The Effect of Railway-Induced Vibrations on Timber Apartment Buildings

Msc. thesis

M. M. de Wit

Delft University of Technology

TUDelft

The Effect of Railway-Induced Vibrations on Timber Apartment Buildings

by

M. M. de Wit

Student Name	Student Number
Marica de Wit	5422159

Thesis committee:	Dr.ir. G.J.P. Ravenshorst (Chair)
	Ir. M. Spanenburg (Company Supervisor, BAM)
	Dr. ir. M. Mirra
	Dr.ir. P.C.J. Hoogenboom
Project Duration:	February, 2023 - April, 2024
Faculty:	Faculty of Civil Engineering and Geosciences, Delft Company:
BAM Advies	Engineering, Bunnik

TU Delft

Preface

This thesis marks the end of my journey, from the premaster in Civil Engineering to obtaining the Master of Science degree at Delft University of Technology. The aim of this research was to investigate the effect of railway-induced vibrations in timber apartment buildings, a topic which combines the two fields that I am most interested in: dynamics and timber. It has given me the opportunity to expand my knowledge on the intricate behaviour of structures under dynamic loads and the opportunities and challenges that lay ahead in the application of timber in modern construction.

I would like to extend my heartfelt gratitude to my assessment committee, beginning with Dr. Ir. Geert Ravenshorst, the chair of the committee, for overseeing the process of my thesis. Your insights and thoughtful feedback have been valuable in approaching the research from different sides and have helped refine the thesis further. To Dr. Ir. Michele Mirra, for always taking the time to sit down with me and for the engaging discussions we have had of the last year. Not in the least, I would like to thank you for the meticulous attention you have given each draft of my report. Your honest and detailed remarks have been very important for the development of my research. To Dr. Ir. Pierre Hoogenboom, for listening attentively to all my presentations and for your feedback, which has helped me to look into underlying principles of difficult concepts, enhancing the clarity of my research.

A special thanks goes out to my company supervisor, Ir. Mark Spanenburg, for your continuous support and keen interest over the last year. Your guidance has helped me through the complexities of this thesis, while always giving me the freedom to follow my own path. I am particularly thankful for your unwavering enthusiasm, which has been a source of inspiration and has motivated me to delve deeper into the topic.

Last but not least, I am eternally grateful for the unconditional support of my friends and family. This thesis, but also the last three years of this academic endeavour, have not been without hurdles. Your encouragement, love, wisdom and believe in me has been the cornerstone in this process. Thank you for having been a part of this journey. I can not express in words how much that means to me.

M. M. de Wit
Delft, April 2024

Abstract

In recent years, the construction industry has witnessed a significant shift towards sustainable materials. Wood, being renewable and able to take up CO2 during its lifetime, offers a more environmentally friendly alternative to concrete or steel. This trend coincides with increasing urbanization and population growth, which leads to more buildings being built in close proximity to the railway tracks in the Netherlands. In 2015, more than 845,000 residential addresses were already located within 300 meters of a railway track and this number is only expected to increase.

This research examines the dynamic behaviour of residential timber buildings subjected to railway-induced vibrations. At present, concrete buildings constitute the most common realized topology. Therefore, the main purpose of this study is to determine if timber building structures can offer sufficient comfort in railway-zones. This is done by analysing the impact of varying different structural parameters on the vibration transmission in the building and comparing the resulting vibrations with those observed in concrete buildings.

To achieve this goal, first a literature study was carried out. The first part of this study focused on the railway-induced vibrations, while the second part investigated the construction of timber multi-storey buildings and the possible building components. Afterwards, an analytical transfer function model is outlined which accounts for foundation and soil-structure interaction (SSI), offering a low-computational alternative to finite element models (FEM) which is an essential consideration for the preliminary design phase this research focuses on. Since this transfer function model is based on a shallow foundation, additional research is carried out to be able to implement a pile foundation into the model. It was found that the behaviour of a pile group is not simply equal to the sum of the stiffness and damping of each of the individual piles and that the piles affect each other, a phenomenon referred to as the 'group effect'. Both the pile dimensions, soil parameters and this group effect are added to the transfer function model in this study. After integrating the pile foundations, the model was implemented in Python and applied to two case studies with concrete buildings. Comparisons between the FEM models provided for these case studies and the results from the transfer function model showed large discrepancies between the results from the FEM models, highlighting the importance of soil-structure interaction.

A parameter study on timber buildings showed that coincidence between the soil-building resonance with the natural frequency of the floors led to significant vibration peaks. Different strategies, such as increasing the natural frequency of the floors and increasing the building mass to prevent this coincidence effectively reduced these peaks. Moreover, it was found that that pile foundations mitigate the railway-induced vibrations more effectively than shallow foundations.

Comparing the timber buildings optimised based on the structural requirements to an equivalent concrete building showed that the timber building exhibited between 108-461 % higher building vibrations. However, increasing the floor thickness, although resulting in less economical floors, reduced this difference substantially to 55-60 %. Furthermore, using fully clamped supports showed a similar reduction. Currently, achieving fully rigid supports between timber walls and floors is technically difficult. These findings suggest that while challenges remain, the adapted transfer function model is able to analyse and compare the behaviour of timber and concrete buildings. Future research into additional mitigation strategies and the kinematic soil-structure effect, combined with pre- and post-building measurements to evaluate the accuracy of the transfer function model could aid in further reducing railway-induced vibrations in both timber and concrete apartment buildings.

Contents

List of Figures

List of Tables

Nomenclature

Abbreviations

Abbreviation	Definition
CLT	Cross-Laminated Timber
FEM	Finite Element Model
GLT	Glued Laminated Timber
LVL	Laminated Veneer Lumber
SLS	Serviceability Limit State
SSI	Soil-Structure Interaction
ULS	Ultimate Limit State

Greek Symbols

Symbol	Definition	Unit
ρ	Density	kg/m^3
ξ	Damping ratio	[-]
ϕ	Phase	radians
ω	Angular frequency	rad/s

Latin/Mathematical Symbols

Symbol	Definition	Unit
$V_{\max}$	Maximum vibration severity	[-]
f	Frequency	Hz
v	Velocity	mm/s
H_v	Weighing function for railway-induced vibrations	$1/mm/s$
E_L, E_T	Elastic modulus parameters	MPa
q_k, g_k	Load parameters	kN/m^2
M_d	Bending moment demand	kNm
V_d	Design shear force	kN
S_{xnet}, I_{xnet}	Sectional properties	cm^3, cm^4
τ_d	Design shear stress	MPa
w_{inst}	Instantaneous deflection	mm
f_1	Fundamental frequency	Hz
L	Span length	m
b, h_{CLT}	Width and height of CLT elements	mm
a_1, t_1, t_2	Dimensions of structural elements	mm

1 Introduction

In recent years, sustainability has become increasingly relevant. This has also become visible in the building industry, amongst others by the rising interest in timber buildings: wood is both renewable and has the ability to take up CO_2 during its growth phase and storing it when used in structures, making it a valuable option when taking into consideration sustainability. Additionally, the lightweight properties of timber can result in lower transport costs and a reduction in the size of the foundation needed, when compared with steel or concrete constructions [21].

At the same time, the growth of the population and increasing urbanisation, result in more buildings being built in close proximity to railways. In 2015 in the Netherlands, more than 845,000 residential addresses were located within 300 meters of a railway track [27], and this number is expected only to rise more in the upcoming years. Besides that, the global goal of becoming more sustainable gives rise to the expansion of the rail network. By 2030, the European Government has planned to double high-speed railway traffic and by 2050, rail freight traffic is scheduled to follow [14]. Sadly, railway-induced vibrations can be the cause of severe annoyance for the occupants of nearby buildings [27]. This stresses the importance of taking into account these vibrations in the design process.

While more studies have been done on the effect of human-induced vibrations in timber buildings, the specific consideration of timber apartment buildings in the context of railway-induced vibrations remains relatively unexplored. Even for concrete buildings, there is still much to be discovered in this area, although much more information is already available. Therefore, this thesis focuses on obtaining a better understanding of the dynamic behaviour of timber structures when subjected to railway-induced vibrations, to offer perspective on whether constructing timber apartments in railway zones is feasible without causing severe annoyance for residents.

1.1. Research objective

The primary objective of this research is to investigate the influence of railway-induced vibrations on timber apartment buildings and assess the likelihood that these vibrations will cause discomfort for residents in the future. To achieve this the goal is to make a model that can be used in the preliminary design phase, in which the structural parameters can be adjusted to study their effect on the resulting vibrations. By using a case study as a reference project and comparing the values of the residential timber building with those of a concrete building, the research aims to provide insights and recommendations for whether it is feasible to build with timber in railway zones while maintaining the livability of the apartment building.

1.2. Research questions

To achieve the research objective, this thesis will strive to answer the following main research question:

> *How does a residential timber apartment building behave when subjected to railway-induced vibrations and how is this influenced by different structural parameters?*

To answer this main question, the research is divided into multiple subquestions.

1. Which **timber building systems** and **components** are currently available and could be used for structural application in timber apartment buildings subjected to railway-induced vibrations?
2. Which factors influence the **characteristics** of the frequencies and amplitudes of **railway-induced vibrations** and how do these vibrations impact the **resident comfort**?
3. How can the railway-induced vibrations be taken into account in the **preliminary design** of apartment buildings to assess the **dynamic response** of the building, exploring how **different structural parameters**, such as the building configuration, influence the building's behaviour under these vibrations?
4. In what way can a timber apartment building be designed such that it is both in compliance with the requirements for the **structural design** and **minimises the resulting vibrations** in the building caused by railway-induced vibrations?
5. How does the dynamic response of a timber apartment building **differ** from that of a **concrete reference building** under similar conditions of railway-induced vibrations, and what insights can be gained from **comparing** their structural performance and serviceability criteria in this context?

1.3. Methodology

The research objective will be achieved through a process that can be divided into three phases:

Literature review
The literature review is conducted to gain insights into the characteristics of railway-induced vibrations and how they propagate through buildings. This part of the thesis also focuses on how the comfort of residents subjected to railway-induced vibrations is quantified in the Netherlands, by considering the SBR guideline: Meet- en beoordelingsrichtlijn voor trillingen:2013 - Deel B - Hinder voor personen in gebouwen [66]. This guideline focuses on the measurements and evaluation of the disturbance in buildings caused by environmental vibrations, such as railway-induced vibrations. Methods of translating railway-induced vibrations are outlined and the model best suited for the preliminary design phase is decided upon, based on computational efficiency and its ability to estimate the building vibration levels. Furthermore, timber structures are studied, and the gained knowledge is used for the design of the timber building that is later analysed.

Structural dynamics
In this chapter, the theory behind the transfer function model, resulting from the literature study, is described and the underlying structural dynamics theory is outlined. The dynamics of shallow foundations and rigid and flexible floors, columns and walls is explored, such that the method can be applied to the concrete buildings from the case study and the timber buildings in the parameter study. Furthermore, this chapter will focus on the dynamics of pile foundations. The transfer function model in the literature is applied to shallow foundations, but many buildings in the Netherlands make use of a pile foundation. Therefore, this chapter also focusses on adapting the transfer function model to implement pile foundations.

Case study
After expanding upon the theory behind the transfer function model, the model is applied to two case studies: ENKA and HERO. For both projects, free-field measurements, specifications of the two concrete building structures and the results of the finite elements model used for the original analysis were

provided. With this information, the building response to the railway-induced vibrations is calculated and compared with the results found with the FEM models.

Parameter study
Finally, in the parameter study, the dynamic model is applied to four variants of a timber building, each with a different type of floor, to study their effect on the vibrations in the building. The types of floors that are analysed are a laminated veneer lumber hollow box floor and a cross-laminated timber floor, each with either a wet or dry screed. Structural design checks are added to the model, to be able to design a building that does not only minimise the railway-induced vibrations but one that is also in compliance with the necessary design checks. The structural and geometrical parameters, such as the thickness of the floors and the number of floors are varied, to analyse how they influence the corresponding transfer functions. This chapter aims to find which parameters are the most efficient in steering the response of the timber buildings.

Comparison
Finally, a comparison is made between timber buildings equivalent to the concrete reference building from the HERO case study, so that a conclusion can be drawn on the differences in the dynamic responses of the different materials.

1.4. Outline

This thesis is organised into distinct chapters, each addressing a different part of the research. **Chapter 2** provides the literature review of railway-induced vibrations necessary to gain an understanding of the different factors that may be of importance in the subsequent analysis. **Chapter 3** focuses on the literature review of timber components, such that a timber floor-, wall and building system can be chosen that will be used as the basis for the analysis. **Chapter 4** dives into the structural dynamics model and its components used to calculate the resulting vibrations in the building caused by the passing trains. In **Chapter 5** two case study projects are evaluated and the model outlined in Chapter 4 is applied, after which the results are compared to the provided results from the FEM models. **Chapter 6** contains the parameter study itself, in which the effects of changing the building parameters on the amplification or attenuation of the vibrations are studied. Finally in **chapter 7**, the resulting vibrations in the concrete building from the HERO case study are compared to those in equivalent timber buildings. After that, changes are made to the timber building design to analyse how this reduces the vibration levels for this specific location. **Chapter 8** discusses the obtained results and limitations of the research, while **chapter 9** contains the conclusion and recommendations for further research.

2

Railway induced vibrations

2.1. Introduction

Generally, the effect of railway-induced vibrations can be explained as the ”gentle shaking or trembling” of a building, often specifically of the floor people stand on. Most of the time, a rumbling sound accompanies this movement [64]. The vibration is found to be too weak to cause actual damage to the structures [47]. Still, it can cause serious annoyance and in some extreme cases, even disturbance of sleep to nearby residents according to the extensive research of Kamp et al. [27].

2.2. Characteristics of railway-induced vibrations

To understand how these railway-induced vibrations can be a nuisance for occupants, it is important to understand how they work. Railway-induced vibrations are defined as the vibrations generated by passing trains. The vibrations are generated at the interface between the wheels and the rails of the train: as the train moves along the track, forces are generated at the points of contact of the wheels and rails, resulting in vibrations. These vibrations are then first transmitted through the track and its supporting structure, after which they propagate through the ground into the foundation of nearby buildings, where they propagate through the building structure as shown in Figure 2.1.

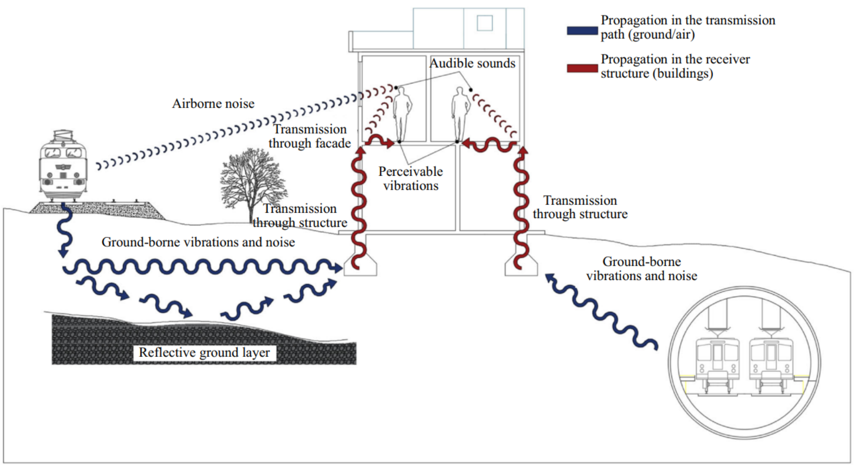

Figure 2.1: Railway-induced vibrations, Ouakka, Verlinden, and Kouroussis [47]

In addition to the vibrations that travel through the ground to nearby buildings, referred to as ground-borne vibrations, the train-track interaction causes two other phenomena: airborne noise and ground-borne noise. As illustrated in Figure 2.1, airborne noise propagates through the air and is then transmitted through the facades of nearby buildings, resulting in audible sounds inside the building. Although both airborne noise and ground-borne noise can cause disturbances in nearby buildings, this research will focus solely on the nuisance caused by the ground-borne vibrations and will disregard the acoustic effects.

2.3. Wave propagation

From the moment railway-induced vibrations are generated to the moment they create vibrations in nearby structures, many variables influence the resulting vibrations in the building. Often, the vibrations are therefore subdivided based on their location: the source, the transmission path and the receiver [9]. The source is the railway and the passing train itself, the transmission path encompasses the ground through which the vibrations are transmitted, and the receiver is the building and its foundation.

2.3.1. Source

The first phase in the transmission of waves is the source, the point where the vibrations are generated. The source includes the train, the tracks, the system below the rails and the ground immediately surrounding it. The vibrations are generated by the interaction between the wheels of the train and the track and are influenced by the properties of the underlying structure and the train itself.

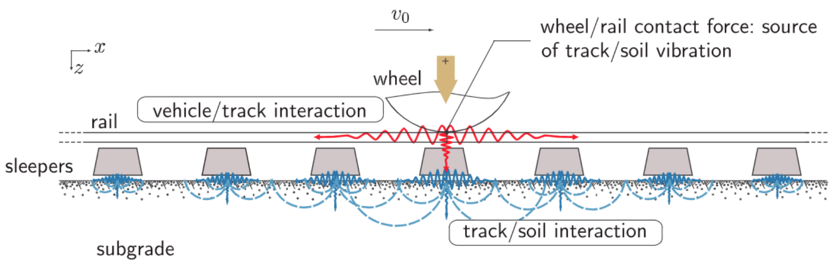

Figure 2.2: Wave generation at the source [61]

At the source, several factors affect the magnitude and frequency of the vibrations. The most significant factors are listed below [24], [64]:

- Irregularities in the wheels of the train increase the vibration levels.
- Irregularities in the track increase the vibration levels.
- Freight trains and high-speed trains generally increase vibration levels.
- Higher speeds in general correspond to higher vibration levels.
- Whether the train is travelling underground or above ground significantly influences the characteristics of the vibrations and the frequencies of the peaks.
- The type of ballast, fasteners, and the material and distance between the sleepers are of influence for the characteristics of the vibrations.

2.3.2. Transmission path

After the generation of the vibrations by the train-track interaction, the vibrations are transmitted to the ground in the form of waves [15], as shown in Figure 2.3. Three main types of waves can be distinguished: compressional waves (P-waves), shear waves (S-waves) and Rayleigh waves. Each of these wave types has different characteristics and propagates differently through the ground. In Figure 2.4, the behaviour of these different wave types is illustrated.

Figure 2.4 shows that compressional waves propagate in the longitudinal direction. These waves are a type of body wave that mainly propagates within the soil rather than at its surface. Shear waves, also a type of body wave, travel transversely. Rayleigh waves, on the other hand, are waves that propagate on the surface of the soil. This type of wave decays as the depth increases.

Compressional and shear waves decay more rapidly than Rayleigh waves, due to geometrical spreading [15]. Geometrical spreading describes how the intensity or energy of a wave decreases as it spreads out

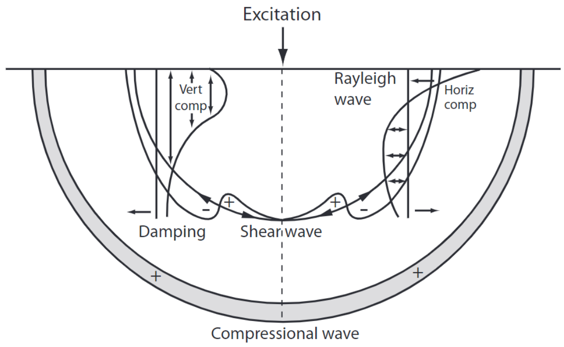

Figure 2.3: Wave generation mechanism [15]

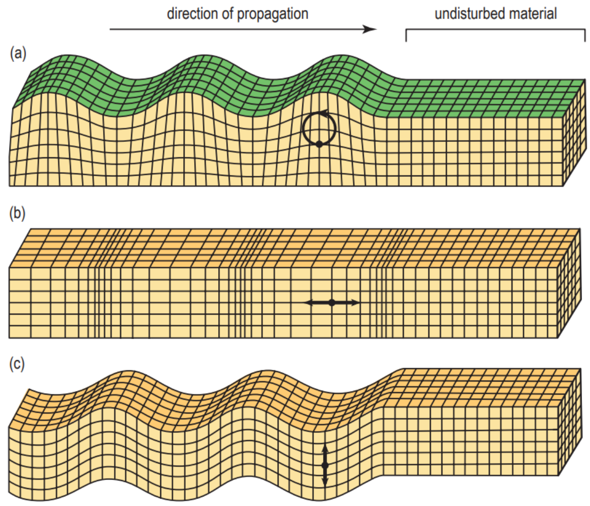

Figure 2.4: Types of waves, with a) Rayleigh waves, b) Compressional waves and c) Shear waves [64]

from its source in three-dimensional space. As a wave spreads out, the total energy remains constant but becomes distributed over a larger area. Therefore, the energy density of the wave decreases. Body waves have a spherical wavefront as shown in Figure 2.5, which means that they propagate in the shape of a half sphere in the soil: both in vertical and horizontal directions. Because Rayleigh waves only propagate over the surface of the soil, they have a circular wavefront on one plane and are two-dimensional instead of three-dimensional. The energy of the waves is only distributed in two directions instead of three, which means that the Rayleigh waves lose their energy less quickly than the body waves. The distribution of the Rayleigh surface waves is also illustrated in Figure 2.5. Due to geometrical spreading, in approximately the first 20 metres of the track, the body waves can be significant. However, for buildings at greater distances, Rayleigh waves are governing [9], [39].

In addition to geometrical spreading, the speed of the waves and their damping are of importance in determining how much energy the waves lose over a distance. This is influenced by the type of soil through which the waves propagate. If the soil is very stiff, for example, the amplitude of waves at lower frequencies is lower than those at higher frequencies. For softer soil, this is the other way around: amplitudes at lower frequencies are higher than those at higher frequencies. Besides that, the overall magnitude of the vibrations is higher for softer soils than for stiffer soils [49], as can be seen in Figure 2.6. For common types of soil, their corresponding modulus of elasticity E_s is summarised in Table 2.1. The variety between values for the soil stiffness per type of soil can be quite large and is dependent on factors such as the water content of the soil, the mass density and the stress history [11].

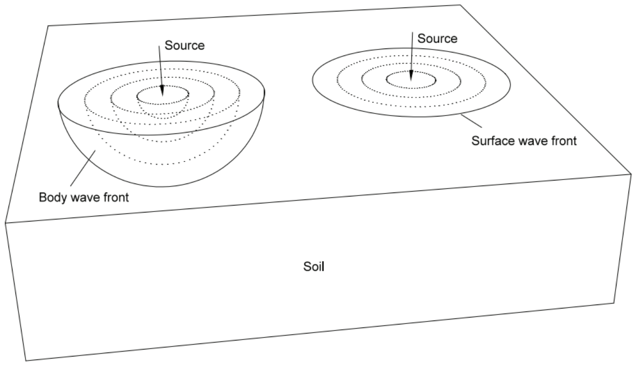

Figure 2.5: The principal of geometrical spreading [49]

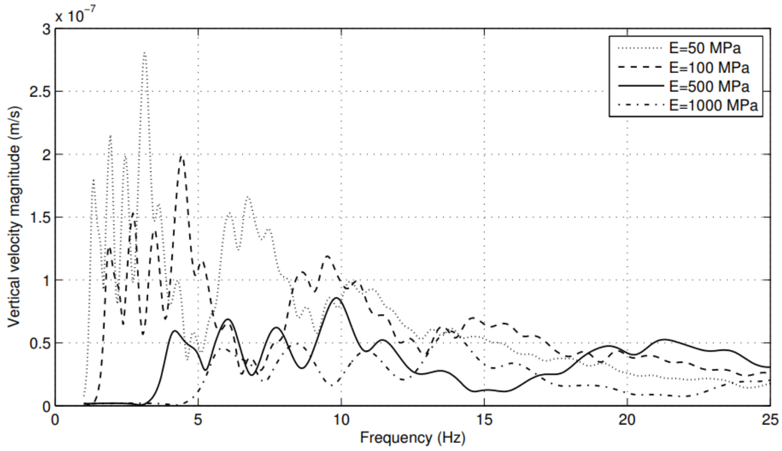

Figure 2.6: The influence of soil stiffness (E) on the frequencies and magnitudes of railway-induced vibrations [49]

2.3.3. Receiver

Lastly, the railway-induced vibrations arrive at the building structure, the receiver. The receiver includes the building itself, its foundation and the immediate surrounding soil. Here, they first reach the foundation of the building, from where they are transmitted to the building itself. Depending on the geometry of the building, the building materials, its superstructure, the type of foundation and the soil properties, the vibrations are either attenuated or amplified.

2.3.4. Variability

One of the problems that arises when considering railway-induced vibrations is that there is a large variability in the factors that influence the frequency range of the vibrations at the receiver, transmission path and source. The characteristics of the vibrations can therefore vary significantly between different sites, tracks, and train types. Therefore, there are no typical railway-induced vibrations and the characteristics of the vibrations have to be analysed locally for each situation [60].

2.4. Human perception

Although railway-induced vibrations are found to be too weak to cause structural damage [47], research shows it is the cause of serious annoyance experienced by residents that live in proximity of the railway tracks. A study, carried out in Sweden by Maclachlan et al. [37], found a positive association between the annoyance experienced by residents and the distance of their homes to the railway track in question. The closer their houses are to the track, the higher the vibration annoyance, up to 400 m. This is in line with the theory behind the Rayleigh waves, which attenuate over distance. Especially freight trains were found to result in severe annoyance. It is noteworthy that a high percentage of the houses had wooden floors, in the living room (60.7 %) and in the bedroom (67.2 %). However, no mention

Table 2.1: Range of values for Young's modulus of different soils E_s [11]

Soil	E_s **[Mpa]**
Clay	
Very soft	2-15
Soft	5-25
Medium	15-50
Hard	50-100
Sandy	25-250
Sand	
Silty	5-20
Loose	10-25
Dense	50-81
Sand and gravel	
Loose	50-150
Dense	100-200

was made of a correlation between the floor type and the level of nuisance experienced by participants. A similar study was carried out by Van Kamp et al. [63] in the Netherlands, with comparable results. In Figure 2.7 the correlation between the distance of the housings of participants of the study and the percentage of participants that experienced nuisance from the railway-induced vibrations is shown. Again, freight trains were found to be of greater nuisance than passenger trains. Another conclusion was that the experienced disturbance was lower for buildings founded on stiff sand soil, compared to other soil types. 39 % of living room floors were wooden floors in this study, but it was not researched whether residents with this floor type experienced greater levels of annoyance. However, a reference is made to a Swedish study by Öhrström and Skånberg [46], in which it is mentioned that the level of disturbance was higher for people living in wooden buildings as opposed to concrete buildings. No further specifications about the type of wooden buildings are, however, provided.

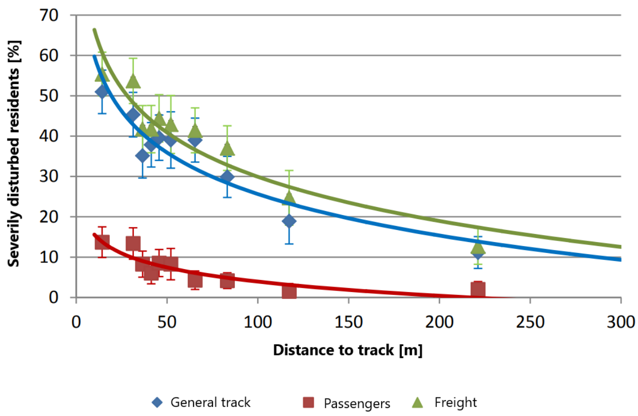

Figure 2.7: Percentage of severely annoyed residents in relation to the distance of their building to the track in the Netherlands[63]

The second problem that can occur when residents are subjected to railway-induced vibrations is sleep disturbance. When looking at purely the effect of noise from traffic such as railway systems, a wide range of research is available. A clear correlation has been found between this type of noise in the nighttime and sleep disturbance of residents in high-traffic exposure areas [54]. Although traffic and noise occur simultaneously, they individually affect the comfort levels of residents. A study carried out by Smith et al. [54], on the influence of both noise and vibration impact of freight trains on people, concludes that train-induced vibrations at night are likely to lead to sleep impairment, independent of the disturbance caused by noise. They found that this negative effect increases with higher vibration amplitudes. Interestingly, this research is carried out by taking into account the vibrations in the horizontal direction instead of the vertical direction. The reasoning behind this choice is that although the highest vibrations are often found in the vertical direction at the mid-span of floors [62], beds are usually placed alongside the edges of a room. At this location and especially at higher storeys of a building, the horizontal vibrations are dominant instead when considering sleep disturbance. However, for vibration analysis in buildings, it is almost always sufficient to only look at the vertical components of the vibration and disregard the transverse vibrations. This is due to both the higher amplitude of the vertical vibrations and the way these vibrations are transmitted more easily through the building foundation than the horizontal ones [24], [52], [18]. Therefore, this research will focus on the propagation of vertical railway-induced vibrations.

2.5. Prediction methods

To predict how railway-induced vibrations will affect nearby buildings such that annoyance for residents can be prevented, different prediction procedures exist. These methods differ in level of detail, but also in which components from the source to the receiver they focus on. Some models start with predicting the force generated by the train and include all the steps up to the building vibrations, but there are also models that make use of free-field measurements instead. Free-field measurements are measurements on the ground which can either be done at the future location of the building or near the track, without any building yet present. These two distinctive approaches are shown in Figure 2.8. The advantage of using measurements on site is that it takes away part of the uncertainty that comes with the assumptions that have to be made at every prediction step, regarding the train, the track, and the propagation through the soil. Although the advantage of models that include the entire system is that a more extensive study can be done to find out how different buildings perform in various circumstances, this research will focus on the building response and use available free-field measurements instead of modelling the source and propagation path explicitly.

The procedures to calculate the building response can be classified into four categories:

- Empirical models
- Experimental methods
- Numerical models
- (Semi-)analytical methods

Empirical models, such as the model developed by the Federal Transit Administration [24], are efficient in use: standardised values for the attenuation and amplification of vibrations travelling from the track to the building have been established based on data from previous projects. However, the accuracy of the predicted vibrations is often low [76]. **Experimental** methods like the method investigated by With and Bodare [69] measure the ground signal and the vibration levels inside an existing building near a railway track to derive functions that determine the ratio between the ground signal and the vibrations inside the building. That information can then be used together with a recorded ground signal at another site, where a similar building will be built, to predict the vibrations inside the new building. The downside of this method is that the building and site of the measured situation have to be very similar to the building that is to be constructed. Another option is to use a **numerical** model such as a finite element model (FEM), which can include the vibration source, the transmission path and the building structure itself or part of the system. However, to create the type of detailed model required to accurately represent the behaviour of the building and subsoil results in models with substantially high computation time [75]. Finally, multiple **analytical** models have been developed, based on mechanics and closed-form equations. Those models make use of simplifications and are not as detailed as a FEM model, but have been proven fast in terms of computation time and have been shown to generate estimations of railway-induced building vibrations comparable to measured results in various studies [76], [7], [6], [75], [2]. Due to the relatively low computational effort required for these models, while still providing sufficiently accurate results for the initial design phases, they are often used for studies into design alternatives [2].

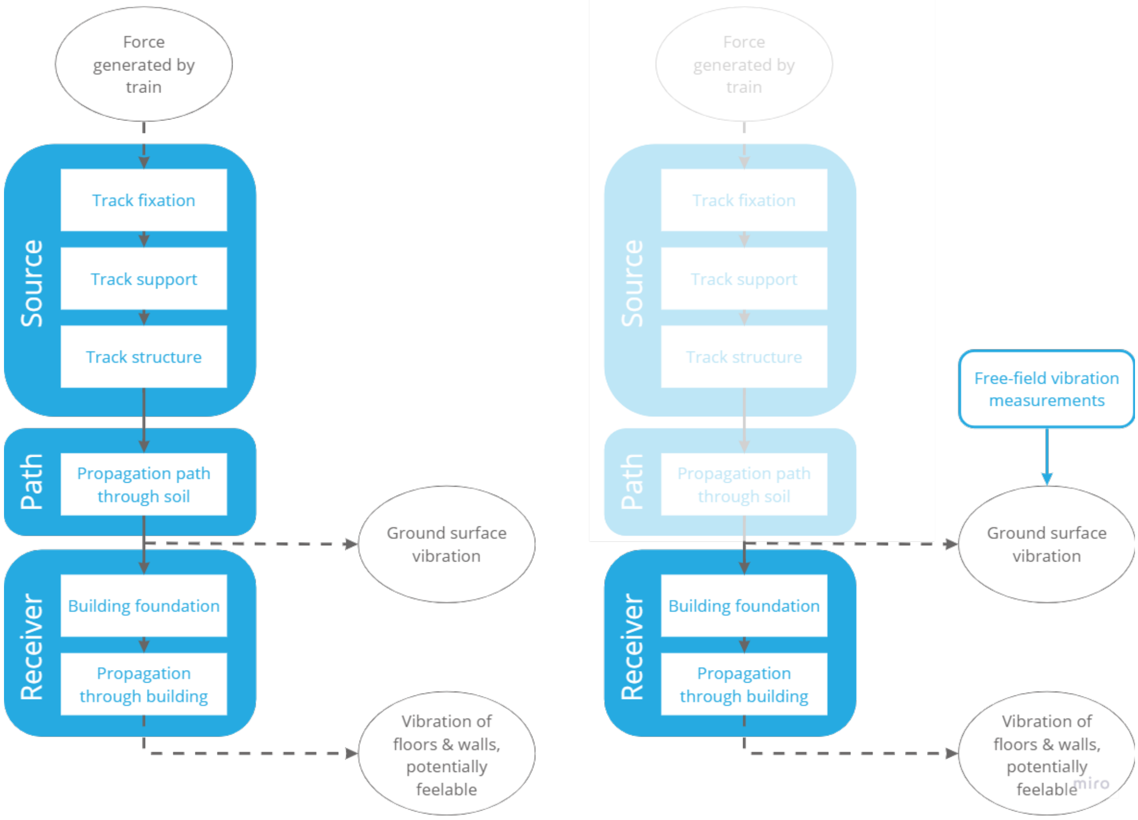

Figure 2.8: Block diagram prediction railway-induced vibrations, partially adapted from Hanson, Towers, and Meister [24]

Impedance modelling is a method that is used in acoustics and mechanics to represent the dynamic response of a system by looking at its impedance (resistance) to vibrations [19]. It is a way to couple individual components to each other to calculate their combined response. It is therefore applicable to many systems. When considering a building structure, the individual physical properties of walls or columns, floors and the foundation can be incorporated into the analysis, and by considering boundary conditions the total structure's resistance can be found and related again to the individual elements. Because this way of modelling allows the structure to be subdivided into elements of which the physical behaviour is well-understood, it is a useful representation of a system when evaluating the effects of modifications on the vibration behaviour. For impedance modelling, all the characteristic matrices of individual elements are combined into one matrix, for which boundary conditions are then used to solve the system. When there are no parallel elements in a system, and it thus only consists of elements that are coupled in series, the impedance matrices can be rewritten as transfer matrices. Although the transfer matrices contain the same information as the impedance matrices, their computation is more straightforward and computationally efficient. For a building system in which the elements are connected from end to end, this is therefore particularly useful, as shown by the research done by Auersch [7]. This methodology simplifies the analysis of complex structures by enabling easier modification and understanding of how changes affect the system's dynamic response.

Furthermore, research from Zou et al. [75] in which an impedance model was used to estimate the building vibrations of two different over-track buildings, has shown good agreement between the measured and estimated vibrations. It should be noted that the study used vibration measurements at the base of the existing building instead of free-field measurements and did therefore not include the building foundation and coupling with the soil. In Figure 2.9 the measured and predicted building vibrations are shown. Both the one-dimensional and the more complicated two-dimensional models show accurate results.

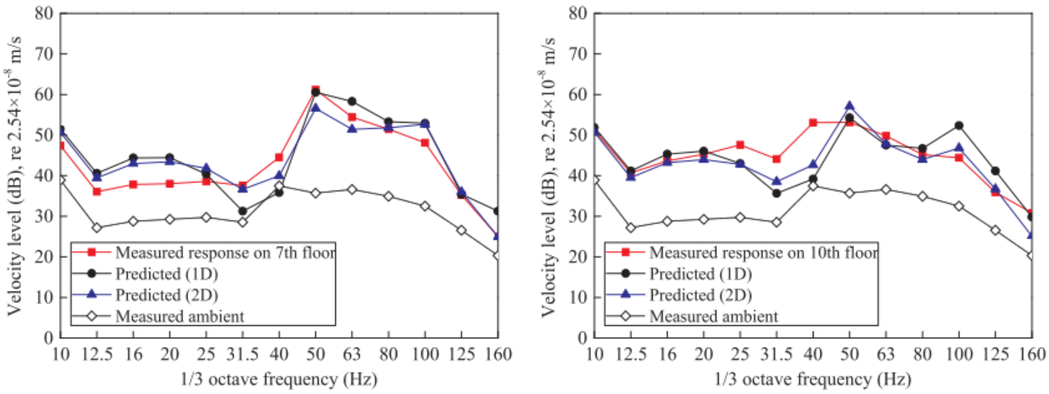

Figure 2.9: Measured and predicted vibrations in a fourteen-storey building, left: on the seventh floor, right: on the tenth floor, from Zou et al. [75]

The research that was carried out by Sanayei et al. [53] validated the analytical predictions of the impedance model with a laboratory scale model building, and it was found that again the predictions accurately represented the measured building response. In Figure 2.10 the measured and predicted velocities on each floor of the building are shown.

Similar conclusions were drawn from the research by Anish et al. [2], who analysed railway-induced vibrations in a four-story building in Boston. They concluded that impedance-based modelling was computationally efficient and that the model predictions matched well with the measured building responses. In this study also measurements on the base level of the building were used instead of free-field measurements since an existing building was studied. In Figure 2.11 the resulting calculated and measured vibration levels in terms of velocity are shown. Above 50 Hz, some deviations between the measured and predicted vibration levels can be noted, which the authors discussed being due to either a measurement error at the base of the building or a difference in the interpretation of the actual behaviour of the composite columns. Although measurements at the base of the building are used and an existing building is regarded, the possibility of including soil-structure interaction and using the model together with free-field measurements for new buildings is recognised.

That is where the research by Auersch [7] expands on the impedance model theory. Whereas Zou et al. [75], Sanayei et al. [53] and Anish et al. [2] use impedance matrices and measurements at the base of the building to prevent having to model soil-structure interaction, Auersch [7] uses transfer matrices and includes a shallow foundation into his model, taking into account soil-structure interaction. The results were validated with three-dimensional finite element method models for multiple buildings. For one of those buildings, the comparison between the transfer functions calculated with the transfer function model and the transfer functions calculated with the finite element model are shown in Figure 2.12. Additionally, for two office buildings, a four-storey concrete building and a six-storey steel frame building, measurements were also carried out. Although a stronger reduction of the vibrations was found for the measured results, the same trend and magnitude of the amplification factors and corresponding frequencies were found, and the transfer function model was concluded to be sufficiently accurate to investigate the building response to railway-induced vibrations, even when considering complex soil-structure interaction. Interestingly, in this study, the transfer function model is not only used to analyse the vibration response of the buildings in proximity of the track but is also shown to be applicable to calculate how the vibrations are transmitted from the train to the soil.

To summarise: the transfer function and impedance model have high computational efficiency, combined with good agreement with both three-dimensional finite element models and measurements in existing buildings. Thirdly, it provides the ability to investigate the influence of changing structural parameters for each of the individual components in the building. Therefore, the transfer function model has shown to be applicable to real-world scenarios and is chosen as the most appropriate model to investigate the building response to railway-induced vibrations in the preliminary design stage.

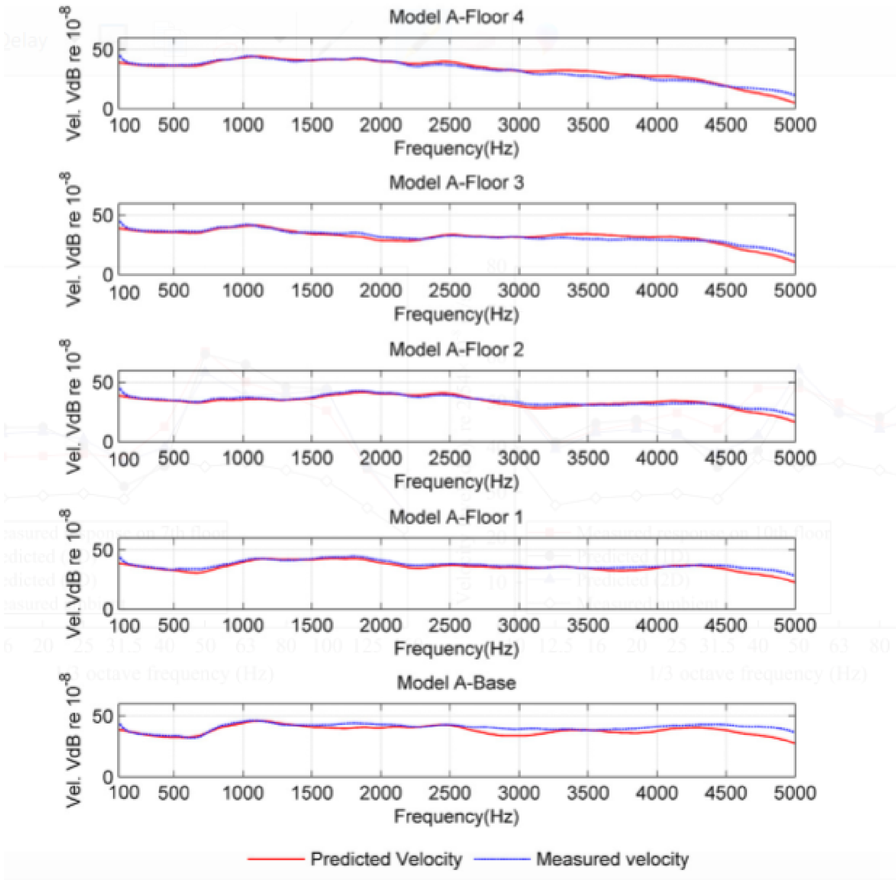

Figure 2.10: Measured and predicted vibrations in a laboratory scale building, from Sanayei et al. [53]

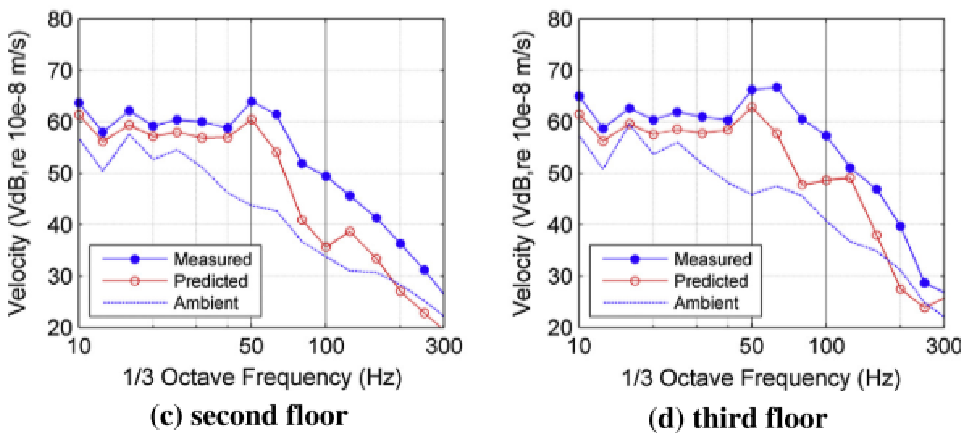

Figure 2.11: Measured and predicted vibrations in a four-storey building, left: on the second floor, right: on the third floor, from Anish et al. [2]

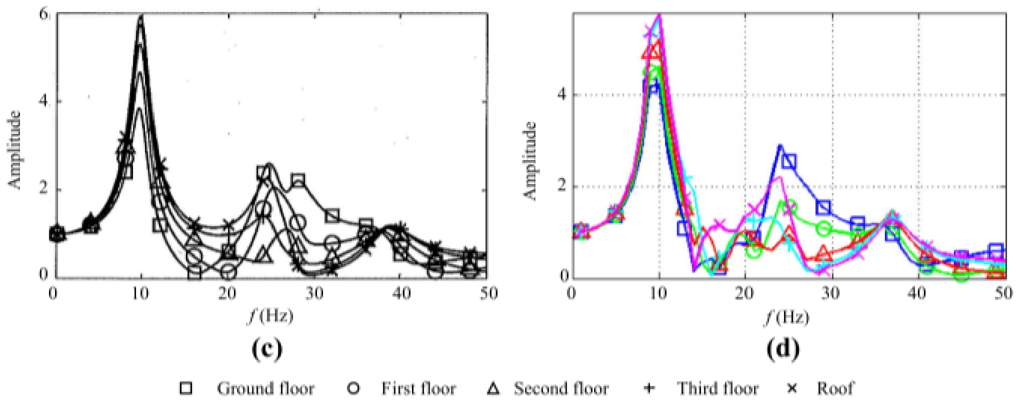

Figure 2.12: Measured and predicted vibrations in a four-storey building, left: calculated transfer functions, right: results finite element model, from Auersch [7]

2.6. Serviceability criteria

Whether the vibrations can be perceived as a nuisance to residents can be estimated in different ways. Although there is currently no legislation in the Netherlands regarding railway-induced vibrations in residential buildings, there are guidelines that focus on preventing nuisance from these vibrations. The most used guideline in the Netherlands to evaluate whether the vibration levels are within the serviceability limits is the "SBR richtlijn, Deel-B". It considers ground-borne vibrations caused by railway traffic from 1 Hz to 80 Hz.

Depending on whether the measured free-field vibrations are provided in terms of acceleration or velocity, a weighing function is applied. For free-field vibrations provided in velocity, Equation 2.1 can be applied. In this equation, v_0 is 1 mm/s, $f_0 = 5.6$ Hz and f is the frequency considered.

$$|H_v(f)| = \frac{1}{v_0} \cdot \frac{1}{\sqrt{1 + (f_0/f)^2}} \tag{2.1}$$

The weighing function over the frequency range of 1-80 Hz for railway-induced vibrations is shown in Figure 2.13. The goal of this function is to reduce peaks in the lower frequency range between 1-16 Hz, that are less perceivable for humans. Because the weighing function divides the input velocity by mm/s, the resulting value is dimensionless.

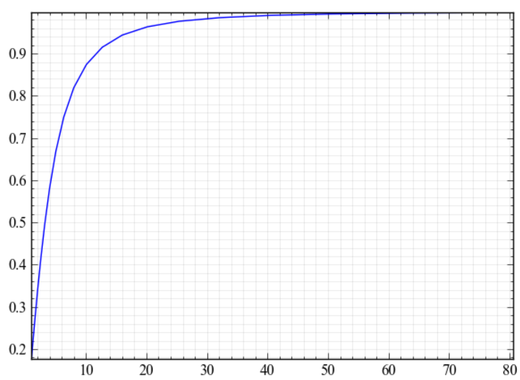

Figure 2.13: Weighing function $|H_v(f)|$ for velocity

This SBR guideline focuses on translating vibration levels of railway-induced vibrations to an effective vibration severity, $v_{eff}(t)$, as shown in Equation 2.2. The maximum value of this effective vibration severity is denoted as V_{max}. This maximum vibration severity is tested against target values, to check whether the vibration levels are below the levels considered undesirable. In the SBR guideline, limits for the vibration levels are specified for different periods, as shown in Table 2.2.

Table 2.2: Time periods as stated in SBR guideline

Period	Timespan	Duration [s]
Day	07:00 until 19:00	43200
Evening	19:00 until 23:00	14400
Night	23:00 until 07:00	28800

$$v_{eff}(t) = \sqrt{\frac{1}{\tau} \cdot \int_0^t g(\xi) v^2(t-\xi) d\xi} \tag{2.2}$$

$$g(\xi) = \exp\left\{\frac{-\xi}{\tau}\right\}$$

$$\tau = 0.125s$$

Besides the maximum vibration severity, the average vibration severity, V_{per}, has to be calculated. V_{per} is the quadratic average of the largest effective value of $v_{eff}(t)$ in an interval of 30 seconds. V_{per} is dependent on both the effective vibration severity and the period in which it occurs. V_{per} is calculated with Equation 2.3 and Equation 2.4.

$$v_{per,meet} = \sqrt{\frac{1}{n} \cdot \sum_{n}^{i=1} v^2_{eff,max,30,i}} \tag{2.3}$$

$$V_{per} = v_{per,meet} \cdot \sqrt{\frac{T_b}{T_0}} \tag{2.4}$$

In which T_b is equal to the duration of the vibration itself and T_0 is equal to the duration of the timespan of the considered period, as given in Table 2.2.

When V_{per} and V_{max} have been determined, these vibration severity values have to be checked against the target values. Depending on the function of the considered building and whether an existing building or a new building is considered, different target values apply. For new buildings near railways, the target values shown in Table 2.3 apply. In this table A_1 is the lower target value for the maximum vibration severity, A_2 is the upper target value and A_3 is the target value for the vibration severity over a specific assessment period.

Table 2.3: Target values SBR guideline

Target value	Day and evening	Night
A1	0.1	0.1
A2	0.4	0.2
A3	0.05	0.05

To check whether the vibration levels are undesirable or acceptable, V_{max} first has to be checked against A_1. If V_{max} turns out to be lower than A_1, the situation is deemed acceptable. If V_{max} turns out to be higher than A_1, it has to be checked against A_2. When V_{max} is between A_1 and A_2, the average vibration severity V_{per} needs to be checked against A_3. If V_{per} is lower than A_3 the situation is again deemed acceptable by the SBR guideline. However, in the case that either V_{max} is higher than A_2 or V_{per} is higher than A_3, the situation is considered undesirable. In that case, the design has to be adjusted to create an acceptable situation for residents. This study focusses on checking the resulting vibrations in the analysed buildings against A_1 and A_2, but does not consider the V_{per} check.

2.7. Mitigation strategies

When the railway-induced vibrations are estimated to be too high in new buildings, or when the measured vibrations in existing buildings exceed the serviceability criteria, measures can be taken to minimise these vibrations. These measures can be taken at either the source, where the vibrations are created, at the transmission path, where the vibrations propagate through, or at the building, where the vibrations are experienced. This research focuses on the building vibrations, but for completeness, the measures at other locations are also briefly discussed.

- **At the source:**
  - Vehicle-based measures
  - Track-based measures, which can be either temporary or permanent. Temporary measures focus on maintenance, which can for example be rail grinding, to create a smoother interface between the rails and the wheels of the train [15].
- **In the transmission path:**
  - Measures in the transmission path in general focus on interrupting the waves propagating away from the source. This can be done by using trenches, for example, filled with low-density materials to reflect part of the propagating waves. Another approach is to stiffen the soil between the source and the receiver to dampen the propagation of the vibrations. The effectiveness of these measures depends on the soil properties [15]. Lastly, an effective way to mitigate railway-induced vibrations in buildings is to increase the length of the propagation path by placing the building further away from the source [47].

When a new railway line is built in the vicinity of an existing neighbourhood, considerations can be made in the design of the railway system itself. However, making changes to existing railway structures and operating trains proves more challenging and is often costly. Measures in the transmission path are therefore typically a more viable option for existing railway lines. Or, for buildings that still have to be developed the third option can be considered, which is to take mitigation measures in the building itself.

Two main components dictate the behaviour of the building when subjected to railway-induced vibrations: soil-structure interaction and the structural design of the building itself. Common measures that can be taken during the design phase of a building are increasing the stiffness of structural elements, increasing the floor thickness [53], and changing the foundation type [25]. Another more costly but effective measure is to use base-isolation [58]. Furthermore, it is suggested by studies based on empirical research such as Hanson, Towers, and Meister [24] and Arnesson [4] that as a general rule, heavier building constructions result in lower vibration levels: wooden structures are generally stated to result in higher amplifications of the imposed railway-induced vibrations. However, measures in existing buildings such as stiffening the floors by adding beams can be efficient, whereas those kinds of adjustments are more difficult for concrete floors [47].

2.8. Soil-structure interaction and building response

Soil-structure interaction (SSI) focuses on the dynamic interaction between the subsoil and the building when subjected to vibrations. Before the building is constructed, vibrations from the track or any other source can propagate freely. These vibrations are known as free-field ground motions. However, when a structure is present, two factors influence these ground motions. Firstly, the presence of the structure alters the free-field ground motions at the location of the structure and its surrounding area, as the vibrations can no longer propagate freely. Secondly, it is important to remember that the ground is a deformable medium and the foundation is not completely rigid. If both were completely rigid, then the ground motions would be fully transmitted to the building: there would be no amplification or attenuation. However, since this is not the case, the stiffness of the soil and the foundation influences the force transferred from the soil to the foundation to the structure [71]. Soil-structure interaction remains subject to significant variability and uncertainty, but nonetheless, an important element when evaluating the effect of railway-induced vibrations [57], [4]. Both predictions and measurements indicate neglecting it can lead to unnecessary conservative building designs [36]. To understand its influence on the vibration behaviour of the building, this section will dive deeper into studies concerning soil-structure interaction for railway-induced vibrations.

2.8.1. The building influence on free-field vibrations

Research carried out by Huang et al. [25] looked amongst others into how the waves propagating from two railway tunnels would influence a theoretical building for different foundations. First, they set up a train-track model to estimate the dynamic loads exerted on the soil, which they then used to calculate the free-field vibrations. They were able to check those vibrations with actual free-field measurements and found they were in good agreement. After that, they modelled a building with different foundations and analysed how that influenced the vibration transmission into the building. The foundations they considered were a pile foundation, raft foundation and strip foundation. By creating a complete model that included the propagation from the source to the receiver, they were not only able to analyse how the vibrations were transmitted into the building but also how the building influenced the propagation of the vibrations through the ground. The first conclusion drawn from their research is that the presence of the building indeed influences the free-field vibrations. For the building with a pile foundation, they discovered that the calculated vibrations in front of the building stay the same, but within the building, the vibrations are already generally suppressed. Especially behind the building, the vibration levels were found to be lowered. This conclusion is supported by the research carried out by Talbot, Edirisinghe, and Sanitate [57], who found that piles stiffen the soil locally, attenuating the propagation of the vibrations. Because of their stiffness, they are not able to follow the movements of the free-field motions, resulting in a different motion at the pile head than in the free-field. Besides this stiffening effect, the piles reflect and scatter the incoming waves. This filtering effect further changes the incoming vibrations [32]. Similar effects are found for other types of foundations [55].

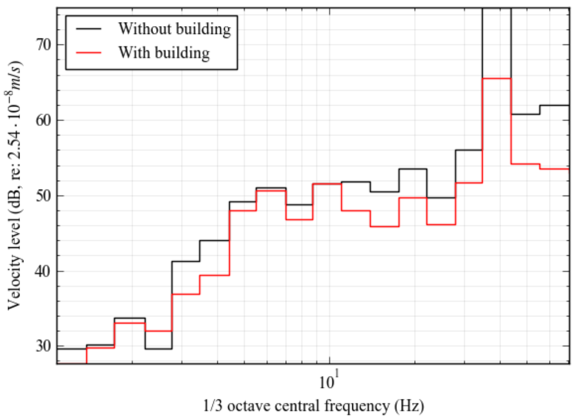

Figure 2.14: Velocity level of railway-induced vibrations on the ground surface of a building with pile foundation, behind the building, adapted from [25]

2.8.2. Transmission through the foundation

Besides the influence of the presence of the building on the free-field vibrations, the interaction between the foundation and the soil influences the transmission of the vibrations into the building. A Swedish study by Arnesson [4] summarises generalized amplification factors used by the industry of 0.3 for pile foundations and 0.6 for on-grade slab foundations, for the transmission of the free-field vibrations to the foundation. Their research then focuses on measurements of 50 buildings with on-grade slab foundations, and although they find a spread between 0.3 and 1.2, they report a mean amplification factor between 0.8-1.1. This is also higher than the often used amplification factors reported by the Federal Railroad Administration [24], who prescribe an attenuation in the range of 0.2-0.6 for masonry buildings on pile foundations and spread footings.

Although using single amplification factors simplifies the estimation of railway-induced vibration levels significantly, research by Kuo et al. [31], Huang et al. [25] and Moskovets and Kanev [42] have shown that these values may be an overestimation of the reduction in transmission. All three studies carried out measurements and found that the transmission is frequency-dependent. The results found by

Huang et al. [25] for a building of four floors, with concrete columns and slabs, are translated[1] to an amplification ratio of the vertical free-field vibrations to the foundations and shown in Figure 2.15. The highest vibration levels are found for the strip foundation, whereas the pile foundation is found to reduce the vibrations the most. At the natural frequency of the structure, amplifications are found instead of attenuation of the vibrations. For this specific site, the pile foundations show the highest overall reduction of the vibrations.

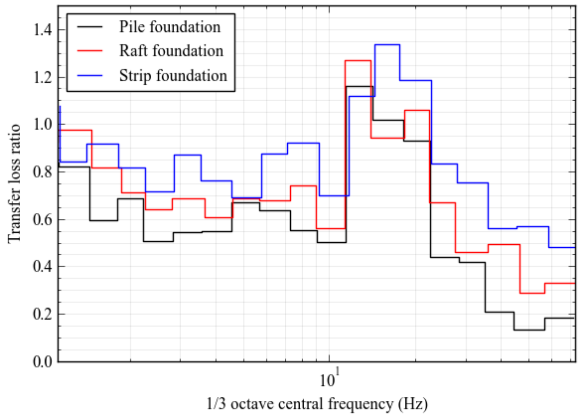

Figure 2.15: Ratio of transmission loss of free-field vibrations for buildings with different foundations at the foundation level, calculated from [25]

2.8.3. Influence of the soil on the building vibrations

Besides the foundation, the soil properties significantly influence the soil-structure interaction. The previously discussed study by Kuo et al. [31] shows this as well. Zakeri, Esmaeili, and Mousavi-Rahimi [72] specifically looked into how foundations and soils of different stiffness influenced not only the vibration levels inside the building but also its effect on the frequency content of the building vibrations. They studied a phenomenon that they refer to as EFRBM: eigenfrequency of rigid body motion. This is the frequency at which the building moves up and down as a whole. This frequency depends on two elements: the mass of the building and the stiffness of the soil. If the mass of the structure stays the same, a soft soil will result in lower eigenfrequencies and stiffer soils will yield higher values. In the study, a model was created that includes the source, the propagation path and a building structure of four floors on a shallow foundation. Both the columns and the floors are made out of concrete.

As expected, the attenuation of the waves created by the train over the distance is the highest for the stiff soil ($V_s = 400$ m/s), which results in lower vibration levels at the building foundation. Interestingly, it was found that when the eigenfrequency of rigid body motion is below the natural frequency of the floors, the soil acts as a damper, lowering the transmission of vibrations throughout the building: the energy in the building can dissipate through the damping of the soil [22]. When the eigenfrequency of rigid body motion is equal to or above the natural frequency of the floors, this dampening effect does not occur, increasing the transmission of vibrations from the foundation into the building. All the vibrations that reach the foundation are intensified instead. The calculated eigenfrequencies of rigid body motion for the building in this study were 24-31 Hz for the stiff soil ($V_s = 400$ m/s), 16-20 Hz for the medium stiff soil ($V_s = 200$ m/s) and 8-10 Hz for the soft soil ($V_s = 100$ m/s). The natural frequency of the floors was between 14-16 Hz. Consequently, the dampening effect of the soil only occurred for the softest soil. Therefore, the vibration levels in the building turned out to be of similar magnitude for the medium stiff soil as for the soft soil, even though the vibrations that reached the building were lower for the medium stiff soil due to the attenuation in the propagation path. In Figure 2.16 the transfer ratios of the vibration levels at the foundation level to the fourth floor of the building are shown, which are calculated based on the data presented in the paper. Although the transfer ratio is the highest for the stiffest soil, the vibrations that reach the foundation are also substantially lower due to this higher

[1] $ratio = 10^{\frac{dB}{20}}$

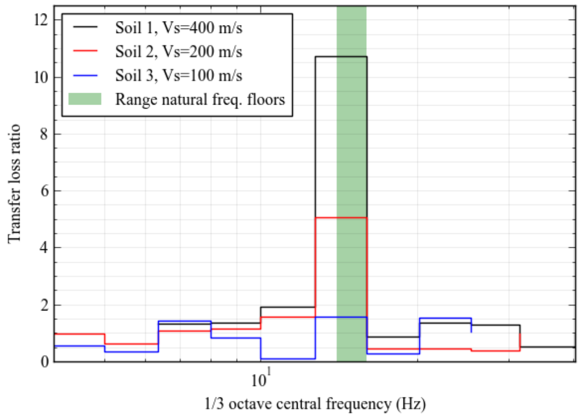

Figure 2.16: Ratio of transmission loss of vibration levels at the foundation for buildings on different types of soil, calculated from [72]

soil stiffness. Therefore, the resulting vibrations in the building are still the lowest for this type of soil.

2.8.4. Quantification of kinematic and inertial effects

All the aforementioned effects of soil-structure interaction can be divided into two categories: kinematic interaction and inertial interaction. Kinematic interaction describes how the free-field vibrations in the soil are altered due to the presence of the building and its foundation. This effect is also referred to as the 'wave scattering' effect or 'wave passage' effect [65] and results in modified vibrations called the foundation input motion (FIM), as shown in Figure 2.17. Inertial interaction is how the building responds to this input motion and how the inertial forces that develop in the structure are transmitted to the soil [32]. It can be taken into account by calculating the stiffness and damping of a foundation and then applying these as springs and dampers to the dynamic system representing the building, as shown in Figure 2.17. This way, the inertial interaction effect can be accounted for analytically.

Taking into account the kinematic effect analytically is however less straightforward. Stewart et al. [55] provides transfer functions for the kinematic interaction of shallow foundations subjected to shear waves, but for the railway-induced vibrations for on-grade railway tracks considered in this research, surface waves are mostly governing. The same focus on shear waves applies to research into the kinematic effect of pile foundation [38], [43], [3]. Furthermore, studies often concentrate on the horizontal component of the waves, since this is the governing direction for seismic analyses.

2.8.5. Building response

After the vibrations have been transmitted through the ground and foundation, they eventually reach the building. Generally, the vibrations on the foundation are amplified over the building height for low frequencies and are the highest mid-span of the floors. High frequencies are generally attenuated. The earlier mentioned study into a four-storey concrete building by Huang et al. [25] also looked into the transmission from the foundation to the top floors of the buildings. The results are translated to an amplification ratio and shown in Figure 2.18. Most of the literature related to railway-induced vibrations focuses on concrete buildings. Generally, two peaks can be distinguished in the building response: one that relates to the EFRBM, also referred to as soil-building resonance frequency and a peak that corresponds to the natural frequency of the floors [34].

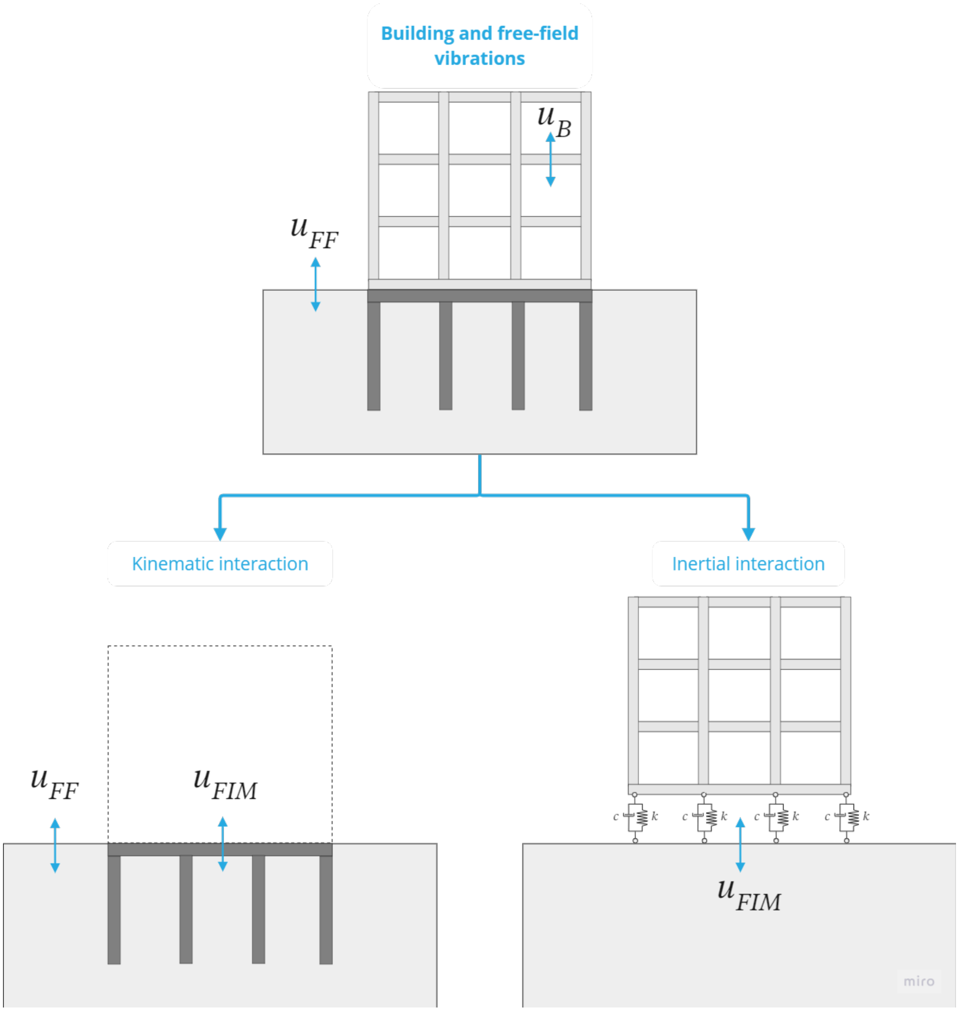

Figure 2.17: From free-field (u_{FF}) ground motion to foundation input motion (u_{FIM}) and building response (u_B), with kinematic and inertial effects

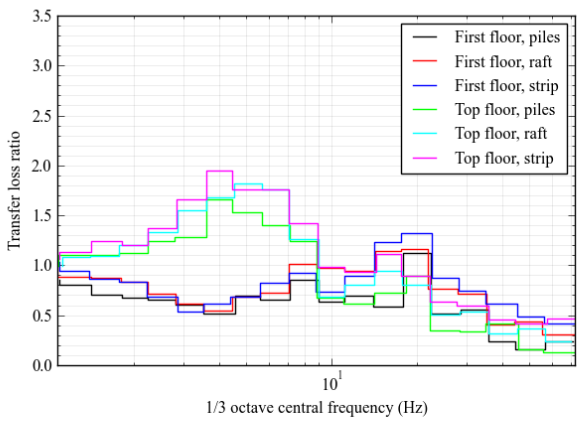

(a) Ratio at the columns

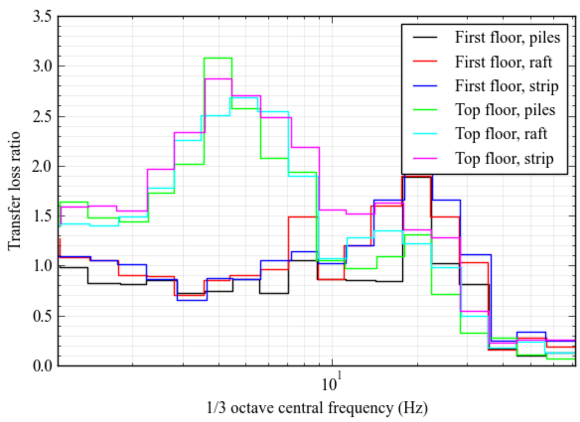

(b) Ratio mid-span of the floors

Figure 2.18: Ratio of transmission loss of free-field vibrations for buildings with different foundations in the building, calculated from [25]

3

Timber Multi-Storey buildings

3.1. Introduction

In the last years, timber construction has proven to be a viable option for the design of mid-rise structures, especially when focusing on the reduction of the environmental footprint [23]. There has been much focus on the serviceability criteria of timber buildings and the influence of walking-induced vibrations on different timber structures and connections ([73], [67]), to solve acoustic and vibrational problems that can occur due to human-induced excitation. There is a wide variety of building systems and floor- and wall configurations available nowadays that can be used in the construction of timber multi-storey apartment buildings. The goal of this chapter is to outline the commonly used components and systems and to narrow this selection down to those that could be used for the structural application in timber apartment buildings subjected to railway-induced vibrations.

3.2. Manufactured wood products

When wood was solely used as solid wood, its dimensions were constrained by the height and size of the tree it was taken from. These days, many engineered wood products have been developed that make it possible to use the beneficial properties of the wood while also making it possible for use when larger dimensions are required. For structural applications, especially glued laminated timber (GLT), cross-laminated timber (CLT) and laminated veneer lumber (LVL) have given a boost to the use of timber in the construction industry.

Glued laminated timber

Glued laminated timber (glulam, GLT) is a product made up of multiple shorter timber boards. The thickness of the individual timber boards is often between 30 and 50 mm. Defects in the timber boards such as knots can be reduced before glueing them together with the use of finger joint connections to create one long board. Then, the finger-jointed board is cut into individual lamellae, after which they are planed and glued together to create a glulam beam of the necessary dimensions [20]. This concept is illustrated in Figure 3.1. Due to its properties, GLT is often used for beam and column elements [28]. The material properties for GLT of strength class GL24h used in this research are shown in Table 3.1.

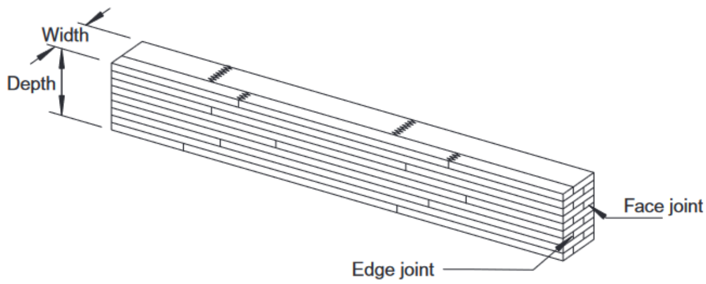

Figure 3.1: Glulam member with finger joints [41]

Table 3.1: Material properties C24 for CLT cross sections

Property	Symbol	GL24	Unit
Bending strength	$f_{m,g,k}$	24	N/mm^2
Tensile strength	$f_{t,0,g,k}$	14	N/mm^2
	$f_{t,90,g,k}$	0.12	N/mm^2
Compression strength	$f_{c,0,g,k}$	21	N/mm^2
	$f_{c,90,g,k}$	2.5	N/mm^2
Shear strength	$f_{v,g,k}$	4	N/mm^2
Rolling shear strength	$f_{r,g,k}$	1.25	N/mm^2
Shear modulus	$G_{g,mean}$	690	N/mm^2
Modulus of elasticity	$E_{0,g,mean}$	12000	N/mm^2
Rolling shear modulus	$G_{r,g,mean}$	50	N/mm^2
Density	$\rho_{g,mean}$	420	kg/m^3

Cross laminated timber

Cross-laminated timber (CLT) is a solid wood-engineered panel product that is made by stacking and glueing together layers of wooden boards referred to as lamellae. The lamellae are orthogonally layered: in each layer, the boards are placed side by side and each lamella is then placed under a 90-degree angle with respect to the adjacent lamellae and connected with an adhesive [41]. Similar to GLT, the number of knots and other defects can be reduced during the production process of the lamellae. Furthermore, the number of lamellae can be customised to achieve different structural requirements. CLT is often used for both floors and walls due to its properties in both transverse and longitudinal directions. An example of a CLT slab is shown in Figure 3.2 and the material properties of the strength class used in this research are shown in Table 3.2.

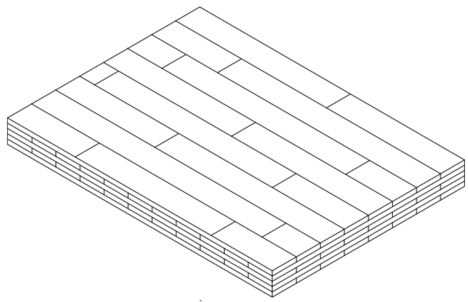

Figure 3.2: Structural floor: cross-laminated timber [28]

Table 3.2: Material properties C24 for CLT cross sections

Property	Symbol	C24	Unit
Bending strength	$f_{m,g,k}$	24	N/mm^2
Tensile strength	$f_{t,0,g,k}$	14.5	N/mm^2
	$f_{t,90,g,k}$	0.4	N/mm^2
Compression strength	$f_{c,0,g,k}$	21	N/mm^2
	$f_{c,90,g,k}$	2.5	N/mm^2
Shear strength	$f_{v,g,k}$	4	N/mm^2
Shear modulus	$G_{g,mean}$	690	N/mm^2
Modulus of elasticity	$E_{0,g,mean}$	11000	N/mm^2
Rolling shear modulus	$G_{r,g,mean}$	50	N/mm^2
Density	$\rho_{g,mean}$	420	kg/m^3

Laminated veneer lumber

Whereas both CLT and GLT are produced from lamellae, LVL is produced from very thin sheets of wood. These sheets are obtained by a peeling process, after which they can be layered to create for example a beam member or a plate by using a resin to glue the individual components together. Generally, the fibres are positioned in the longitudinal direction of the member, with deviations up to 25 % perpendicular to this main direction [10].

Table 3.3: Material properties LVL 32S and LVL 50S

Property	Symbol	LVL 32S	LVL 50S	Unit
Bending strength	$f_{m,0,edge,k}$	27	44	N/mm^2
	$f_{m,0,flat,k}$	32	50	N/mm^2
Tensile strength	$f_{t,0,k}$	24	35	N/mm^2
	$f_{t,90,edge,k}$	0.5	0.8	N/mm^2
Compression strength	$f_{c,0,k}$	26	35	N/mm^2
	$f_{c,90,edge,k}$	4	6	N/mm^2
	$f_{c,90,flat,k}$	1	1.8	N/mm^2
Shear strength	$f_{v,0,edge,k}$	2.4	4.1	N/mm^2
	$f_{v,0,flat,k}$	1.3	2.3	N/mm^2
Shear modulus	$G_{0,edge,mean}$	400	500	N/mm^2
	$G_{0,flat,mean}$	400	500	N/mm^2
Modulus of elasticity	$E_{0,mean}$	10000	13800	N/mm^2
Density	ρ_{mean}	440	510	kg/m^3

Rib floors

Besides the solid wood CLT, GLT and LVL elements, rib floors can be used in cases where large spans or a high load-bearing capacity is needed. These types of floors consist of flat wood panels, with supporting ribs in between, connected together with structural adhesives. The wood panels are often made from CLT, GLT or LVL panels, whereas for the ribs either GLT or LVL is common, making use of the high bending strength of these materials. The floors are either fully closed, as shown in Figure 3.3a and referred to as hollow box floors, fully open, or partially open, as shown in Figure 3.3b.

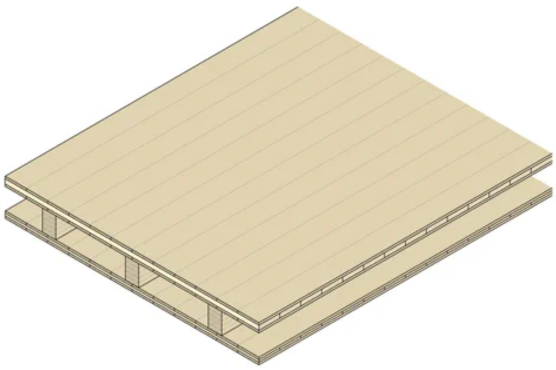

(a) Hollow box rib floor, CLT and GLT

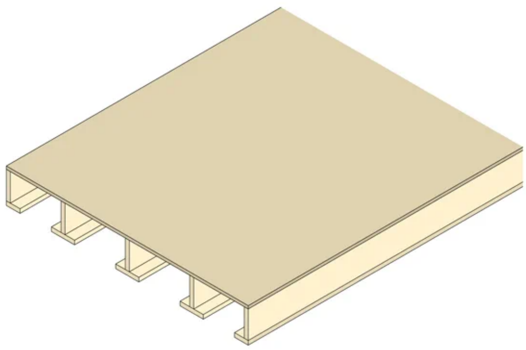

(b) Partially open rib floor, LVL

Figure 3.3: Types of rib floors [56]

3.3. Timber building systems

There are many ways to build a timber apartment building. Different load-bearing systems exist, each with its own benefits and disadvantages. Kolb [30] divides the building systems into two categories:

- Linear-supported structures,
- Point-supported structures.

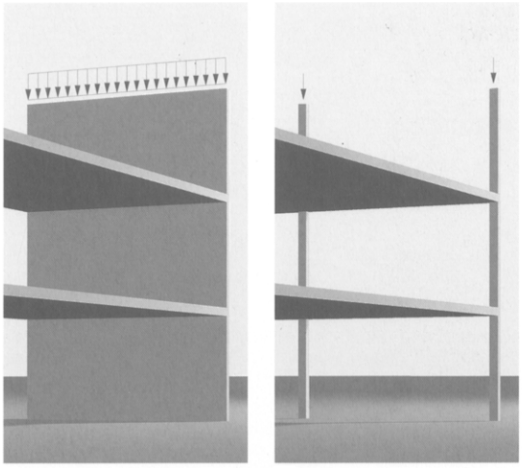

Figure 3.4: Linear-supported timber system (left) and point-supported timber system (right) [30]

Linear-supported structures are systems in which the loads are distributed along linear elements. In this system, elements such as walls transfer the loads that act on the floors to the foundation of the structure. This distribution of forces can be advantageous because it reduces the reaction forces on the components. Besides that, in some cases, the linear elements can function as part of the building envelope and as a bracing structure simultaneously. Contrarily, in **Point-supported systems** such as the post-and-beam system, the loads are concentrated into the columns and beams that the system is comprised of. An advantage of this system is that the load paths are clearly visible. On the downside, to enable the transference of loads between the beams and columns sometimes additional measures are needed due to these high load concentrations that occur there. In Figure 3.4 these two systems are illustrated.

3.3.1. Solid timber structure

An example of a linear-supported structure is the Via Cenni complex in Milan, Italy. It is a social housing apartment building located in one of Italy's seismic zones. This building's load-bearing system is linear-supported and consists of CLT wall and floor elements, combined with CLT cores around the stairs and elevator shaft. Since the vertical load-bearing elements are solid walls, they also determine the layout of the building, which is often cellular for that reason [23]. The project is shown in Figure 3.5.

Figure 3.5: Via Cenni residential complex, Italy [28]

One of the advantages of a solid timber panel system is that openings for walls and windows can already be included during the prefabrication process, making quick on-site assembly of the building possible [30].

3.3.2. Post- and beam structure

An example of a post-and-beam timber building is the Wood Innovation and Design centre (WIDC). It is made up out of GLT columns and beams for the load-bearing structure of the building. Both the floor panels and the walls are made from CLT. The building has a CLT core in which the elevator and staircase are located, providing lateral stability. Because the floor is made solely out of timber and no concrete layover was used, additional measures such as an acoustically insulated subfloor system had to be taken to comply with the building codes. The building steps of this building are demonstrated in Figure 3.6. This figure shows that the facades are placed in front of the load-bearing structure so that it is completely protected against the weather whilst creating an airtight structure (Kolb 2008).

The advantage of this structure is that relatively large spans can be achieved and that there is more flexibility in the design of the interior layout. Lateral stability can sometimes be an issue, in which case bracing or shear walls are applied, which was not necessary in this case [23].

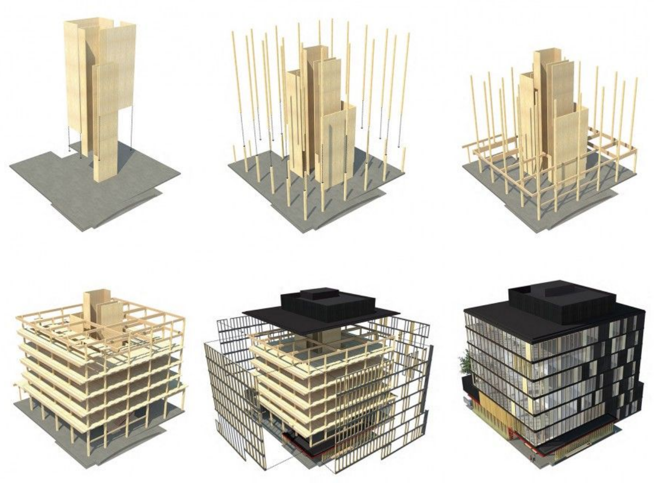

Figure 3.6: The wood innovation and design centre in Canada [23]

3.4. Floor systems

Based on the wood-engineered products introduced in section 3.2 and the building systems discussed in section 3.3, two different floor systems can be considered for the structural application in timber apartment buildings subjected to railway-induced vibrations: hollow box floors and CLT floors.

A timber floor system generally consists of multiple layers to be able to provide sound insulation properties and fire resistance. The layers can be subdivided into three parts: the structural floor, the floor finish and the ceiling structure. The structural floor is the part of the floor system that has a load-bearing function, in this case the hollow box or the CLT floor. In terms of floor finishes, either wet or dry screed is often applied [30]. Since the floor finish influences the mass of the floor and thus influences its dynamic behaviour, different finishes for each structural floor system are considered. The floor configurations that will be used in this research and their corresponding properties that will be used for the design of the timber floors are summarized in Table 3.4 and Table 3.4. For all floor types, gypsum plasterboard is used for the ceiling. It is assumed that this is sufficient to comply with the fire safety of the structure.

Table 3.4: Floor systems for CLT slabs and LVL hollow box floors

CLT slab					
Wet screed			**Dry screed**		
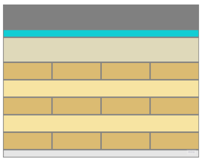			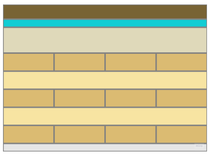		
Layer	*mm*	kg/m^2	*Layer*	*mm*	kg/m^2
Cement screed	70	175	Plasterboard	12.5	10
Sound insulation	30	2	Underlayment (OSB)	25	20
Fill, sand	50	75	Sound insulation	30	2
Cross laminated timber	variable	variable	Cross laminated timber	variable	variable
Plasterboard	12.5	10	Plasterboard	12.5	10
Total finishes	**162.5**	**262**	**Total finishes**	**80**	**42**
Hollow box floor					
Wet screed, without infill			**Dry screed, with fill**		
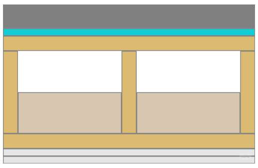			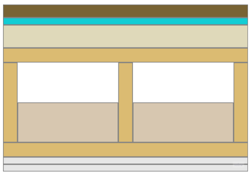		
Layer	*mm*	$kg/m2$	*Layer*	*mm*	$kg/m2$
Cement screed	70	175	Underlayment (OSB)	25	20
Sound insulation	30	2	Sound insulation	30	2
LVL-X	variable	variable	Fill, sand	50	75
Mineral wool	100	2	LVL-X	variable	variable
LVL-S I-joist	variable	variable	Mineral wool	100	2
LVL-X	variable	variable	LVL-S I-joist	variable	variable
Plasterboard	25	20	LVL-X	variable	variable
			Plasterboard	25	20
Total finishes	**125**	**199**	**Total finishes**	**155**	**119**

Damping ratio's

An important aspect of any structure subjected to vibrations is the damping ratio. This ratio causes the imposed vibrations to reduce over time and eventually come to a halt. The higher the damping ratio, the quicker the vibrations are dissipated. However, many different sources influence the total damping ratio of a building, which makes estimating the damping ratio of entire structures difficult. Furthermore, it is hard to measure the amount of energy that is being dissipated by the structure. Luckily, for individual components, such as floors, research has been carried out that aims to determine their damping ratio [26]. Therefore, in this research, it is chosen to use the values that are proposed for the revised Eurocode 5 [45], which are presented in Table 3.5. These values are in agreeance with the damping factors found by Abeysekera et al. [1].

Table 3.5: Damping ratio ξ for different timber floors [45]

	ξ without floating floor	ξ with floating floor
Timber joisted floors	0.02	0.03
Timber-concrete floors, rib-type floors and slab type floors	0.25	0.04

3.5. Connections

For the connection between the load-bearing walls and the floors, there are essentially two different methods that can be considered: the suspended floor structure and the supported floor structure [28]. With the suspended floor structure, as the name suggests, the floor is hung between two load-bearing walls. This principle is shown in Figure 3.7a. The advantage of this method is that there are no large vertical loads imposed on the timber floor structure perpendicular to the grain. Loads perpendicular to the grain can pose challenges in the structural design of the floors, since the mechanically properties of timber are substantially lower in this direction [10]. A downside of this connection is that for high vertical loads, it may be difficult to find transmission strips that have sufficient load-bearing capacity. This can for example be the case in tall buildings. Also, an additional bending moment is imposed on the walls due to the eccentricity created with this connection. With the second connection method, the supported floor structure, the floors are clamped between the walls of two subsequent storeys, as shown in Figure 3.7b. This connection is easier to construct and also avoids that the loads from the floors are imposed eccentrically. However, the disadvantage of this connection is that the placement of the wall on top of the floor results in high vertical loads perpendicular to the grain. Therefore, flanking transmission strips are placed between the floors and the walls, to account for this pressure [59].

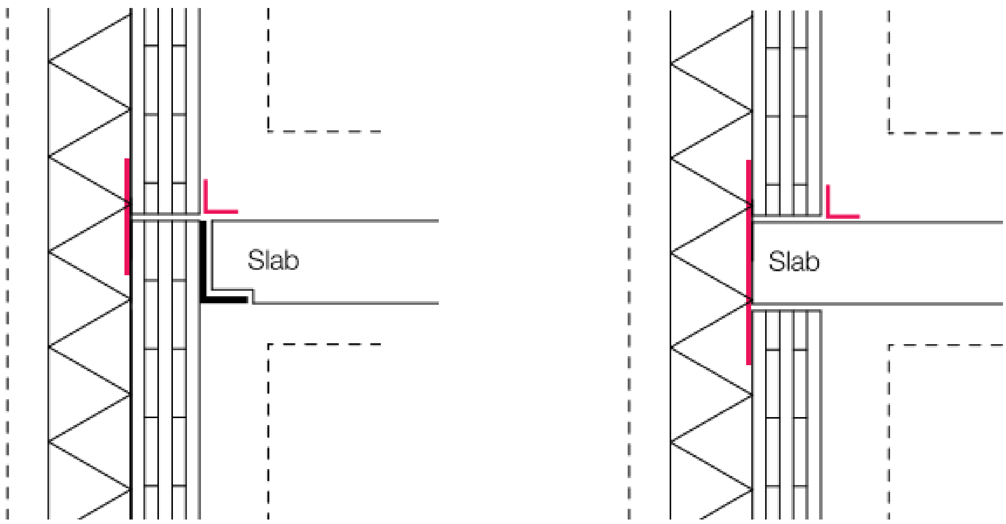

(a) Suspended floor **(b)** Supported floor

Figure 3.7: Types of connections [28]

4 Structural dynamics

4.1. Introduction

To investigate the building response to railway-induced vibrations, this chapter will focus on the structural dynamics theory behind the transfer matrix model that is used. First, general dynamics concepts are briefly outlined, after which the focus will shift to the framework for the transfer function method discussed in chapter 2. The corresponding matrices for a shallow and pile foundation, walls and columns, and floors are derived and elaborated on. Lastly, the boundary conditions needed to calculate the building response are presented. The dynamic formulations in this chapter are then implemented in a Python script that is used to analyse the buildings from the case studies in chapter 5, the parameter study in chapter 6 and the comparison of concrete and timber apartment buildings in chapter 7.

4.2. Single degree of freedom system

Buildings are complicated systems with many degrees of freedom, but to analyse the response of smaller parts of the structure, a single-degree-of-freedom (SDOF) system can be used. The response of this system subjected to an external force can be described by its displacement u, velocity $\dot{u}$ and its acceleration $\ddot{u}$ as shown in Figure 4.1.

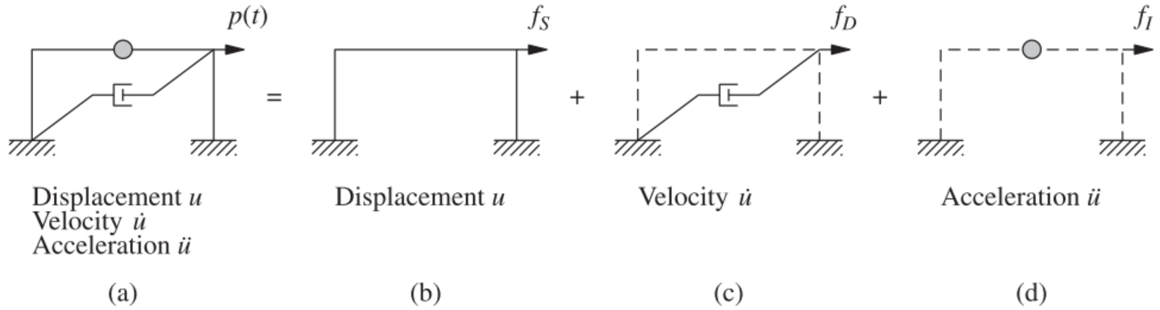

Figure 4.1: (a) System; (b) stiffness component; (c) damping component; (d) mass component from [13]

The stiffness component of the system k results in the elastic resisting force f_S, which is related to the displacement u of the system, whereas the damping component c of the structure is related to its velocity $\dot{u}$ resulting in the damping resisting force f_D. Lastly, the inertia force resulting from the mass component m is associated with the acceleration $\ddot{u}$, resulting in f_I. In order for the system to be in equilibrium, the externally applied force $p(t)$ has to be equal to the sum of these resisting forces. This results in Equation 4.1.

$$p(t) = f_I + f_S + f_D \tag{4.1}$$

Substituting the components and their relationship to the displacement, velocity and acceleration results in the well-known equation of motion (EOM) in Equation 4.2.

$$m\ddot{u} + c\dot{u} + ku = p(t) \tag{4.2}$$

However, in the case of railway-induced vibrations, the force is applied to the base of the structure and is described by a displacement of the ground as illustrated in Figure 4.2. Both vertical and horizontal vibrations have to be considered, but both systems are identical in terms of their equation of motion. The absolute displacement of the mass $u_t(t)$ is now the summation of the displacement of the system itself $u(t)$ and the displacement of the ground $u_g(t)$. The relation between these displacements is shown in Equation 4.3.

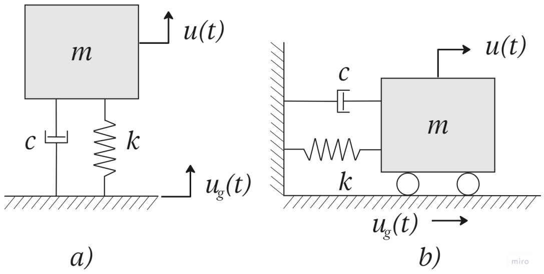

Figure 4.2: a) generalised SDOF vertical vibrations and b) horizontal vibrations

$$u_t(t) = u_g(t) + u(t) \tag{4.3}$$

Since the elastic forces and damping forces are only caused by the relative displacement of the system, f_S and f_D of equation Equation 4.1 do not change. The inertia force is however related to the absolute acceleration, and by substituting Equation 4.3 thus becomes:

$$f_I = m\ddot{u}_t = m\ddot{u} + m\ddot{u}_g \tag{4.4}$$

Substituting this relation into Equation 4.1 together with the unchanged elastic and damping resisting forces results in the equation of motion as shown in Equation 4.5.

$$m\ddot{u} + c\dot{u} + ku = -m\ddot{u}_g = p_{eff}(t) \tag{4.5}$$

4.3. Frequency and time domain

Vibrations are oscillating motions, which can be described by their amplitude and frequency. The higher the amplitude, the higher the strength of the vibrations. Vibrations related to earthquakes and structural damage for example have substantially higher amplitudes than vibrations related to traffic-induced vibrations. Besides their amplitude, vibrations are described by their frequency. When expressing the frequency in Hertz (Hz), this is the number of times an oscillation occurs in one second. Every element has their own natural frequency: if the element is excited by a force with the same frequency, it will start to vibrate with increasing amplitudes. This phenomenon is called resonance. This effect can cause the element to deflect much more than if the deflection had been caused by a static force of the same magnitude [12]. To minimise vibrations in structures, it is therefore the goal to avoid resonance from occurring.

To predict the response of a structure, there are two different approaches: the time domain method and the frequency domain method [68]. Both methods are related to each other, but represent the vibrations the system is subjected to and its response differently. Where the time domain approach shows the vibrations as a function of time, the frequency domain method represents time series in terms of their frequency content. The relationship between these two methods is shown in Figure 4.3. The graph that represents the vibrations in the frequency domain is also referred to as the spectrum. The advantage of considering vibrations in the frequency domain is that it can easily be seen which frequencies have the highest energy content. This is important, because when the strongest frequency of the railway-induced

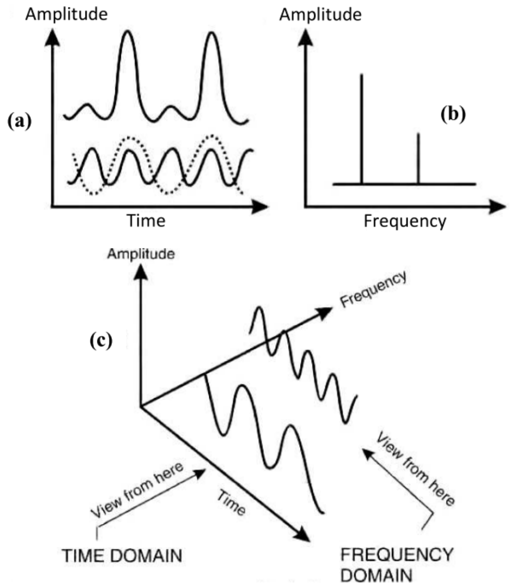

Figure 4.3: Relationship between frequency and time domain, with a) time domain, b) frequency domain, and c) the relationship between the frequencies, amplitudes and time, from [48]

vibrations coincides with the natural frequency of the structure or structural components, they will amplify each other, resulting in high resonance.

4.4. Dynamic building response

As described in chapter 2, one of the ways to study the effect of imposed vibrations on a structure is to use transfer matrices. Generally speaking, transfer matrices translate an input, such as free-field measurements, to an output, in this case the building response. This principle is illustrated in Figure 4.4.

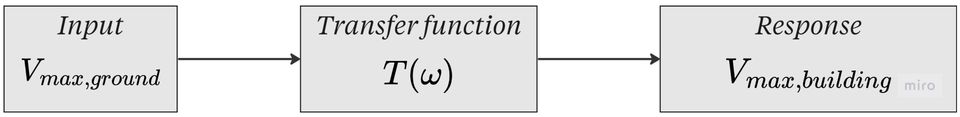

Figure 4.4: Principle of transfer functions

Now, delving into the specifics: a simple building in proximity to a railway is considered, for which the building response to the railway-induced vibrations has to be calculated. An example building is illustrated in Figure 4.5. First, the vibrations travel through the soil, until they reach the foundation of the building. Here, they are influenced by the foundation of the building, through which they reach the ground floor of the building. The vibrations are considered to be axially propagating waves, because as explained in chapter 2, vertical vibrations are considered governing for railway-induced vibrations. The waves propagate axially through the load-bearing structure and cause vertical displacements at the connection of the walls with the floor elements. At this connection, they also radiate out into the floors as transverse bending waves [76].

To be able to calculate the response of the building to the railway-induced vibrations with the transfer function method, the building is simplified into a 1D structure. Because it is assumed that the excitation of the foundation is uniform, a representative section of the building can be taken to calculate the attenuation or amplification of the imposed vibrations. In Figure 4.5 two different building sections are highlighted. Then, for each building element in each section, transfer matrices can be found that translate the ground-borne vibrations to vibrations in the foundation, floors, and walls or columns. The foundation can be simplified to one spring and damper element per section. Next, the walls or columns can be simplified as rods, taking into account the area of the load-bearing walls or columns in the investigated section. The same can be done for the floors, although in a slightly more complex way. The eigenfrequency of each floor is taken into account, using the entire floor span of that specific floor. For the two highlighted sections in Figure 4.5, the span is the same. The difference between the two highlighted sections is however the participating portion of the floor, which is factored into the calculation of the floor mass.

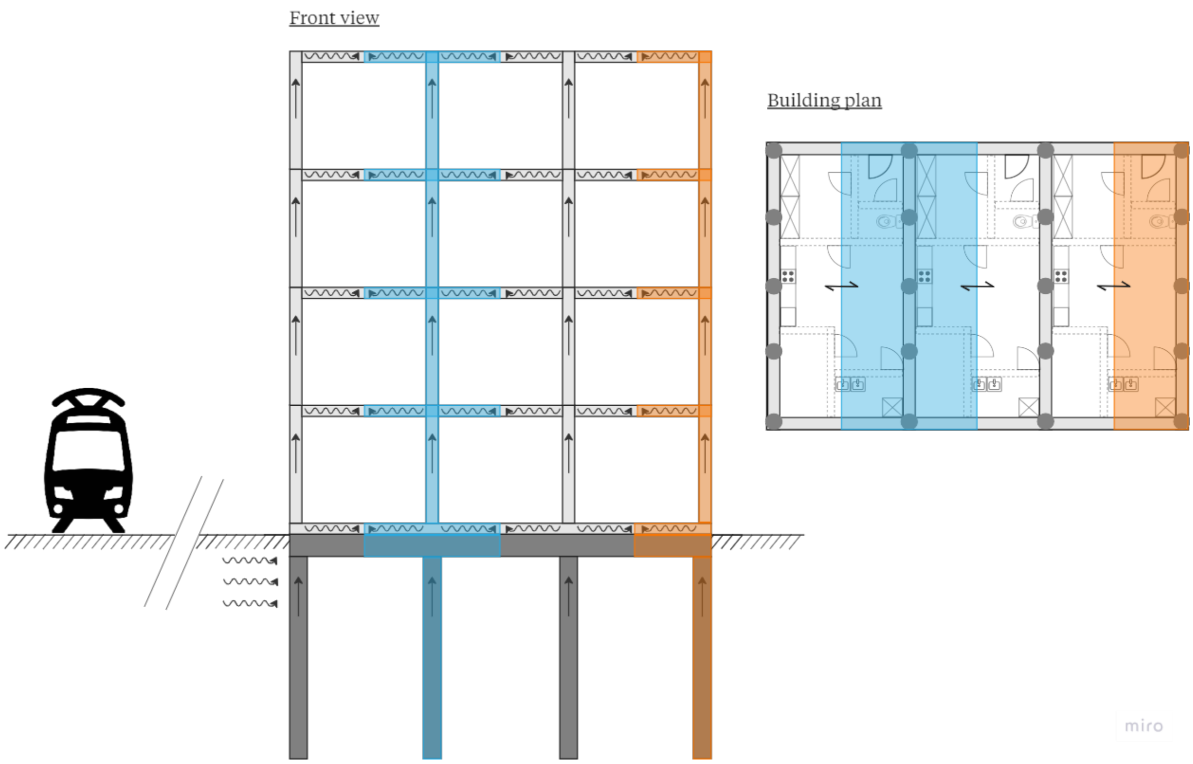

Figure 4.5: Theoretical building structure subjected to railway-induced vibrations

4.4.1. Soil-structure interaction

As explained in chapter 2, an important factor to consider when assessing the response of the building is the effect of the Soil-Structure Interaction (SSI). There are multiple ways to take into account soil-structure interaction, but the more extensive methods often have high computational costs and need large amounts of data. There will still be many uncertainties, because determining the soil profile and corresponding properties is complex. There are also more simplified models, which can still capture the most important features of the principle of soil-structure interaction [70]. Although soil-structure interaction consists of both kinematic and inertial interaction, as described in chapter 2, only the inertial interaction is considered for the transfer function model. The main reason is that the kinematic interaction is not influenced by the building itself: it focusses on how the foundation influences incoming waves without the building being present, as shown in Figure 2.17. Inertial interaction, which describes the building response to this input motion and the reaction of the soil and foundation, is dependent on the building parameters. Therefore, this section focusses on how to take this into account in the transfer function model. For the vertical vibrations considered in this research, the simplified model combines the foundation characteristics with the soil parameters, allowing the combined system to be modelled as a spring and damper element as shown in Figure 4.6. This method is widely used [74] and simplifies the soil-structure problem significantly.

The equations corresponding to the spring and dashpot system shown in Figure 4.6 can easily be derived:

$$\begin{aligned} p_1 &= k(u_1 - u_2) + c(\dot{u}_1 - \dot{u}_2) \\ p_2 &= -p_1 \end{aligned} \tag{4.6}$$

By assuming harmonic excitation of the system, the external force p can be written as follows:

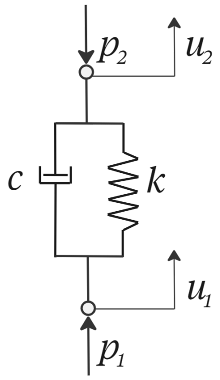

Figure 4.6: Spring- damper element to take into account soil-structure interaction

$$p = P\exp\{i\omega t\} \tag{4.7}$$

The displacement response is then assumed to be of the same form:

$$\begin{aligned} u &= U\exp\{i\omega t\} \\ \dot{u} &= i\omega U\exp\{i\omega t\} \end{aligned} \tag{4.8}$$

By substituting Equation 4.7 and Equation 4.8 in Equation 4.6 and dividing by $\exp\{i\omega t\}$, the equations can be written in matrix form:

$$\begin{bmatrix} P_1 \\ P_2 \end{bmatrix} = \begin{bmatrix} k + i\omega c & -(k+i\omega c) \\ -(k+i\omega c) & k + i\omega c \end{bmatrix} \begin{bmatrix} U_1 \\ U_2 \end{bmatrix} \tag{4.9}$$

This matrix equation can also be written in a transfer matrix form, using the same relations described in Equation 4.22, which results in the matrix T_S used by Auersch [6]:

$$\begin{bmatrix} U_2 \\ P_2 \end{bmatrix} = \begin{bmatrix} 1 & \frac{1}{k+i\omega c} \\ 0 & 1 \end{bmatrix} \begin{bmatrix} U_1 \\ P_1 \end{bmatrix} \tag{4.10}$$

The parameters k and c, respectively the stiffness and damping of the system, are determined by the type of foundation and the soil parameters. In types of foundations, two distinctions will be made: a shallow foundation and pile foundation will be considered.

Shallow foundation

For a shallow foundation as shown in Figure 4.7, the spring constant k and the damping factor c for vertical vibrations can be chosen as follows [51]:

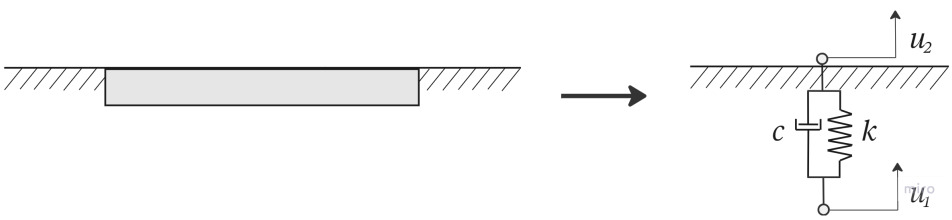

Figure 4.7: Representation of a shallow foundation with spring and damper

$$\begin{aligned} k &= \frac{4G_s\sqrt{\frac{A_s}{\pi}}}{1-\nu} \\ c &= \frac{3.4}{1-\nu}\frac{A_s}{\pi}\sqrt{\rho_s G_s} \end{aligned} \tag{4.11}$$

Poisson's ratio ν is taken as 0.33, that results in the approximation of $k \approx 3.4 \cdot G_s \sqrt{A_s}$ and the damping by $c \approx 1.6\sqrt{G_s \rho_s} A_s = 1.6 \rho_s \nu_s A_s$ as used by Auersch [5]. A_s represents the foundation area, G_s the shear modulus of the soil, ρ_s the mass density and ν_S the shear wave velocity of the soil, which is equal to $\nu_s = \sqrt{\frac{G_s}{\rho_s}}$.

Pile foundation

When considering a pile foundation instead of a shallow foundation, again the surrounding soil and the piles can also be represented by springs and dampers as shown in Figure 4.8.

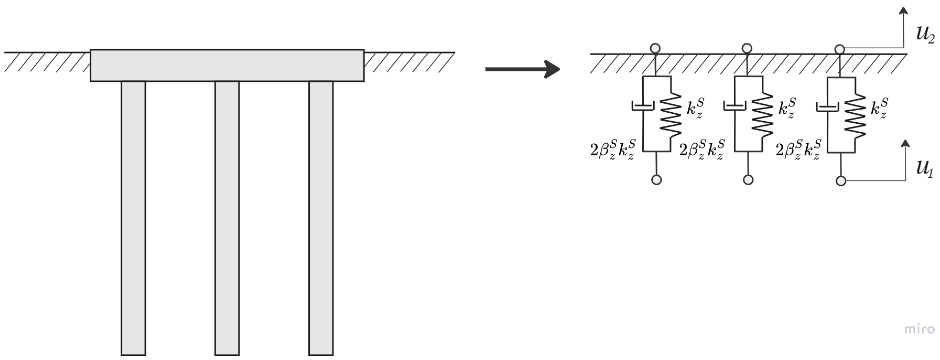

Figure 4.8: Representation of the individual piles of a pile foundation with springs and dampers

For a single pile, the vertical dynamic stiffness k_z^S can be calculated by taking into account its static stiffness, K_z^S, and α_z^S, a dynamic modifier factor. This results in Equation 4.12 [55].

$$k_z^S = K_z^S \cdot \alpha_z^S \tag{4.12}$$

The static stiffness K_z^S can be calculated with the help of formulas that take into account both the pile and the soil stiffness. The damping ratio β_z^S can also be calculated. These equations can be found in Appendix A. The soil in this model is assumed to be homogeneous. Alternatively, Equation 4.13 can be written as:

$$\begin{bmatrix} U_2 \\ P_2 \end{bmatrix} = \begin{bmatrix} 1 & \frac{1}{k_z^S(1+2i\beta_z^S)} \\ 0 & 1 \end{bmatrix} \begin{bmatrix} U_1 \\ P_1 \end{bmatrix} \tag{4.13}$$

However, a pile foundation for a building structure is rarely composed of just one pile. The problem with pile foundations is that it is not possible to simply use superposition to calculate the dynamic stiffness and damping of the entire group of piles. For the dynamic building response, one value for the stiffness and damping of the foundation is necessary. Luckily, it is possible to calculate the group stiffness k_z^G and damping β_z^G as illustrated in Figure 4.9 using interaction factors [17]. This interaction factor method has been shown to agree well with the more rigorous dynamic methods [29].

If a pile foundation is excited, the piles undergo oscillations, creating circular wavefronts as shown in Figure 4.10a. These waves are assumed to propagate away from the piles horizontally, over the length of the pile (Figure 4.10a). As the waves propagate away from the active piles, they reach nearby piles, which are then influenced by these waves. With the interaction factors as presented by Dobry and Gazetas [17], the influence of all the piles in the pile group can be calculated, to find one dynamic stiffness and damping factor.

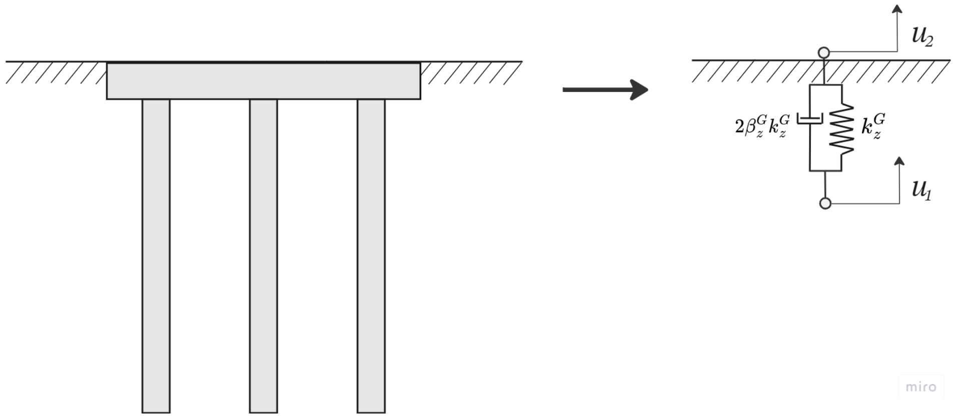

Figure 4.9: Representation of a pile group foundation with spring and damper

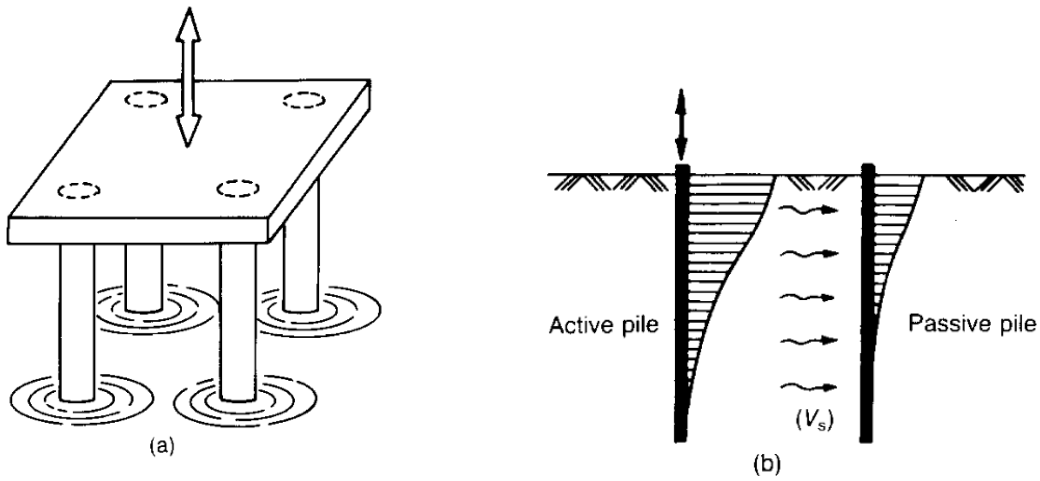

(a) Effect of spreading waves in a pile group **(b)** Effect of oscillations of active pile on passive pile

Figure 4.10: Visualisation of pile group effects from Dobry and Gazetas [17]

The interaction factors are highly dependent on the geometry of the pile group: whether it is a row of piles, a grid of piles or another geometry. In Appendix B, the equations for a two by two pile group and a three by three pile group are derived.

4.4.2. Column- and wall elements

The vertical railway-induced vibrations are primarily transmitted axially through the walls, as illustrated in Figure 4.11. The contribution of bending effects is deemed negligible, considering their comparatively smaller magnitude. Therefore, the columns and wall segments are idealised as finite rod elements as shown in Figure 4.12.
The governing differential equation needed to obtain the transfer matrix for such a rod element is as follows [35]:

$$EA\frac{\mathrm{d}^2U}{\mathrm{d}x^2} + \rho A\omega^2 U(x) = 0 \tag{4.14}$$

In Equation 4.14, E is the modulus of elasticity of the column or wall element, ρ denotes its mass density, A the cross-sectional area, ω the angular frequency and $U(x)$ represents the amplitude of the resulting vibrations. Furthermore, the differential equation for the longitudinal force acting on the element is as shown in Equation 4.15:

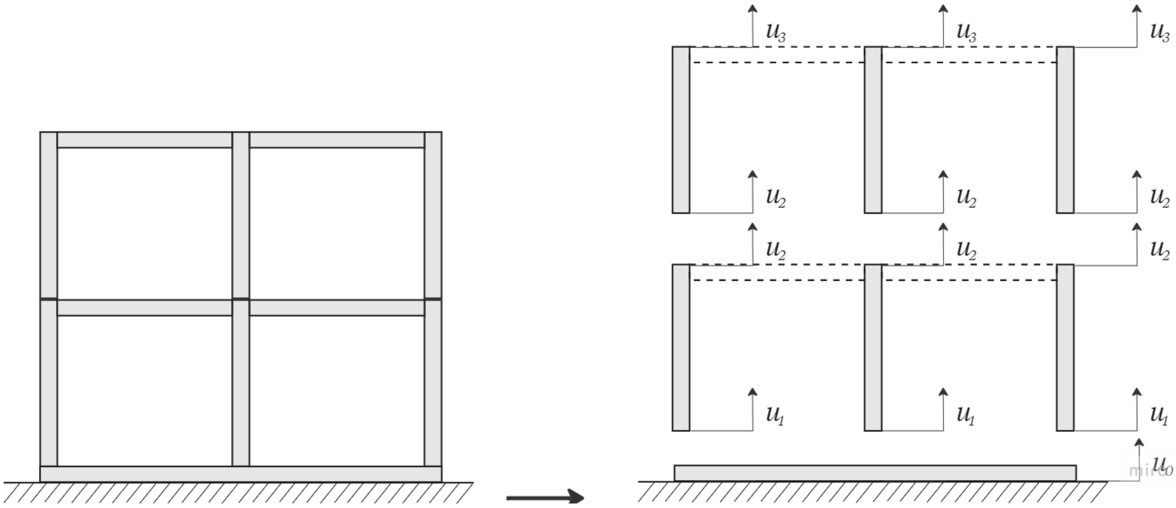

Figure 4.11: Displacements of walls or columns caused by vertical dynamic loads

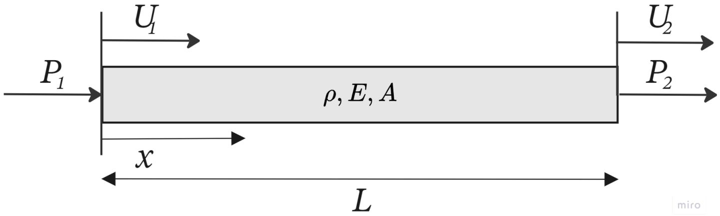

Figure 4.12: Rod element representing wall or column elements

$$P(x) = EA\frac{\mathrm{d}U}{\mathrm{d}x} \tag{4.15}$$

Equation 4.16 can be obtained as the solution for Equation 4.15, with constants $C1$ and $C2$ and $a = \sqrt{\frac{E}{\rho}}$:

$$U(x) = C_1 \cos\left(\frac{\omega}{a}x\right) + C_2 \sin\left(\frac{\omega}{a}x\right) \tag{4.16}$$

The boundary conditions for the rod element shown in Figure 4.12 can be defined as well. As can be seen, at $x = 0$, the displacement of the rod is equal to $U1$ and at $x = L$ the displacement is equal to $U2$. The same can be argued for the force $F(x)$, resulting in the following boundary conditions:

$$\begin{gathered} U(0) = U_1, U(L) = U2 \\ F(0) = -P_1, F(L) = P_2 \end{gathered} \tag{4.17}$$

Substituting Equation 4.17 into Equation 4.16 and Equation 4.15 results in two systems of equations, both written in terms of C_1 and C_2 with $\alpha = \frac{\omega L}{a}$:

$$\begin{bmatrix} U_1 \\ U_2 \end{bmatrix} = \begin{bmatrix} 1 & 0 \\ \cos\alpha & \sin\alpha \end{bmatrix} \begin{bmatrix} C_1 \\ C_2 \end{bmatrix} \tag{4.18}$$

$$\begin{bmatrix} P_1 \\ P_2 \end{bmatrix} = EA \begin{bmatrix} 0 & -\frac{\omega}{a} \\ -\frac{\omega}{a}\sin(\alpha) & \frac{\omega}{a}\cos(\alpha) \end{bmatrix} \begin{bmatrix} C_1 \\ C_2 \end{bmatrix} \tag{4.19}$$

$C1$ and $C2$ can be eliminated from Equation 4.18 and by rewriting and combining these equations, resulting in the following matrix equation:

$$\begin{bmatrix} P_1 \\ P_2 \end{bmatrix} = \frac{EA\alpha}{L} \begin{bmatrix} \cot(\alpha) & -\csc(\alpha) \\ -\csc(\alpha) & \cot(\alpha) \end{bmatrix} \begin{bmatrix} U_1 \\ U_2 \end{bmatrix} \tag{4.20}$$

Which is equal to $\mathbf{P} = \mathbf{KU}$. Because the problem is one-dimensional and the elements (soil and foundation, walls or columns and floors) are all connected end to end, it is useful to use the transfer matrix representation [19], which is also what is done by Auersch [6]. The general transfer matrix formulation is as follows:

$$\begin{bmatrix} U_2 \\ P_2 \end{bmatrix} = \begin{bmatrix} T_{11} & T_{12} \\ T_{21} & T_{22} \end{bmatrix} \begin{bmatrix} U_1 \\ P_1 \end{bmatrix} \tag{4.21}$$

Using the relations [19]:

$$\begin{aligned} T_{11} &= -K_{12}^{-1} K_{11} \\ T_{12} &= -K_{12}^{-1} \\ T_{21} &= K_{21} - K_{22} K_{12}^{-} 1 K_{11} \\ T_{22} &= -K_{22} K_{12}^{-1} \end{aligned} \tag{4.22}$$

Results in the transfer matrix T_W formulation for a rod:

$$\begin{bmatrix} U_2 \\ P_2 \end{bmatrix} = \begin{bmatrix} \cos(\alpha) & \frac{L \sin(\alpha)}{EA\alpha} \\ -\frac{\sin(\alpha) EA\alpha}{L} & \cos(\alpha) \end{bmatrix} \begin{bmatrix} U_1 \\ P_1 \end{bmatrix} \tag{4.23}$$

Equation 4.23 is equivalent to the transfer matrix used by Auersch [6]. In this equation, A is the area of the wall. In case columns are taken into account instead, A will be the total area of the columns considered instead.

4.4.3. Floor elements

Through the columns, the railway-induced vibrations are transmitted to the floors. At the point where the floors are connected to the walls, the displacement of the floor will be the same as the displacement of the supporting walls or columns. Over the relatively short height of the wall compared to the height of the walls or columns, the effect of extension is deemed negligible. The mass of the floor does however influence the force that is being transmitted. This principle is illustrated by first considering a rigid floor as shown in Figure 4.13.

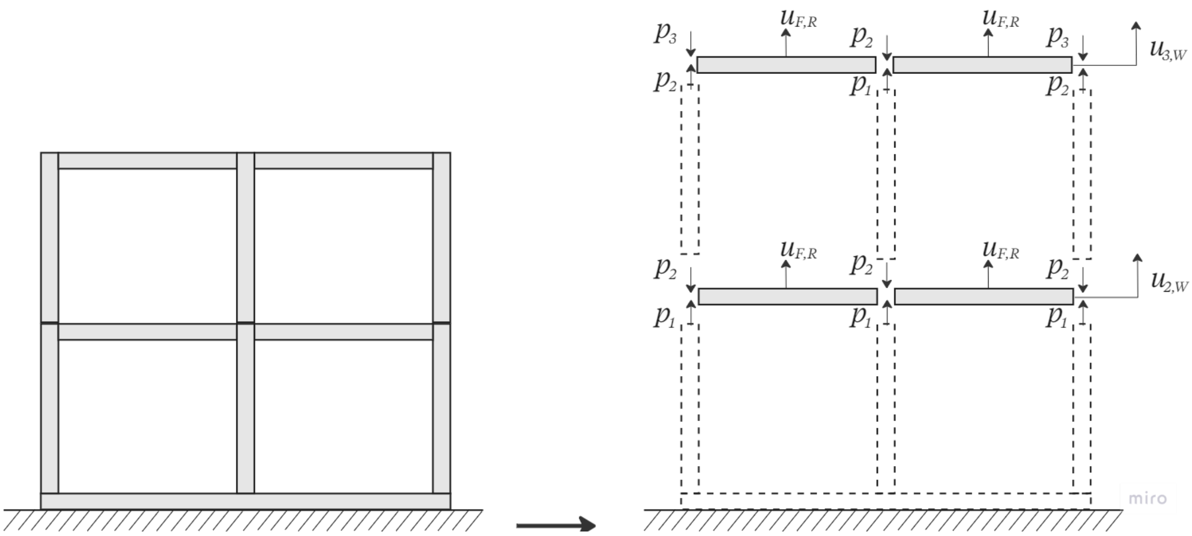

Figure 4.13: Displacements and force transfer of a rigid floor caused by vertical dynamic loads

If the floor is rigid, the effect of bending is not taken into account. Therefore it could be modelled as a simple lumped mass element as illustrated in Figure 4.14. Because any extension of the floor in vertical direction is deemed negligible, $u_1 = u_2$ and is equal to the displacement of the supporting walls or columns. The mass of the floor m_F does however create an inertial force equal to the mass times the acceleration, which has to be taken into account in the equilibrium of the forces. These two considerations result in the following two equations:

$$\begin{aligned} p2 - p1 &= m_F \ddot{u}_1 \\ u1 &= u2 \end{aligned} \tag{4.24}$$

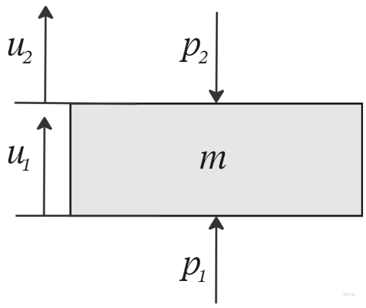

Figure 4.14: Lumped mass element representing rigid floor

By then assuming the same harmonic force excitation as in Equation 4.7, the displacement can be found:

$$\begin{aligned} u &= U \exp\{i\omega t\} \\ \ddot{u} &= -\omega^2 U \exp\{i\omega t\} \end{aligned} \tag{4.25}$$

Substituting Equation 4.25 in Equation 4.24, dividing by $\exp\{i\omega t\}$ and rearranging the terms, the transfer matrix T_F can again be found:

$$\begin{bmatrix} U_2 \\ P_2 \end{bmatrix} = \begin{bmatrix} 1 & 0 \\ -m_F\omega^2 & 1 \end{bmatrix} \begin{bmatrix} U_1 \\ P_1 \end{bmatrix} \tag{4.26}$$

However, floors are rarely fully rigid and the waves that propagate through the columns or walls also cause the floor to be subjected to bending, as shown in Figure 4.15.

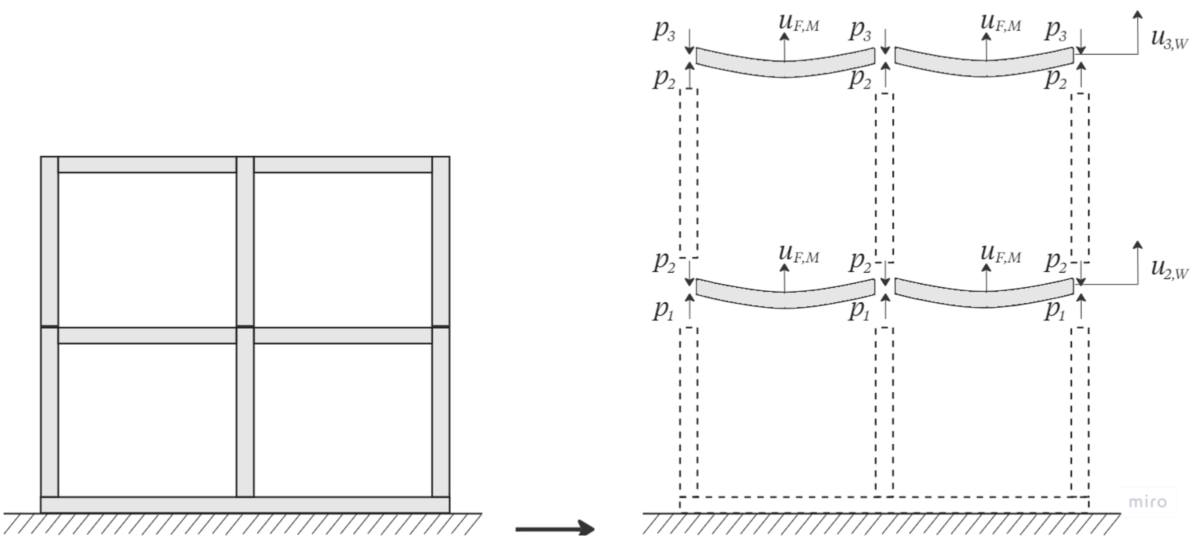

Figure 4.15: Displacements mid-floor caused by vertical dynamic loads

This effect can be taken into account by adjusting T_{21} in the transfer matrix T_F of Equation 4.26 and by instead modelling the floor as an elastic plate. The term T_{21} for an elastic plate then becomes the transfer function between the wall-column displacement and the force acting on the location where the floor is supported. That way, the force P_2 becomes the sum of the effect of the force resulting from the floor $P_{F,W}$ and the initially imposed force (P_1) from the supporting element.

$$\begin{bmatrix} U_2 \\ P_2 \end{bmatrix} = \begin{bmatrix} 1 & 0 \\ \frac{P_{F,W}}{U_{F,W}} & 1 \end{bmatrix} \begin{bmatrix} U_1 \\ P_1 \end{bmatrix} \tag{4.27}$$

The equation for the transfer function between the support force of the floor $P_{F,W}$ and the displacement at this location $U_{F,W}$ is as follows [6]:

$$\begin{aligned} \frac{P_{F,W}}{U_{F,W}} &= -(2\pi f)^2 (m_F + \mu \frac{f^2}{(1+2ci) f_{0,F}^2 - f^2}) \\ \mu &= \frac{(\int \phi_n \, dm)^2}{m_F \int \phi_n^2 \, dm} = \frac{(\int_0^t \int_0^b \int_0^a \phi_n \rho \, dx \, dy \, dz)^2}{\rho bta \int_0^t \int_0^b \int_0^a \phi_n^2 \rho \, dx \, dy \, dz} \end{aligned} \tag{4.28}$$

In this equation, f represents the forcing frequency, $f_{0,F}$ the eigenfrequency of the floor, c the damping, m_F the mass of the floor and μ a factor that takes into account the mode shape ϕ. In the equation for μ, ρ represents the mass density of the floor and t is the corresponding thickness of the plate. When analysing Equation 4.28, it can be seen that the equation takes into account rigid body movement in the same manner as in Equation 4.26 ($-m_F\omega^2 = -m_F(2\pi f)^2$) but adds an extra term which takes into account the effect of bending. The derivation of this term can be found in Appendix C .

After finding $P_{F,W}$ and $U_{F,W}$, the effect of bending is the highest at mid-span. The displacement at mid-span $U_{F,M}$ can be calculated by using the transfer function between the floor at mid-span at $x_{F,M}$ and the floor support:

$$\begin{aligned} \frac{U_{F,M}}{U_{F,W}} &= 1 + \alpha \frac{f^2}{(1+2ci) f_{0,F}^2 - f^2} \\ \alpha = \phi_n(x_{F,M}) \frac{\int \phi_n \, dm}{\int \phi_n^2 \, dm} &= \phi_n(x_{F,M}) \frac{\int_0^t \int_0^b \int_0^a \phi_n \rho \, dx \, dy \, dz}{\int_0^t \int_0^b \int_0^a \phi_n^2 \rho \, dx \, dy \, dz} \end{aligned} \tag{4.29}$$

The way the slab reacts to the imposed vibrations depends on the stiffness, mass and damping, but also on the boundary conditions, which can also be seen in Equation 4.28. The boundary conditions determine how the floor element deforms and thus determine the mode shape ϕ, which can be explained as the shape of the deformation. For the situation in which the slab is modelled as a one-way slab (see Figure 4.16), the behaviour of the plate is similar to that of a simply supported beam.

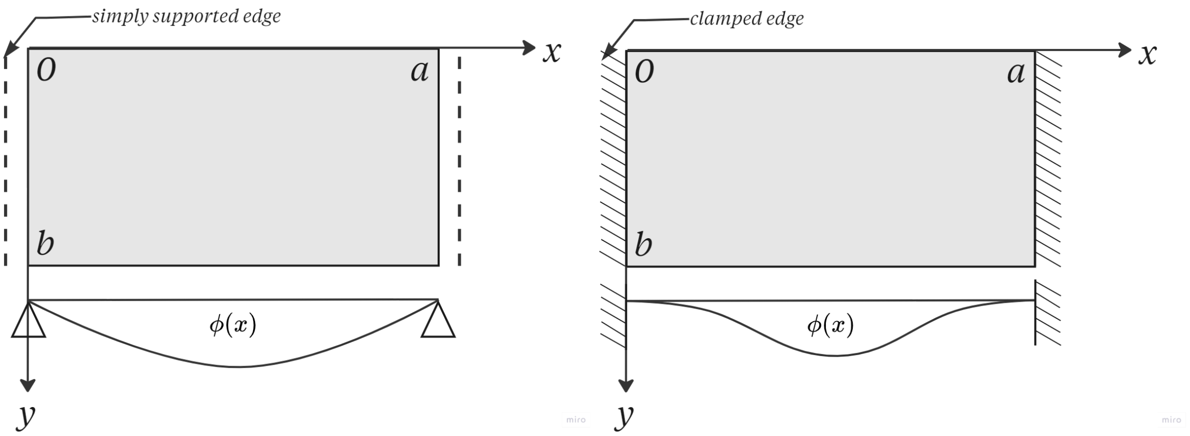

(a) Simply supported edges (SFSF) **(b)** Clamped edges (CFCF)

Figure 4.16: Plates representing one-way slab floor

The eigenfrequency of the floor $f_{0,F}$ and mode shape can be calculated for each of the boundary conditions shown in Figure 4.16 [33]. With the mode shapes, the values for α and μ can also be determined. These values are only dependent on the mode shape and represent a ratio factor, independent of the actual values of the width, length, thickness and mass density of the plate. Table 4.1 summarises these equations and values.

Table 4.1: Eigenfrequency $f_{0,F}$, mode shape $\phi(x)$ and α, μ one-way slab

	$f_{0,F}$ [Hz]	$\phi(x)$	μ	α
SFSF	$\sqrt{\frac{\pi^4 D}{a^4 \rho t}}\frac{1}{2\pi}$	$\sin\frac{\pi x}{a}$	$\frac{64}{\pi^4}$	$\frac{16}{\pi^2}$
CFCF	$\frac{2\sqrt{3}\pi}{3}\sqrt{\frac{D}{a^4 \rho t}}$	$\cos\frac{2\pi x}{a} - 1$	$\frac{2}{3}$	$\frac{4}{3}$

In the equations from Table 4.1, D represents the flexural rigidity of the floor in which ν is its Poisson's ratio and E its modulus of elasticity:

$$D = \frac{Et^3}{12(1-\nu^2)} \tag{4.30}$$

4.4.4. Assembly of the system

When all the necessary values for each of the elements are found, the response of the building can be found by multiplying the transfer matrices with each other. For example, a five-story building would be represented by the matrix chain:

$$T_B = \underbrace{T_F \cdot T_W}_{Roof} \underbrace{T_F \cdot T_W}_{5^{th} floor} \cdot \underbrace{T_F \cdot T_W}_{4^{th} floor} \cdot \underbrace{T_F \cdot T_W}_{3^{rd} floor} \cdot \underbrace{T_F \cdot T_W}_{2^{nd} floor} \cdot \underbrace{T_F \cdot T_W}_{1^{st} floor} \cdot \underbrace{T_F \cdot T_S}_{Ground\ floor} \tag{4.31}$$

After multiplying all the element matrices with each other, the transfer matrix of the building T_B can be used to find the relation between the forces and displacements at the roof level and at the foundation:

$$\begin{bmatrix} U_R \\ P_R \end{bmatrix} = \begin{bmatrix} T_{B11} & T_{B12} \\ T_{B21} & T_{B22} \end{bmatrix} \begin{bmatrix} U_0 \\ P_0 \end{bmatrix} \tag{4.32}$$

Then, by taking into account that the force acting on the roof of any building $P_R = 0$ and that the input displacement U_0 at the foundation level is known, the force acting on the foundation P_0 and the displacement at the roof U_R can be calculated:

$$\begin{aligned} P_0 &= \frac{-T_{B21}U_0}{T_{B22}} \\ U_R &= T_{B11}U_0 + T_{B12}P_0 \end{aligned} \tag{4.33}$$

With these values, all the transfer functions at the location where the floors are connected to the walls can be calculated. By making use of Equation 4.29 the displacements at mid-span of the floor at each storey can also be calculated. In Figure 4.17 the locations and denotation of both types of transfer functions is shown.

Due to different mechanisms, resonance can occur at various frequencies. At these frequencies, the transfer functions will show peaks Besides the natural frequencies of the floors, two other theoretical resonance frequencies can be calculated. The first one is the soil-building resonance frequency, which is related to the stiffness of the soil and foundation and the mass of the building. This is the frequency at which the building behaves similar to a rigid body, therefore also referred to as EFRBM (eigenfrequency of rigid body motion) [34]. The theoretical value can be calculated with Equation 4.34, with k_S the stiffness of the soil-foundation system and m_B the total mass of the building. For shallow foundations, a constant value can be found, because the stiffness of the foundation is independent of the frequency. However, the stiffness of a pile foundation is frequency dependent, so in this case the soil-building frequency is approximated. This is done by considering a shallow foundation and using the corresponding equations for the stiffness of the soil.

$$f_B = \frac{1}{2\pi}\sqrt{\frac{k_S}{m_B}} \tag{4.34}$$

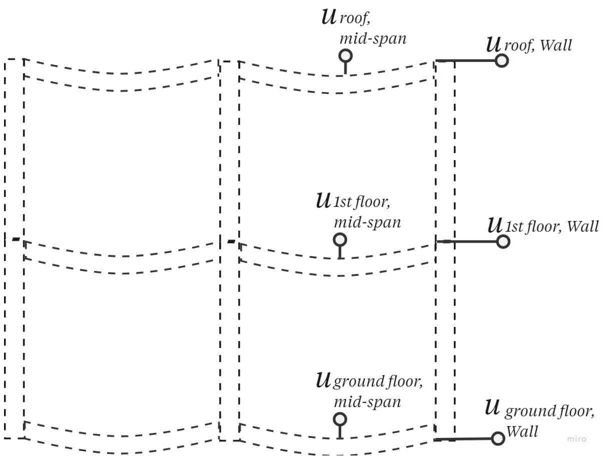

Figure 4.17: Locations of the transfer functions, mid-span of the floors and at the wall-floor supports

The third theoretical resonance frequency is related to the walls. This theoretical value can be calculated with Equation 4.35 [6]:

$$f_W = \frac{vL}{4H} \tag{4.35}$$

In which $vL = \sqrt{E_W/\rho_W}$ is the wavesp eed of the walls, with E_W the corresponding Young's modulus of the walls and ρ_W the mass density of the walls. H denotes the total building height. As explained for the soil-building resonance frequency and the natural frequency of the floors in subsection 2.8.3, it is possible that two or more resonance frequencies coincide, amplifying each other. Also, coupling between different mechanisms can result in lower frequencies than the theoretically calculated values and due to this coincidence between frequencies, it is not always the case that distinct peaks in the transfer functions can be found for each of the mechanisms [8]. Nevertheless, calculating the theoretical resonance frequencies can give insight in which mechanisms are coupled in the building and is a useful tool in estimating around which frequencies resonance will occur.

5
Case studies

5.1. Introduction

To be able to assess whether the transfer matrix model can be used for the preliminary design of apartment buildings, the model is applied to two case studies. For both case studies, free-field vibration measurements at the building locations are available. Furthermore, the vibration levels for the design of a concrete apartment building were evaluated with a finite element method programme and checked against the serviceability criteria of the SBR. Therefore, reference values for the vibration levels in the original design are available. By also modelling the concrete building with the transfer method analysis laid out in this report, the two methods can be compared, giving insight into the spread of the results of these distinct methods. With this information, a conclusion can be drawn on how the transfer function model can be used in the preliminary design of apartment buildings to assess the dynamic response of the buildings. This will help interpret the results of the parameter study in chapter 6.

5.2. Case study - Hero

The first case study to be considered is the Hero project, for which two concrete apartment buildings were designed in close proximity to the railway tracks. In Figure 5.1 the location of the two buildings (DD and DAT) is shown. For the case study, apartment building DD will be considered.

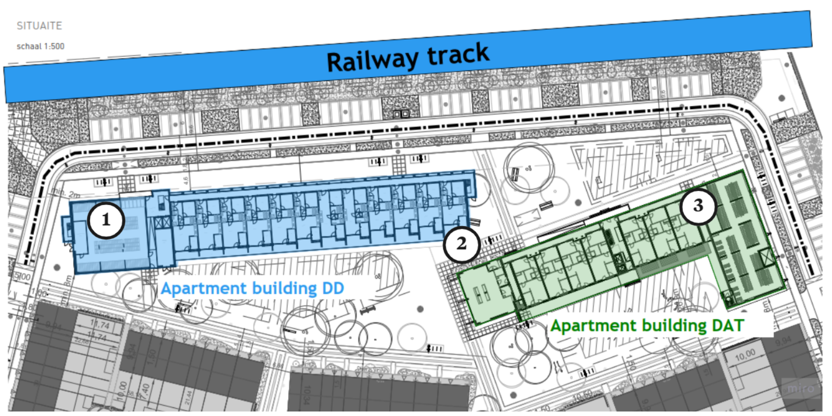

Figure 5.1: Hero location overview and measurement locations 1, 2 and 3

5.2.1. Data railway-induced vibrations

Since the planned location of the apartments was close to the railway tracks, during one week, measurements were carried out on locations 1, 2 and 3 shown in Figure 5.1, in x-, y- and z-direction. The measurements were carried out in the ground, before the construction of the two buildings. As mentioned in chapter 2, in this research only the vertical vibrations in z-direction are taken into account.

The spectra resulting from these measurements are shown in Figure 5.2. The weighing function H_f, from Equation 2.1 is already included in these spectra, therefore the amplitudes are dimensionless. Each of the different measurements represents the passage of a different train at a different time. To find out if the building of the case study satisfies the requirements of the SBR guideline, the buildings vibrations will have to be checked for each of these passages. The spectra from locations 1 and 2 are used as input for the calculation of the response of the DD apartment building.

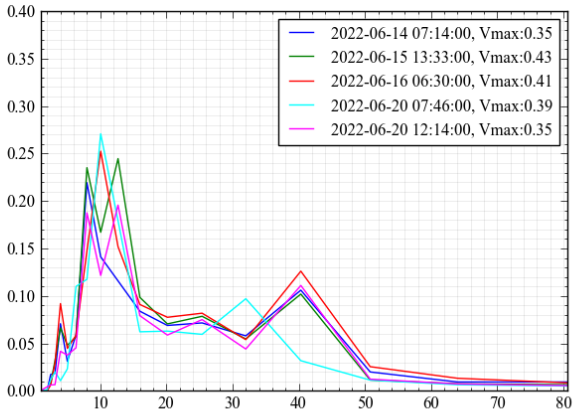

(a) Data location 1, z-direction

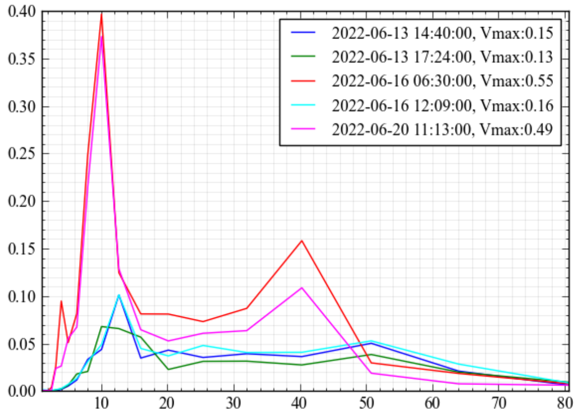

(b) Data location 2, z-direction

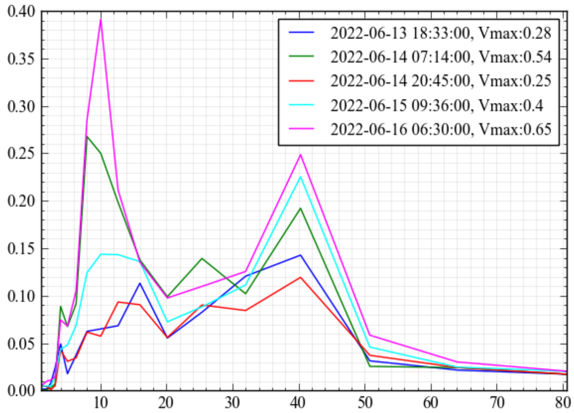

(c) Data location 3, z-direction

Figure 5.2: Vertical velocity vibration levels obtained from measurements for the case study Hero

The V_{max} value in the frequency domain can be found with the following equation, which takes into account the total energy per one-third octave-band:

$$V_{max} = \sqrt{\sum_{i=1}^{n} A_i^2} \tag{5.1}$$

In which i denotes the one-third octave band that is considered and A signifies the corresponding amplitude at that specific frequency. In Table 5.1 these values are calculated for each of the three locations. Comparing these values with the serviceability criteria of $V_{max} \leq 0.1$, it can be seen that the criteria are exceeded even without the presence of a building.

Table 5.1: V_{max} measurements location 1, 2 and 3 HERO project, with orange denoting the values that are below the A_2 limit but above A_1 and red the values that are above A_2

Location 1	V_{max}	Location 2	V_{max}	Location 3	V_{max}
2022-06-14 07:14:00	0.35	2022-06-13 14:40:00	0.15	2022-06-13 18:33:00	0.28
2022-06-15 13:33:00	0.43	2022-06-13 17:24:00	0.13	2022-06-14 07:14:00	0.54
2022-06-16 06:30:00	0.41	2022-06-16 06:30:00	0.55	2022-06-14 20:45:00	0.25
2022-06-20 07:46:00	0.39	2022-06-16 12:09:00	0.16	2022-06-15 09:36:00	0.4
2022-06-20 12:14:00	0.35	2022-06-20 11:13:00	0.49	2022-06-16 06:30:00	0.65

5.2.2. Soil- and foundation structure

Based on the CPT values available for the Hero project, the subsoil is considered to be sandy. Although the soil is not homogeneous, the transfer function model used in this research does assume homogeneity. Therefore, one type of subsoil is determined and used throughout the case study. The corresponding soil parameters are shown in Table 5.2.

Table 5.2: Subsoil characteristics

		Subsoil	
Shear wave velocity	V_s	150	m/s
Modulus of Elasticity	E_S	$50 \cdot 10^6$	N/m^2
Mass density	ρ_s	1800	kg/m^3
Poisson modulus	ν_s	0.25	[-]

As for the pile foundations, three different sizes are being used, which are indicated with the colours red, green and blue in the building plans in the following chapters. The corresponding pile specifications are shown in Table 5.3.

Table 5.3: Pile foundation specification HERO. The colours green, blue and red correspond to the colours of the piles in the building layouts

		Pile type 1	**Pile type 2**	**Pile type 3**	
Pile length	L_d	15.5	15.5	21	m
Diameter	d	0.5	0.6	0.65	m
Modulus of Elasticity	E_p	$15 \cdot 10^9$	$15 \cdot 10^9$	$15 \cdot 10^9$	N/m^2
Mass density	ρ_p	2500	2500	2500	kg/m^3

5.2.3. Apartment building DD

In Figure 5.3 the layout of the ground floor of apartment building DD is shown, including the pile foundation. The sections that will be used as input for the case study are also named here from A to D. In Figure 5.4 the south view of apartment building DD is portrayed. The sections differ from each other in the number of storeys and in terms of building layout. The number of storeys varies from five storeys for sections A and B, to seven storeys for section D, to eight storeys for section C. All the floors are considered to be one way slabs with **clamped edges**. This is because the concrete floors are poured in-situ and the connection between the floors and the walls is fully moment-resistant. Therefore, the floors are schematized as one-way slabs that are clamped on two sides. These boundary conditions are important for the calculation of the natural frequency of the floors, because clamped floors result in higher natural frequencies than simply supported floors.

Section A

Section A consists of a foundation of 4 piles, as shown in Figure 5.5 with a pile length of 15 m. The highlighted part of the building is translated to a 1D structure, as explained in chapter 4. In Figure 5.4 it is shown that this part of the building contains five storeys. The floors are designed as monolithic

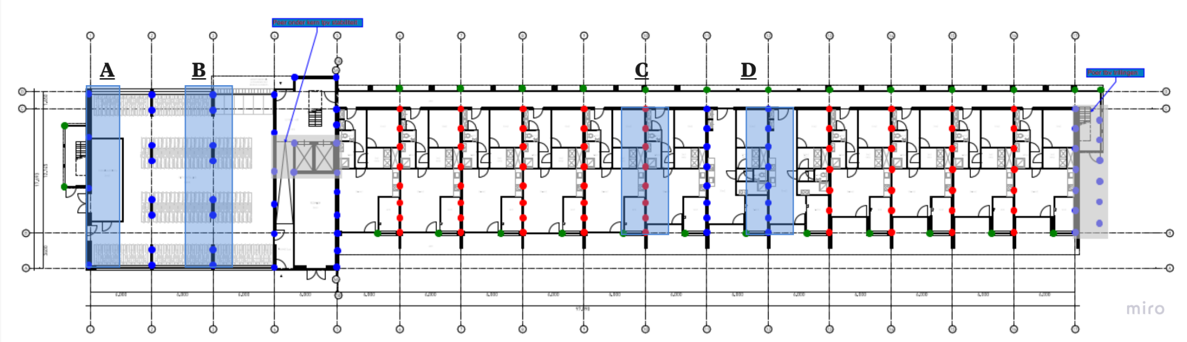

Figure 5.3: Building layout ground floor Hero, building DD

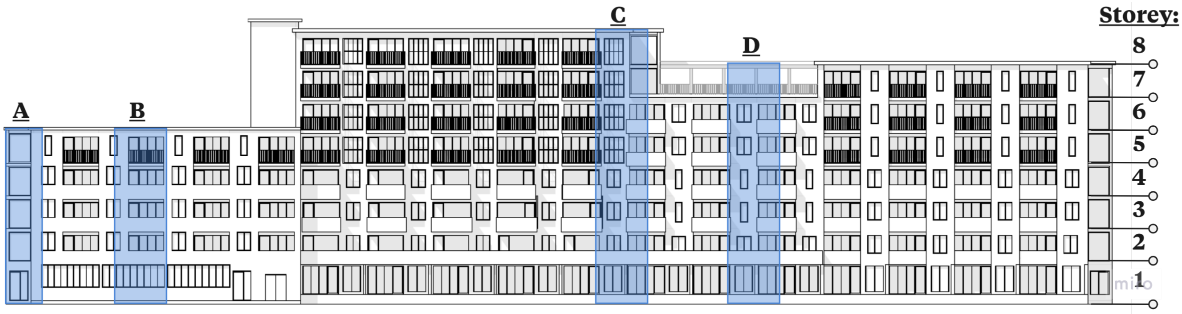

Figure 5.4: South view Hero, building DD

slabs with an anhydrite screed for which an equivalent mass density, height and modulus of elasticity are determined. The upper floors of the other sections are designed similarly. A schematization of this floor is shown in Figure 5.6. The ground floor of section A has a slightly different cross-section. Instead of a monolithic slab, this floor is carried out as a hollow core slab. The ground floor also differs from the other floors in terms of layout, as can be seen in Figure 5.5. This is taken into account in the transfer function model by assigning a transfer matrix with different properties to the ground floor, for both the walls and the floors. The concrete strength class used for all the walls in this section is C45/55. The corresponding building parameters relevant to the dynamic analysis are summarised in Table 5.4.

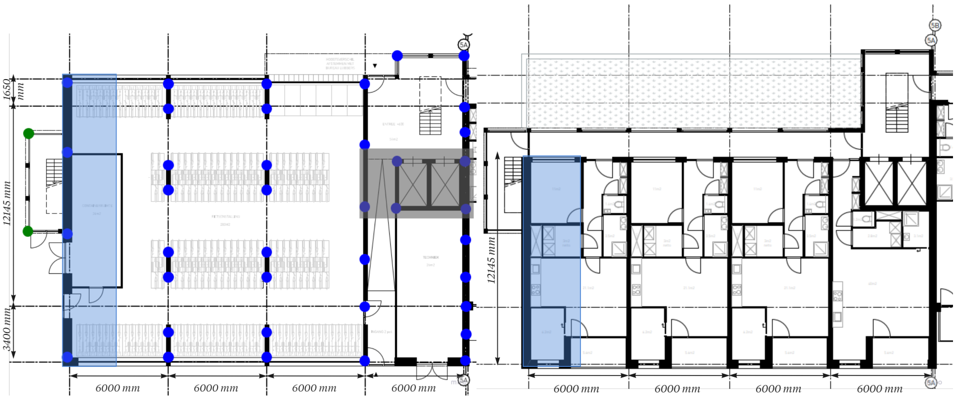

(a) Ground floor **(b)** Upper floors

Figure 5.5: Building DD, Section A

Table 5.4: Material properties apartment building DD, section A

		Ground floor	Floor	Wall, ground floor	Wall, upper floors	Units
Mass density	ρ	2750	3232	2500	2500	kg/m^3
Modulus of elasticity	E	$28 \cdot 10^9$	$28 \cdot 10^9$	$36 \cdot 10^9$	$36 \cdot 10^9$	N/m^2
Thickness	t	0.3	0.28	0.35	0.25	m
Area	A	3×17.693	3×12.145	0.35×17.693	0.35×12.145	m^2
Span	L	6	6	-	-	m

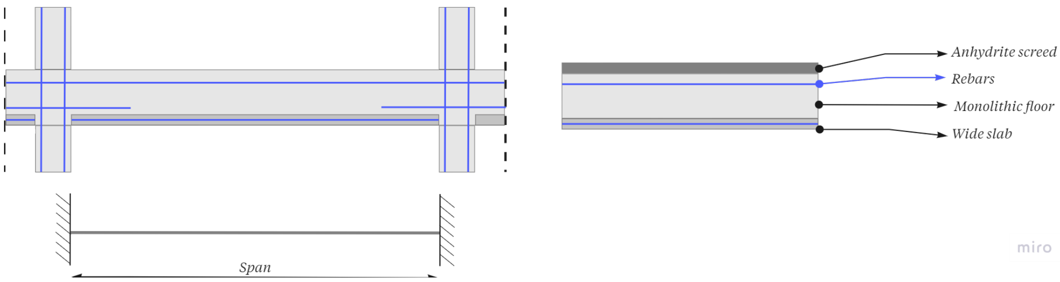

Figure 5.6: Schematization of the concrete floors for the upper storeys of the HERO building

In Figure 5.7 the calculated transfer functions per storey are depicted. The first peak around 8 Hz corresponds to soil-building resonance of the building. The next peak occurs around the natural frequency of the upper floors, which is 24.5 Hz and the natural frequency of the ground floor, which is equal to 28.4 Hz. At these two frequencies, it can be seen in Figure 5.7a that the amplitude of the walls approaches zero. This signifies an anti-phase vibration between the walls and the floors, indicating that the walls are moving in the opposite direction to the floors at these specific natural frequencies. Although the overall amplification at different frequencies of this building section is relatively low, the building resonance takes place at around the same frequency where the peaks in the spectrum of the ground measurements are the highest. This observation is confirmed by the calculation of V_{max} for each storey. Each measurement of location 1 is multiplied by the transfer function of the mid-span of the floor of each storey, after which Equation 5.1 is applied to find V_{max} per measurement per storey. The maximum resulting V_{max} per storey is shown in Figure 5.8.

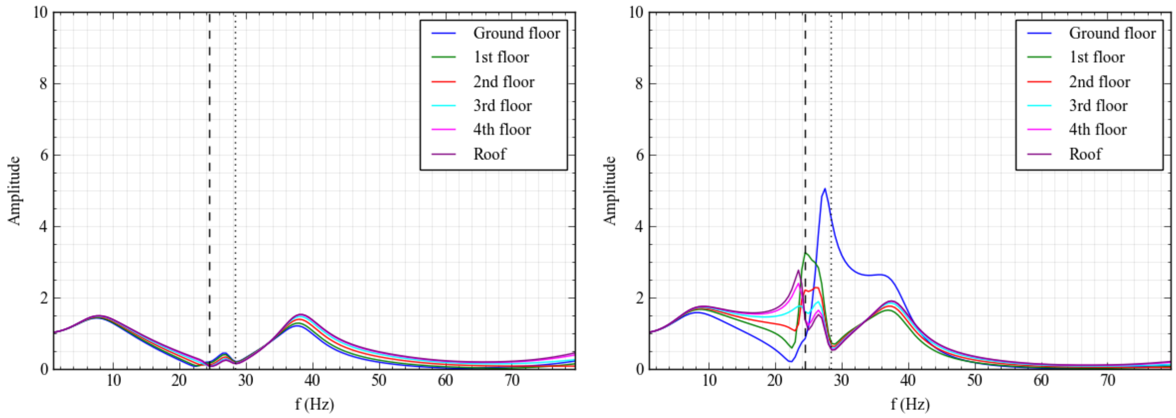

(a) Transfer functions walls

(b) Transfer functions mid-span floors

Figure 5.7: Transfer functions section A, floor frequencies denoted with vertical lines

From Figure 5.8 it can be concluded that none of the storeys comply with the serviceability criteria target values of A_1 or A_2 when using the transfer function method. The amplification of the initially measured free-field vibrations is still relatively low, less than a factor of 2. However, the measured vibrations would have to be attenuated by a factor of 4, to be below the highest target value A_2.

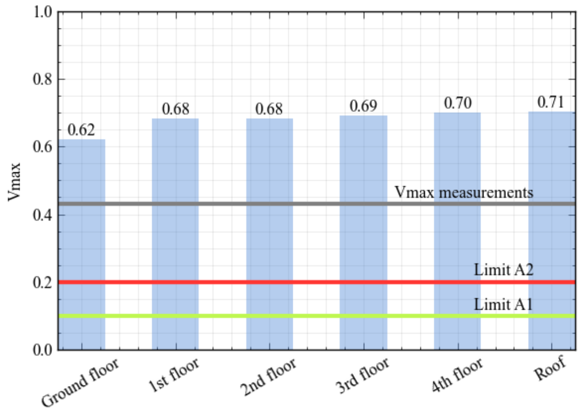

Figure 5.8: V_{max} mid-span floors section A, with the serviceability A1 limit of 0.1 and the A2 limit of 0.2 [66] and the highest found value of V_{max} of the free-field measurements at this location

Section B

Section B consists of a foundation of 8 piles of a pile length of 21 m, as shown in Figure 5.9. As can be seen from Figure 5.4, this part of the building contains four storeys. The highlighted part of the building is translated to a 1D structure, as explained in chapter 4. The floors are again designed as monolithic slabs with an anhydrite screed as shown in Figure 5.6. The floors of all storeys have the same dimensions, but the ground floor has a slightly different cross-section. Instead of a monolithic slab, this floor is carried out as a hollow core slab, similar to section A. Additionally, the ground floor has a different layout from the upper floors, which is taken into account in the transfer function model by assigning a distinct transfer matrix to the ground floor and walls at this level. The relevant corresponding building parameters are summarised in Table 5.5.

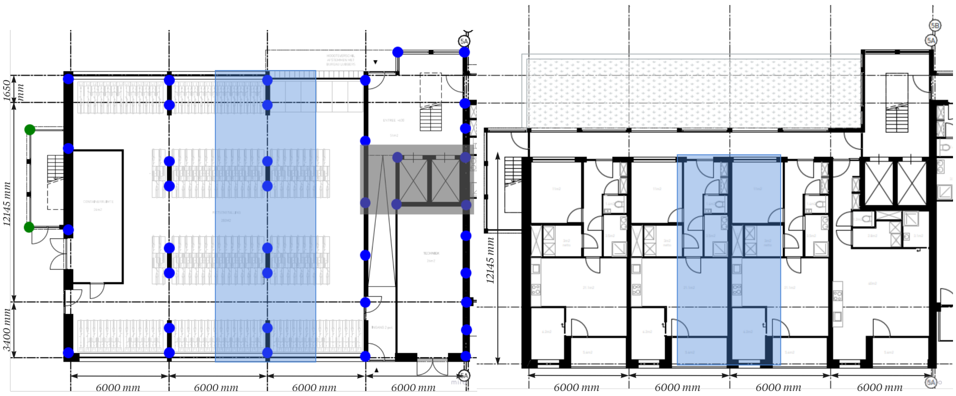

(a) Ground floor **(b)** Upper floors

Figure 5.9: Building DD, Section B

Table 5.5: Material properties apartment building DD, section B and D

		Ground floor	Floor	Wall, ground floor	Wall, upper floors	Units
Mass density	ρ	2750	3232	2500	2500	kg/m^3
Modulus of elasticity	E	$28 \cdot 10^9$	$28 \cdot 10^9$	$36 \cdot 10^9$	$36 \cdot 10^9$	N/m^2
Thickness	t	0.3	0.28	0.25	0.25	m
Area	A	6×17.693	6×12.145	0.25×7.25	0.25×12.145	m^2
Span	L	6	6	-	-	m

Given that the floor spans and the number of storeys for section A and section B are the same, it is consistent with the expectations that the transfer functions are also similar. In Figure 5.10 it can be observed that compared to section A, the amplification between storeys is slightly higher for section B. This can be explained by the column-like structure of the walls on the ground floor of section B and the generally smaller area of the walls per storey, compared to section A. This results in more extension of the walls, which in turn results in an amplification of the vibrations from one element to the next.

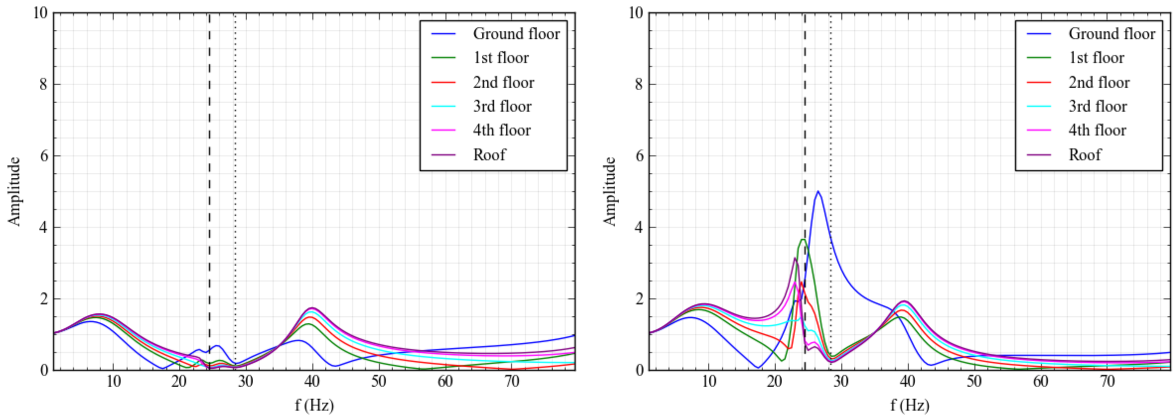

(a) Transfer functions walls

(b) Transfer functions mid-span floors

Figure 5.10: Transfer function section B, floor frequencies denoted with vertical lines

Similar to section A, the maximum resulting V_{max} values are calculated for each storey with Equation 5.1 and the measurements from location 1. The results are of the same magnitude, but the slightly higher amplification per storey can also be seen in the resulting V_{max} values. Besides that, the V_{max} of the ground floor of section B is discernibly lower than the V_{max} value of section A. This can be understood through the higher damping of the more closely spaced pile group foundation of eight piles of section B compared to the more sparsely spaced pile group foundation of similar piles for section A.

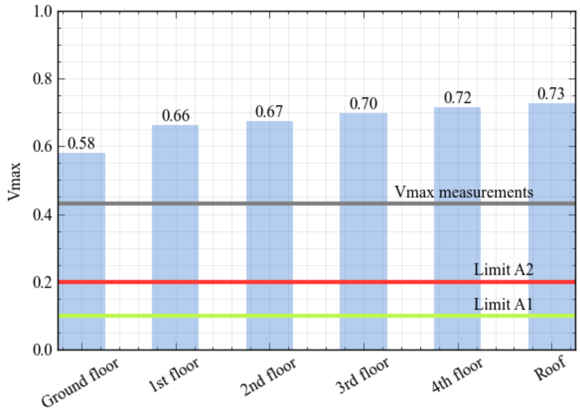

Figure 5.11: V_{max} mid-span floors section B, with the serviceability A1 limit of 0.1 and the A2 limit of 0.2 [66] and the highest found value of V_{max} of the free-field measurements at this location

Section C and D

Section C consists of a foundation of 8 piles with a pile length of 21 m, as shown in Figure 5.12a. This section is chosen for the analysis because an expansion joint is placed at the edge of this section as shown with the yellow dashed line in Figure 5.12a. That means that only half of the mass of the floor is acting as effective mass, which will have an effect on the transfer functions of this section. Also, this part of the building has the highest number of storeys. Section D is very similar to section C, except that this part of the building consists of seven storeys instead of eight and the pile length is 15 m instead of 21 m. Also, this part of the cross-section does not contain an expansion joint, meaning that the effective width will be equal to the entire span of the floor multiplied with its width. Section D is shown in Figure 5.12b. The floors for both sections are again designed as monolithic slabs with an anhydrite screed for which an equivalent mass density, height and modulus of elasticity are determined. The floors of all storeys have the same dimensions, but the ground floor has a slightly different cross-section. Instead of a monolithic slab, this floor is carried out as a hollow core slab. The walls in this section are concrete walls of C45/55 and have the same length and thickness, both on the ground floor and the upper floors. The relevant corresponding building parameters are summarised in Table 5.6.

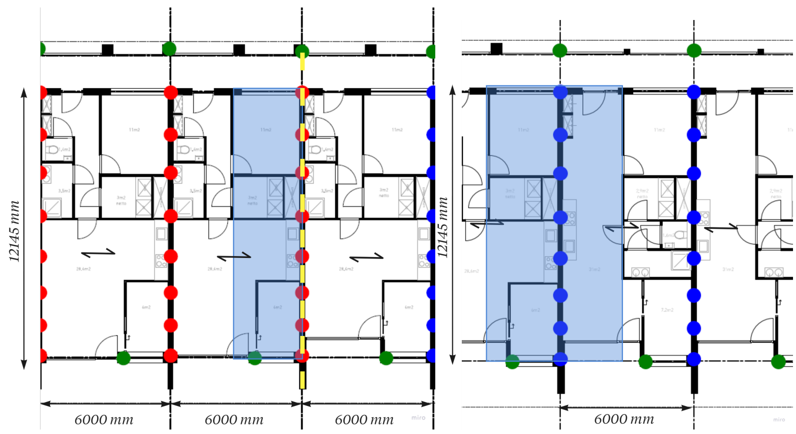

(a) Building DD, section C **(b)** Building DD, section D

Table 5.6: Material properties apartment building DD, section C and D

		Ground floor	Floor	Wall	Units
Mass density	ρ	2750	3232	2500	kg/m^3
Modulus of elasticity	E	$28 \cdot 10^9$	$28 \cdot 10^9$	$36 \cdot 10^9$	N/m^2
Thickness	t	0.3	0.28	0.25	m
Area section C	A	3×12.145	3×12.145	0.25×12.145	m^2
Area section D	A	6×12.145	6×12.145	0.25×12.145	m^2
Span	L	6	6	-	m

In Figure 5.13 the calculated transfer functions for sections C and D are shown. The floors have the same thickness, mass density, span and modulus of elasticity as the floors in section A and B, resulting in the same natural frequency of 24.5 Hz for the upper floors and 28.4 Hz for the ground floor. However, due to the lower effective mass of the floors of section C, the floors are more easily excited at their natural frequency, resulting in higher peaks in the spectrum of the transfer functions. Furthermore, although section C consists of one additional storey compared to section D, the total weight of this section is lower, resulting in a slightly higher building resonance frequency. This is reflected in the first peak of the transfer functions, which takes place around 5 Hz for section D and around 9 Hz for section C.

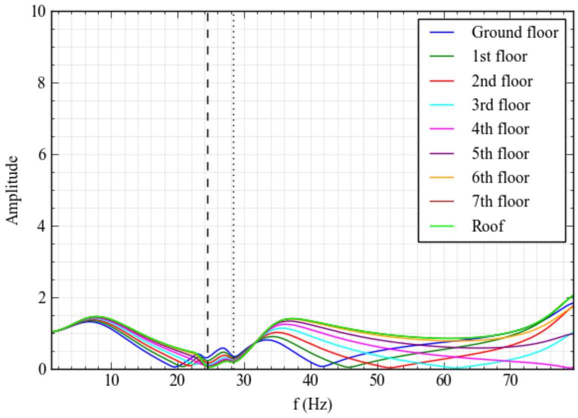

(a) Section C: Transfer functions walls

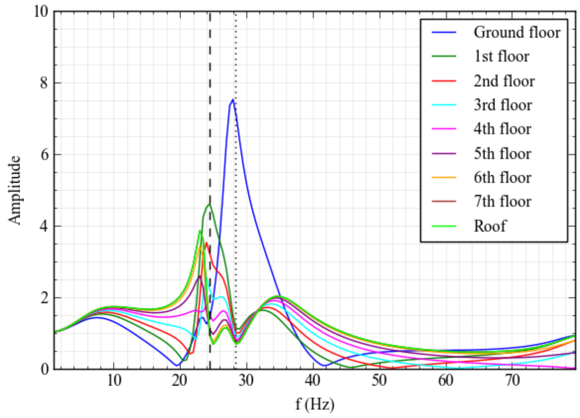

(b) Section C: Transfer functions mid-span floors

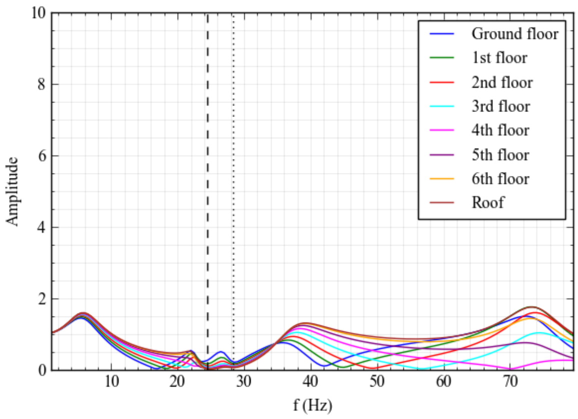

(c) Section D: Transfer functions walls

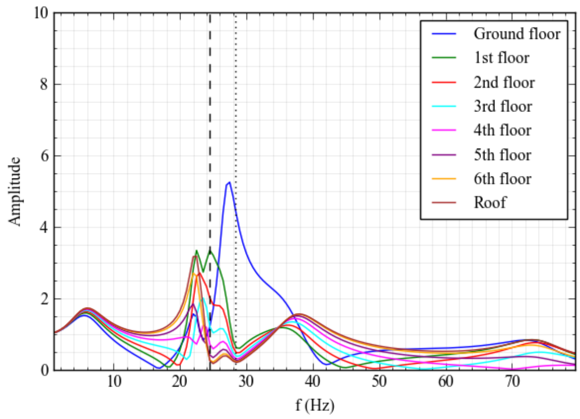

(d) Section D: Transfer functions mid-span floors

Figure 5.13: Transfer functions walls and floors section C and D, apartment building DD, floor frequencies denoted with vertical lines

To find the maximum values of V_{max}, the transfer functions of section C are multiplied with the free-field measurements of location 1 and the transfer functions of section D are multiplied with the measurements of location 2. Analogous to section A and B, Equation 5.1 is then used to calculate the values per storey of V_{max}. The maximum values for each of the storeys of each of the buildings are shown in Figure 5.14. In Figure 5.14 it can be seen that the V_{max} values for both sections are quite comparable, even though the transfer functions for section C are less favourable. However, it is important to highlight that the maximum value of V_{max} is higher for the free-field measurements at location 2 compared to those of location 1, which is the main cause for this difference. When comparing the values for V_{max} for the ground floors of both sections, the effect of the higher amplification factor of section C for this floor can nevertheless be observed, since this peak takes place outside of the first peaks of the free-field spectra of both locations 1 and 2. The maximum value for V_{max} of the free-field spectra at the natural frequency of the ground floor is around 0.1. Multiplication with the transfer functions of section C and D results in a lower V_{max} value for section D, consistent with the predictions.

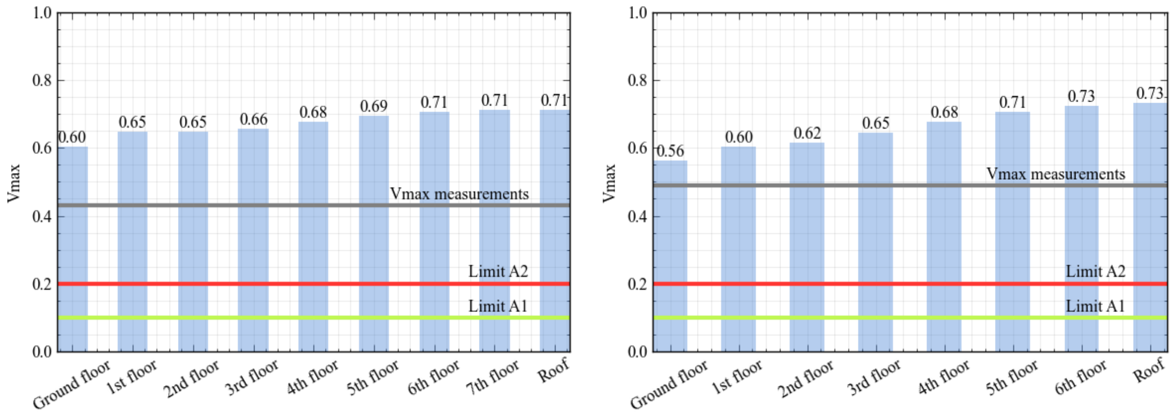

(a) Section C

(b) Section D

Figure 5.14: V_{max} mid-span floors section C and D, with the serviceability A1 limit of 0.1 and the A2 limit of 0.2 [66] and the highest found value of V_{max} of the free-field measurements at this location

Serviceability criteria comparison

From the analysis of the sections A, B, C and D for the HERO apartment building, it can be concluded that in all the sections and for every storey, the target values for V_{max}, A_1 and A_2, are exceeded. The highest V_{max} values are found on the roof of sections D and B. However, the vibrations will be the most perceivable on the floor below, since the roof is not used as living area. As a result, the sixth floor of section D and the fourth floor of section B are the floors where the model estimates the highest nuisance. However, the difference between the other sections in terms of maximum V_{max} values is only ≈ 0.02. For the actual case study, an initial estimation of the range within which the resulting vibrations would fall was made, before the finite element model was set up. The first estimation only took into account the free-field vibrations and common building amplification factors. This resulted in an expected value of V_{max} of 1.1 in the building at location 1 and a value of 1.2 at location 2. When taking into account the building parameters, a more positive estimation was derived, indicating V_{max} for location 1 to be 0.4 and for location 2 to be 0.5. Finally, the results from the finite element analysis showed even more positive results: the target value of A_2 was only exceeded at one location in the DD building, and marginally. The highest calculated V_{max} value was 0.26 at section A, at the edge of the building. All these values are compared to the results from the application of the transfer function model and are shown in Figure 5.15.

Although the results from the transfer function model are within the range of the original estimations for the HERO building, there is still a large difference with the results from the Finite Element Model. The transfer functions yield outcomes that are approximately 2.7 times higher. There can be multiple explanations for this difference. Firstly, the building components of the different sections of the DD apartment building are coupled. Stiffer areas of the building, such as the elevator and staircase shaft, could have a positive effect on the vibrations in more vulnerable areas of the building. In the transfer function model, this is not taken into account, since the building is simplified to a 1D structure. Secondly, the soil around the building is completely modelled in the FEM model. All the soil elements

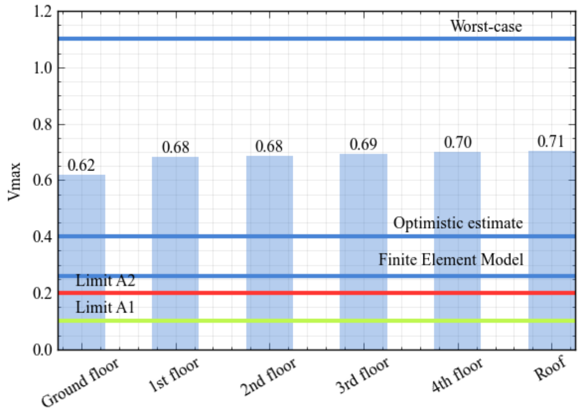

Figure 5.15: Comparison of V_{max} at mid-span of the floors in section A, with the serviceability A1 limit of 0.1 and the A2 limit of 0.2 [66] and the results from the FEM model provided by the case study. Worst-case and optimistic estimate represent the initial estimations provided by the case study

are connected to the foundation and the building itself. Since there is a high dependency between the foundation characteristics and the building response, this could have a significant effect on the results [50].

A change in the soil parameters immediately affects the values that are found for V_{max}. To illustrate this effect, the V_{max} values are recalculated with the transfer function model for section A and different types of soils. The different types of subsoil are summarised in Table 5.7 and the calculated transfer functions are shown in Figure 5.16. The corresponding values for V_{max} per storey are displayed in Figure 5.17. In line with the literature study, softer soils provide more damping compared to stiff soils. Furthermore, the building response peak moves to a lower frequency when the soil is less stiff, causing the soil-building resonance frequency to coincide less with the highest peaks in the railway-induced vibration spectra, which results in lower vibrations.

Also, in the transfer function model, it is assumed that the building is uniformly excited with the same free-field ground motion from the measurements. However, in reality, the surface waves that cause the vibrations are partially absorbed, scattered or reflected. Especially in the case of the pile foundation, this could reduce the vibrations that excite the building. This effect, which was also outlined in the literature study in chapter 2, is the kinematic soil-structure effect that is not taken into account in the calculations with the transfer function model. The FEM model provided in the case study used an approach in which the free-field measurements were first translated back to the location of the track, in a model which only contained the soil. Then, a model was created that included the building itself and the load was applied at the location of the railway tracks. That way, the way the foundation influences the propagation of the waves could be taken into account, which would lower the vibrations that are transmitted through the building at the foundation level.

Even though the V_{max} values were close to the limit value of A_2, to comply with the serviceability criteria for V_{max}, it was decided to stiffen the foundation at section A by adding beams and additional weight. Those adjustments were applied to the FEM model and turned out to be sufficient for lowering the value of V_{max} below the A_2 limit. This adjustment is a relatively economical option compared to other options such as applying base isolation.

Table 5.7: Different subsoil parameters

Soil	E_s **[Mpa]**	G_s **[Mpa]**	V_s **[m/s]**
Soft clay	10	12	100
Medium clay	20	15	200
Loose sand	25	20	150
Dense, stiff sand	75	70	300

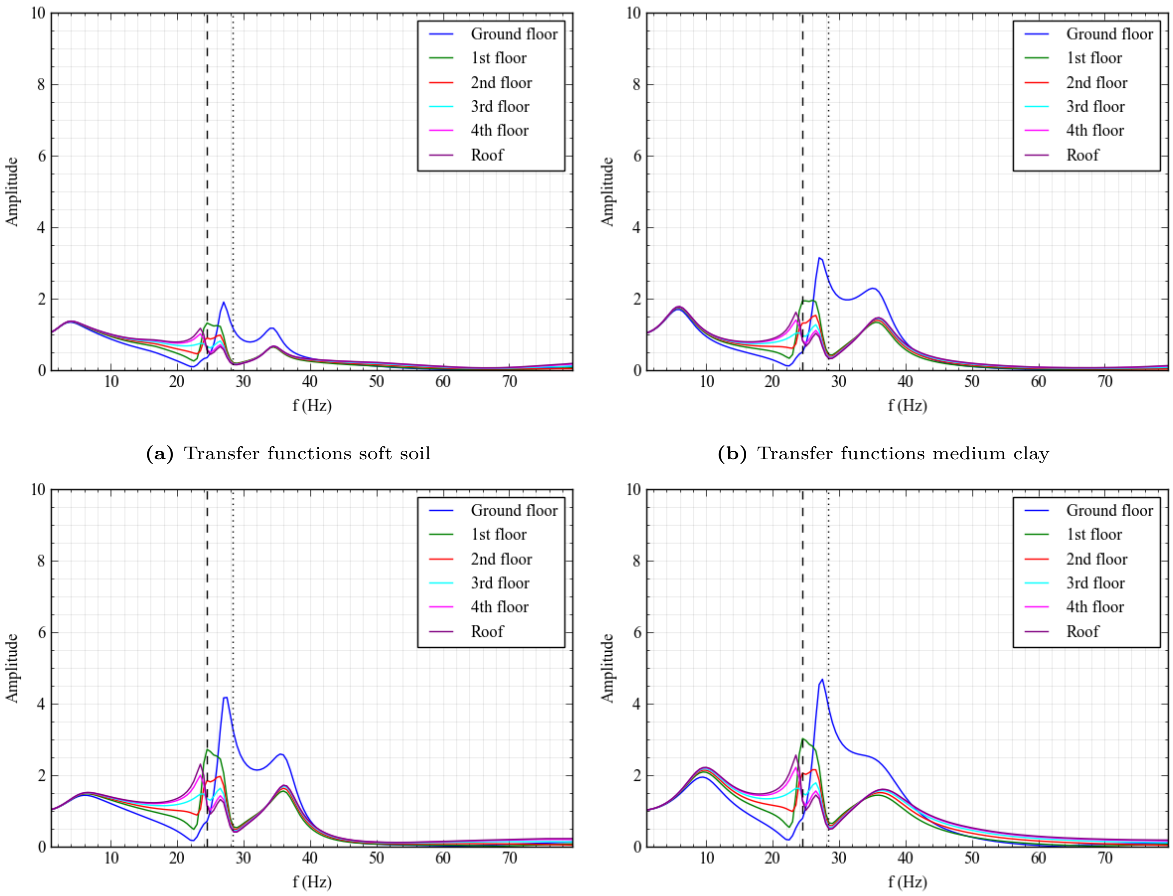

(a) Transfer functions soft soil

(b) Transfer functions medium clay

(c) Transfer functions loose sand

(d) Transfer functions dense, stiff sand

Figure 5.16: Variation in transfer functions for section A with changing subsoil parameters, floor frequencies denoted with vertical lines

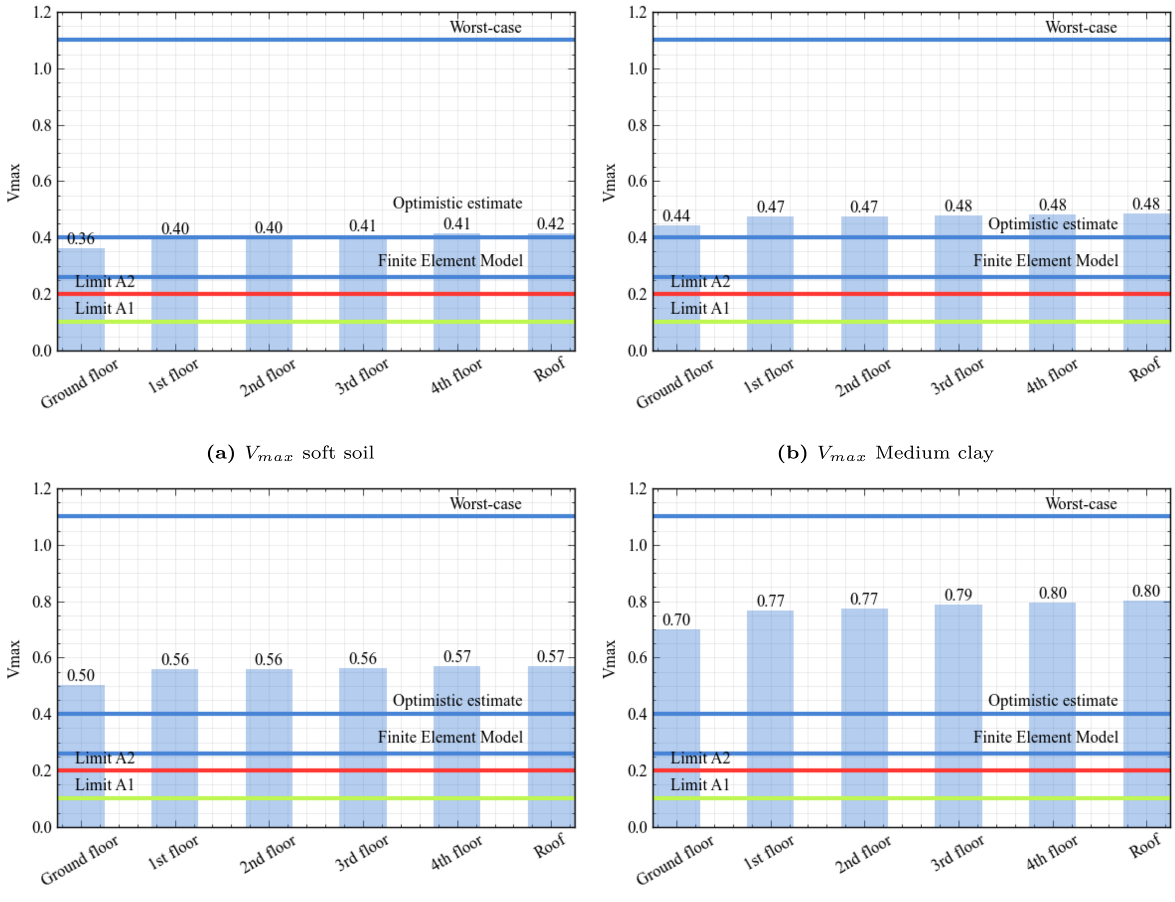

(a) V_{max} soft soil

(b) V_{max} Medium clay

(c) V_{max} Loose sand

(d) V_{max} Dense, stiff sand

Figure 5.17: Variation in V_{max} with changing subsoil parameters, with V_{max} mid-span floors of section A, with the serviceability A1 limit of 0.1 and the A2 limit of 0.2 [66] and the results from the FEM model provided by the case study. Worst-case and optimistic estimate represent the initial estimations provided by the case study

5.3. Case study - Enka

The second case study to be analysed is the ENKA project. This project is located near the railway track from Ede to Arnhem, close to station Ede-Wageningen. The construction of the buildings is planned at a distance of approximately 39 meters from the ground-level railway track. In Figure 5.18 the location of the two buildings in relation to the track is shown. For this case study, apartment buildings H2A and H4F will be analysed.

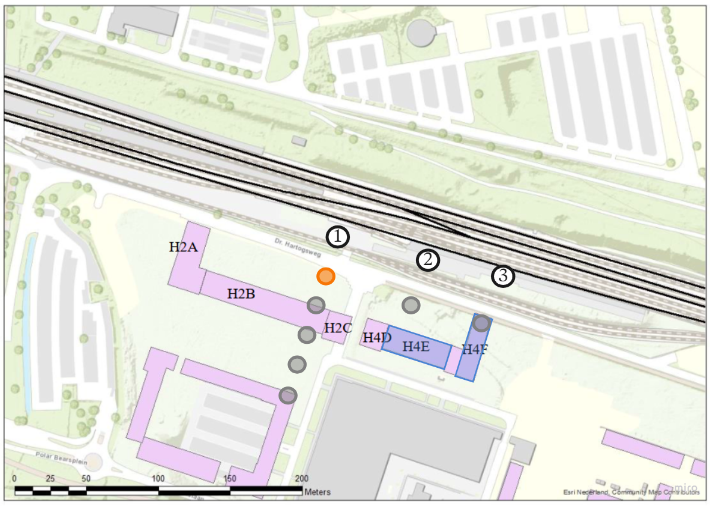

Figure 5.18: Location ENKA buildings and measurements

5.3.1. Data railway-induced vibrations

The measurements for this case study differ from those carried out for the HERO project. Instead of two extended-duration measurements at the planned location of the buildings, one extended-duration measurement is carried out, and six additional short-duration measurements are taken at different locations. The location of the extended-duration measurement is indicated in orange in Figure 5.18 and the short-duration measurements are denoted in grey. The multiple short-duration measurements are intended to assess the variation in soil composition and its effect on the distribution of the vibration levels, whereas the extended-duration measurement is used to determine the characteristic spectrum for the railway-induced vibrations. In Figure 5.19a this characteristic spectrum resulting from the extended-duration measurement is shown. The same axes are used for the HERO case study, from which can be seen that the vibrations for the ENKA project are generally lower. Whereas the main peak for the HERO project takes place between 1-20 Hz, the main peak for ENKA is at a much higher frequency, between 60-70 Hz.

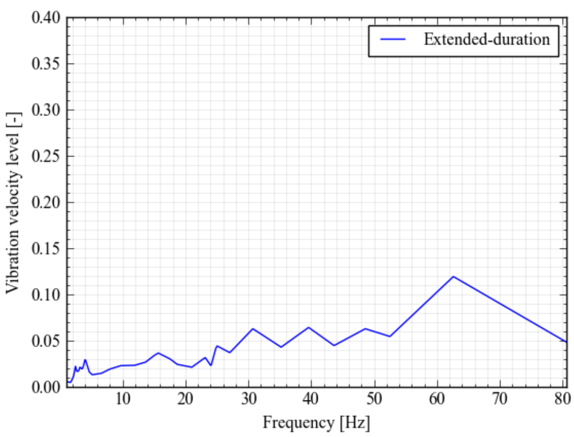

(a) Data extended-duration measurement ENKA case study

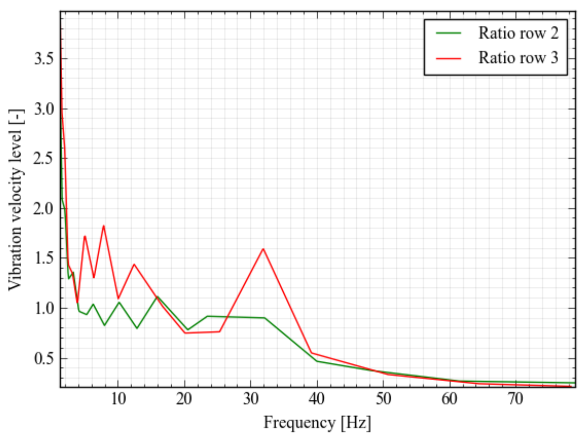

(b) Ratio measurements row 2 and 3

To determine the transmission of the railway-induced vibrations over the distance and to obtain the characteristic spectrum at the second and third rows as shown in Figure 5.18, the ratio between the extended-duration measurements at row 1 and the short-duration measurements in row 2 and 3 is calculated. This ratio is shown in Figure 5.19b. Subsequently, the spectrum of the railway-induced vibrations at rows 2 and 3 can be calculated by multiplying this ratio with the spectrum of the extended-duration meeting. The resulting spectra are shown in Figure 5.20a and Figure 5.20b. Although they differ from the spectrum of the first row for the frequencies above 40 Hz, the vibrations barely change in the range of 0-40 Hz.

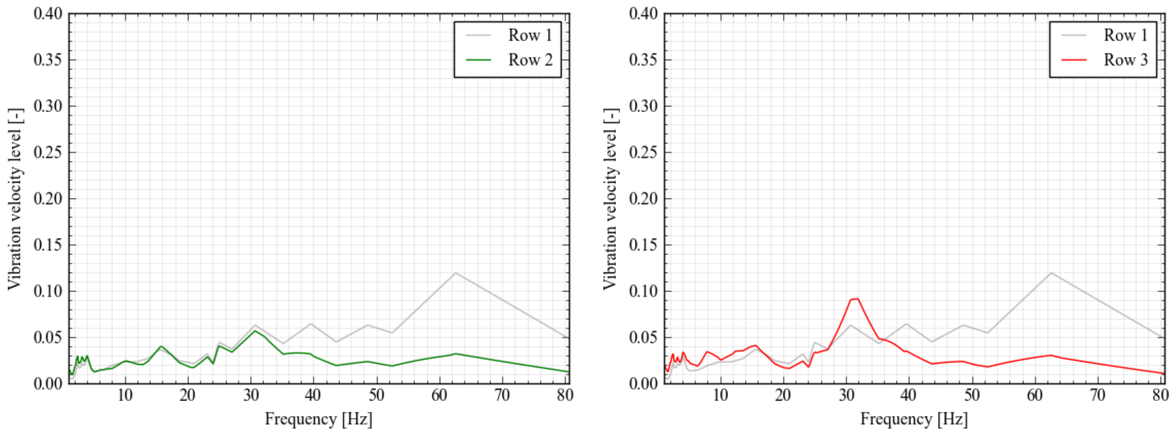

(a) Calculated spectrum row 2 **(b)** Calculated spectrum row 3

5.3.2. Soil- and foundation structure

Based on the CPT values available for the ENKA project, the subsoil is considered to be medium stiff and sandy. Similar to the HERO project, the soil is treated as homogeneous. The corresponding soil parameters are shown in Table 5.8.

Table 5.8: Subsoil characteristics

		Subsoil	
Shear wave velocity	V_s	200	m/s
Modulus of Elasticity	E_S	$50 \cdot 10^6$	N/m^2
Mass density	ρ_s	1800	kg/m^3
Poisson modulus	ν_s	0.3	[-]

Both building H4E and H4F are founded on a pile foundation consisting of mortar screw piles. The diameter of the piles varies between 500 and 550 mm and the length between 4.5 and 12.5 m. The characteristics of the piles are summarised in Table 5.9 for the two buildings that are analysed in this case study, H4E and H4F.

Table 5.9: Pile foundation specification ENKA

		Pile type H4E	**Pile type H4F**	
Pile length	L_d	5	8	m/s
Diameter	d	0.5	0.5	N/m^2
Modulus of Elasticity	E_p	$15 \cdot 10^9$	$15 \cdot 10^9$	kg/m^3
Mass density	ρ_p	2500	2500	[-]
Center-to-center distance	S	1500	1250	mm

5.3.3. Building H4E

In Figure 5.21 the south view of the H4E and H4F building is shown. The section that will be analysed for the case study is highlighted in blue. This section of the building contains five storeys and is founded on a pile foundation.

Figure 5.21: South view building H4E and H4F

The load-bearing structure of this section consists of concrete walls of C30/37 combined with concrete floors of C30/37 with an anhydrite finish of 60 mm. The ground floor differs from the upper floors and is designed as a hollow core slab with a screed of 170 mm and the same anhydrite finish as used for the floors on the upper storeys of 60 mm. An equivalent mass density is calculated for both the ground floor and the upper floors. The main building parameters are summarised in Table 5.10.

Table 5.10: Material properties apartment H4E

		Ground floor	Floor	Wall	Units
Mass density	ρ	2675	3172	2500	kg/m^3
Modulus of elasticity	E	$32 \cdot 10^9$	$32 \cdot 10^9$	$32 \cdot 10^9$	N/m^2
Thickness	t	0.28	0.29	0.25	m
Area	A	6.9×13.8	6.9×13.8	0.25×13.8	m^2
Span	L	6.9	6.9	-	m

In Figure 5.22 the layout of one of the upper floors of the building section is shown. Each floor has a span of 6.9 meters and the entire apartment spans a length of 13.8 meters. The building section is founded on a group of eight piles, with an average centre-to-centre distance of 1.5 meters.

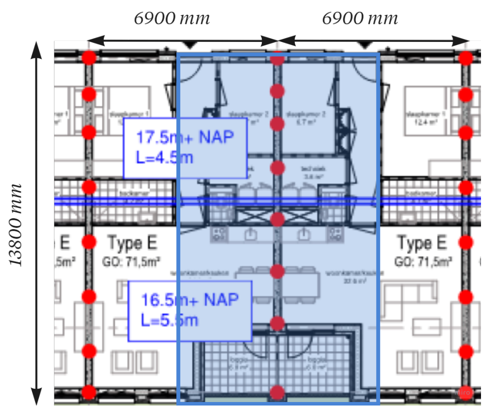

Figure 5.22: Section of building H4E

The calculated transfer functions are shown in Figure 5.23. The first peak is related to the soil-building resonance and occurs around 5 Hz. At this frequency, the entire building vibrates in the same phase. The second peak is related to the natural frequency of the floors, which is 20.68 Hz for the upper floors and 21.74 Hz for the ground floor. At the natural frequency of the floors, the amplitudes of the transfer functions for the walls approach zero, indicating that the floors and walls move out of phase. Similar to the HERO project, the amplification of the free-field vibrations is relatively low and stays below a factor of two. Although the dimensions of the building are similar to the dimensions of HERO, the floors used in the ENKA project are stiffer: C30/37 concrete is used instead of the C20/25 that was applied for HERO. Therefore, the amplification between the different storeys is less for the ENKA project.

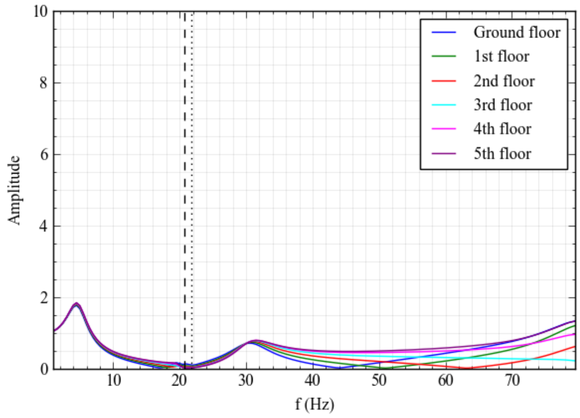

(a) Section H4E: Transfer functions walls

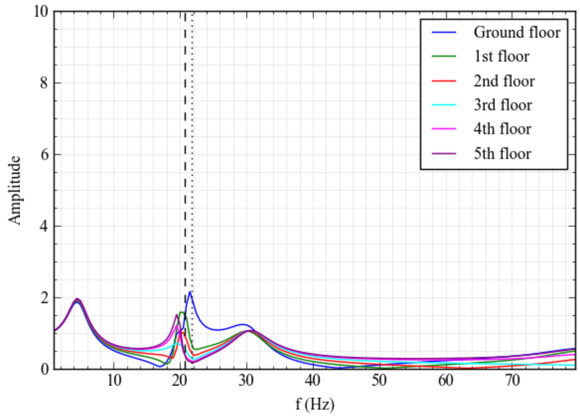

(b) Section H4E: Transfer functions mid-span floors

Figure 5.23: Transfer function walls and floors section H4E, ENKA building, floor frequencies denoted with vertical lines

5.3.4. Building H4F

In Figure 5.24 the east view of the H4F building is shown. Highlighted in blue is the section that will be analysed for the case study. The main difference between this section and section H4E is the number of storeys: building H4F consists of six storeys instead of five. Also, the pile lengths are longer than those applied for section H4E. Lastly, the span of the floors is for this section also 6.9 meters, but the width of the apartments is 9.87 m. In Figure 5.25 the layout of the section that is to be analysed is shown. This section is founded on a group of eight piles, similar to the section of building H4F. The parameters important for the calculation of the transfer function can be found in Table 5.11.

Figure 5.24: East view building H4F

Because the building geometry of building section H4F is similar to that of H4E, it is in line with the expectations that the transfer functions are alike as well. Although the floors of both sections have the same natural frequency of 20.68 Hz for the upper floors and 21.74 Hz for the ground floor, the floors of section H4F are more easily excited due to their lower mass. Therefore, the peaks in the transfer function at the natural frequency of the floors are higher for this section. Furthermore, the lower mass causes a slightly higher amplification from storey to storey. Lastly, it shifts the resonance frequency of the soil-building frequency of the building to a slightly higher frequency, since this is dependent on the stiffness of the soil and the mass of the entire building.

Table 5.11: Material properties apartment H4F

		Ground floor	Floor	Wall	Units
Mass density	ρ	2675	3172	2500	kg/m^3
Modulus of elasticity	E	$32 \cdot 10^9$	$32 \cdot 10^9$	$32 \cdot 10^9$	N/m^2
Thickness	t	0.28	0.29	0.25	m
Area	A	6.9×9.87	6.9×9.87	0.25×9.87	m^2
Span	L	6.9	6.9	-	m

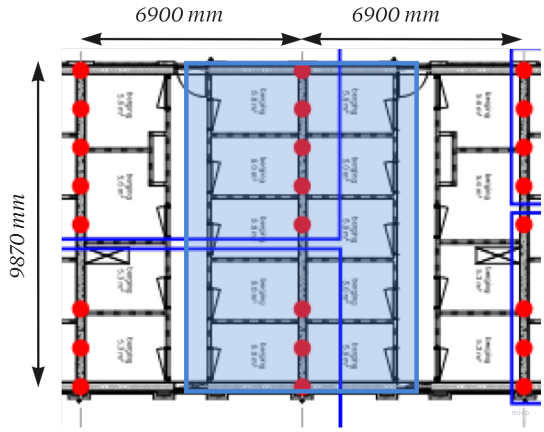

Figure 5.25: Section of building H4F

Serviceability criteria comparison

Besides the difference in the execution of the measurements for ENKA when compared to HERO, the modelling approach of this case study is also different. Whereas for the HERO project the entire building including the surrounding soil was modelled, for ENKA only the building structure was modelled with a finite element model. To calculate the transmittance of the measured free-field vibrations to the building, a standardized function is used. This function is shown in Figure 5.27. All vibrations until 10 Hz are reduced with a factor of 0.72 and after 10 Hz this factor linearly decreases until it reaches a plateau at 50 Hz of a factor of 0.35.

The assumptions on which this transmission function is based are not described in the case study. It is not fully clear whether a distinction is made in the type of foundation or subsoil, or whether this is a transmission function that is generally applied for all soil conditions and foundation types. However, the ENKA case study also provides the transfer functions obtained from the finite element model. These transfer functions show the transmission from the lowest floor to the upper floor of each building.

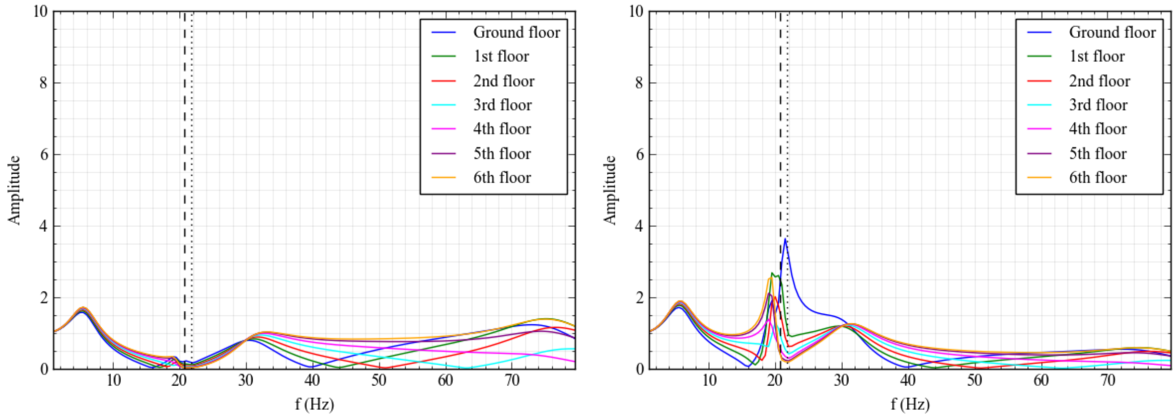

(a) Transfer functions walls

(b) Transfer functions mid-span floors

Figure 5.26: Transfer function walls and floors section H4F, ENKA building, floor frequencies denoted with vertical lines

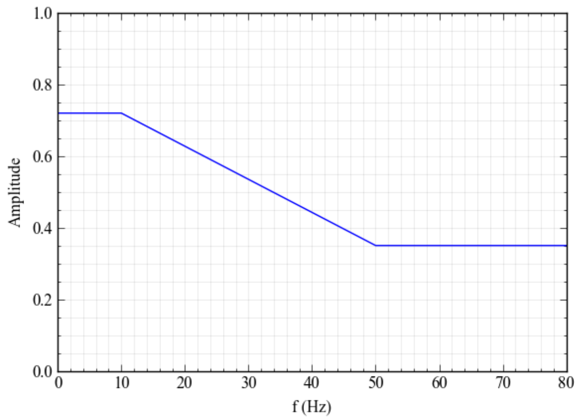

Figure 5.27: Transmission function foundation to building, ENKA

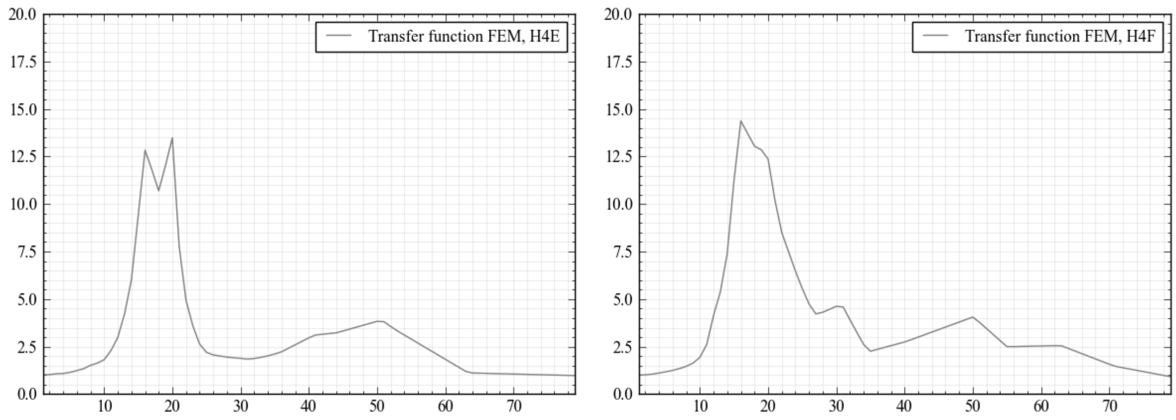

(a) Section H4E: provided transfer function FEM model

(b) Section H4F: provided transfer function FEM model

Figure 5.28: Provided transfer functions FEM model, ENKA

By multiplying the transmission function shown in Figure 5.27 with these FEM transfer functions of the building, the transfer functions including the soil-structure interaction are obtained, which can be compared with the transfer functions calculated with the transfer function model for these sections.

The comparison is shown in Figure 5.29. Please note that the scale used in Figure 5.28 differs from the scale used in Figure 5.29.

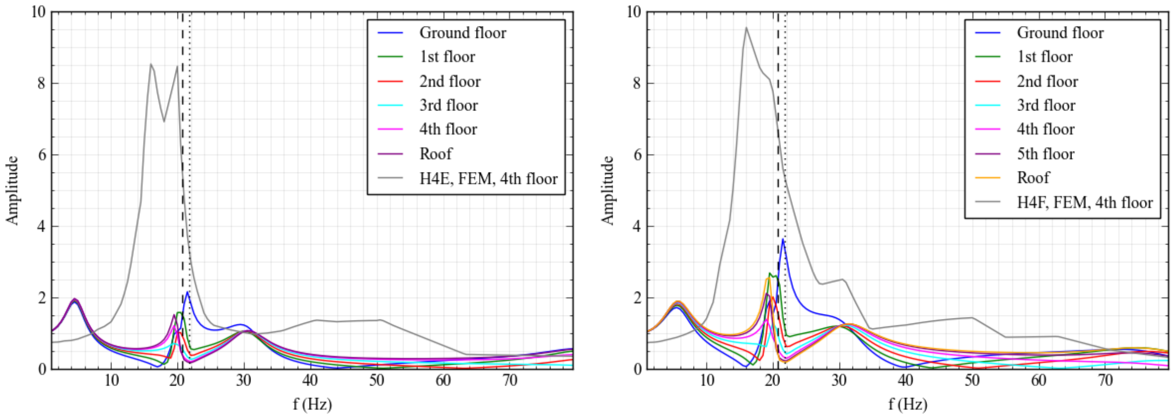

(a) Section H4E: comparison transfer functions walls **(b)** Section H4F: Transfer functions mid-span floors

Figure 5.29: Comparison transfer functions FEM model ENKA and transfer function model, floor frequencies denoted with vertical lines

Two interesting observations can be made from this comparison. The first one is that the transfer functions from the FEM model do not contain the peak corresponding to the soil-building resonance frequency of the entire building. This conforms however to the principles of the soil-structure interaction: this resonance is a combination of the stiffness of the soil-foundation system and the mass of the building. This is illustrated in Figure 5.30. In the case of the FEM transfer functions for ENKA, there is no spring and damper system present and the vibrations are just applied to the base of the building. Although the vibrations are reduced with the transmission function, the damping effect due to the inertial interaction of the building with the soil does not take place, resulting in higher amplifications of the imposed vibrations.

The second observation is the large discrepancy between the amplitudes of the transfer function model and the transfer functions provided in the original case study. The peaks take place around the natural frequency for both models, which implies that the same boundary conditions were used for the floors in the FEM model. However, the amplitudes calculated with the FEM model are approximately four to five times larger than those calculated with the transfer function method. This is particularly interesting because when comparing the results from the transfer function model with the results of the HERO case study, the conclusion was that the transfer function model seemed to overestimate the transmittance of the vibrations when compared to the FEM model. In the FEM model of the HERO project, the amplitude of the V_{max} free field vibrations was reduced by a factor of approximately 0.5, whereas the transfer functions for the HERO project suggest an amplification factor of 8 to 9 times the free-field vibrations. The building geometry for both case studies is however very similar and the same type of medium stiff soil is assumed. The most feasible explanation for this discrepancy is therefore again the difference in the modelling of the soil-structure interaction.

Because the V_{max} values calculated with the FEM model for ENKA did not comply with the target values A_1 or A_2, different measures were researched to lower the vibrations in the building. The effects of adding additional walls, lowering the number of storeys, changing the mass of the floors, adding mass to the foundation and using base isolation were considered. Due to the high costs of base isolation, the effect of the other measures was first analysed. According to the ENKA FEM model combined with their transmission function, none of these measures could lower the values for V_{max} sufficiently. Therefore it was decided to use base isolation, which reduced the V_{max} values sufficiently.

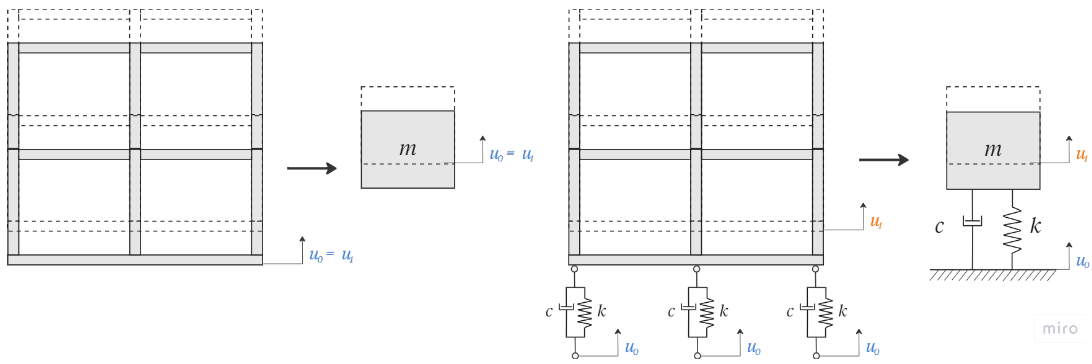

Figure 5.30: Left: no soil-building resonance, right: soil-building resonance

5.3.5. Comparison ENKA, HERO and transfer function method

Based on the background of railway-induced vibrations and the highlighted importance of soil-structure interaction, the decision for the most accurate model leans toward the HERO model: it takes into account both the inertial and kinematic soil-structure interaction. It is nonetheless difficult to determine this with certainty, since there were no measurements carried out in the buildings after their construction to validate the accuracy of the models. Also, although the kinematic interaction effect does lower the imposed vibrations, the main reductions are generally found for higher frequencies, whereas mainly the peaks between 0-15 Hz contribute to the exceedance of the serviceability criteria for the V_{max} values. This first soil-building resonance peak in the transfer function model would have to be reduced by an additional 70 % to obtain the same V_{max} values as found by the FEM study, which is considerably high.

5.4. Conclusion

The results from the FEM models of both case studies differ significantly, although the building geometry and soil conditions are comparable. The transfer function model results are in between those of both case studies. The FEM model for the HERO project suggests that the relatively high free-field vibrations will be more than halved by the combination of soil-structure interaction. Measures taken for this project are solely the addition and stiffening of the foundation of specific areas of the building. On the other hand, the calculations for the ENKA project suggest that the relatively low free-field vibrations are instead amplified substantially and conclude that the only way to reduce these vibrations is to use costly base isolation. Soil-structure interaction is modelled in the HERO project, but for the ENKA project only a general transmission function is used. Additional damping by the inertial interaction of the building with the soil is therefore not accounted for, which leads to conservative results, in line with the findings from the literature study in chapter 2. For the transfer function method, the inertial soil-structure interaction is accounted for, but the kinematic interaction is not taken into account. However, the peaks that correspond the most to the high V_{max} values for the HERO project are in the lower frequency range, whereas the literature study in chapter 2 shows that kinematic interaction mainly reduces the higher frequencies substantially and the effect is lesser for lower frequencies.

The main difficulty when comparing the results of the case studies and the transfer function model is that for both projects, no measurements after the construction of the building inside the building are available for comparison. Therefore, no conclusion can be drawn on how the resulting railway-induced vibrations in the building are best estimated. The peaks in the transfer function model are however supported by theory and changes in the building parameters can clearly be distinguished in the transfer function spectra. Therefore, the transfer function model is considered to be suitable for the preliminary design of apartment buildings subjected to railway-induced vibrations to assess how different structural parameters influence the building's behaviour.

6 Parameter study

6.1. Introduction

Now that the method for analysing the effect of different structural parameters on the building response is established, this chapter will focus on varying these parameters to find a residential timber building design in which the railway-induced vibrations are minimised. The resulting vibrations in the building are highly dependent on the free-field vibrations the structure is subjected to. However, these vibrations are location-specific and can vary greatly between different projects. Therefore, first, the influence of the different structural parameters on the transfer functions of the building is analysed. The effect of changes in the floor- and wall configuration, soil- and foundation characteristics and the number of storeys in the building are investigated. This way, the necessary knowledge is gained to optimise the building such that the peaks of the transfer function coincide minimally with the peaks in the free-field ground vibration spectra.

6.2. Building section

For the basis of the parameter study, a simple apartment building of four storeys is used, as shown in Figure 6.1. Since a section of the structure is simplified to a 1D structure for the transfer function model, as explained in chapter 4, the number of apartments next to each other is arbitrary for the dynamic analysis. The storey height throughout the parameter study is chosen to be 3.3 m. In Figure 6.2, the floor plan of two apartments next to each other in the timber apartment building is shown. Each floor has a span of 3.6 m and the initial width of the apartments is chosen to be 10.8 m, resulting in apartments with an area of 78 m^2. The soil- and foundation parameters, the wall configuration and the floor configurations that are used for the initial design of the building are discussed subsequently.

6.2.1. Soil- and foundation parameters

Initially, the soil is chosen to be similar to the soil used in the HERO case study: a medium stiff sand soil. The corresponding parameters are included in Table 6.1. The design of a pile foundation is outside the scope of this research, but because the soil is chosen to be equal to the soil for the HERO case study, it is assumed that the same pile foundation can be applied. Based on the total weight of the timber apartment building compared to the concrete building of the HERO case study, it is assumed that the pile dimensions can be reduced from a pile diameter d of 0.5 m to a pile diameter of 0.3 m. The chosen pile foundation dimensions are given in Table 6.2. Because the design of the pile foundation is beyond the scope of this thesis, the pile characteristics are derived from the pile foundation used for the HERO case study. The diameter of the piles is however reduced, due to the much lower weight of timber when compared to concrete. Equivalent to the case study, a pile group of eight piles is used for the parameter study. The piles are spaced evenly over the width of the apartment.

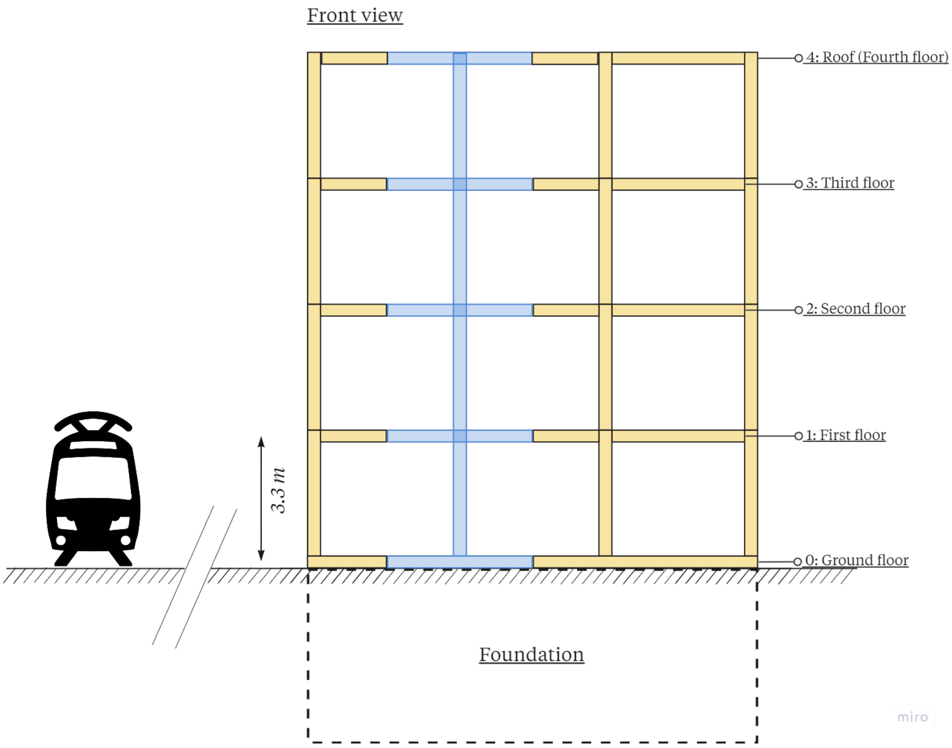

Figure 6.1: Timber building structure

Table 6.1: Subsoil characteristics

		Subsoil	
Shear wave velocity	V_s	150	m/s
Modulus of Elasticity	E_S	$50 \cdot 10^6$	N/m^2
Mass density	ρ_s	1800	kg/m^3
Poisson modulus	ν_s	0.3	[-]

Table 6.2: Pile characteristics

		Pile type
Pile length	L_d	15.5
Diameter	d	0.3
Modulus of Elasticity	E_p	$15 \cdot 10^9$
Mass density	ρ_p	2500

6.2.2. Initial wall configuration

The initial layup for the walls of the timber apartment building is CLT 100 L5S: the cross-section consists of five layers, each with a thickness of 20 mm, resulting in a total thickness of 100 mm. For the four-storey apartment building used as the basis for the parameter study, the checks for buckling and axial stress as described in Appendix E are carried out for the CLT 100 L5S cross-section. The detailed results can be found in Appendix G. The checks are performed for each of the four floor configurations which are discussed in subsection 6.2.4, since all these floors have a different mass. The resulting unity checks are summarised in Table 6.3.

Whereas the concrete walls in both case studies were isotropic, not all layers in the CLT wall have the same stiffness in the axial direction. Only the layers with a fibre orientation in the axial direction

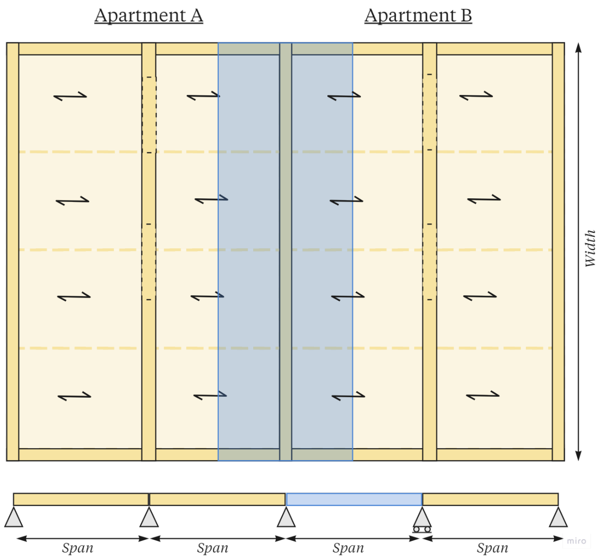

Figure 6.2: Floor plan timber apartments

Table 6.3: Summary of unity checks walls, for each of the four floor configurations

	Axial stress	Buckling, compression	Buckling, combined
CLT-W	0.13	0.43	0.33
CLT-D	0.09	0.29	0.26
HB-W	0.11	0.35	0.29
HB-D	0.1	0.32	0.27

participate in the axial stiffness. Therefore, to accommodate the CLT walls in the transfer function model, an equivalent Young's modulus is calculated. That way, the entire area of the walls is still taken into account for the calculation of the mass of the building, but only the layers of the wall that contribute to the axial stiffness are taken into account for the calculation of the transmission of the vibrations. If a symmetric CLT layup is assumed, the equivalent Young's modulus for the five-layer CLT wall considered is calculated by taking the ratio of the thickness of the effective layers to the total thickness of the wall panel and multiplying this with the Young's modulus:

$$E_{effective} = E_{0,g,mean} \cdot \frac{t_{effective}}{t_{total}} = 6600\, N/mm^2 \tag{6.1}$$

6.2.3. Initial connection

For the initial connection between the floors and the walls, the suspended floor method outlined in chapter 3 is implemented. It is assumed that for the mid-rise buildings considered in this parameter study, the transmission strips will have sufficient load-bearing capacity to resist the vertical forces. By using the suspended floor connection, high vertical forces perpendicular to the grain of the floor are avoided. For this connection, the support conditions of the floors are assumed to be hinged. The structural verification of the connection is considered beyond the scope of the study.

6.2.4. Initial floor configuration

As discussed in section 3.4, four different floor systems are considered for the parameter study. Each floor configuration differs from the others in terms of mass and natural frequency, due to the type of floor system and type of finish used. The structural verifications as specified in the NEN-EN 1995-1-1+C1+A1:2011 in terms of bending, shear force and deformations are used to determine the cross-sectional properties of each of the floors. For the walking vibrations, the prEN 1995-1-1:2023 is consulted. In Appendix E these structural verifications are outlined and the corresponding calculations

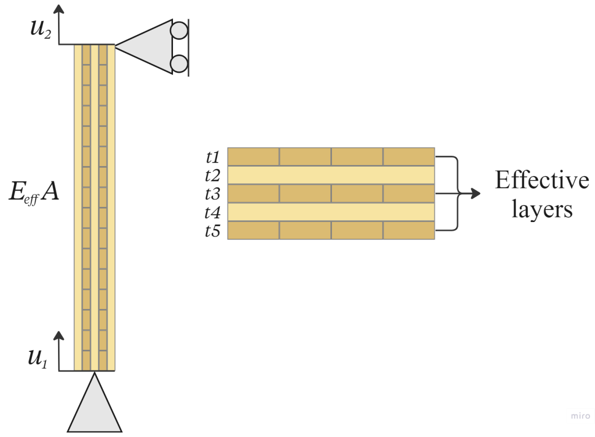

Figure 6.3: Equivalent Young's modulus $E_{effective}$ for wall system

can be found in Appendix G.

In Table 6.4, the unity checks for the CLT floors can be found. The same layup of 140 L5S[1] is used for both floor types. From Table 6.4 it can be seen that the deformations are governing in the design of the CLT floor with a wet screed, with a unity check of 0.94 and the walking-induced vibrations in terms of stiffness are the limiting factor of the CLT floor with a dry screed, with a value of 0.98. The deformation check is higher for the CLT floor with a wet screed because the imposed permanent load is higher due to the additional weight of the screed and floor finishes as described in section 3.4. Also, the stiffness of the screed is only taken into account for the vibration checks, in accordance with the prEN 1995-1-1:2023, but not included in the other cross-sectional checks, complying with the NEN-EN 1995-1-1+C1+A1:2011. This additional mass of the screed does however have a positive effect on the walking induced vibrations. Here, the additional flexural rigidity is accounted for, both in longitudinal direction EI_L and transverse direction EI_T. Those two factors combined result in a lower unity check for the walking-induced vibrations when compared to the lighter and less stiff CLT floor with a dry screed.

Below, the parameters used for the transfer function model are shown for both CLT floors. The finishes as specified in section 3.4 are included in the mass of the floor m_F. Furthermore, an additional mass of 75 kg/m^2 is added to account for the presence of furniture and partitional walls, equivalent to the added weight to the floors in the case studies. In the flexural rigidity EI_L, the stiffness of the wet screed is also included. With these values, the natural frequency of the floors $f_{0,F}$ is calculated for a one-way slab with a span of 3.6 meters, simply supported on both sides. The natural frequency ClT floor with a wet screed is 10.18 Hz, 2.76 Hz lower than the natural frequency of the CLT floor with a dry screed. This is due to the fact that the mass of the floor with a wet screed is almost twice as high in comparison to the mass of the floor with a dry screed, which lowers the natural frequency more than the flexural rigidity is increased due to the additional stiffness of the wet screed.

Table 6.4: Summary of unity checks CLT floors

	Bending	Shear	Rolling shear	Deformations	Vibrations, stiffness	Vibrations, velocity
CLT-W	0.3	0.06	0.32	0.94	0.53	0.29
CLT-D	0.21	0.04	0.22	0.59	0.98	0.6

[1]**5** layers, **s**ymmetric and a total thickness of 140 mm

CLT-W: CLT floor, wet screed

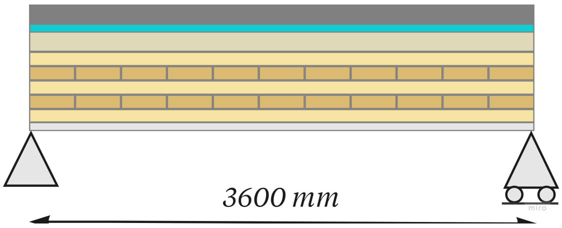

Layup: [40, 20, 20, 20, 40]

$$m_F = 405.6\,kg/m^2$$

$$EI_L = 2.86 \cdot 10^6\,Nm^2/m$$

$$f_{0,F} = \frac{\pi^2}{2\pi L^2} \cdot \sqrt{\frac{EI_L}{m_F}} = 10.18\,Hz$$

$$\zeta = 0.04$$

CLT-D: CLT floor, dry screed

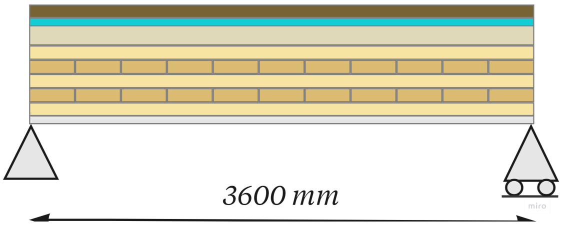

Layup: [40, 20, 20, 20, 40]

$$m_F = 185.6\,kg/m^2$$

$$EI_L = 2.12 \cdot 10^6\,Nm^2/m$$

$$f_{0,F} = \frac{\pi^2}{2\pi L^2} \cdot \sqrt{\frac{EI_L}{m_F}} = 12.94\,Hz$$

$$\zeta = 0.04$$

Similar to the CLT floors, the LVL hollow box floors are designed such that they satisfy the structural requirements outlined in Appendix G. For the design of the cross-sections, the standard dimensions from Storaenso [2] are consulted. The provided tables used for the design can be found in Appendix F. Both the upper and lower panel are designed as LVL-X panels, whereas the rib is designed with LVL-S. It was again possible to use the same cross sectional properties for both the hollow box floor with a wet screed and the hollow box floor with a dry screed, analogous to the CLT floors. Using the minimum thicknesses prescribed in Appendix F for the flanges and height of the ribs, both floors satisfy the structural requirements. The resulting unity checks are summarised in Table 6.5. For the hollow box floor with a wet screed, it can be seen that the check on shear force is governing, with a value of 0.82, whereas the check for walking-induced vibrations in terms of stiffness of 0.84 is governing for the hollow box floor with a dry screed. The shear force check is higher for the hollow box floor with a wet screed due to the higher permanent load, which in turn positively influences the response to walking-induced vibrations. The difference in performance on the walking-induced vibration checks is in the case of the hollow box sections mainly caused by the low transverse stiffness of the LVL cross-section. For the velocity criteria check, this lower transverse stiffness results in a much higher multiplication factor[3], automatically resulting in a higher root mean square velocity v_{RMS} and thus a higher unity check. A similar effect occurs when considering the stiffness unity check for the walking-induced vibrations. This unity check calculates the deformation of the slab when subjected to a load of 1 kN[4]. A higher value of the effective width b_{ef}, which is incorporated in this calculation, results in a lower deformation and thus a lower unity check. The transverse stiffness of the cross-section is an important parameter in the calculation of this effective width, with a higher transverse stiffness resulting in a higher effective width. This, combined with the higher longitudinal stiffness of the hollow box floor with a wet screed results in a ≈3.23 times lower unity check compared to the hollow box floor with a dry screed.

Displayed below are the parameters used for the transfer function model for both LVL hollow box floors. Again, the finishes as specified in section 3.4 are included in the mass of the floor m_F and the additional mass of 75 kg/m^2 is added. Equivalent to the CLT floors, the stiffness of the wet screed is included in the flexural rigidity EI_L for the dynamic calculations, but excluded for the other cross-sectional checks. Taking into account a simply supported one-way slab with a span of 3.6 m results in a natural frequency for the LVL hollow box floor with wet screed $f_{0,F}$ of 20.42 Hz and a higher natural frequency of the LVL hollow box floor with a dry screed of 22.69 Hz. This difference can be explained with the same reasoning as for the CLT floor.

[2] Stoarenso, producer of amongst others LVL hollow box floors: https://www.storaenso.com/en/products/mass-timber-construction/building-products/rib-panels

[3] k_{imp}, see calculations in Appendix G

[4] See calculations for w_{1kN} in **??**

HB-W: LVL hollow box floor, wet screed

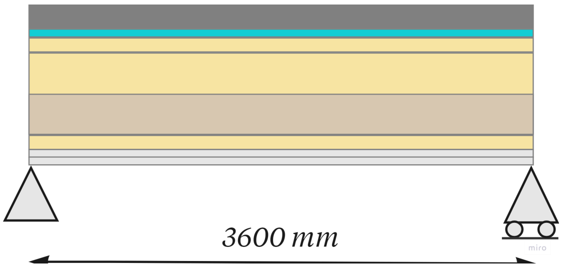

Centre-to-centre ribs: 600 mm
Height rib: 200 mm
Thickness rib: 45 mm
Thickness upper flange: 27 mm
Thickness lower flange: 27 mm

$$m_F = 309.19\ kg/m^2$$

$$EI_L = 8.77 \cdot 10^6\ Nm^2/m$$

$$f_{0,F} = \frac{\pi^2}{2\pi L^2} \cdot \sqrt{\frac{EI_L}{m_F}} = 20.42\ Hz$$

$$\zeta = 0.04$$

HB-D: LVL hollow box floor, dry screed

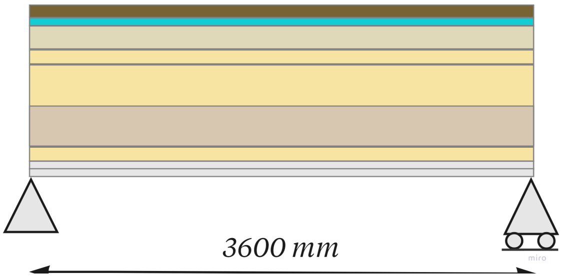

Centre-to-centre ribs: 600 mm
Height rib: 200 mm
Thickness rib: 45 mm
Thickness upper flange: 27 mm
Thickness lower flange: 27 mm

$$m_F = 229.19\ kg/m^2$$

$$EI_L = 8.03 \cdot 10^6\ Nm^2/m$$

$$f_{0,F} = \frac{\pi^2}{2\pi L^2} \cdot \sqrt{\frac{EI_L}{m_F}} = 19.53\ Hz$$

$$\zeta = 0.04$$

Table 6.5: Summary of unity checks LVL hollow box floors

	Bending, middle	Bending, edge	Shear, middle	Shear, edge	Deformations	Vibrations, stiffness	Vibrations, velocity
HB-W	0.08	0.08	0.82	0.75	0.26	0.26	0.19
HB-D	0.07	0.07	0.73	0.67	0.23	0.84	0.62

6.2.5. Evaluation initial building section

With the parameters described in the previous chapters, the first transfer functions are set up. A transfer function at the **connection of the floors with the walls** and a transfer function **mid-span of the floors** is calculated for each of the floor configurations. These locations are visualised in Figure 6.4. For the initial evaluation, the function is shown for each of the storeys. The amplification between floors can be visualised this way. For the remainder of the parameter study, only the transfer function that displays the highest amplification factor per floor type will be presented, for the sake of clarity. In practice, the maximum amplification often occurs at the highest storey of the building [40]. Lastly, it should be noted that the scale of the graphs in this section differs from the scale used in the graphs for the case study due to the generally higher amplitudes found for the timber buildings in this section.

CLT floor systems

In Figure 6.5 the transfer functions for the floor configuration of a CLT slab with a wet screed are shown. The natural frequency of the floor of 10.18 Hz can clearly be distinguished and is annotated with a dashed line in the graph. At this natural frequency, it can be seen that the transfer function of the walls approaches zero, whereas there is a peak in the transfer functions at mid-span of the floors. This means that the walls at this frequency move out of phase with the floors. The amplification factor is relatively high, with a maximum factor of 12.5 at the natural frequency of the floors. This means that the free-field vibrations at this frequency are amplified substantially. This is related to the effect that was described in subsection 2.8.3: when the soil-building frequency is higher than the natural frequency of the floors, the soil damping effect does not occur. The vibrations are intensified instead, resulting in higher vibration transmission from the free-field vibrations to the building. For the concrete buildings in the case study, the theoretical soil-building frequency took place around 10 Hz and the

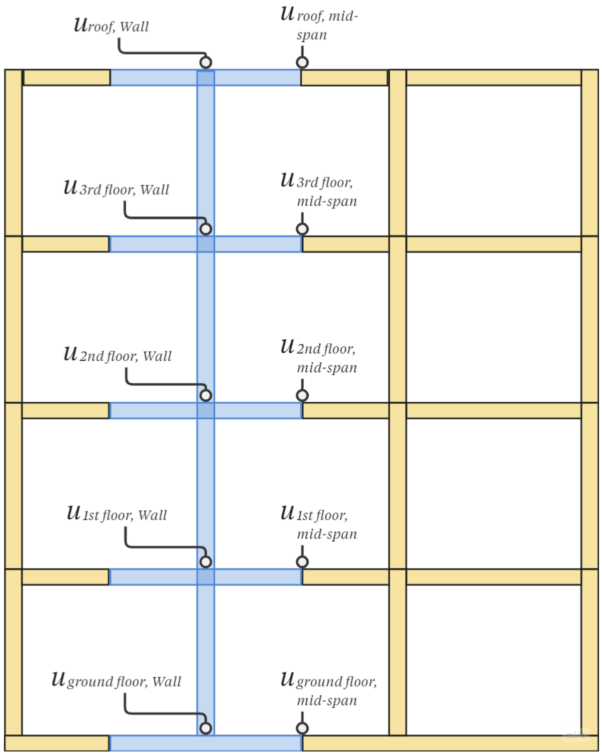

Figure 6.4: Positions for which the transfer functions are calculated. The connection with the walls $u_{storey,Wall}$ and mid-span of the floors $u_{storey,mid-span}$

clamped floors had a natural frequency of above 20 Hz. Due to its weight, the much lighter CLT timber building considered now has a significantly higher theoretical soil-building resonance frequency of 23.5 Hz, whereas the natural frequency of the simply supported floors is much lower, at 10.18 Hz.

Because the high amplification factors found for the initial building due to the lack of soil damping, the parameter study will also focus on ways to mitigate this effect. There are two measures that can aid in this goal: increasing the mass of the building, which will lower the theoretical soil building resonance, or increasing the natural frequency of the floors. Both can be achieved in different ways. The mass of the building can for example be increased by increasing the area of the apartments, adding additional storeys or considering carrying out the ground floor in concrete. The natural frequency of the floors can be increased by increasing the stiffness of the floors, decreasing the span or if different boundary conditions are applied. Lastly, softer soils will also result in lower soil-building resonance frequencies. However, the soil stiffness is location dependent and can not be used as a measure to mitigate the vibrations.

The second peak in the transfer functions of the CLT floors is related to the walls. Because the walls have the same properties for all the four floor configurations, it results in the same natural frequency for each of the floors, 69.5 Hz. However, as explained in chapter 4, the floors influence the transmittance of forces between the storeys, influencing the natural frequency of the walls. Therefore, the second peak is shifted to a lower frequency and is different for each of the floor types. Furthermore, it can be concluded that at this frequency, the peaks in the transfer functions at the walls are higher than the peaks in the transfer functions mid-span of the floors. This signifies that the floors dampen the vibrations imposed by the walls and both the floors and walls move in-phase with each other.

The CLT floor with a dry screed displays similar behaviour to the CLT floor with a wet screed. The transfer functions shown in Figure 6.6 show comparable interaction and amplification of the soil-building resonance frequency with the natural frequency of the floors. Furthermore, the same out of phase movement of the walls can be detected in the transfer functions at the location of the connection of the floors with the walls, at the natural frequency of 12.93 Hz. However, for the CLT floor with a dry screed, the maximum amplification factor is 15, significantly higher than the 12.5 found for the CLT floor with a wet screed. This occurs due to the lower mass of the building with the CLT floor with a dry screed when compared to the Clt floor with a wet screed. Due to this lower mass, less energy is needed to excite the system, which results in higher amplitudes at the resonance frequencies of the building.

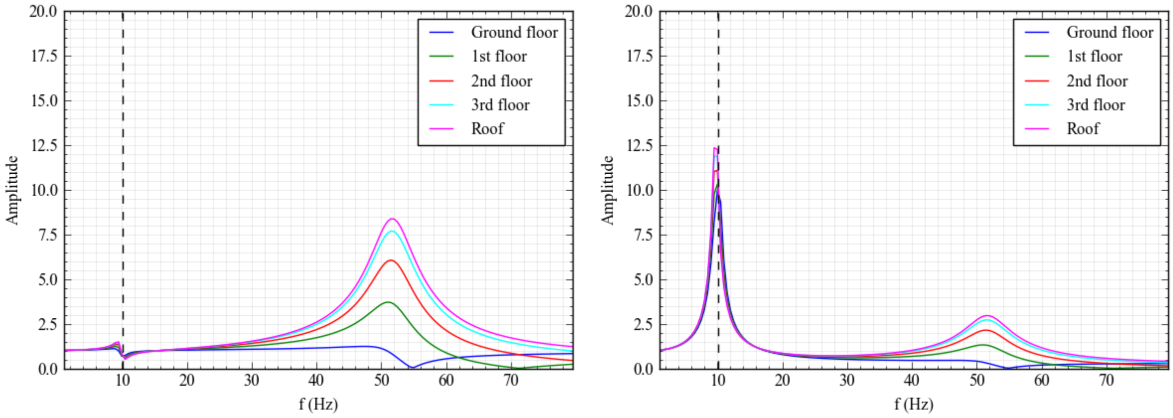

(a) Transfer functions walls

(b) Transfer functions mid-span floors

Figure 6.5: Transfer functions CLT slab, wet screed, for initial parameters. The vertical line highlights the natural frequency of the floors

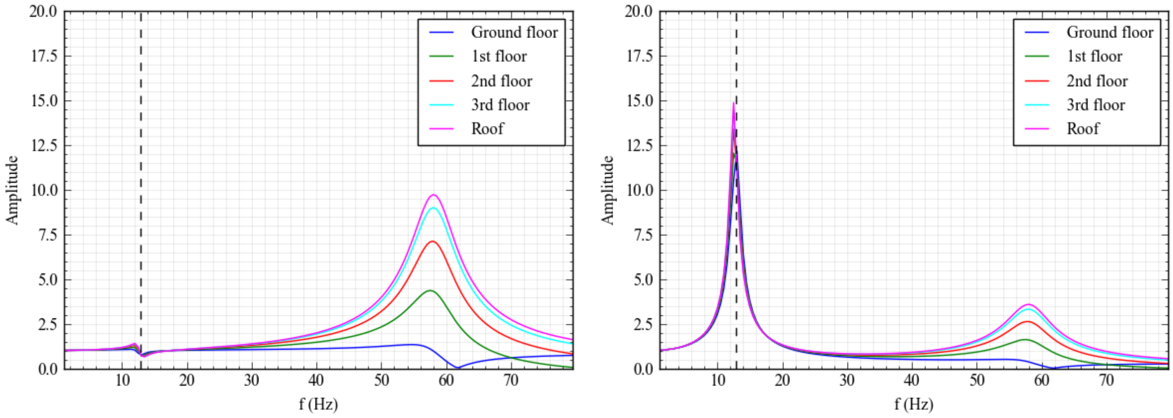

(a) Transfer functions walls

(b) Transfer functions mid-span floors

Figure 6.6: Transfer functions CLT slab, dry screed, for initial parameters. The vertical line highlights the natural frequency of the floors

Hollow box floor systems

When comparing the transfer functions of the LVL hollow box systems with those of the CLT floors, there are shared characteristics. For both the transfer function of the hollow box slab with a wet screed, shown in Figure 6.7 and the transfer function of the hollow box slab with a dry screed, shown in Figure 6.8, the amplitudes in the transfer functions at the walls approach zero where the natural frequency of the floors occurs. Again, the natural frequency of the hollow box slab with a wet screed of 20.42 Hz and of the hollow box slab with a dry screed of 22.28 Hz can clearly be distinguished and is annotated with the dashed line in the graphs. Furthermore, the walls move out of phase when the natural frequency of the floors occurs. Since the natural frequencies of both hollow box floors are higher than those of the CLT floors and, although still lower, closer to the theoretical soil-building frequency, the peaks of those two different resonance phenomena do not coincide fully. Similar to the CLT floors, the soil does not exhibit its full damping potential. The maximum amplitudes found for the transfer functions are 13 for the hollow box floor with a wet screed and 13.5 for the hollow box floor with a dry screed. The theoretical wall resonance frequency is influenced and shifted to a lower frequency by the natural frequency of the considered floors, in the same way as was explained for the CLT floors. For the hollow box floor with a wet screed, wall resonance occurs at $\approx$ 58 Hz and for the hollow box with a dry screed at $\approx 60Hz$. At this frequency, the walls move in phase with the floors. From the lower amplitude of the peak mid-span of the floors, it can be seen that the floors have a damping effect at the wall resonance frequency.

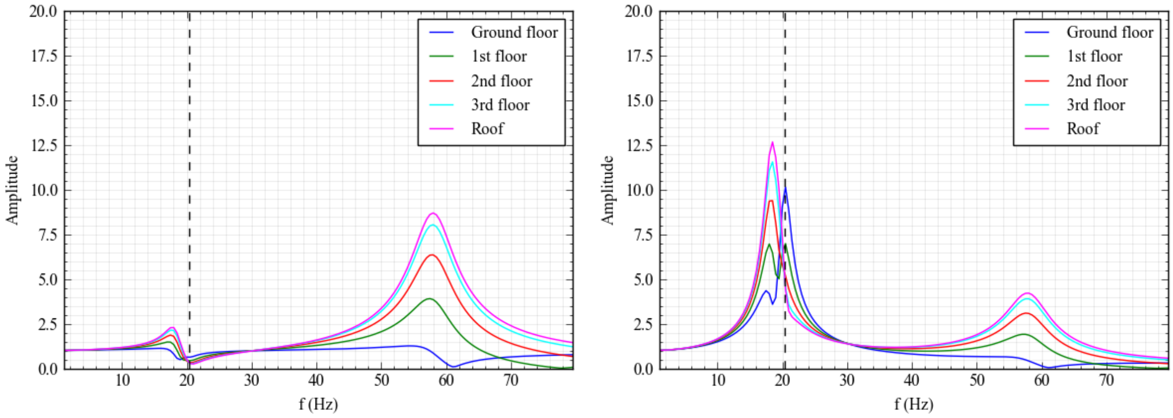

(a) Transfer functions walls

(b) Transfer functions mid-span floors

Figure 6.7: Transfer functions hollow box slab, wet screed, initial parameters. The vertical line highlights the natural frequency of the floors

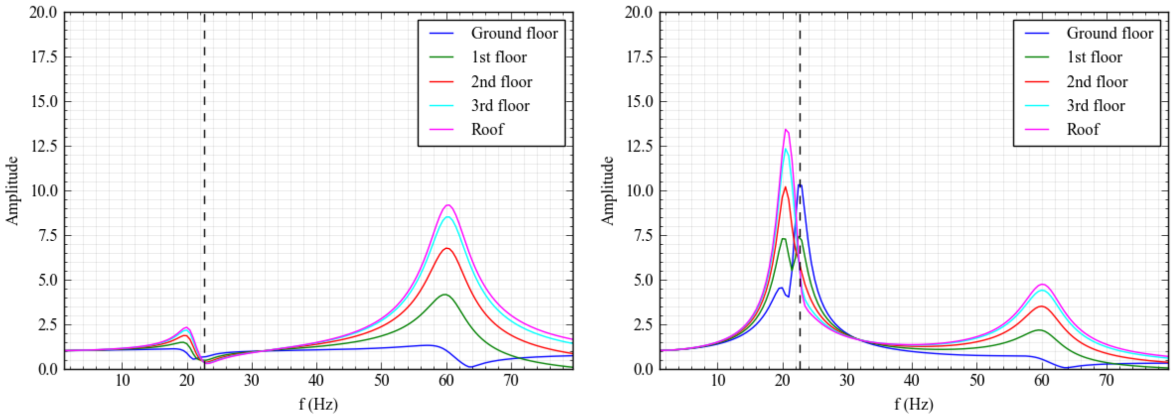

(a) Transfer functions walls

(b) Transfer functions mid-span floors

Figure 6.8: Transfer functions hollow box slab, dry screed, initial parameters. The vertical line highlights the natural frequency of the floors

6.3. Influence of soil-structure interaction

The first variable for which its effect on the transfer functions of the different floor configurations is analysed is the soil-structure interaction. For the initial pile foundation, the effect of different types of soils on the transfer functions is researched. These types of soils are equivalent to the types of soils analysed in the case study and are repeated in Table 6.6. Additionally, the pile foundation is compared to a shallow foundation. Subsequently, the influence of the area of the shallow foundation is mapped out.

Table 6.6: Different subsoil parameters

Soil	E_s **[Mpa]**	G_s **[Mpa]**	V_s **[m/s]**
Soft clay	10	12	100
Medium clay	20	15	200
Loose sand	25	20	150
Dense, stiff sand	75	70	300

6.3.1. Pile foundation

To analyse the effect of different soil types on the response of the timber apartment buildings, the transfer functions at mid-span are examined for the four floor configurations. In line with the findings for the concrete buildings in the case study, the softer soil dampens the overall building response whereas higher amplifications are found for the response of buildings founded on stiffer soils. In Figure 6.9 the transfer functions for the building with a CLT floor with a wet screed and for the CLT floor with a dry screed are included and in Figure 6.9 the transfer functions for the building with respectively the hollow box section with a wet screed and the hollow box section with a dry screed are shown.

In general, by changing the soil parameters, the soil-building frequency shifts to a lower or higher frequency. Since this frequency is dominated by the natural frequency of the floors for all the four floor configurations, this effect is not evident in Figure 6.9. In Table 6.7, the maximum found amplification factors are summarised for each of the floors and each of the soil types analysed. For each of the floor types, the highest amplification factor is found for the dense and stiff soil, which is in line with the findings of chapter 2. The highest amplification factor is found for a CLT floor with a dry screed, of 15.39. This is consistent with the expectations, since for the initial evaluation the CLT floor with a dry screed also yielded the highest amplification factor. From the initial observation of solely these transfer functions, it may seem that a softer soil results in lower amplification of the free-field vibrations. Although this trend is true for the transfer functions, with the softer soil providing a higher damping, it should be taken into account that for these type of softer soils, the peaks found in the free-field response spectrum are also generally higher. Hence, it can not be presumed that locations with softer soil types automatically have a positive effect on the resulting building vibrations.

Table 6.7: Maximum amplification factors for different soil types

	Soft clay	Medium clay	Loose sand	Dense, stiff sand
CLT-W	9.7	11.2	11.49	14.05
CLT-D	11.82	12.47	13.54	15.39
HB-W	8.39	8.39	10.04	11.48
HB-D	9.36	9.36	10.88	12.21

6.3.2. Shallow foundation

Although pile foundations are most commonly applied in the Netherlands for apartment buildings, there are areas in which shallow foundations can be applied as well. Therefore, the difference between these two foundations is also analysed in the parameter study. Since shallow foundations are applicable for stiffer soils such as the medium stiff sand soil used for the initial building section, the main parameter that will be varied for this type of foundation is the foundation area. As elaborate calculations are typically carried out for the design of a building foundation, the results presented in this section are purely exploratory. The variation in the area of the foundation solely focuses on investigating the impact of this parameter on the transfer function of the building.

Three different situations are analysed for the shallow foundation. The area of the foundation is once taken as equal to the floor area, meaning that the shallow foundation consists of one large slab equal to the area of the building. Secondly, the transfer functions are calculated for a strip foundation, equal to half of the area of the floor plan. Lastly, a strip foundation equal to a quarter of the ground floor is

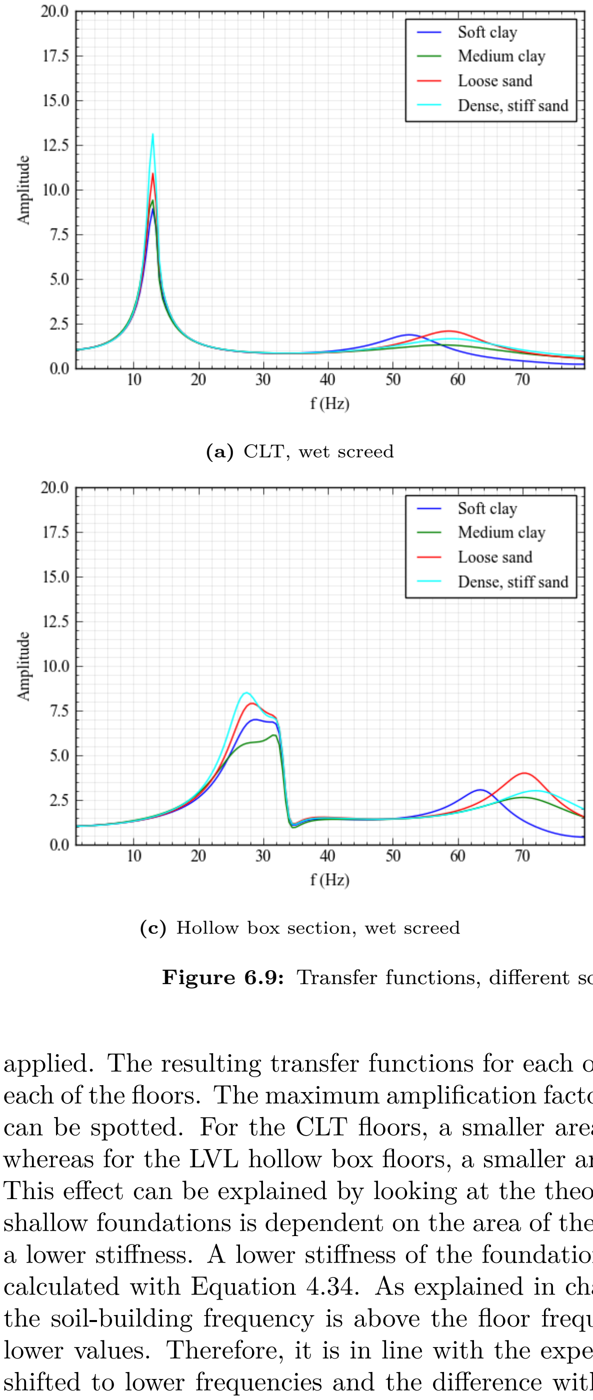

(a) CLT, wet screed

(b) CLT, dry screed

(c) Hollow box section, wet screed

(d) Hollow box section, dry screed

Figure 6.9: Transfer functions, different soil types and pile foundation, mid-span floors

applied. The resulting transfer functions for each of these three situations are shown in Figure 6.10 for each of the floors. The maximum amplification factors are summarised in Table 6.8. Two different trends can be spotted. For the CLT floors, a smaller area results in a *higher* maximum amplification factor, whereas for the LVL hollow box floors, a smaller area results in a *lower* maximum amplification factor. This effect can be explained by looking at the theoretical soil-building frequencies. The stiffness of the shallow foundations is dependent on the area of the shallow foundation, with a smaller area resulting in a lower stiffness. A lower stiffness of the foundation results in a lower soil-building frequency, which is calculated with Equation 4.34. As explained in chapter 2, the highest amplification is found for when the soil-building frequency is above the floor frequencies and the soil-building frequency is shifted to lower values. Therefore, it is in line with the expectations that when the soil-building frequencies are shifted to lower frequencies and the difference with the natural frequencies of the floor decreases, the amplitudes also decrease, as is the case for the LVL hollow box floors. In Table 6.9 the theoretical soil-building frequencies are shown for each of the shallow foundations and compared to the natural frequencies for each of the floors. Conversely, for the CLT floor with a lower natural frequency, the peaks continue to coincide. This occurs because the soil-building frequency can not be shifted to lower frequencies, bounded by the area between 0-10 Hz, leading to higher amplification even with a smaller difference between the soil-building frequency and the natural frequency of the floors. Therefore, it is concluded that whether it is beneficial or disadvantageous to increase the foundation area is strongly dependent on the theoretical soil-building frequency and the natural frequency of the regarded floor.

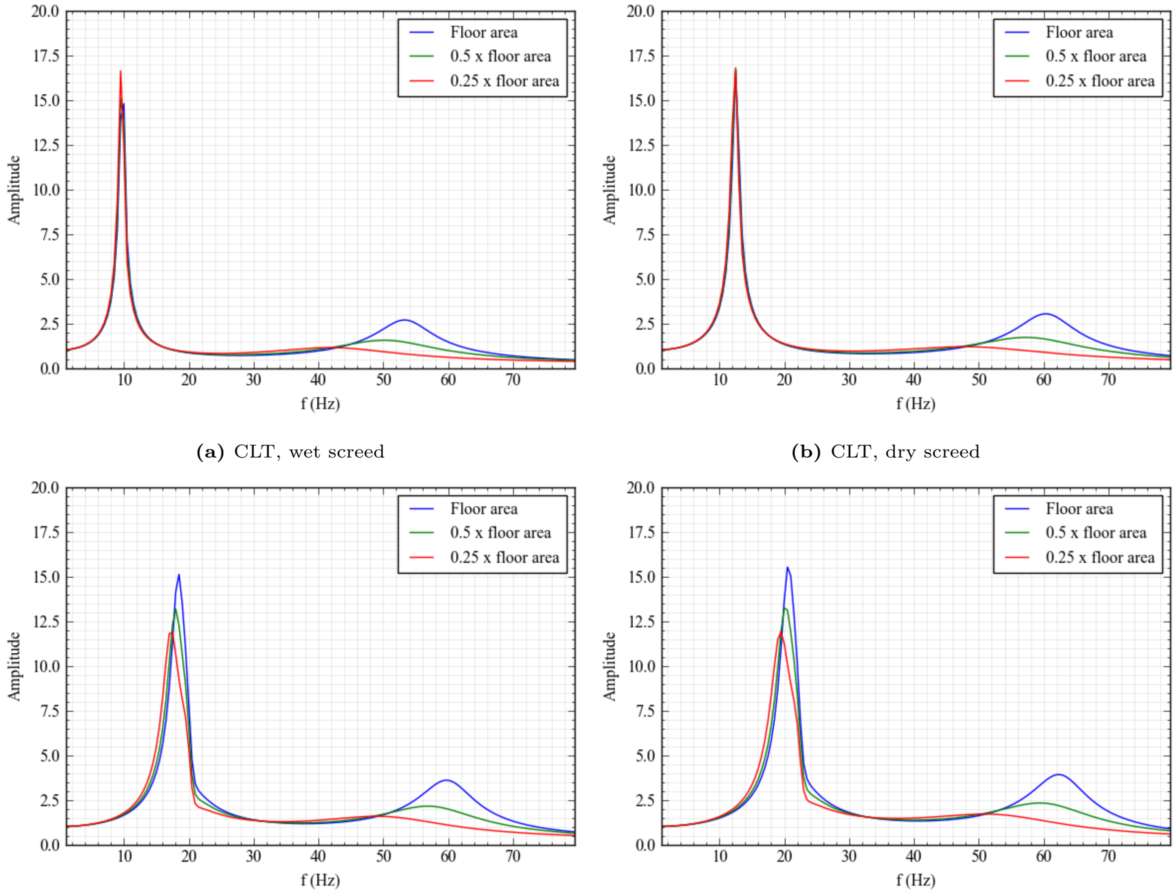

(a) CLT, wet screed

(b) CLT, dry screed

(c) Hollow box section, wet screed

(d) Hollow box section, dry screed

Figure 6.10: Transfer functions mid-span floors, variation in shallow foundation area

Table 6.8: Maximum amplification factors for different shallow foundations

	Floor area	0.5 x floor area	0.25 x floor area
CLT-W	14.8	15.09	16.63
CLT-D	16.67	16.81	16.72
HB-W	15.12	13.18	11.86
HB-D	15.53	13.24	11.91

Table 6.9: Building frequencies f_B compared to f_F for different shallow foundations

	Floor area		0.5 x floor area		0.25 x floor area	
	f_B [Hz]	$f_B - f_F$ [Hz]	f_B [Hz]	$f_B - f_F$ [Hz]	f_B [Hz]	$f_B - f_F$ [Hz]
CLT-W	23.51	*13.33*	19.77	*9.59*	16.62	*6.44*
CLT-D	33.19	*20.25*	27.91	*14.97*	23.47	*10.53*
HB-W	26.59	*6.17*	22.36	*1.94*	18.8	*-1.62*
HB-D	33.36	*10.69*	28.05	*5.38*	23.49	*0.82*

6.4. Number of storeys

One of the parameters that has a significant influence on the transfer functions of the timber apartment buildings is the number of storeys. The transfer functions at mid-span are shown for all four different floor configurations in Figure 6.11. Since the natural frequency of the walls is partially determined by the number of storeys, as can be seen in Equation 4.35, it is within the line of expectations that for each of the floor configurations, the peak corresponding to the natural frequencies of the walls shifts to lower frequencies with an increasing number of storeys. Furthermore, increasing the number of storeys increases the mass of the building, which decreases the theoretical soil-building resonance frequency calculated with Equation 4.34. The same trend can be seen as for the shallow foundations: for the LVL hollow box sections, this results in smaller amplitudes in the transfer functions due to the smaller difference between the natural frequencies of the floors compared to the higher theoretical soil-building frequency. In Table 6.10 the maximum amplitudes per floor configuration per number of storeys is summarised.

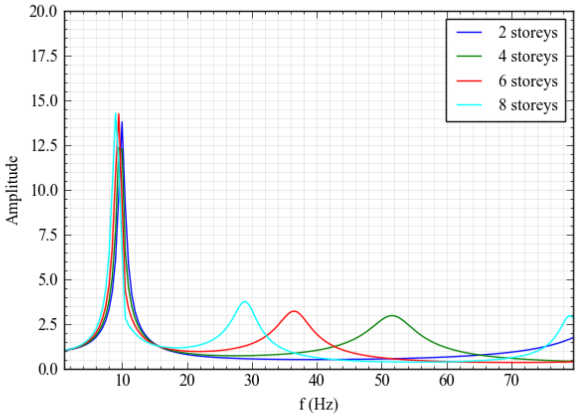

(a) CLT, wet screed

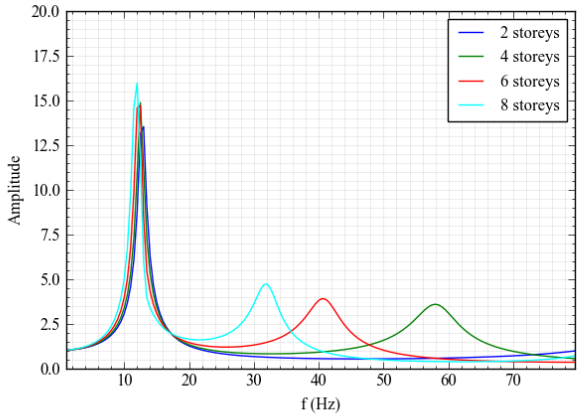

(b) CLT, dry screed

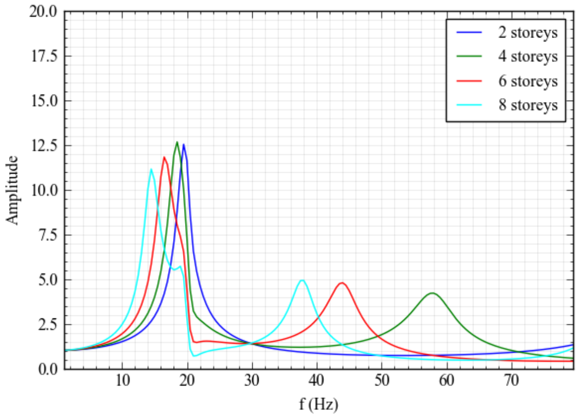

(c) Hollow box section, wet screed

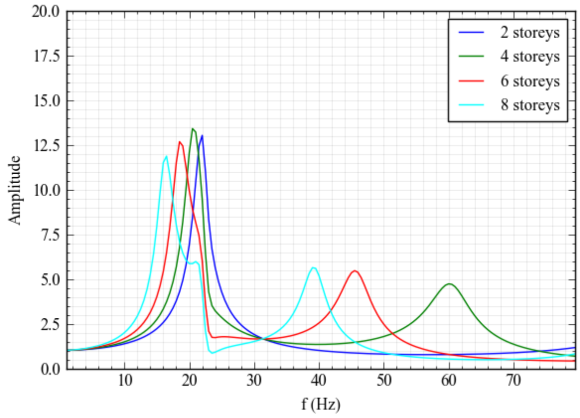

(d) Hollow box section, dry screed

Figure 6.11: Transfer functions mid-span floors, variation in number of storeys

Table 6.10: Maximum amplification factors for different number of storeys

	2 storeys	4 storeys	6 storeys	8 storeys
CLT-W	13.79	12.33	14.24	14.27
CLT-D	13.53	14.87	14.71	15.97
HB-W	13.03	13.42	12.68	11.87
HB-D	12.54	12.67	11.82	11.15

6.5. Floor configuration

When considering the floor configuration, there are two variables that can be adjusted to change the response of the building: the natural frequency of the floors can be adapted and the mass of the floor can be varied. This can be done in multiple ways. To increase or decrease the natural frequency of the floors, for example, different floor spans can be considered. Alternatively, the cross-section of the floors can be modified. Because it will be necessary to change the cross-sectional properties of the floors when increasing the span to make sure that the slab is still compliant with the structural requirements, in this section the floor thickness will be altered to analyse the effect of changing the natural frequency of the slabs. Likewise, to change the mass of the floor, the most significant variations can be made by either modifying the span or the width of the floor. The difference between a heavier floor with a wet screed and a floor with a dry screed is already taken into account by analysing the four different floor configurations.

6.5.1. Floor thickness

In Figure 6.12, the effect of increasing the floor thickness is shown. For the CLT floors, the layup is varied from 140 L5S to 200 L5S. Since the span of the floors is kept at the initial length of 3.6 meters and the floor thickness is only increased, the floors will still meet the structural requirements. For the LVL hollow box floors, the floor thickness is increased by increasing the height of the ribs from 200 mm to 360 mm. The highest maximum amplitudes for each of the variations for the CLT floors can be found in Table 6.11 and for the LVL hollow box floors in Table 6.12.

When increasing the thickness of the CLT floors, Figure 6.12 shows that although the peak corresponding to the natural frequency of the floor shifts to the higher natural frequency of the adjusted floors, there is little attenuation of the peaks. The amplitude of the CLT floor with a wet screed is reduced the least, by 1.36 %, when adding 60 mm to the layup of the floors, going from a 140 mm thickness to a 200 mm thickness. The amplitude of the CLT floor with a dry screed is reduced a bit more with 6.7 %, but the maximum amplitude with a layup of 200 L5S is still higher for the CLT floor with a dry screed when compared with the amplitude of the CLT floor with a wet screed and the same layup.

Increasing the rib height h_2 of the LVL hollow box floors has a more pronounced effect on the transfer functions, as can be seen in Figure 6.12. First of all, the increased height of the ribs visibly shifts the peak to the higher corresponding natural frequencies, similar to the CLT floors. Secondly, since the difference between the natural frequencies of the floors and the natural frequency of the walls is reduced with increasing rib height, it can be seen that the peaks corresponding to the wall resonance are shifted to a higher frequency as well. Thirdly, the earlier described effect of the natural frequency of the floors approaching and eventually surpassing the theoretical soil-building frequency is again evident. Because the additional height of the ribs barely increases the total weight of the building, the theoretical soil-building frequency is not affected substantially. For the LVL hollow box floor with a dry screed, this frequency occurs around $\approx$ 33 Hz and for the LVL hollow box floor with a wet screed this frequency takes place around $\approx$ 29 Hz. In Table 6.13, the difference between the theoretical soil-building frequency and the natural frequency of each of the floors with varying rib height is recorded. When considering these aspects, it is in line with the expectations that the floor with the highest natural frequency and a rib height of 360 mm yields the lowest amplification factor. Increasing the rib height from 200 mm to 360 mm reduces the maximum amplification factor with 28.5 % for the hollow box floor with a wet screed and with 22.2 % for the hollow box floor with a dry screed.

Table 6.11: Maximum amplification factors for different CLT floor layups

	140 L5S	160 L5S	180 L5S	200 L5S
CLT-W	13.89	13.42	13.31	13.02
CLT-D	14.88	14.82	14.77	14.68

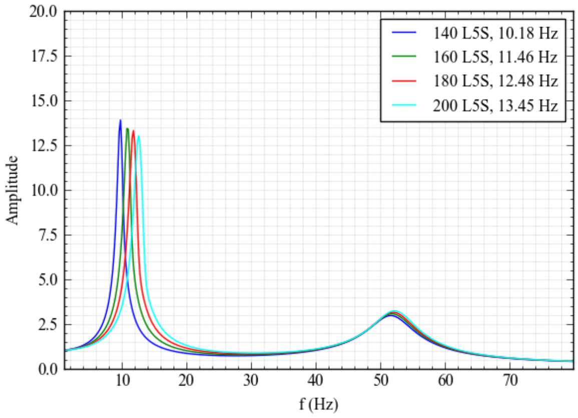

(a) CLT, wet screed

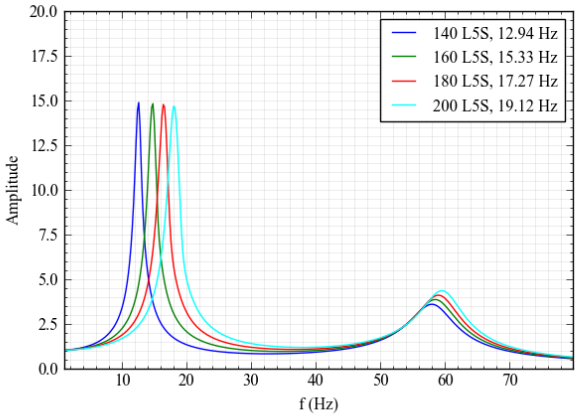

(b) CLT, dry screed

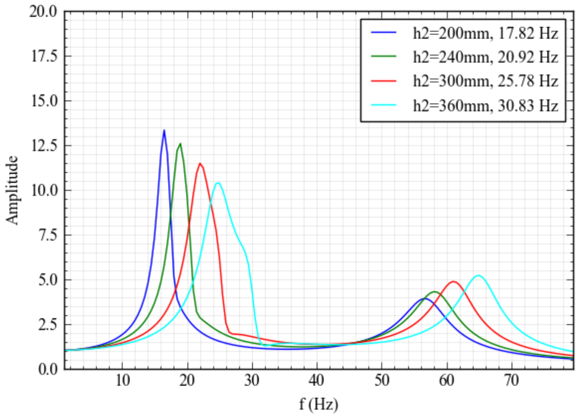

(c) Hollow box section, wet screed

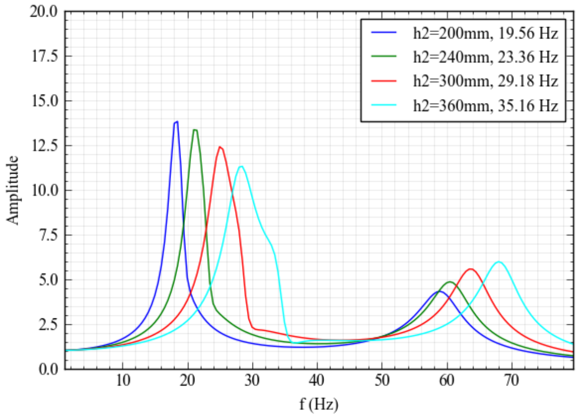

(d) Hollow box section, dry screed

Figure 6.12: Transfer functions mid-span floors, variation in floor thickness

Table 6.12: Maximum amplification factors for different LVL hollow box floor rib heights, h_2

	h2 = 200 mm	h2 = 240 mm	h2 = 300 mm	h2 = 360 mm
HB-W	13.33	12.58	11.48	10.37
HB-D	13.81	13.35	12.4	11.3

Table 6.13: Difference between soil-building frequency f_B and the natural frequencies f_F of the floors for different rib heights

	h2 = 200 mm	h2 = 240 mm	h2 = 300 mm	h2 = 300 mm
	$f_B - f_F$ [Hz]	$f_B - f_F$ [Hz]	$f_B - f_F$ [Hz]	$f_B - f_F$ [Hz]
HB-W	14.24	10.34	4.38	-1.74
HB-D	11.83	8.66	3.6	-1.44

6.5.2. Floor area

In Figure 6.13 the effect of increasing the floor area on the transfer functions for each of the four floor configurations is shown. Two observations can be made: increasing the area of the floor has the most significant effect on the LVL hollow box sections, for which the peaks corresponding to the combined floor and soil-building resonance are reduced. This effect is again less evident for both the CLT floors. Secondly, the change in soil-building frequency also influences the peaks corresponding to the natural frequency of the walls by shifting them to lower frequencies.

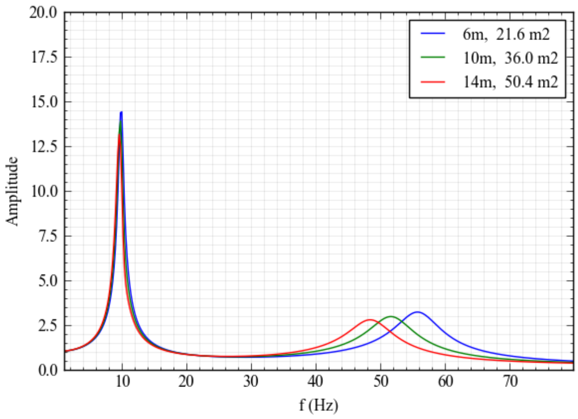

(a) CLT, wet screed

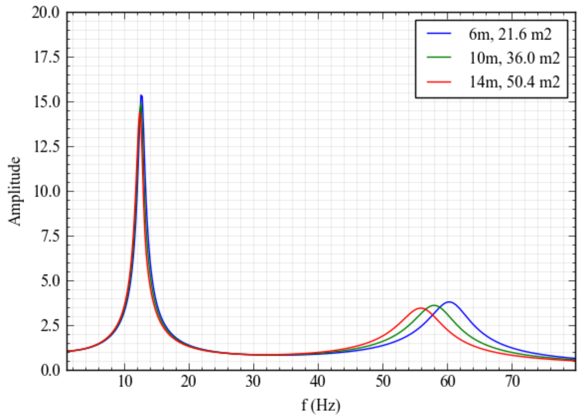

(b) CLT, dry screed

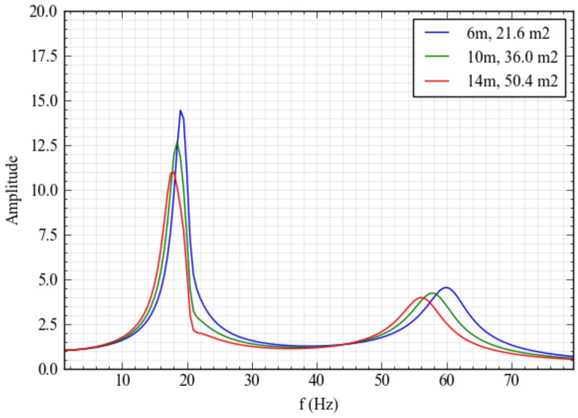

(c) Hollow box section, wet screed

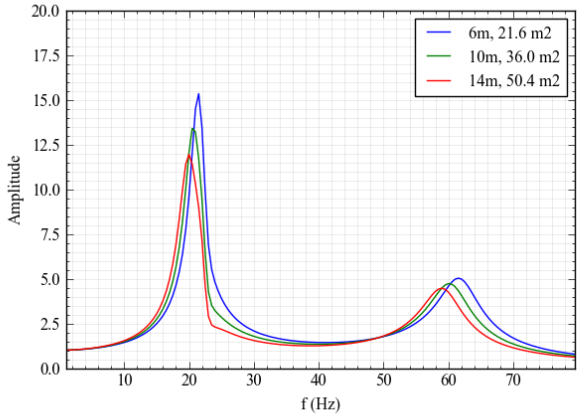

(d) Hollow box section, dry screed

Figure 6.13: Transfer functions mid-span floors, variation in floor area

6.6. Wall configuration

In Figure 6.14 the influence of the CLT wall layup on the response of the building is shown for each of the four floor configurations. Presumably, an increase in the wall thickness would also decrease the amplification between the storeys. From the transfer functions it can be seen that by increasing the wall thickness from 100 mm to 200 mm, mainly the peaks corresponding to the wall resonance at higher frequencies are reduced and shifted. Insightfully, doubling the wall thickness has only a marginal impact on the highest peaks in the spectrum, which are attributed to the combined resonance of the floors and the soil-building resonance. This is in line with the expectations, since altering the wall thickness does not have an influence on the natural frequency of the floors and only a small impact on the total mass of the building.

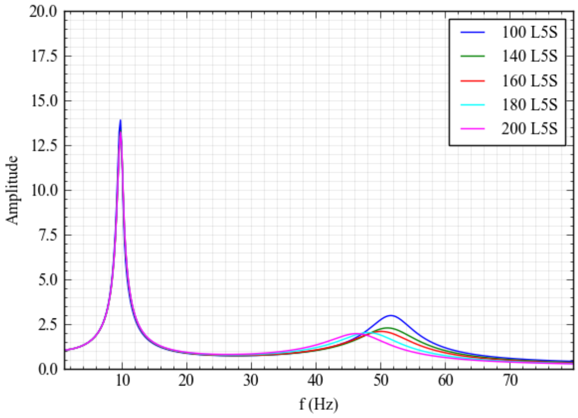

(a) CLT, wet screed

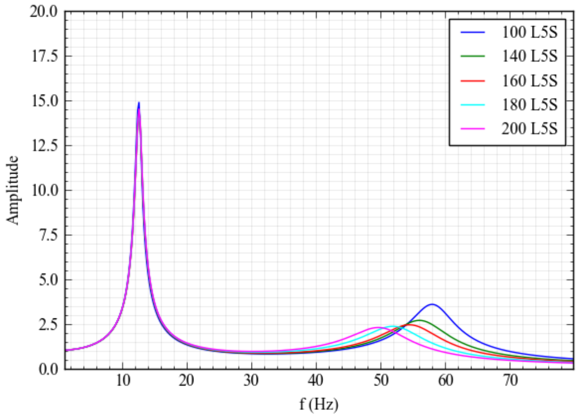

(b) CLT, dry screed

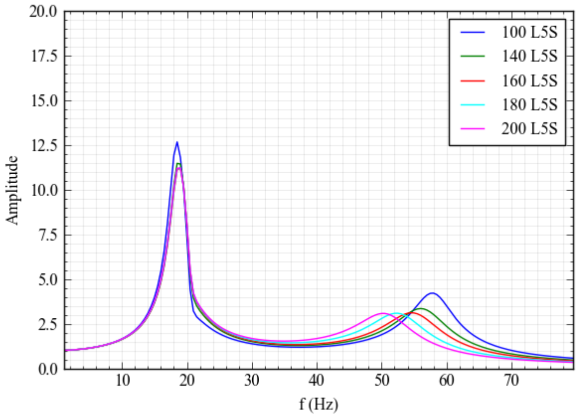

(c) Hollow box section, wet screed

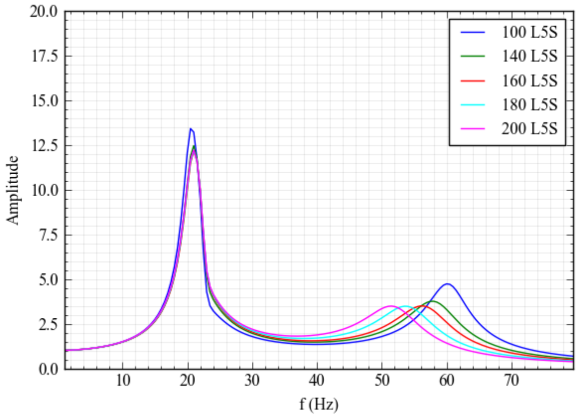

(d) Hollow box section, dry screed

Figure 6.14: Transfer functions at mid-span floors, variation in wall layup

6.6.1. Support conditions

In the previous calculations, it is assumed that the connection of the floors with the walls is hinged. However, it is also possible to design a more rigid connection. If the floor is clamped or partially clamped, the natural frequency of the floor is increased, compared to the simply supported case. Generally, considering a slab that is clamped instead of hinged results in a higher natural frequency of the floors, because the floor exhibits higher stiffness due to the restriction of the rotation at the supports. The increased natural frequencies of the floors are summarised in Table 6.14 for each of the floor types. As established during the parameter study, shifting the natural frequency of the floors closer to or to a higher frequency than the theoretical soil-building resonance generally results in lower maximum amplitudes. In the calculated transfer function shown in Figure 6.15, it can be seen that the maximum occurring amplitudes of the LVL hollow box floor with a wet screed and the dry screed are now below 10.5. The highest amplification factor found for the CLT floor with a wet screed is also decreased when compared to the suspended floor connection, from 12.5 to 11. The CLT floor with a dry screed still yields the highest maximum amplification, but also this value is reduced from 15 to 14.5.

In Figure 6.15, one of the other effects that can be distinguished clearly is that high amplification takes place from floor to floor, which was much lower for the concrete buildings. The higher floor-to-floor amplifications are likely related to the lower wall stiffness of the timber apartment buildings, resulting in more transmission between storeys. chapter 7 will analyse and compare the two types of buildings in more detail. Achieving fully clamped support conditions is however difficult. The supported floor connection described in chapter 3 is more rigid than the suspended floor connection since the floor for the supported floor connection is clamped between the walls of two subsequent storeys. Although the supported floor connection will result in higher natural frequencies for the floors, the actual stiffness of the connection is not known.

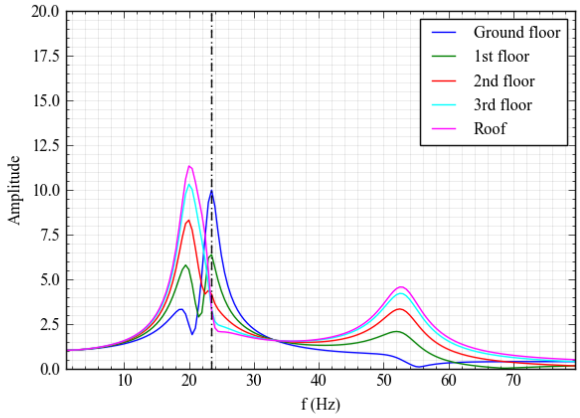

(a) CLT, wet screed

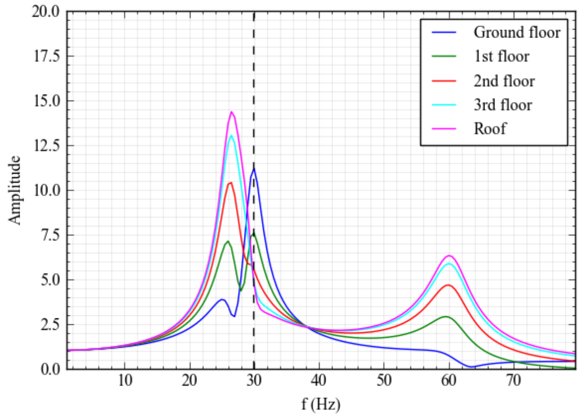

(b) CLT, dry screed

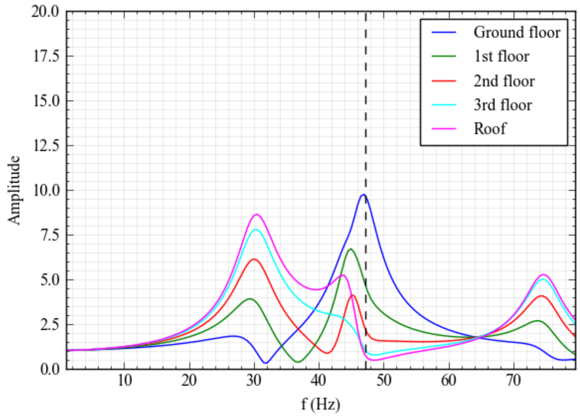

(c) Hollow box section, wet screed

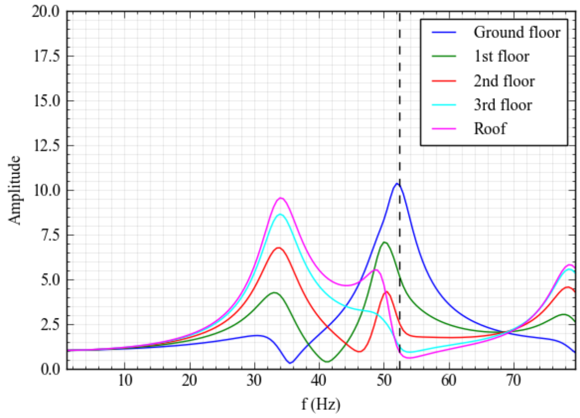

(d) Hollow box section, dry screed

Figure 6.15: Transfer functions, for clamped-clamped connection (CFCF)

Table 6.14: Natural frequencies for clamped-clamped slabs (CFCF), supported floor connections

	Natural frequency floor f_F, CFCF
CLT-W	23.51 Hz
CLT-D	29.88 Hz
HB-W	47.14 Hz
HB-D	69.51 Hz

6.7. Findings from the parameter study

The findings from the parameter study are as follows:

- The timber buildings have a relatively low mass, which results in higher soil-building frequencies. The natural frequencies of the floors when simply supported on two sides are lower than this soil-building resonance frequency. Therefore, the effect of soil damping is less prominent, which is in line with the findings from the literature study in chapter 2.
- The timber buildings with pile foundations on medium stiff soil yield lower overall amplification factors than the buildings on shallow foundations, which is in line with the results of the literature study in chapter 2. The pile foundation on soft soil dampens the vibrations the most, although it should be taken into account that for softer soils, the peaks found in the free-field response of the railway-induced vibrations are also generally higher.
- It was found that when the natural frequencies of the floors is below the soil-building resonance frequency, reducing this difference has a positive effect on the reduction of the transmission of the vibrations. Shifting the natural frequency of the floors above the soil-building frequency yields the lowest maximum amplifications for each of the floor types. The easiest way to achieve this is to change the boundary conditions from simply supported to clamped; however, creating fully clamped connections between CLT walls and timber floors is not feasible currently. Increasing the stiffness of the connection could be achieved by using the suspended floor connection described in chapter 3, but the exact stiffness of this connection is not known. Increasing the floor thickness also shifts the combined soil-building resonance peak to higher frequencies and reduces the amplitudes, especially for the LVL hollow box floors.
- Out of the four floor configurations, the LVL hollow box floors generally display lower maximum amplitudes when compared to the CLT floors.
- Doubling the wall thickness influences the peaks corresponding to the natural frequency of the walls by lowering them but does have less effect on the highest peaks in the transfer functions mid-span of the floors. This is because these peaks are governed by the coupling between the soil-building resonance and the natural frequency of the floors.
- Increasing the number of storeys is another way of increasing the mass of the building, but it should be taken into account that this also shifts the peak corresponding to the natural frequencies of the walls to a substantially lower frequency.

7 Comparative analysis

7.1. Introduction

At first glance, the differences in the transfer function between the timber buildings analysed in chapter 6 and the concrete buildings from chapter 5 are quite significant. This chapter will analyse what the dissimilarities are between the two materials that explain these differences. To do so, a comparison will be made between the transfer functions of the concrete building and a timber building with a LVL hollow box floor and a dry screed. After this comparison, for each of the timber floor configurations a timber building is designed. The first design is based on the structural unity checks. The free-field railway-induced vibrations are imposed on the buildings, after which their building response is calculated and compared. As mentioned in chapter 5 and chapter 2, railway-induced vibrations are highly location dependent. For the measured free-field vibrations for the HERO project, the timber buildings will be optimised based on the findings of the parameter study, to find out to what degree the resulting building vibrations can be minimised.

7.2. Transfer functions: Concrete vs. timber

To analyse where the differences in transfer functions and thus the dynamic behaviour of the concrete and the timber buildings stem from, one of the sections of the HERO building from the case study is compared to an equivalent timber building. Only a building with an LVL hollow box floor and dry screed is considered since the behaviour of all the four floor configurations is comparable. Although the ground floor of the original HERO building has a ground floor with different properties, the same properties are applied to each storey for this comparison. The floors both span 6 m, and the building has a width of 12.145 m, the same as in the case study and the considered section contains five storeys. The LVL hollow box floor is optimised based on the structural unity checks, which are shown in Table 7.1 and for the concrete floor it is assumed that a similarly optimised design was chosen for the case study. As discussed in chapter 5, the monolithic moment resisting connection of the concrete floor is a rigid connection, thus the supports are considered to be clamped. The corresponding transfer functions are shown in Figure 7.2. Because of these boundary conditions, the soil-building frequency is lower than the natural frequency of the floors for the concrete apartment building. Therefore, the soil exhibits damping, which is one of the reasons for the lower amplification factors for the concrete building. Due to the coupling between the soil-building frequency and the natural frequency of the floors for the timber building, the higher damping factor that is assigned to the timber floors has little effect.

In Figure 6.15, it was already shown that changing the boundary conditions of the timber floors reduces the building amplifications, but not to the same level as the concrete floors. Although the monolithic connection is rigid for the concrete building, for comparison, in Figure 7.1b the situation is shown in case the connection would have been simply supported. Again, it can be seen that although this results in a coupled mode between the soil-building frequency and the natural frequency of the floors, which is now 10.59 Hz the amplification is still much lower. This can be explained by comparing the other properties of the two building systems. One of the other dissimilarities is the effective thickness of the walls. The concrete walls of 250 mm have a much larger effective area than the effective 60 mm of the CLT 100 L5S. Combined with the lower modulus of Elasticity of the CLT walls, this results in a lower wall stiffness for the timber building, which in turn results in the higher storey-to-storey amplifications that can be seen in Figure 7.1b. This is in line with the results found by Auersch [6] for column-type buildings, which also have a lower effective area and higher amplification factors. To highlight this effect, the transfer function model with the rigid instead of flexible floor is shown in Figure 7.1a.

HB-D: LVL hollow box floor, dry screed

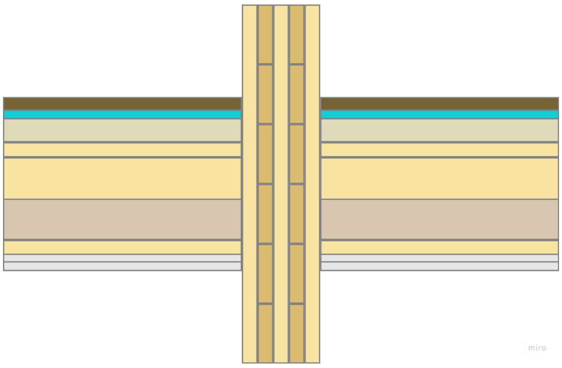

Height floor: 407 mm
Modulus of Elasticity: $10.5 - 13.8 \cdot 10^9\ N/m^2$
Supports: SFSF[1]

$$m_F = 236.45\ kg/m^2$$

$$EI_L = 2.58 \cdot 10^7\ Nm^2/m$$

$$f_{0,F} = \frac{\pi^2}{2\pi L^2} \cdot \sqrt{\frac{EI_L}{m_F}} = 14.23\ Hz$$

$$\zeta = 0.04$$

(Effective) thickness walls: 60 mm
Modulus of Elasticity: $11 \cdot 10^9\ N/m^2$

CON: Concrete floor HERO

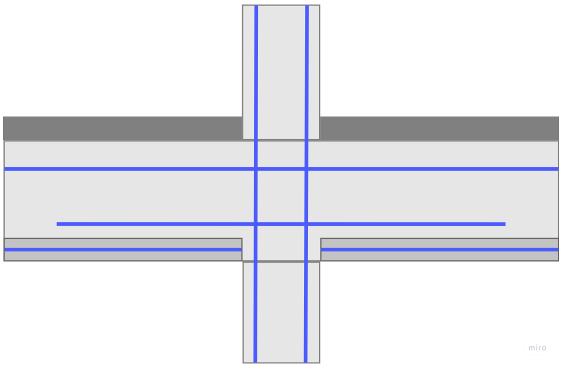

Height floor: 280 mm
Modulus of Elasticity: $28 \cdot 10^9\ N/m^2$
Supports: CFCF[2]

$$m_F = 904.96\ kg/m^2$$

$$EI_L = 5.49 \cdot 10^7\ Nm^2/m$$

$$f_{0,F} = \frac{2\sqrt{3}\pi}{3L^2} \sqrt{\frac{D}{m_F}} = 24.5\ Hz$$

$$\zeta = 0.03$$

(Effective) thickness walls: 250 mm
Modulus of Elasticity: $36 \cdot 10^9\ N/m^2$

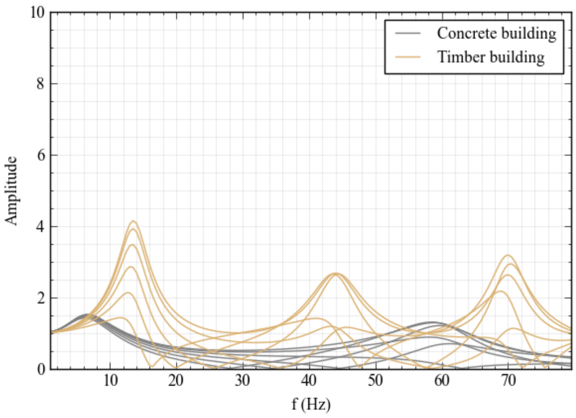

(a) Rigid floor transfer function model for the concrete and timber building

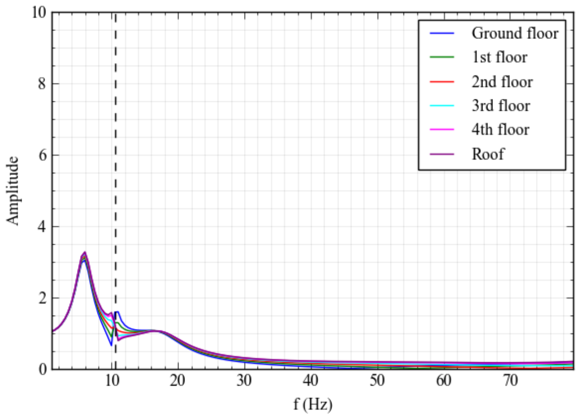

(b) Transfer functions for concrete building with simply supported floors

Figure 7.1: Differences between concrete and timber building

[1]One-way slab, simply supported
[2]One-way slab, clamped edges

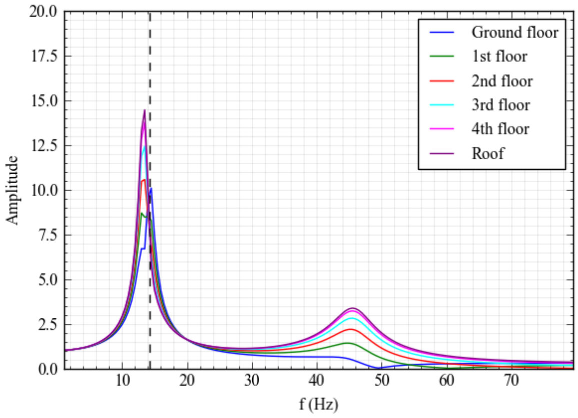

(a) LVL hollow box floor, dry screed, mid-span floors

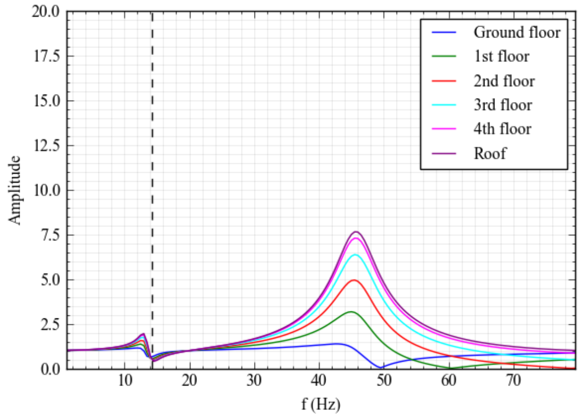

(b) LVL hollow box floor, dry screed, walls

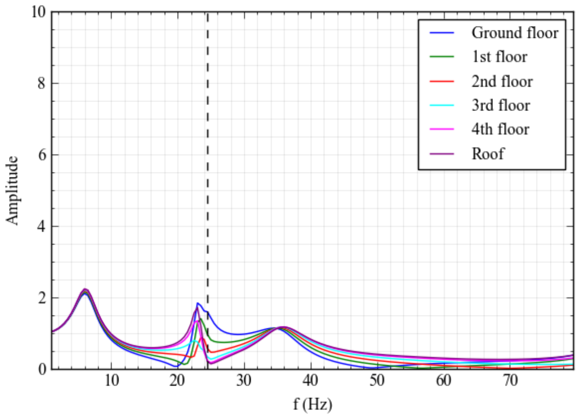

(c) Concrete floor, mid-span floors

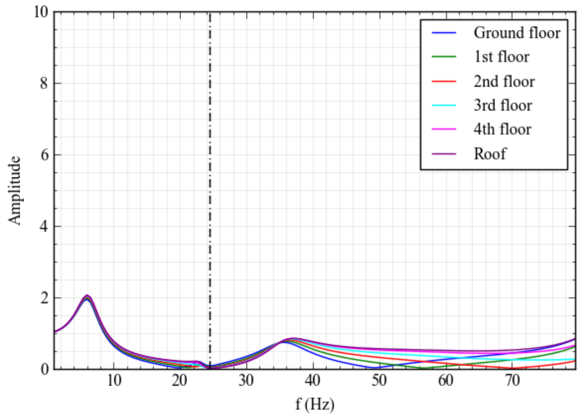

(d) Concrete floor, walls

Figure 7.2: Transfer functions for concrete and LVL hollow box floors, for comparison

7.3. HERO case study - structural optimisation

Although the transfer functions of the timber buildings show higher amplification factors than the concrete building, the final response of the buildings to railway-induced vibrations depends on the imposed vibrations. Therefore, the free-field vibrations of the HERO building are imposed on the four timber buildings and compared to the equivalent concrete building discussed in section 7.2. In Figure 7.3, the measured railway-induced vibrations for the HERO case study are repeated, that will be further used in this chapter.

7.3.1. Building section

The same building section as described in section 7.2 is used for the comparison between the four timber buildings, for each of the four floor configurations described in subsection 6.2.4. However, for the CLT floors, a seven-layer layup would be needed to span the apartment length of 6 meters, which is not customary. Therefore, a partition wall is added for this floor configuration. In Figure 7.4 an overview is given of all the timber floor configurations, as well as the monolithic concrete floor.

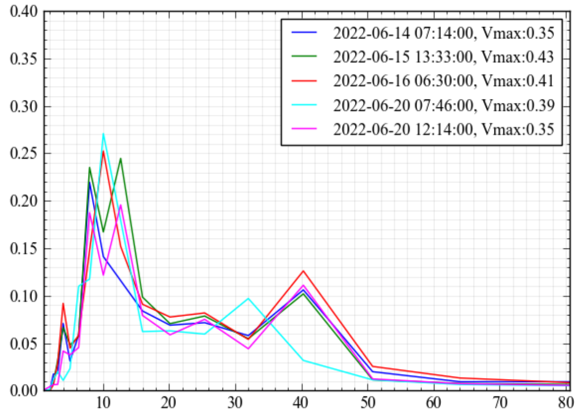

Figure 7.3: Input free-field vibrations HERO, location 1

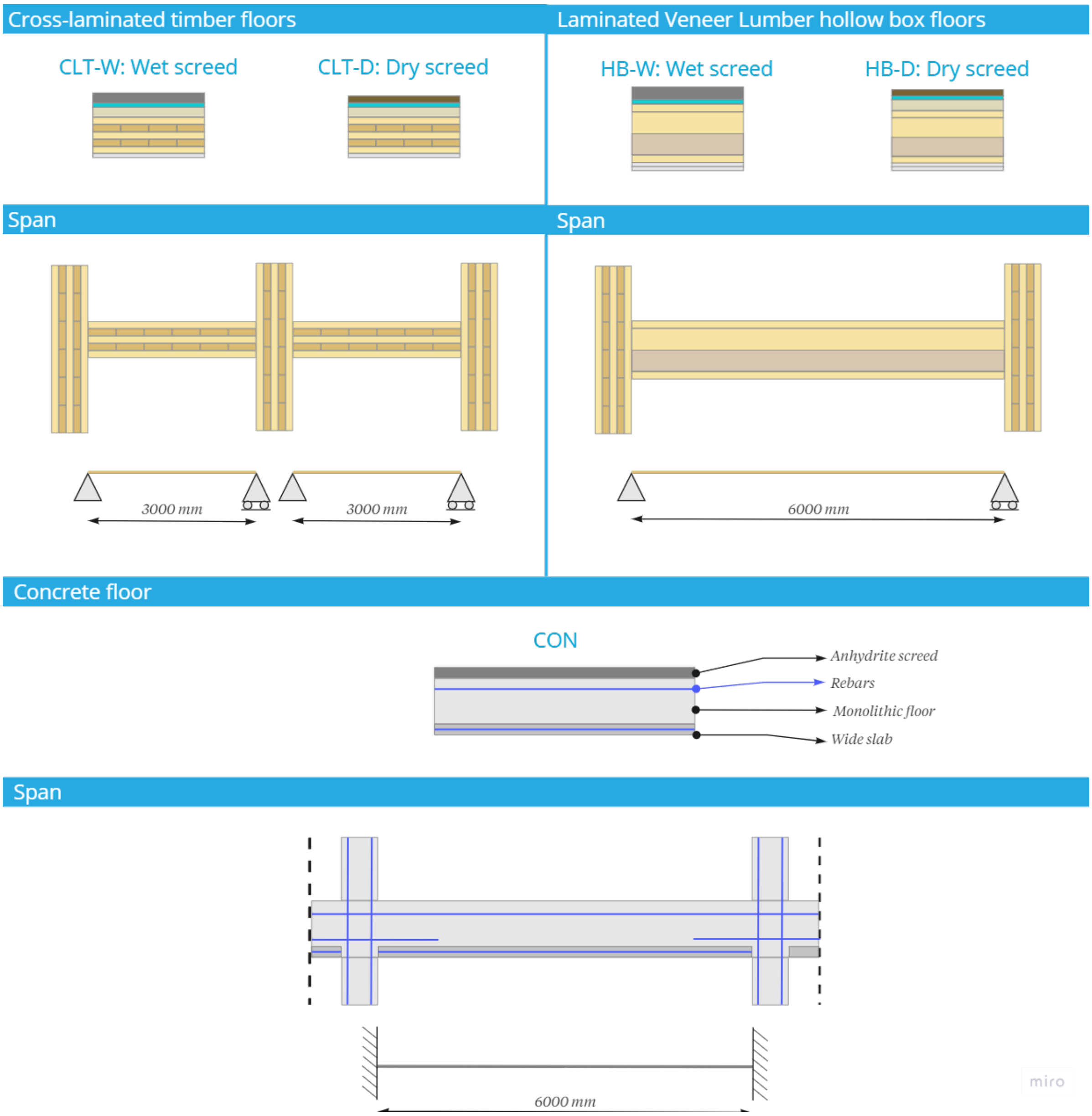

Figure 7.4: Different floor configurations for the comparative analysis

7.3.2. LVL hollow box floors

Based on the systems shown in Figure 7.4, a design is made for the LVL hollow box floors such that they both satisfy the structural requirements. The corresponding unity checks are shown in Table 7.1. The stiffness and mass of the LVL hollow box floor with a wet screed aids in satisfying the walking-induced vibration requirements and could therefore be designed with a lower rib height. On the other hand, the stiffness of the hollow box floor with a dry screed had to be increased to meet these requirements, resulting in a 50 mm higher rib height and a 3 mm higher thickness of the lower flange. The corresponding unity checks are shown in Table 7.1.

HB-W: LVL hollow box floor, wet screed

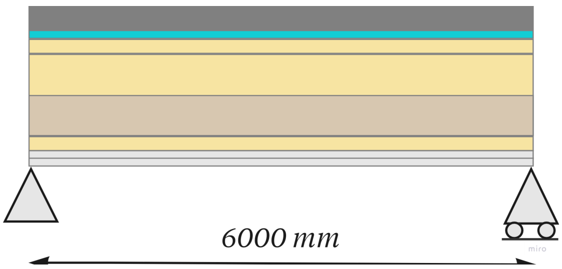

Centre-to-centre ribs: 600 mm
Height rib: 300 mm
Thickness rib: 45 mm
Thickness upper flange: 27 mm
Thickness lower flange: 27 mm

$$m_F = 313.02\ kg/m^2$$

$$EI_L = 18.26 \cdot 10^6\ Nm^2/m$$

$$f_{0,F} = \frac{\pi^2}{2\pi L^2} \cdot \sqrt{\frac{EI_L}{m_F}} = 10.54\ Hz$$

$$\zeta = 0.04$$

HB-D: LVL hollow box floor, dry screed

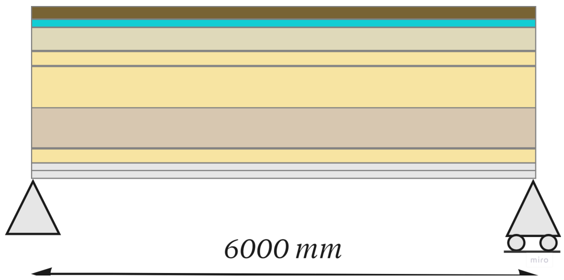

Centre-to-centre ribs: 600 mm
Height rib: 350 mm
Thickness rib: 45 mm
Thickness upper flange: 27 mm
Thickness lower flange: 30 mm

$$m_F = 236.45\ kg/m^2$$

$$EI_L = 25.14 \cdot 10^6\ Nm^2/m$$

$$f_{0,F} = \frac{\pi^2}{2\pi L^2} \cdot \sqrt{\frac{EI_L}{m_F}} = 14.23\ Hz$$

$$\zeta = 0.04$$

Table 7.1: Summary of unity checks LVL hollow box floors

	Bending, middle	Bending, edge	Shear, middle	Shear, edge	Deformations	Vibrations, stiffness	Vibrations, velocity
HB-W	0.15	0.13	0.93	0.82	0.46	0.38	0.22
HB-D	0.11	0.09	0.68	0.58	0.29	0.95	0.62

For both floors, the corresponding transfer functions for the seven-storey building of the case study are calculated. Then, similar to the case study, the values of V_{max} are calculated based on the input free-field vibrations shown in Figure 7.3. When comparing the transfer functions, it can be seen that the results are quite similar. However, the resulting V_{max} values for the LVL hollow box floor with a dry screed are significantly lower. This is due to the lower natural frequency of the LVL hollow box floors with a wet screed, which causes the highest peaks in the railway-induced vibration spectra to coincide with the highest peaks in the transfer functions. The higher natural frequency of the floors with a dry screeds lowers this coincidence, resulting in lower building vibrations.

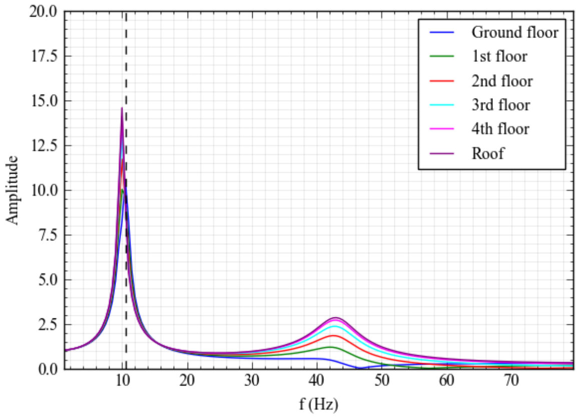

(a) Transfer functions mid-span floors, HB-W

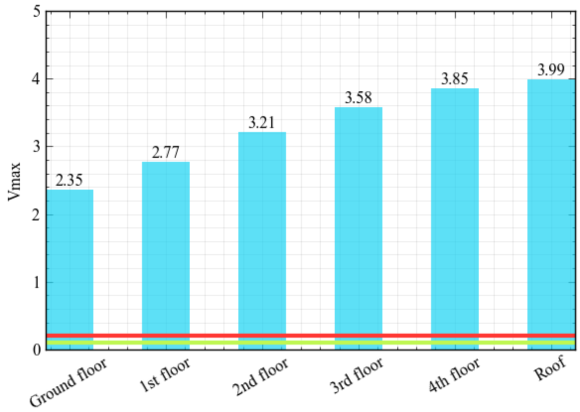

(b) V_{max} LVL hollow box floor, HB-W

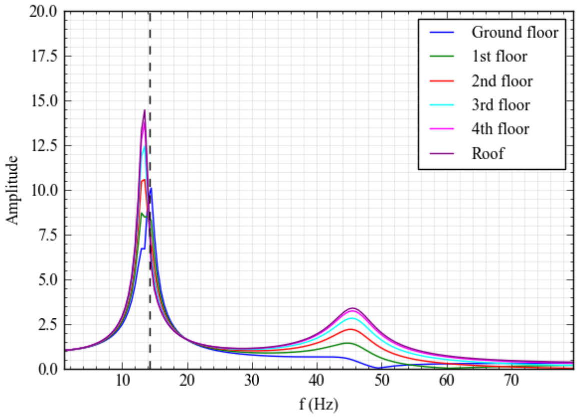

(c) Transfer functions mid-span floors, HB-D

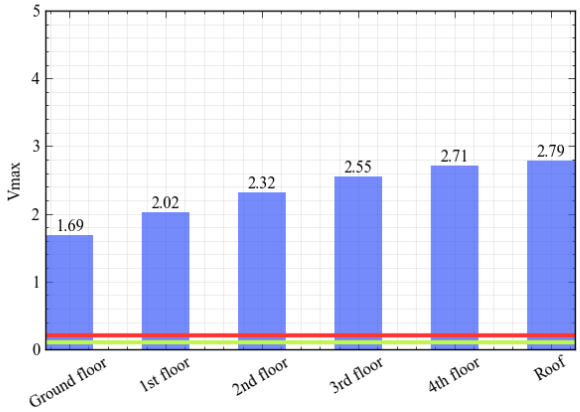

(d) V_{max} LVL hollow box floor, HB-D

Figure 7.5: Transfer function and V_{max} values serviceability criteria for LVL hollow box floors, structurally optimised design

7.3.3. CLT floors

Similar to the LVL hollow box floors, the CLT floors are designed such that they meet the structural requirements. The unity checks can be found in Table 7.2. Again, due to the walking-induced vibration requirements, it was necessary to use a layup with a higher thickness for the CLT floor with a dry screed. The layout, flexural stiffness, mass and natural frequency that corresponds to each of the floors are shown below.

CLT-W: CLT floor, wet screed

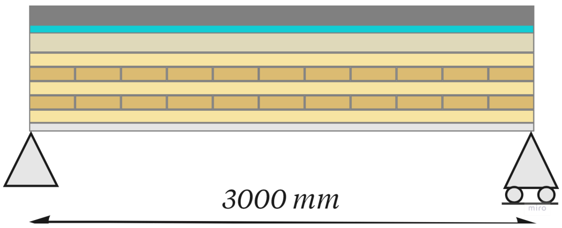

Layup: [30, 20, 20, 20, 30]

$$m_F = 395.8\ kg/m^2$$

$$EI_L = 1.98 \cdot 10^6\ Nm^2/m$$

$$f_{0,F} = \frac{\pi^2}{2\pi L^2} \cdot \sqrt{\frac{EI_L}{m_F}} = 12.36\ Hz$$

$$\zeta = 0.04$$

CLT-D: CLT floor, dry screed

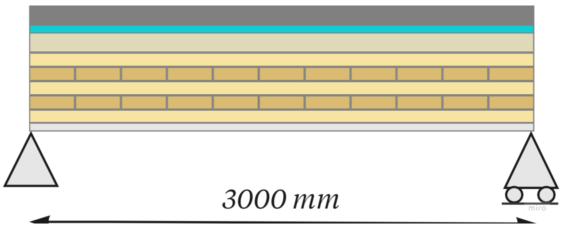

Layup: [40, 20, 20, 20, 40]

$$m_F = 185.6\ kg/m^2$$

$$EI_L = 2.02 \cdot 10^6\ Nm^2/m$$

$$f_{0,F} = \frac{\pi^2}{2\pi L^2} \cdot \sqrt{\frac{EI_L}{m_F}} = 18.21\ Hz$$

$$\zeta = 0.04$$

Table 7.2: Summary of unity checks CLT floors

	Bending	Shear	Rolling shear	Deformations	Vibrations, stiffness	Vibrations, velocity
CLT-W	0.29	0.05	0.30	0.91	0.48	0.29
CLT-D	0.14	0.03	0.19	0.36	0.71	0.49

In Figure 7.6 the transfer functions and the resulting building vibrations in terms of V_{max} are shown. Similar to the LVL hollow box floors, the floor with a dry screed outperforms the floor with a wet screed. Again, this is due to the higher natural frequency of the CLT floors with a dry screed, which shifts the peak corresponding to the coincidence of the natural frequency of the floors and the soil-building resonance to a higher frequency.

7.3.4. Comparison timber and concrete buildings

In Figure 7.7 the comparison between the resulting structurally optimised timber buildings with the equivalent concrete building is shown. It can be seen that the concrete building yields lower building vibrations for each of the storeys, compared to each of the timber buildings. This is in line with the expectations, because the highest peaks of the free-field response of the railway-induced vibrations takes place between ≈ 8-16 Hz. This is also the frequency range in which the highest amplifications are found for the timber buildings, which are much higher than the maximum amplification factors found for the concrete buildings due to the earlier described effects of coupling between modes and a higher transmission between storeys. The second conclusion that can be drawn from this comparison is that the higher natural frequency of the CLT floors with a dry screed results in the lowest building out of the four floor configurations. This is because the highest peak in the transfer function is shifted away from the highest peak in the spectra of the measured railway-induced vibrations. Still, the building vibrations are 108 % higher for the building with a CLT floor with a dry screed, compared to the equivalent concrete building. For the CLT floor with a wet screed this is 288 %. For the timber building with a LVL floor with a wet screed, the building vibrations are 461 % higher and for the LVL floor with a dry screed 293 %.

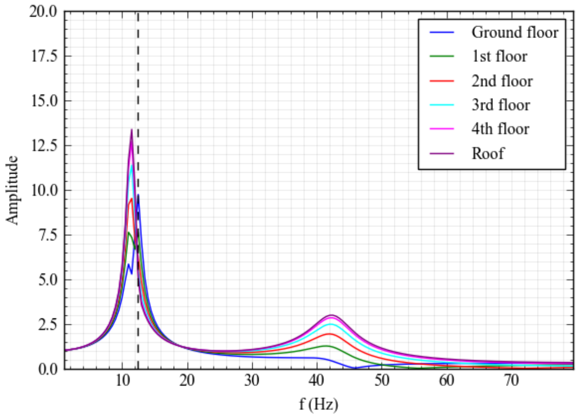

(a) Transfer functions mid-span floors, CLT-W

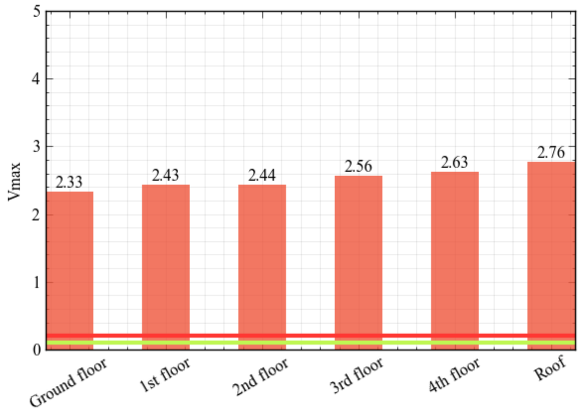

(b) V_{max} CLT floor, CLT-W

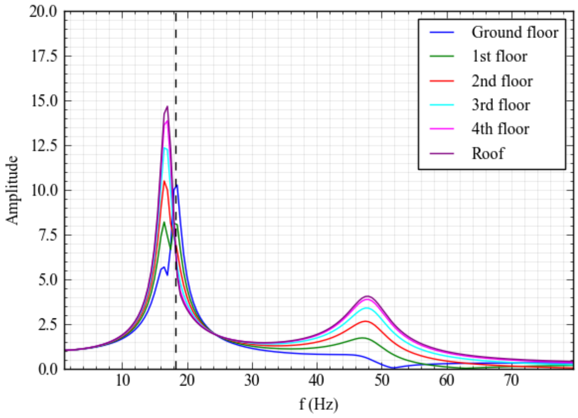

(c) Transfer functions mid-span floors, CLT-D

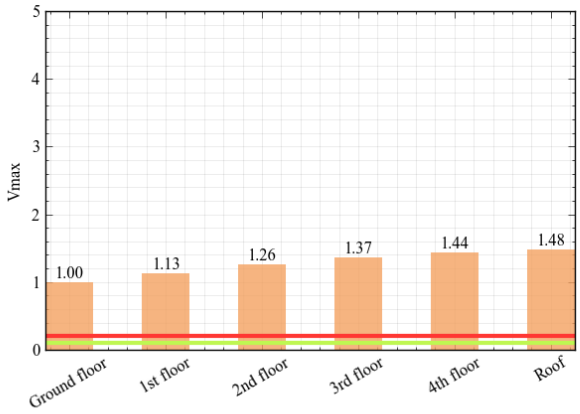

(d) V_{max} CLT floor, CLT-D

Figure 7.6: Transfer function and V_{max} values serviceability criteria for CLT floors, structurally optimised design

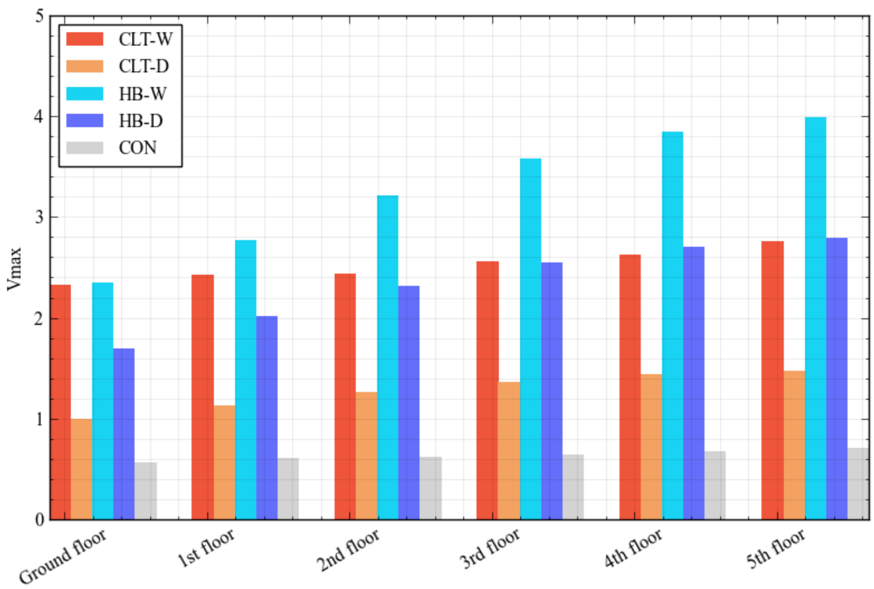

Figure 7.7: Comparison transfer functions concrete and timber buildings in terms of serviceability criteria V_{max}, mid-span of the floors

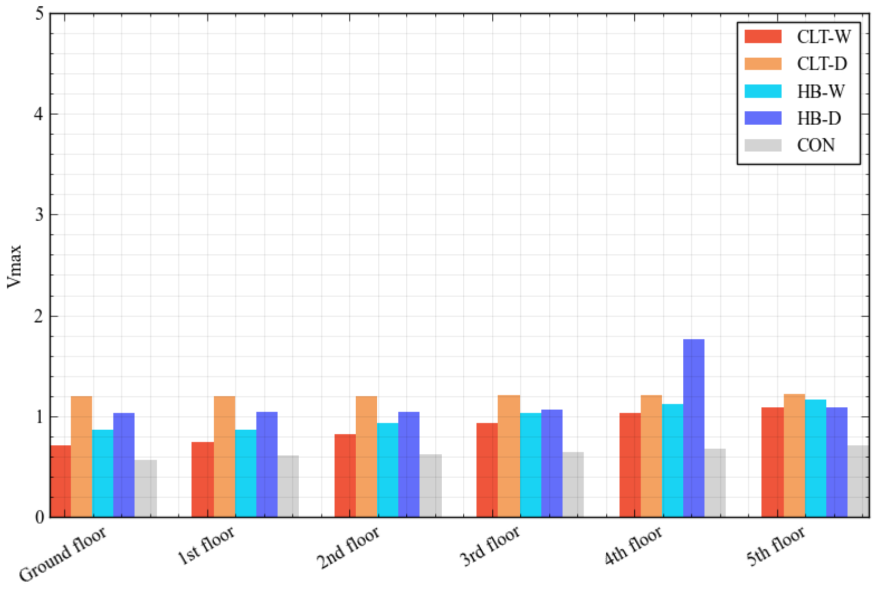

Figure 7.8: Comparison transfer functions concrete and timber buildings in terms of serviceability criteria V_{max}, mid-span of the floors, for fully clamped supports (CFCF)

7.4. HERO case study - railway-induced vibration optimisation

To be able to design an optimised timber building, it is important to prevent coincidence between the peaks in the free-field railway-induced vibrations and the peaks in the transfer functions of the timber buildings. In Figure 7.3 it can be seen that the highest peaks of the measured free-field vibrations take place between ≈ 8-16 Hz. The second peak takes place around 40 Hz. The effect of three different measures on the building response is researched in this section.

7.4.1. Clamped supports

Another way to shift the peaks with the highest amplification factors in the transfer functions of the timber building away from the peaks in the measured railway-induced vibrations is if the connections of the floors with the walls were to be clamped. To show the effect stiffening the connections can have, this section takes into account rigid connections of each of the timber floor configurations with the walls. It should be noted however that it has been established that currently, a fully clamped connection between the CLT walls and timber floor configurations is likely not feasible. However, it may be possible to apply connections that are stiffer than the simply supported connections considered so far. In Figure 7.9 the resulting transfer functions and the corresponding building vibrations in terms of V_{max} are shown.

Applying fully clamped supports increases the natural frequency of the floors significantly. The adjusted natural frequencies of the floors are shown with a dashed line in Figure 7.9. Although the amplification factors are still high, as expected they coincide less with the peaks found for the measured free-field vibrations. Furthermore, the amplitudes in the transfer functions of each of the timber buildings is lowered because there is less coincidence between the soil-building frequency and the floor resonance frequency, an effect described in chapter 6. Therefore, the V_{max} values found for the floors with clamped supports are significantly lowered for each of the floors. In Figure 7.8 the resulting building frequencies are again compared to those found for the equivalent concrete building. Now, the differences between the concrete and timber buildings are much lower. The timber building with the CLT configuration with a wet screed has the lowest V_{max} values of the timber structures. Without the clamped support optimisation, this floor yielded V_{max} values which were 288 % higher than those found for the concrete building. With the clamped supports, this is reduced to only 55 % higher building vibrations.

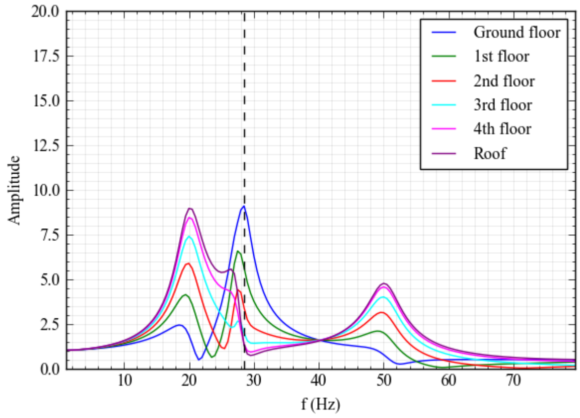

(a) Transfer functions mid-span floors, CLT-W

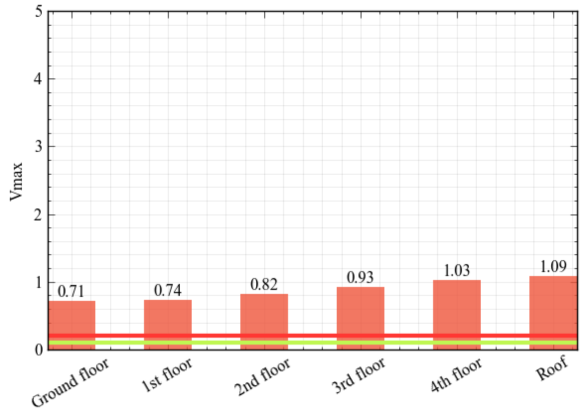

(b) V_{max} CLT floor, CLT-W

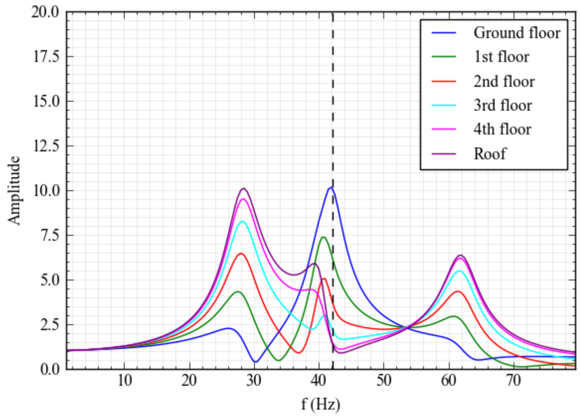

(c) Transfer functions mid-span floors, CLT-D

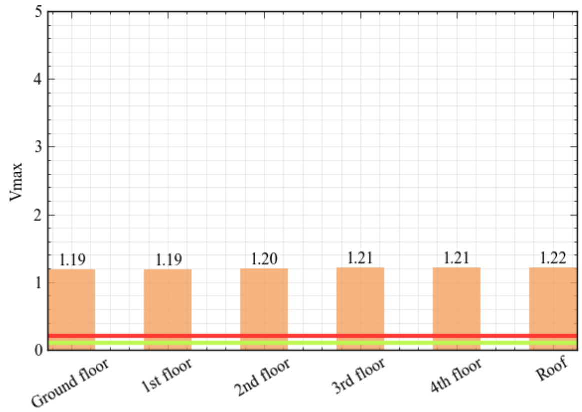

(d) V_{max} CLT floor, CLT-D

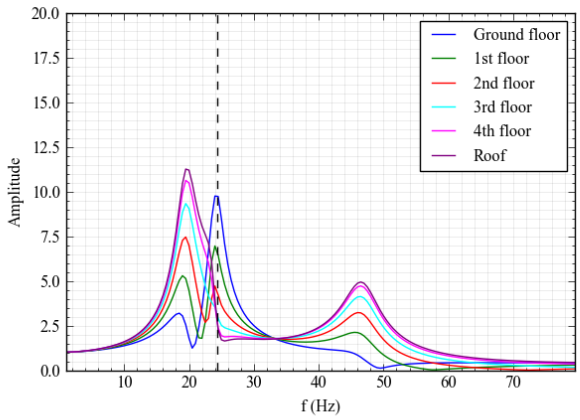

(e) Transfer functions mid-span floors, LVL hollow box floor, HB-W

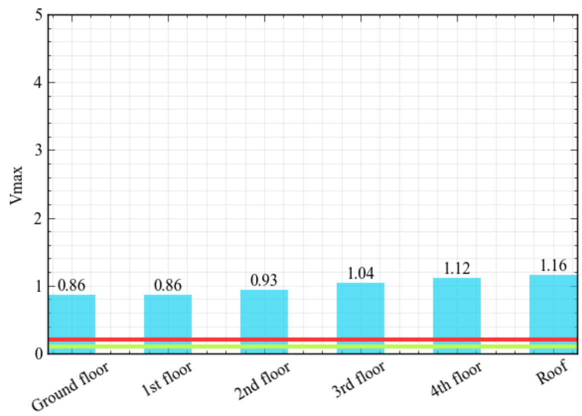

(f) V_{max} LVL hollow box floor, HB-W

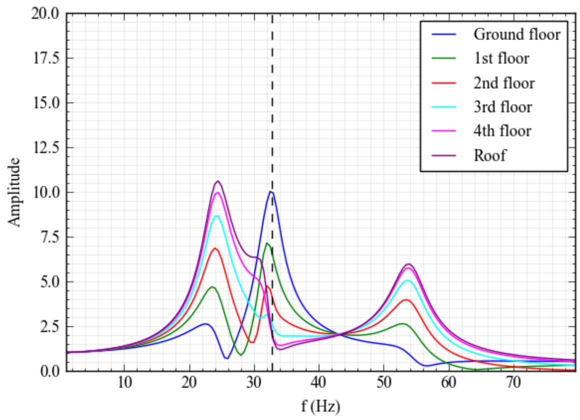

(g) Transfer functions mid-span floors, LVL hollow box floor, HB-D

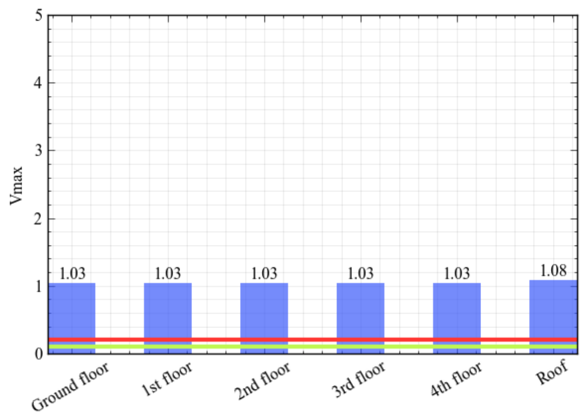

(h) V_{max} LVL hollow box floor, HB-D

Figure 7.9: Transfer function and V_{max} values serviceability criteria for fully clamped supports (CFCF)

7.4.2. Increasing the floor thickness

Increasing the thickness of the floors increases their natural frequency, due to their higher stiffness. By increasing the natural frequency of the floors, the peaks with the highest amplification factors in the transfer functions can be shifted away from the 8-16 Hz area where the railway-induced vibrations display the highest amplification factors. The floor thickness of the CLT floors is increased to 200 mm and the rib height of the LVL hollow box floors is increased to 600 mm. The new floor configurations are shown below. The corresponding unity checks for the CLT floors are included in Table 7.3 and for the LVL hollow box floors in Table 7.4. The resulting transfer functions and V_{max} values per storey are shown in Figure 7.10. In Figure 7.11 the results are compared with the V_{max} values of the concrete apartment building.

CLT-W: CLT floor, wet screed

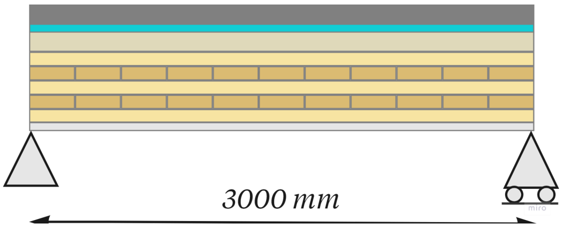

Layup: [40, 40, 40, 40, 40]

$$m_F = 435.0\, kg/m^2$$

$$EI_L = 4.98 \cdot 10^6\; Nm^2/m$$

$$f_{0,F} = \frac{\pi^2}{2\pi L^2} \cdot \sqrt{\frac{EI_L}{m_F}} = 18.68\; Hz$$

$$\zeta = 0.04$$

HB-W: LVL hollow box floor, wet screed

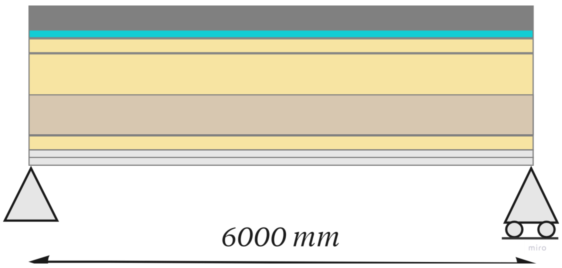

Centre-to-centre ribs: 600 mm
Height rib: 600 mm
Thickness rib: 45 mm
Thickness upper flange: 33 mm
Thickness lower flange: 33 mm

$$m_F = 330.61\, kg/m^2$$

$$EI_L = 88.86 \cdot 10^6\; Nm^2/m$$

$$f_{0,F} = \frac{\pi^2}{2\pi L^2} \cdot \sqrt{\frac{EI_L}{m_F}} = 22.62\; Hz$$

$$\zeta = 0.04$$

CLT-D: CLT floor, dry screed

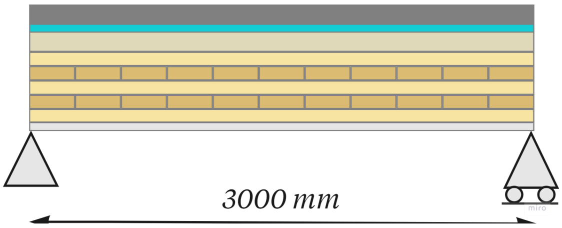

Layup: [40, 40, 40, 40, 40]

$$m_F = 215.0\, kg/m^2$$

$$EI_L = 4.24 \cdot 10^6\; Nm^2/m$$

$$f_{0,F} = \frac{\pi^2}{2\pi L^2} \cdot \sqrt{\frac{EI_L}{m_F}} = 24.51\; Hz$$

$$\zeta = 0.04$$

HB-D: LVL hollow box floor, dry screed

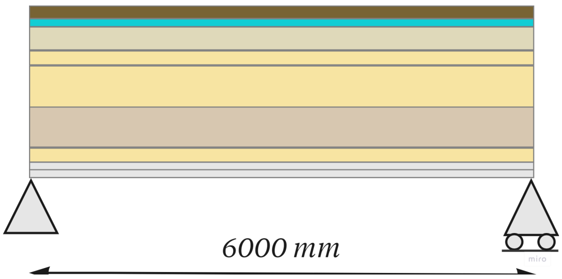

Centre-to-centre ribs: 600 mm
Height rib: 600 mm
Thickness rib: 45 mm
Thickness upper flange: 33 mm
Thickness lower flange: 33 mm

$$m_F = 250.61\, kg/m^2$$

$$EI_L = 88.11 \cdot 10^6\; Nm^2/m$$

$$f_{0,F} = \frac{\pi^2}{2\pi L^2} \cdot \sqrt{\frac{EI_L}{m_F}} = 25.87\; Hz$$

$$\zeta = 0.04$$

Table 7.3: Summary of unity checks CLT floors, for increased floor thickness

	Bending	Shear	Rolling shear	Deformations	Vibrations, stiffness	Vibrations, velocity
CLT-W	0.12	0.03	0.18	0.28	0.19	0.14
CLT-D	0.09	0.02	0.13	0.18	0.24	0.18

Table 7.4: Summary of unity checks LVL hollow box floors, for increased floor thickness

	Bending, middle	Bending, edge	Shear, middle	Shear, edge	Deformations	Vibrations, stiffness	Vibrations, velocity
HB-W	0.06	0.05	0.45	0.37	0.14	0.12	0.09
HB-D	0.05	0.04	0.39	0.32	0.11	0.33	0.25

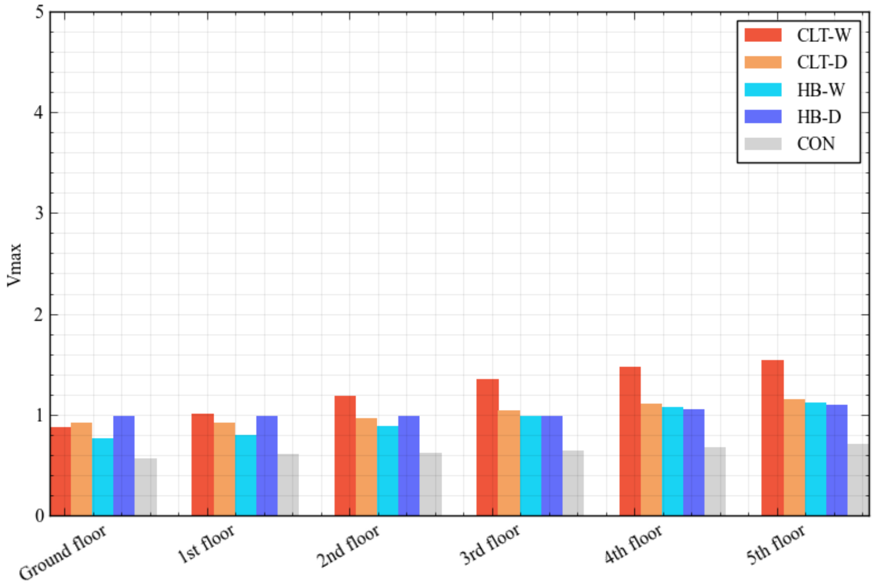

Figure 7.11: Comparison transfer functions concrete and timber buildings in terms of serviceability criteria V_{max}, mid-span of the floors, for increased floor thickness

By increasing the floor thickness and shifting up the natural frequencies of the floors, the building vibrations are again lowered compared to the initial design based on the structural design checks. The LVL hollow box floor with a dry screed yields the lowest vibration levels. The building vibrations are now only 55% higher for this floor type compared to the vibrations in the equivalent concrete building. However, in Table 7.3 and Table 7.4 it can be seen that the unity checks of the floors are now also significantly lower. The highest unity check for the CLT floor with a wet screed is now only 0.28 compared to the initial 0.91 and for the CLT floor with a dry screed the initial check of 0.71 is lowered to 0.24. Similar for the LVL hollow box floor, the unity check is lowered from 0.93 to 0.45 for the floor with a wet screed and from 0.95 to 0.39 for the floor with a dry screed. In terms of the structural ULS and SLS checks, the floors are overdimensioned and less efficient. When considering material efficiency, this is important to consider. However, the highest vibration levels in each of the buildings are lowered by 44.2 % for the CLT floor with a wet screed, by 22.3 % for the CLT floor with a dry screed, by 71.93 % for the LVL hollow box floor with a wet screed and 60.57 % for the LVL hollow box floor with a dry screed. Especially for both the LVL hollow box floors these reductions are substantial.

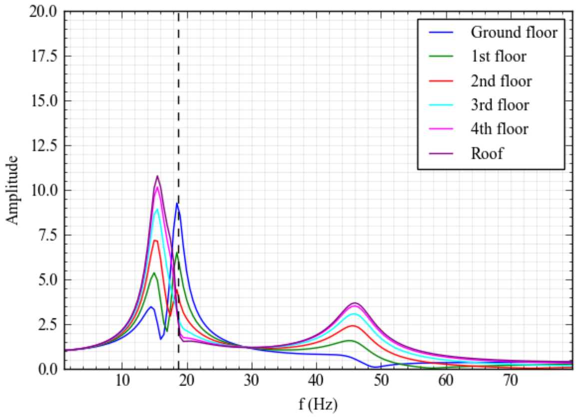

(a) Transfer functions mid-span floors, CLT-W

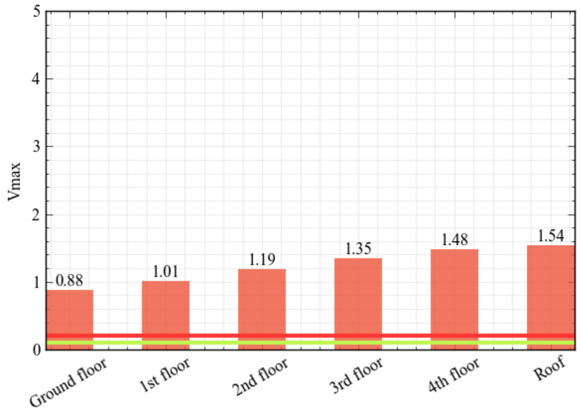

(b) V_{max} CLT floor, CLT-W

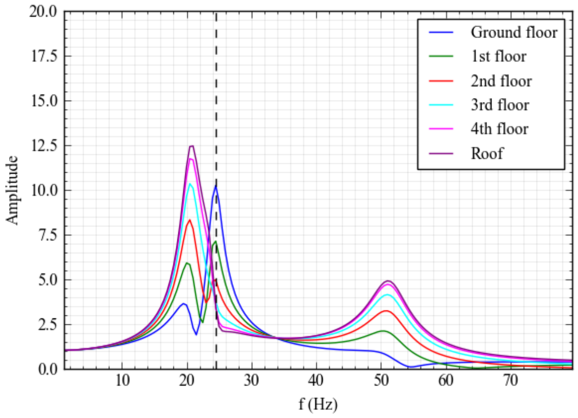

(c) Transfer functions mid-span floors, CLT-D

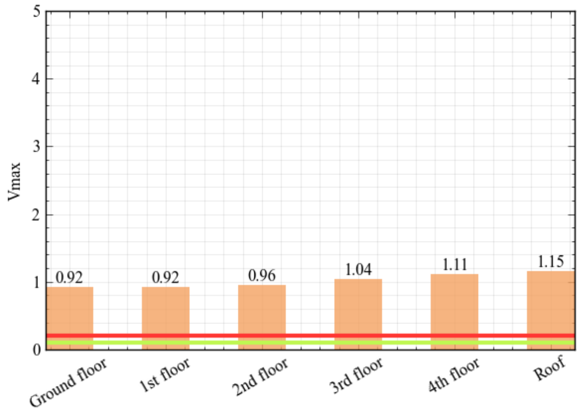

(d) V_{max} CLT floor, CLT-D

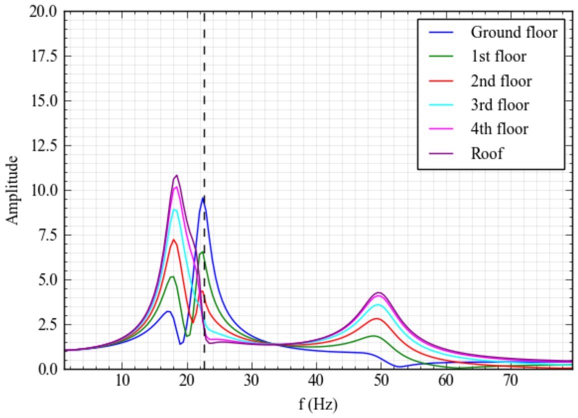

(e) Transfer functions mid-span floors, LVL hollow box floor, HB-W

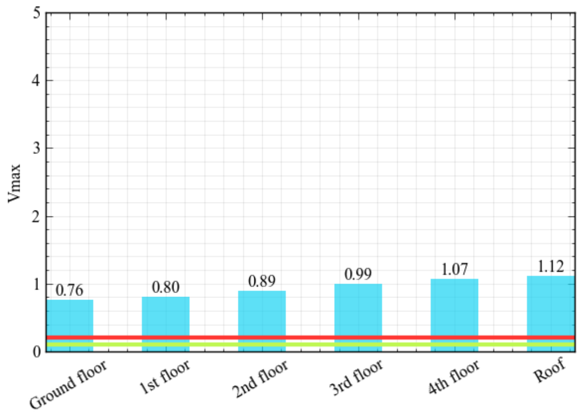

(f) V_{max} LVL hollow box floor, HB-W

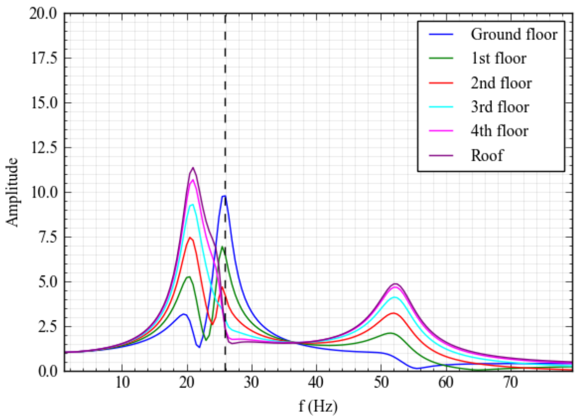

(g) Transfer functions mid-span floors, LVL hollow box floor, HB-D

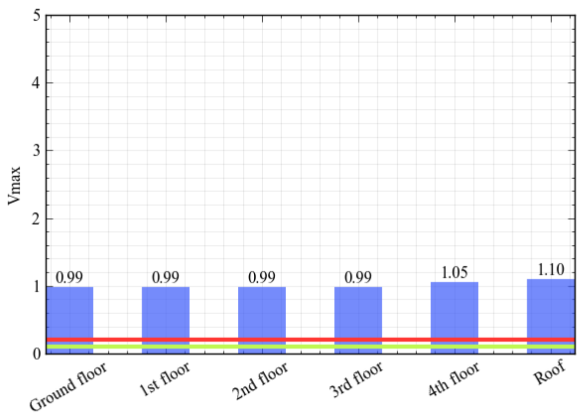

(h) V_{max} LVL hollow box floor, HB-D

Figure 7.10: Transfer function and V_{max} values serviceability criteria for increased floor thickness

7.4.3. Changing the number of storeys

The third measure that was shown to be effective in lowering the first peak in the transfer functions of the timber buildings is increasing the number of storeys. However, increasing the number of storeys also shifts the peak corresponding to the resonance frequencies of the walls to a lower frequency. Also, the peak corresponding to the combined soil-building resonance and natural frequency of the floors is shifted to a lower frequency. In this case, that would shift the frequencies into the range where they coincide with the highest peaks in the measured railway-induced vibrations. Therefore, it is more feasible to reduce the number of storeys, to shift the frequency corresponding to the natural frequency of the walls to a higher frequency instead. The highest number of storeys resulting in the lowest building response for this specific situation is three storeys. The results are shown in Figure 7.13. In Figure 7.12 the calculated V_{max} values are again compared to the values found for the concrete building. Compared to the initial building design, the vibration levels are reduced by 12.32 % for the CLT floor with a wet screed, 25.68 % for the CLT floor with a dry screed, 8.52 % for the LVL hollow box floor with a wet screed and lastly 28.67 % for the LVL hollow box floor with a dry screed. The lowest building vibrations are found for the CLT floor with a dry screed, which are now 71 % higher than the building vibrations for the equivalent concrete three storeys building.

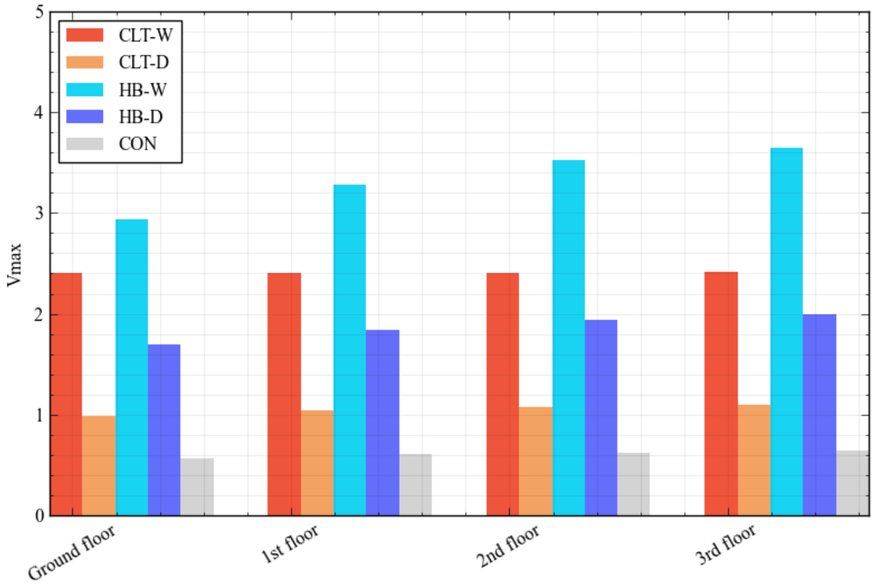

Figure 7.12: Comparison transfer functions concrete and timber buildings in terms of serviceability criteria V_{max}, mid-span of the floors, for three storeys instead of five

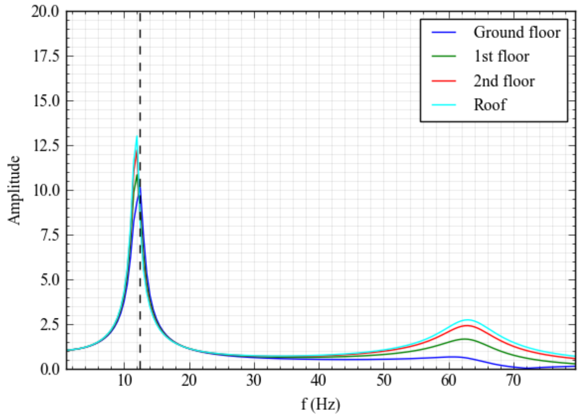

(a) Transfer functions mid-span floors, CLT-W

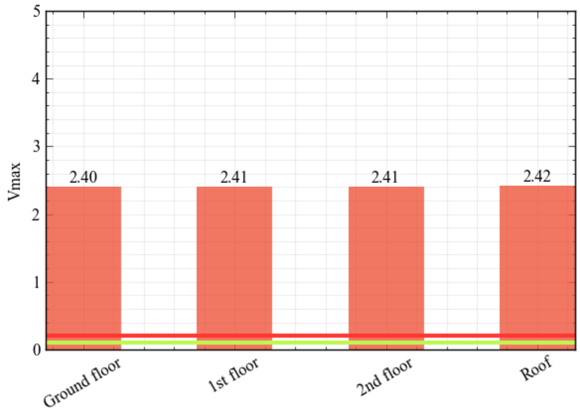

(b) V_{max} CLT floor, CLT-W

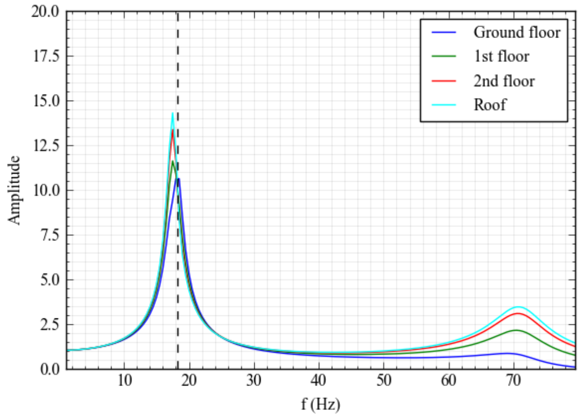

(c) Transfer functions mid-span floors, CLT-D

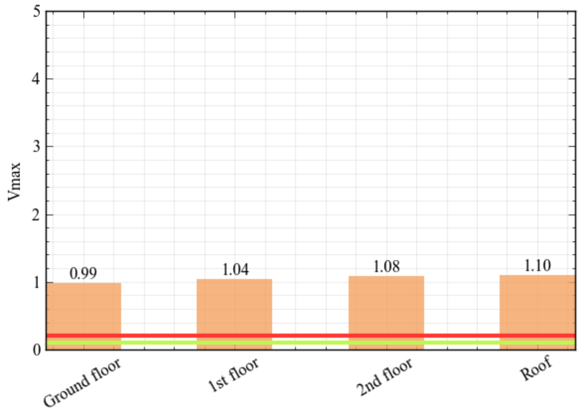

(d) V_{max} CLT floor, CLT-D

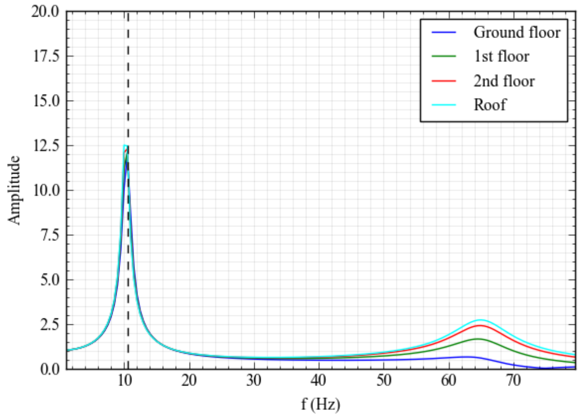

(e) Transfer functions mid-span floors, LVL hollow box floor, HB-W

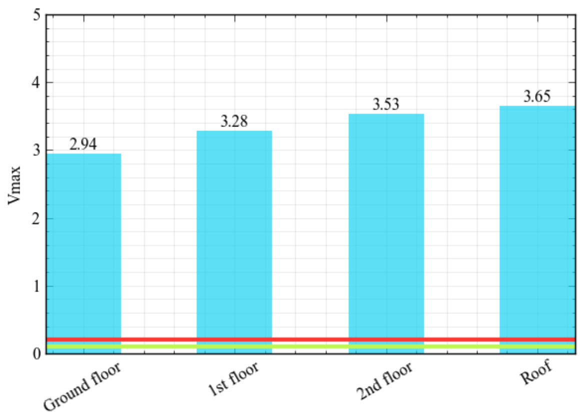

(f) V_{max} LVL hollow box floor, HB-W

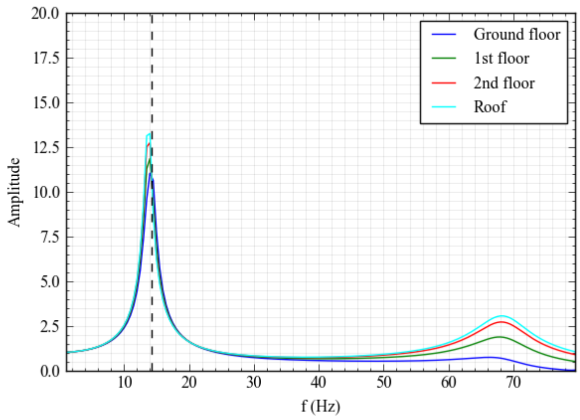

(g) Transfer functions mid-span floors, LVL hollow box floor, HB-D

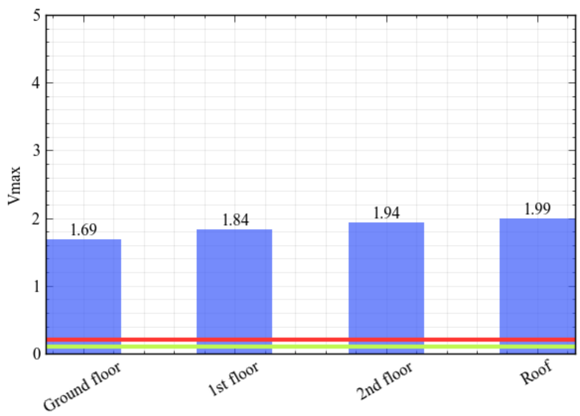

(h) V_{max} LVL hollow box floor, HB-D

Figure 7.13: Transfer function and V_{max} values serviceability criteria for three storeys instead of five

8
Discussion

The outcomes of the research have provided insight into the behaviour of residential behaviour of timber apartment buildings subjected to railway-induced vibrations and the effect of varying structural parameters such as the building geometry, the foundation, floor configurations and the walls. However, there are limitations that should be considered as well and the results should be interpreted carefully. This chapter focuses on a reflection of the research carried out. Possible limitations and potential consequences are outlined, followed by their corresponding implications on the interpretation of the results. Recommendations for future research can be found in chapter 9.

8.1. Interpretation

By comparing the timber buildings optimised based on the structural unity checks, the building vibrations are 108 % higher for the building with a CLT floor with a dry screed, 288 % for a CLT floor with a wet screed, 461 % higher for the LVL hollow box floor with a wet screed and for the LVL floor with a dry screed 293 %, compared to the equivalent concrete building. This difference is traced back to the interaction between the natural frequencies of the floors with the soil-building resonance, which results in high amplifications for the timber apartment buildings. Also, the effective area of the CLT walls is much lower than that of the concrete walls, resulting in higher storey-to-storey amplifications. The higher natural frequency of the concrete floors compared to the timber floors is also due to the clamped boundary conditions. The comparative analysis in chapter 7 shows that when considering fully rigid supports for the timber buildings, the difference between concrete and timber is reduced to 55-60%. However, creating fully rigid moment resisting connections between the timber CLT walls and floor configurations is currently challenging. Considering the connections to be fully simply supported may underestimate the connections, especially when considering supported floor connections instead of suspended connections. Research into the actual stiffness of timber connections when subjected to railway-induced vibrations may result in higher natural frequencies and will be beneficial for the overall building response.

Furthermore, the parameter study indicates that it is possible to adjust the design of timber apartment buildings to change their transfer functions. By doing so, it can be prevented that the peaks in the railway-induced spectra align with those of the building, lowering the vibration levels in the building. One of the options is to increase the natural frequency of the floors by increasing the floor thickness. The research demonstrates that by optimising the timber apartment buildings to lower the vibration levels, the cross-sections of the floors are overdimensioned; they have excessive capacity when considering the structural unity checks. The design considerations are however effective: for the building with the CLT floors, the vibrations are lowered by 44.2 % when a wet screed is applied and 22.3 % when a dry screed is considered. For the building with the LVL hollow box floor with a wet screed the reduction is 71.93 % when compared to the more economical design for each of the floors. For the LVL hollow box floor with a dry screed this is 60.56 %. Another measure that effectively reduces the building vibrations is adjusting the number of storeys. When decreasing the number of storeys for the building considered in chapter 7 from five to three, reductions in the building vibrations between 8.52-28.67 % are found.

When comparing the resulting building vibrations for the most effective and feasible method, increasing the floor thickness, the building vibrations are reduced from between 108-461 % higher to 55-65 % higher than those found for the equivalent concrete building.

Additionally, studying the buildings and provided Finite Element models (FEM) of the case studies indicates the way soil-structure interaction is taken into account makes a significant difference in the estimation of vibration levels in the buildings. For the HERO project, the soil-structure interaction is modelled extensively in the FEM model, whereas a linear transmission function is used for the ENKA project. The comparison of the two projects shows that taking into account soil-structure interaction by modelling the soil, as done for the HERO project, results in more attenuation of the vibrations. The calculations of the transfer function model show higher amplifications for the concrete building than those found in the HERO case study and lower amplifications for the ENKA case study.

8.2. Implications

This research highlights implications for constructing buildings near railway tracks, particularly emphasizing the critical role of soil-structure interaction (SSI) in determining vibration levels. The case studies show how much the estimated building vibrations can vary when different methods are used to take this soil-structure interaction into account. This conclusion is supported by the literature study, in which the importance of taking into account soil-structure interaction is stressed due to its effect on the building behaviour. It advocates for the necessity of real-world measurements within buildings in areas near railway tracks to identify which methods yield the most accurate results for assessing the building vibration levels. This does not only apply to residential timber apartment buildings, but is also important for the concrete alternatives.

Moreover, in literature it is often advised against using timber as building material in areas exposed to railway-induced vibrations. The results from this research partially fit with this theory, because when comparing the results from the concrete building of the HERO case study with the optimised timber buildings, the resulting vibration levels in the concrete building are lower for both cases. However, the transfer function model demonstrates how changes in the structural parameters of the building can influence the response of the building. Also, the spectra of the vibrations turn out to be very location dependent. The research shows that using the location-specific spectra of the railway-induced vibrations to design the timber apartment building, results in significant reductions in the resulting building vibration levels. Therefore, implementing the transfer function model in the preliminary design stages of a project is an easy way to optimise the structure and compare alternatives, such as a concrete building and a timber building. It has demonstrated to be a useful tool for optimising the building structure compared to computationally intensive alternative FEM models.

8.3. Limitations

One of the limitations of this research is that only the free-field measurements form the HERO case study are used to analyse whether the timber residential building exceeds the serviceability criteria V_{max}. Even though two case studies were available, only the data from the HERO case study could be reproduced. Calculating the values for V_{max} for the ENKA building for the supplied data results in much lower values of V_{max} than those reported in the provided report. The spectra of the railway-induced vibrations of this project could therefore not be used to analyse the response of the timber building. Because the railway spectra for this second location shows less peaks and lower amplification factors compared to the spectra of the railway-induced vibrations of HERO in the frequency range in which the highest amplification factors are found for the residential timber apartment building, imposing the vibrations corresponding to this spectrum is likely to lead to lower values of V_{max}. Therefore, although the building that was optimised to minimise the effect of the railway-induced vibrations does not meet these criteria for the HERO project, this does not mean that building with timber should automatically be disregarded in railway areas.

Furthermore, an important limitation of this research is that for neither of the case studies measurements after construction of the building are available. This limits the interpretation of the comparison with the transfer function model used in this research. Although the buildings considered for both the case studies are comparable and the soil conditions are also similar, the results from the provided FEM models used to analyse the vibration levels in the building differ substantially. The main difference can be found in the way the soil-structure interaction is taken into account in each of the FEM models. However, with the lack of measurements in either of the completed buildings, it is difficult to estimate which project is the most accurate representation of the real-world buildings. How the transfer function model relates to reality for these two situations can therefore also not be determined within this research, even though the model has been verified with both measurements and FEM models as described in the literature study. Especially since none of the considered cases in literature includes a pile foundation, which was added to the model in this study. Pre- and post-building measurements would aid in gaining more clarity on these relationships.

Another limitation of the research is the simplifications made in the transfer function model. For the application in the context of preliminary design, the transfer function model achieves its purpose. However, for more complex building geometry a more detailed FEM model can give additional insight into the behaviour of the building. The effect of a stability system such as a core is in the current research not taken into account, although this could potentially influence the building response positively. Also, in a FEM model the coupling between the soil and the building could be taken into account more elaborately, although again the need for measurements in a completed building are stressed to compare this FEM model to. One of the effects that is considered in the FEM model but not in the transfer function model is the kinematic soil-structure interaction. The literature study has however shown that this can further reduce the building vibrations, particularly at frequencies above 10 Hz. Especially for the optimised timber buildings, which have peaks in this higher frequency range, this could substantially reduce the resulting vibrations. If the same foundation is applied for both the timber and concrete building, the reduction of the free-field motions will have the same effect for both buildings. This is because the kinematic effect is solely dependent on the foundation characteristics. However, in the current study, a smaller pile diameter was used for the timber buildings based on the lower building mass. For piles with a smaller pile diameter, the kinematic reduction is slightly lower.

Additionally, as mentioned, the connections of the floors to the walls are considered to be hinged for the parameter study. This might be a conservative estimation, especially for the supported floor connections. Furthermore, the timber building may exhibit more damping through the connections and walls than currently taken into account for only the floors. However, more research into the propagation of vertical railway-induced vibrations through the building would have to be carried out to be able to determine these damping values.

Lastly, this research focused solely on the vertical railway-induced vibrations in the building. That means that the effect of the horizontal vibrations which are also generated by the railway system are not taken into account. Although the vertical vibrations were found to be governing for both the concrete buildings in the case studies, literature research showed that horizontal vibrations can also be the cause of disturbance for residents. Due to the lower stiffness of the walls and connections, the timber apartment buildings may be more prone to these horizontal vibrations than their concrete counterparts.

9 Conclusion

9.1. Conclusions

This research aimed to investigate the response of a residential timber building when subjected to railway-induced vibrations. A parameter study was carried out to analyse the influence of different structural parameters and the results were compared to the response of a concrete reference building from a case study. The following main research question was formulated:

> *How does a residential timber apartment building behave when subjected to railway-induced vibrations and how is this influenced by different structural parameters?*

Railway-induced vibration characteristics

- The transmission of the railway-induced vibrations can be divided into three phases, from the point where the vibrations are generated (source), the medium through which it then propagates (transmission path) to the building (receiver). At each of these stages, there is a large number of variables that influences the transmission of the vibrations. Therefore, railway-induced vibrations are highly location dependent. To analyse the effect of these vibrations on buildings in close proximity to the railway track, the use of measurements carried out on the ground before the construction of new buildings is often a recommended method.
- Especially the type of soil influences the attenuation or amplification of the railway-induced vibrations, with softer soils yielding higher overall free-field vibrations compared to stiffer soils. Contrastingly, softer soils also yield more damping due to the inertial interaction of the buiding with the soil.
- A positive correlation was found between the distance of residential buildings from the train track and the perceived annoyance of residents. Additionally, the vibrations that can occur in residential buildings near railways are shown to cause sleep disturbance in high traffic exposure areas.
- Although there is currently no legislation in the Netherlands regarding railway-induced vibrations, the serviceability criteria can be checked with the guideline "SBR richtlijn, Deel-B". The vibrations are translated to V_{max} after which they are checked against limiting values A_1 and A_2.

Dynamic preliminary design response

- An analytical transfer function model is decided upon for the parameter study. This model has low computational effort compared to numerical models such as a finite element model (FEM). Furthermore, this model has been shown to provide sufficiently accurate results for the initial design phases and it provides the possibility to closely monitor the effect of modifications in the building parameters.
- An additional advantage of the transfer function model is that the foundation and soil-structure interaction (SSI) can be taken into account, which has been recorded to influence the dynamic response in buildings significantly.

- By coupling the foundation, floors and walls, the transfer function model is able to take into account interaction between the building components.
- The transfer function model used in other research uses a shallow foundation. This study has shown that the transfer function model can be adjusted to take into account pile foundations as well, by creating a transfer matrix that takes into account the stiffness and the damping of the piles and soil.
- Research into pile foundations has shown that the behaviour of a pile group is not simply equal to the sum of the stiffness and damping of each of the individual piles and that the piles affect each other, a phenomenon referred to as 'group effect'. This was also taken into account in the adapted transfer function model.

Case studies for concrete buildings

- The two case studies that were provided to investigate railway-induced vibrations analyse two similar buildings. However, there is a large difference in how the dynamic analyses were carried out and also in the amplification and attenuation of the imposed vibrations. The FEM model that was used for the HERO project, which extensively includes soil-structure interaction, concludes that the designed building reduces the imposed railway-induced vibrations by ≈ 0.35 %. The ENKA case study also used a FEM model for the building, but without modelling the soil. The highest peak in the transfer function from the FEM model for the ENKA project increases the vibrations from the foundation to the top of the building with a factor eight.
- Applying the transfer function model to the HERO project resulted in two times higher V_{max} values than those obtained by the provided FEM model.
- Contrarily, when applying the transfer function model to the ENKA project, the amplitudes of the transfer functions model are around four times smaller compared to the values obtained by the ENKA FEM model.
- For neither of the buildings, measurements after the construction of the building are available. Therefore, it is difficult to draw conclusions on how the resulting railway-induced vibrations are best estimated.

Parameter study

- The parameter study shows that the highest peaks in the transfer functions are found around the natural frequencies of the considered floors. Interaction between the soil-building frequency and the natural frequency of the floors results in increased amplification factors. The amplification factors can be reduced by:
  - Increasing the natural frequencies of the floors. This can be done by increasing the stiffness, shortening the span, or by implementing a more rigid connection.
  - Increasing the total mass of the building. Effective measures are increasing the number of storeys or increasing the width of the floors.
  - Using a pile foundation instead of a shallow foundation.

Building optimisation and comparison

- The optimisation of the timber apartment buildings with the conclusions drawn from the parameter study and the comparison with an equivalent concrete building results in the following conclusions:
  - One of the main differences between the concrete building and the timber apartment building is that due to the lower mass of the timber building combined with lower natural frequencies of the floors, the soil-building frequency coincides with the natural frequency of the floors, resulting in higher building amplifications. This takes place because the soil does not exhibit its full damping potential due to this effect, which is in line with the results from the literature study.
  - The response of the timber buildings is also distinct from the concrete equivalent building because the CLT walls have a significantly smaller effective area and lower modulus of elasticity compared to the concrete walls. This results in higher storey-to-storey amplifications.

- The initial design of the timber buildings, optimised based on the structural design checks, yield between 108-461 % higher building vibrations for the HERO free-field vibrations compared to an equivalent concrete building.
- Considering stiffer support conditions for the timber buildings, such as fully clamped supports, increases the natural frequencies of the floors and reduces the building response substantially. However, creating fully rigid moment resisting connections between the timber CLT walls and floor configurations is currently challenging. Considering the support to be fully simply supported may be an underestimation of their natural frequency.
- When increasing the thickness of the floors, the imposed vibrations are reduced significantly. The floors are then overdimensioned when considering the structural unity checks. However, the difference with the equivalent concrete building is reduced to 55-60 % instead of the initial 108-461 %.
- Adjusting the number of storeys from five to three for the timber buildings reduces the building vibrations between 8.52-28.67 % for the HERO railway-induced vibrations.
- With the transfer function analysis, neither the concrete building nor the timber apartment building yield building vibrations lower than the serviceability criteria of either A_1 or A_2. However, considering the free-field vibrations and using the transfer function model to analyse the effect of mitigation measures for railway-induced vibrations has shown to be an effective and computationally efficient method for early design phases.

9.2. Recommendations

This section of the research presents recommendations for further research in the field of railway-induced vibrations in timber apartment buildings:

1. **Building measurements**
   The most important recommendation relates to the measurement of building vibrations. If both free-field measurements are available before the construction of the building and measurements are carried out in the building after its construction, the accuracy of the transfer function model, but also of the FEM models can be analysed. Ideally, measurements in a timber apartment building would also be carried out, to find out amongst others if the system displays more damping in the structural components than only the damping currently considered for the floors.

2. **Base-isolation**
   For the concrete building of the ENKA project, base isolation was implemented to lower the resulting building vibrations so that the serviceability criteria of the SBR guideline were satisfied. Although these measures are costly, it may provide a solution for residential timber apartment buildings and it is therefore recommended to further research how this effect can be accounted for and what effects it yields on the building response. It can then be compared to the costs of stiffening the floors by increasing their thickness, to analyse which method is more efficient in mitigating building vibrations. Besides the costs of both methods, the environmental costs should then also be considered.

3. **Complex building geometry**
   The transfer function model simplifies the building geometry. There are however components that could be used in the design of the building that may positively influence the building response to railway-induced vibrations. For example, the presence of a stability system such as a core could stiffen the building and lower the resulting building vibrations. Other factors that could alter the building response positively are differentiating between floor spans, considering the placement of the building relative to the railway track and adding a basement to the building structure. To be able to take these factors into account it is recommended to set up a finite element model for future research.

4. **More elaborate research into soil-structure interaction**
   Currently, the inertial effect of the soil-structure interaction is taken into account in the transfer function model. This accounts for the interaction between the building and the soil when the building is excited by the railway-induced vibrations. However, the presence of the building also

alters the free-field vibrations by reflection and refraction of the waves that propagate through the ground. This kinematic interaction effect is taken into account for the HERO case study and although it can not directly be derived from the provided data what this effect is, it is likely to further reduce the free-field vibrations that are now used. The literature study has also acknowledged this effect. Further research into implementing this in the transfer function model is therefore recommended.

5. **Horizontal vibrations**
   The last recommendation is to consider horizontal vibrations in future research. The focus in this research was on the vertical building vibrations, which were shown to be governing for both the considered case studies. It would however be interesting to further analyse the differences between the response of concrete and timber buildings by also considering horizontal vibrations. Potentially, the transfer function model can be adjusted so that it can be used for horizontal vibrations as well. The focus should then also be on verifying this adjusted model with measurements.

Bibliography

[1] Ik Abeysekera et al. *DEVELOPMENT OF A FLOOR VIBRATION DESIGN METHOD FOR EUROCODE 5 Federation of the Finnish woodworking industries, Finland*. Tech. rep. 1.

[2] Kayiparambil P. Anish et al. "An impedance model approach to predicting train-induced vibrations in buildings". In: *Structures Congress 2015 - Proceedings of the 2015 Structures Congress*. American Society of Civil Engineers (ASCE), 2015, pp. 864–875. ISBN: 9780784479117. DOI: 10.1061/9780784479117.074.

[3] George Anoyatis et al. "Kinematic response of single piles for different boundary conditions: Analytical solutions and normalization schemes". In: *Soil Dynamics and Earthquake Engineering* 44 (Jan. 2013), pp. 183–195. ISSN: 02677261. DOI: 10.1016/j.soildyn.2012.09.011.

[4] Matilda Arnesson. *Analysis and Estimation of Residential Vibration Exposure from Railway Traffic in Sweden*. Tech. rep. 2016.

[5] L Auersch. "Dynamic Stiffness of Foundations on Inhomogeneous Soils for a Realistic Prediction of Vertical Building Resonance". In: (). DOI: 10.1061/ASCE1090-02412008134:3328.

[6] Lutz Auersch. *Building Response due to Ground Vibration-Simple Prediction Model Based on Experience with Detailed Models and Measurements*. Tech. rep. 2010.

[7] Lutz Auersch. "Simple and fast prediction of train-induced track forces, ground and building vibrations". In: *Railway Engineering Science* 28.3 (Sept. 2020), pp. 232–250. ISSN: 26624745. DOI: 10.1007/S40534-020-00218-7/FIGURES/15. URL: https://link.springer.com/article/10.1007/s40534-020-00218-7.

[8] Lutz Auersch and Susanne Ziemens. "The response of different buildings to free-field excitation - a study using detailed finite element models". In: *Proceedings of the International Conference on Structural Dynamic , EURODYN* 2 (2020), pp. 4560–4576. ISSN: 23119020. DOI: 10.47964/1120.9371.19375.

[9] Mehdi Bahrekazemi. "Train-Induced Ground Vibration and Its Prediction". In: (Jan. 2004).

[10] Hans Joachim Blaß and Carmen Sandhaas. *Timber Engineering - Principles for Design*. en. KIT Scientific Publishing, 2017. URL: https://publikationen.bibliothek.kit.edu/1000069616%20files/521/Bla%C3%9F%20and%20Sandhaas%20-%202017%20-%20Timber%20Engineering%20-%20Principles%20for%20Design.pdf.

[11] Joseph E. Bowles. *Foundation analysis and design*. McGraw-Hill, 1996, p. 1175. ISBN: 0079122477.

[12] H A Buchholdt and S E Moossavi Nejad. *Structural Dynamics for Engineers (2nd Edition)*. URL: https://app.knovel.com/hotlink/toc/id:kpSDEE0001/structural-dynamics-engineers/structural-dynamics-engineers.

[13] Anil K Chopra. "Dynamics of structures : theory and applications to earthquake engineering". In: (2011). URL: https://books.google.com/books/about/Dynamics_of_Structures.html?hl=nl&id=IH-zzgEACAAJ.

[14] European Commission. "Mobility Strategy". en. In: *Sustainable and Smart Mobility Strategy – putting European transport on track for the future* (2020), p. 25. URL: https://transport.ec.europa.eu/transport-themes/mobility-strategy_en%20files/48/mobility-strategy_en.html.

[15] D P Connolly et al. "Benchmarking railway vibrations-Track, vehicle, ground and building effects". In: (2014). DOI: 10.1016/j.conbuildmat.2014.07.042. URL: http://dx.doi.org/10.1016/j.conbuildmat.2014.07.042.

[16] R Dobry and G Gazetast. *Simple method for dynamic stiffness and damping of floating pile groups*. Tech. rep.

[17] R. Dobry and G. Gazetas. “Simple method for dynamic stiffness and damping of floating pile groups”. In: *Geotechnique* 38.4 (Dec. 1988), pp. 557–574. ISSN: 17517656. DOI: 10.1680/GEOT.1988.38.4.557.

[18] Tisal Edirisinghe and James Talbot. *Some observations on the transmission of ground-borne vibration into base-isolated buildings.* Sept. 2022.

[19] Frank Fahy and John Walker. *Advanced Applications in Acoustics, Noise and Vibration.* Tech. rep. 2004.

[20] Gerhard Fink, Andrea Frangi, and Jochen Köhler. “Influence of varying material properties on the load-bearing capacity of glued laminated timber”. en. PhD thesis. 2014. URL: http://hdl.handle.net/20.500.11850/81314%20files/523/Fink%20-%202014%20-%20Influence%20of%20varying%20material%20properties%20on%20the%20lo.pdf.

[21] Ola Flodén, Kent Persson, and Göran Sandberg. “Numerical Investigation of Vibration Reduction in Multi-storey Lightweight Buildings”. en. In: ed. by Juan Caicedo and Shamim Pakzad. Conference Proceedings of the Society for Experimental Mechanics Series. Springer International Publishing, 2015, pp. 443–453. ISBN: 978-3-319-15248-6. DOI: 10.1007/978-3-319-15248-6{_}45. URL: files/55/Flod%C3%A9n%20et%20al.%20-%202015%20-%20Numerical%20Investigation%20of%20Vibration%20Reduction%20in%20.pdf.

[22] S François et al. “The influence of dynamic soil–structure interaction on traffic induced vibrations in buildings”. en. In: *Soil Dynamics and Earthquake Engineering* 27.7 (July 2007), pp. 655–674. ISSN: 02677261. DOI: 10.1016/j.soildyn.2006.11.008. URL: https://linkinghub.elsevier.com/retrieve/pii/S0267726106002028.

[23] Michael Green and Jim Taggart. *Tall Wood Buildings.* 2017. DOI: 10.1515/9783035604764.

[24] Carl E Hanson, David A Towers, and Lance D Meister. “Transit Noise and Vibration Impact Assessment”. In: 2006. URL: https://www.transit.dot.gov/sites/fta.dot.gov/files/docs/FTA_Noise_and_Vibration_Manual.pdf.

[25] Shan Huang et al. “Train-induced environmental vibrations by considering different building foundations along curved track”. In: *Transportation Geotechnics* 35 (July 2022), p. 100785. ISSN: 22143912. DOI: 10.1016/j.trgeo.2022.100785. URL: https://linkinghub.elsevier.com/retrieve/pii/S2214391222000691.

[26] Jarnerö$_I$*nlIndd*. “Vibrations in timber floors-Dynamic properties and human perception”. In: (2014).

[27] I Van Kamp et al. “Health effects of vibrations due to trains”. en. In: (2015).

[28] Hermann Kaufmann, Stefan Krötsch, and Stefan Winter. *Manual of Multistorey Timber Construction.* München: DETAIL, 2018. ISBN: 978-3-95553-395-3. URL: https://doi.org/10.11129/9783955533953%20files/537/Kaufmann%20et%20al.%20-%202018%20-%20Manual%20of%20Multistorey%20Timber%20Construction.pdf.

[29] A.M. Kaynia and E. Kausel. *Dynamic Stiffness and Seismic Response of Pile Groups.* 1982. URL: https://www.researchgate.net/publication/260539543_Dynamic_Stiffness_and_Seismic_Response_of_Pile_Groups/citations.

[30] Josef Kolb. *Systems in timber engineering: loadbearing structures and component layers.* ger. Basel Boston: Birkhäuser, 2008. ISBN: 978-3-7643-8690-0. URL: https://ebookcentral-proquest-com.tudelft.idm.oclc.org/lib/delft/reader.action?docID=3063845.

[31] K A Kuo et al. “The coupling loss of a building subject to railway induced vibrations: Numerical modelling and experimental measurements”. In: *Journal of Sound and Vibration* 442 (2019), pp. 459–481. DOI: 10.1016/j.jsv.2018.10.048. URL: https://doi.org/10.1016/j.jsv.2018.10.048.

[32] Raffaele Di Laora and Luca De Sanctis. “Piles-induced filtering effect on the Foundation Input Motion”. In: (2013). DOI: 10.1016/j.soildyn.2012.12.007. URL: http://dx.doi.org/10.1016/j.soildyn.2012.12.007.

[33] A. Leissa. *Vibration of plates.* Tech. rep. National Aeronautics and space administration (NASA), 1969.

[34] Xuming Li et al. "Building coupling loss measurement and prediction due to train-induced vertical vibrations". In: *Soil Dynamics and Earthquake Engineering* 164 (Jan. 2023). ISSN: 02677261. DOI: 10.1016/j.soildyn.2022.107644.

[35] Xiang Liu et al. "Dynamic stiffness method for exact longitudinal free vibration of rods and trusses using simple and advanced theories". In: *Applied Mathematical Modelling* 104 (Apr. 2022), pp. 401–420. ISSN: 0307904X. DOI: 10.1016/j.apm.2021.11.023.

[36] Mott Macdonald Group et al. *Simplified models to inform the base-isolation design of buildings*. Tech. rep. 2023. URL: https://www.researchgate.net/publication/374164043.

[37] Laura Maclachlan et al. "Annoyance in Response to Vibrations from Railways". In: *International Journal of Environmental Research and Public Health* 15.9 (Sept. 2018), p. 1887. ISSN: 1661-7827. DOI: 10.3390/ijerph15091887. URL: https://www.ncbi.nlm.nih.gov/pmc/articles/PMC6163999/.

[38] Rosa Maria Stefania Maiorano et al. "Kinematic response analysis of piled foundations under seismic excitation". In: *Canadian Geotechnical Journal* 46.5 (May 2009), pp. 571–584. ISSN: 00083674. DOI: 10.1139/T09-004/ASSET/IMAGES/T09-004IE8H.GIF. URL: https://cdnsciencepub.com/doi/10.1139/T09-004.

[39] Jens Malmborg. "Vibrations from Railway Traffic: Computational Modeling and Analysis". PhD thesis. Division of Structural Mechanics, LTH, Sept. 2022.

[40] Christian Meinhardt. "Einflussgrößen für das Schwingungsverhalten von Gebäuden zur Prognose von Erschütterungsimmissionen". PhD thesis. Jan. 2008. DOI: 10.14279/depositonce-1875.

[41] H R Milner and A C Woodard. "8 - Sustainability of engineered wood products". In: *Sustainability of Construction Materials (Second Edition)*. Ed. by Jamal M Khatib. Second Edition. Woodhead Publishing Series in Civil and Structural Engineering. Woodhead Publishing, 2016, pp. 159–180. ISBN: 978-0-08-100995-6. URL: https://www.sciencedirect.com/science/article/pii/B9780081003701000081%20files/466/Milner%20and%20Woodard%20-%202016%20-%208%20-%20Sustainability%20of%20engineered%20wood%20products.pdf.

[42] Mariya Moskovets and Nikolay Kanev. "Assessment of Rail Vibration Transmission from the Ground to the Foundation of a Building". In: *MATEC Web of Conferences* 320 (2020), p. 00005. ISSN: 2261-236X. DOI: 10.1051/MATECCONF/202032000005. URL: https://www.matec-conferences.org/articles/matecconf/abs/2020/16/matecconf_aso2020_00005/matecconf_aso2020_00005.html.

[43] George Mylonakis. *SIMPLIFIED MODEL FOR SEISMIC PILE BENDING AT SOIL LAYER INTERFACES*. Tech. rep. 4. 2001, pp. 47–58.

[44] George Mylonakisi and George Gazetasii. "VERTICAL VIBRATION AND ADDITIONAL DISTRESS OF GROUPED PILES IN LAYERED SOIL". In: *SOILS AND FOUNDATIONS* 38.1 (1998), pp. 1–14.

[45] NEN. "NEN-EN 1995-1-1:2023 Ontw. en". In: *Netherlands Standards Institute, Delft (NL)* (2023).

[46] E. Öhrström and A. B. Skånberg. "A FIELD SURVEY ON EFFECTS OF EXPOSURE TO NOISE AND VIBRATION FROM RAILWAY TRAFFIC, PART I: ANNOYANCE AND ACTIVITY DISTURBANCE EFFECTS". In: *Journal of Sound and Vibration* 193.1 (May 1996), pp. 39–47. ISSN: 0022-460X. DOI: 10.1006/JSVI.1996.0244.

[47] Slimane Ouakka, Olivier Verlinden, and Georges Kouroussis. "Railway ground vibration and mitigation measures: benchmarking of best practices". en. In: *Railway Engineering Science* 30.1 (Mar. 2022), pp. 1–22. ISSN: 2662-4745, 2662-4753. DOI: 10.1007/s40534-021-00264-9. URL: https://link.springer.com/10.1007/s40534-021-00264-9.

[48] A Oulmane, A A Lakis, and N Mureithi. *A Method for Analyzing Rotating Machinery Faults using Time-Frequency Application*. Tech. rep. 2. 2013, pp. 21–34.

[49] Nils Persson. *Predicting railway-induced ground vibrations*. Tech. rep. 2016. URL: www.byggmek.lth.se.

[50] P Persson et al. “Effect of structural design on traffic-induced building vibrations”. en. In: *Procedia Engineering* 199 (2017), pp. 2711–2716. ISSN: 18777058. DOI: 10.1016/j.proeng.2017.09.577. URL: https://linkinghub.elsevier.com/retrieve/pii/S1877705817340961%20files/63/Persson%20et%20al.%20-%202017%20-%20Effect%20of%20structural%20design%20on%20traffic-induced%20bui.pdf.

[51] Jr. Richart F. E. *Vibrations of Soils and Foundations*. 1970.

[52] Masoud Sanayei, Pradeep Maurya, and James A Moore. “Measurement of building foundation and ground-borne vibrations due to surface trains and subways”. In: (2013). DOI: 10.1016/j.engstruct.2013.03.038. URL: http://dx.doi.org/10.1016/j.engstruct.2013.03.038.

[53] Masoud Sanayei et al. “Prediction and Mitigation of Building Floor Vibrations Using a Blocking Floor”. In: *Journal of Structural Engineering* 138.10 (Oct. 2012), pp. 1181–1192. ISSN: 0733-9445. DOI: 10.1061/(asce)st.1943-541x.0000557.

[54] Michael G. Smith et al. “On the Influence of Freight Trains on Humans: A Laboratory Investigation of the Impact of Nocturnal Low Frequency Vibration and Noise on Sleep and Heart Rate”. In: *PLoS ONE* 8.2 (Feb. 2013). ISSN: 19326203. DOI: 10.1371/JOURNAL.PONE.0055829. URL: /pmc/articles/PMC3567002/%20/pmc/articles/PMC3567002/?report=abstract%20https://www.ncbi.nlm.nih.gov/pmc/articles/PMC3567002/.

[55] Jonathan Stewart et al. *Soil-Structure Interaction for Building Structures*. en. 2012. URL: https://tsapps.nist.gov/publication/get_pdf.cfm?pub_id=915495.

[56] Storaenso. *Rib Panels*. URL: https://www.storaenso.com/en/products/mass-timber-construction/building-products/rib-panels#Tbcb28296-fbfc-4b59-9673-95271c39ed36.

[57] James Talbot, Tisal Edirisinghe, and Giuseppe Sanitate. *The influence of foundation and building structures on ground-borne vibration: What we might expect and what we find in practice*. July 2023.

[58] James P. Talbot. *Base-isolated buildings: Towards performancebased design*. Aug. 2016. DOI: 10.1680/jstbu.15.00057.

[59] *The CLT Handbook CLT structures-facts and planning*. Tech. rep. URL: www.traguiden.se,.

[60] David Thompson. “Chapter 12 - Low Frequency Ground Vibration∗”. en. In: *Railway Noise and Vibration*. Ed. by David Thompson. Oxford: Elsevier, 2009, pp. 399–435. ISBN: 978-0-08-045147-3. URL: https://www.sciencedirect.com/science/article/pii/B9780080451473000128%20files/39/Thompson%20-%202009%20-%20Chapter%2012%20-%20Low%20Frequency%20Ground%20Vibration%E2%88%97.pdf%20files/38/B9780080451473000128.html.

[61] David J. Thompson, Georges Kouroussis, and Evangelos Ntotsios. “Modelling, simulation and evaluation of ground vibration caused by rail vehicles*”. In: *Vehicle System Dynamics* 57.7 (July 2019), pp. 936–983. ISSN: 17445159. DOI: 10.1080/00423114.2019.1602274.

[62] I. H. Turunen-Rise et al. “Vibration in dwellings from road and rail traffic — Part I: a new Norwegian measurement standard and classification system”. In: *Applied Acoustics* 64.1 (Jan. 2003), pp. 71–87. ISSN: 0003-682X. DOI: 10.1016/S0003-682X(02)00052-X.

[63] I Van Kamp et al. “Wonen langs het spoor - Gezondheidseffecten trillingen van treinen”. In: *RIVM rapport 2014-096* (2014). ISSN: 2014-0096.

[64] Paul de Vos. “Railway induced vibration - State of the art report”. en. In: *International Union of Railways* (Nov. 2017). Ed. by Nick Craven and Linus Grob, p. 82. URL: https://uic.org/com/enews/nr/571-sustainable-development/article/vibrations-state-of-the-art-report.

[65] Ing C Vrettos and Georgia Efthymiou. *NUMERICAL STUDY ON THE KINEMATIC RESPONSE OF PILED FOUNDATIONS TO A STATIONARY OR MOVING LOAD*. Tech. rep. 2023.

[66] A.C.W.M. Vrouwenvelder. *SBR richtlijn Meet- en beoordelingsrichtlijn voor trillingen:2013 - Deel B - Hinder voor personen in gebouwen*. SBRCURnet, 2013. URL: https://www.briswarenhuis.nl/docs/cur/menbrl-deelb-2013/menbrl-deelb-2013.

[67] J Weckendorf et al. “Vibration serviceability performance of timber floors”. en. In: *European Journal of Wood and Wood Products* 74.3 (2016), pp. 353–367. ISSN: 0018-3768, 1436-736X. DOI: 10.1007/s00107-015-0976-z. URL: http://link.springer.com/10.1007/s00107-015-0976-z%20files/51/Weckendorf%20et%20al.%20-%202016%20-%20Vibration%20serviceability%20performance%20of%20timber%20flo.pdf.

[68] Martin Williams. *Structural dynamics*, p. 265. ISBN: 9780415427326.

[69] Christoffer With and Anders Bodare. “Prediction of train-induced vibrations inside buildings using transfer functions”. In: *Soil Dynamics and Earthquake Engineering* 27.2 (Feb. 2007), pp. 93–98. ISSN: 02677261. DOI: 10.1016/j.soildyn.2006.06.003.

[70] John P Wolf. *Simple Physical Models for Foundation Dynamics*. Tech. rep. 1995. URL: http://scholarsmine.mst.edu/icrageesdhttp://scholarsmine.mst.edu/icrageesd/03icrageesd/session16/5.

[71] John P. Wolf. “Dynamic Soil-Structure Interaction”. In: *Prentice-Hall International Series in Civil Engineering and Engineering Mechanics* (1985).

[72] Jabbarali Zakeri, Morteza Esmaeili, and Mehrad Mousavi-Rahimi. “Effect of foundation shape and properties of the adjacent buildings on the railway-induced vibrations”. In: *Asian Journal of Civil Engineering* 21.7 (Nov. 2020), pp. 1095–1108. ISSN: 2522011X. DOI: 10.1007/S42107-020-00264-W.

[73] Binsheng Zhang et al. “Comparison of vibrational comfort assessment criteria for design of timber floors among the European countries”. In: *Engineering Structures* 52 (July 2013), pp. 592–607. ISSN: 01410296. DOI: 10.1016/j.engstruct.2013.03.028. URL: https://linkinghub.elsevier.com/retrieve/pii/S014102961300151X.

[74] Mi Zhao et al. *An analytical solution for the dynamic response of an end-bearing pile subjected to vertical P-waves considering water-pile-soil interactions*. Feb. 2022. DOI: 10.1016/j.soildyn.2021.107126.

[75] Chao Zou et al. “Efficient impedance model for the estimation of train-induced vibrations in over-track buildings”. In: *JVC/Journal of Vibration and Control* 27.7-8 (Apr. 2021), pp. 924–942. ISSN: 17412986. DOI: 10.1177/1077546320935285.

[76] Chao Zou et al. “Impedance model for estimating train-induced building vibrations”. In: *Engineering Structures* 172 (Oct. 2018), pp. 739–750. ISSN: 18737323. DOI: 10.1016/j.engstruct.2018.06.032.

A

Dynamic stiffness and damping single pile

To calculate the values for the transfer matrix of the soil-foundation element, Equation 4.10, the vertical dynamic stiffness k_z^p and the damping ratio β_z^p have to be calculated [55]. The dynamic stiffness is a combination of the static stiffness K_z^p and a dynamic modification factor α_z^p:

$$k_z^p = K_z^p \cdot \alpha_z^p \tag{A.1}$$

The static stiffness K_z^p can be calculated with the following formulas [55]:

$$\begin{aligned}
K_z^p &= \chi_z E_s d \\
\chi_z &= \sqrt{\frac{\pi\delta_z}{2}}\sqrt{\frac{E_p}{E_s}}\frac{\Omega + \tanh(\lambda L_p)}{1 + \Omega\tanh(\lambda L_p)} \\
\Omega &= \frac{2}{(\sqrt{\pi\delta_z})(1-\nu^2)}\frac{1}{\sqrt{\frac{E_p}{E_s}}} \\
\lambda L_p &= \sqrt{\frac{4\delta_z}{\pi}}\frac{1}{\sqrt{\frac{E_p}{E_s}}}\frac{L_p}{d} \\
\delta_z &= 0.6; (L_p/d > 10, \frac{E_p}{E_s} > 100)
\end{aligned} \tag{A.2}$$

In Equation A.2, the subscripts p and s represent, respectively, whether the parameter belongs to the pile or soil material. d is the pile diameter; L_p the pile length; E_j the Young's modulus; ρ_j the mass density; ν Poisson's ratio of the soil; V_s the shear wave velocity of the soil and w_{pz}, w_{sz} and w_{bz} are weight factors.

The factor α_z^p from Equation A.1 can also be calculated with formulas given in Stewart et al. [55]:

$$\begin{aligned}
\alpha_z^p &= 1 - w_{sz}\left[\left(\frac{\pi}{8\delta_x}\right)\left(\frac{\frac{\rho_p}{\rho_s}}{1+\nu}\right)(a_o^p)^2 - \frac{1}{2}\sqrt{a_o^p}\right] \\
w_{sz} &= \frac{-2[(\lambda L_p)(\Omega^2 - 1) + \Omega] + 2\Omega\cosh(2\lambda L_p) + (1+\Omega^2)\sinh(2\lambda L_p)}{4\cosh^2(\lambda L_p)[\Omega + \tanh(\lambda L_p)][1 + \Omega\tanh(\lambda L_p)]} \\
\delta_z &= 2\left(\frac{E_p}{E_s}\right)^{\frac{-3}{40}} \\
a_o^p &= \frac{\omega d}{V_s}
\end{aligned} \tag{A.3}$$

Lastly, the damping ratio β_z^p can be calculated as follows [55], [44]:

$$\beta_z^p = w_{pz}\beta_p + (w_{sz} + w_{pz})\beta_s + \beta_{rz}w_{pz} = 1 - (w_{sz} + w_{bz})$$
$$w_{bz} = \frac{2\Omega}{2\Omega\cosh(\lambda L_p) + (1+\Omega^2)\sinh(\lambda L_p)} \tag{A.4}$$
$$\beta_{rz} = \frac{1}{\alpha_z^p}\left[w_{sz}\frac{1.2\pi}{4(1+\nu)\delta_z}(a_o^p)^{\frac{3}{4}} + w_{bz}0.21a_o^p\right]$$

In this equation, β_p and β_s are respectively the hysteretic damping ratios of the pile and soil.

The equations for the stiffness and damping of the single piles are checked with the results presented by Stewart et al. [55], presented in Figure A.1.

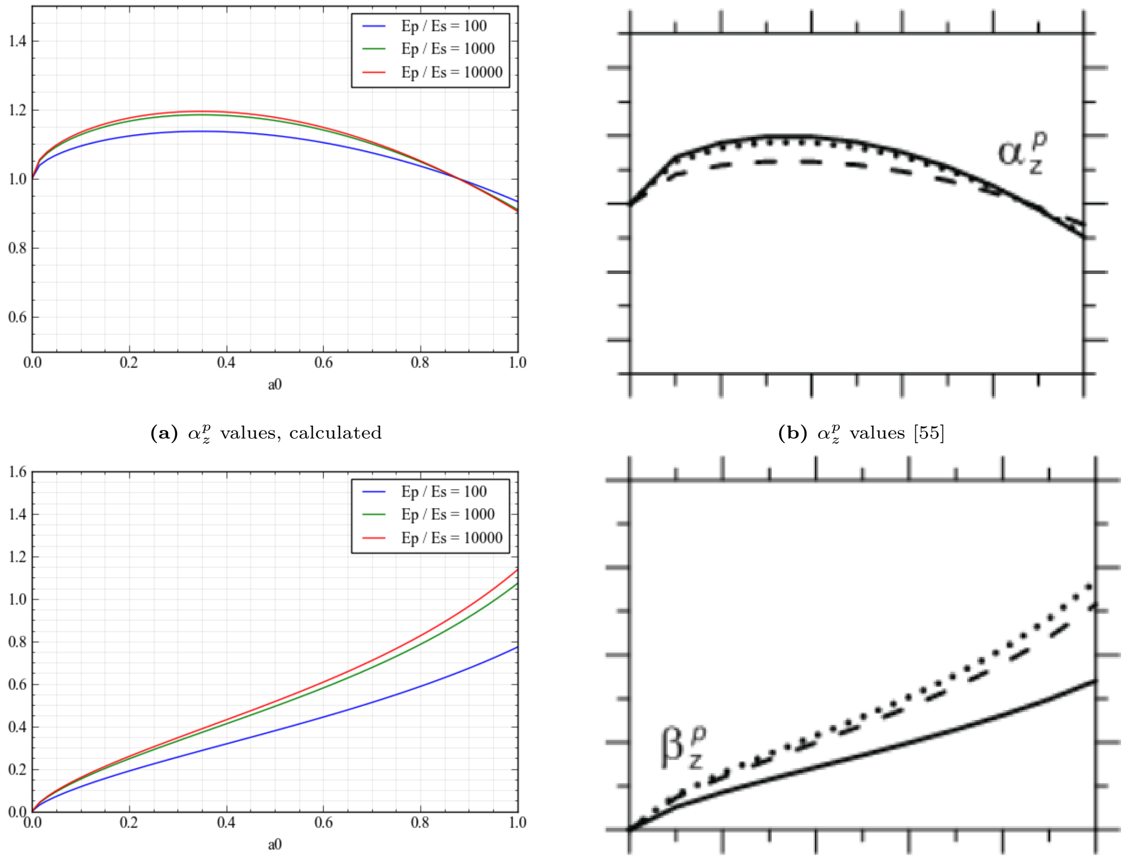

(a) α_z^p values, calculated

(b) α_z^p values [55]

(c) β_z^p values, calculated

(d) β_z^p values [55]

Figure A.1: Verification damping and stiffness of single piles

B

Dynamic stiffness and damping pile group

B.1. Verification two by two pile group

The stiffness and damping of a group of piles can be calculated using the impedance $\mathscr{K}^G$. For a pile group of two by two, the results are verified against the results obtained by Dobry and Gazetast [16].

The piles are equally spaced with a distance S in the horizontal and vertical directions. Therefore, the diagonal distance between the piles in the corners is $S\sqrt{2}$, as shown in Figure B.1.

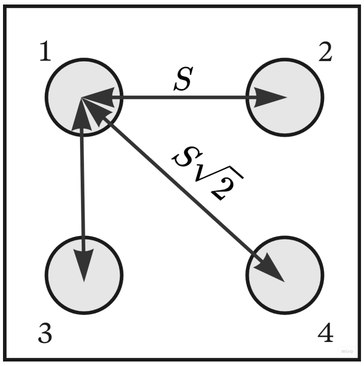

Figure B.1: 2x2 pile group

The effect of the vibration of pile p on pile q can be calculated with the dynamic interaction factor α_v, which depends on the distance between the piles and the frequency, according to Dobry and Gazetast [16]:

$$\alpha_v(S) = \left(\frac{S}{r_0}\right)^{-1/2} \exp(-\beta_s \omega S/V_s) \cdot \exp(-i\omega S/V_s) \tag{B.1}$$

In which $r0 = d/2$ with d being the diameter of the piles, S the distance between the considered piles, V_s the shear wave velocity of the soil, β_s the damping factor of the soil and ω the frequency, equal to $2\pi f$ in which f is the frequency in Hz. Both piles with distance S and those with distance $S\sqrt{2}$ are close enough to influence each other's vibrations, so α_v must be calculated for both distances, resulting in $\alpha_v(S)$ and $\alpha_v(S\sqrt{2})$.

The load applied to the pile group is in this case equally distributed due to symmetry. Therefore, $F_1 = F_2 = F_3 = F_4 = F$. The displacement of pile 1 w_1 can be described by the effect of the displacement of the pile itself and the displacement of pile 1 caused by the other 3 piles:

$$w_1 = w_{11} + w_{12} + w_{13} + w_{14} \tag{B.2}$$

Since the distance between pile 2 and 1 and pile 3 and 1 is the same, it can be derived that $w_1 2 = w_1 3$. By taking into account the interaction factors, the unknowns can be removed from the equation:

$$w_1 = w_{11}(1 + 2\alpha_v(S) + \alpha_v(S\sqrt{2})) \tag{B.3}$$

The impedance of a single pile is defined as follows:

$$\mathscr{K}_z^{\mathbf{S}}(\omega) = \bar{K}_z^{\mathbf{S}}(\omega) + ia_0 C_z^{\mathbf{S}}(\omega) = F^{\mathbf{S}}/w^{\mathbf{S}} \tag{B.4}$$

Therefore, w_{11} can be expressed in terms of the impedeance of a single pile, which in turn can be calculated with the equations from Appendix A:

$$w_1 = \frac{F}{\mathscr{K}_z^S}(1 + 2\alpha_v(S) + \alpha_v(S\sqrt{2})) \tag{B.5}$$

By definition, the group impedance $\mathscr{K}^G$ is equal to Equation B.6.

$$\mathscr{K}_{\mathrm{z}}^{\mathrm{G}} = \bar{K}_{\mathrm{z}}^{\mathrm{G}} + ia_0 C_{\mathrm{z}}^{\mathrm{G}} = F^{\mathrm{G}}/w^G \tag{B.6}$$

Therefore, the group impedance for a pile group of two by two $\mathscr{K}^G$ can be determined with Equation B.7.

$$\mathscr{K}_{\mathrm{z}}^{\mathrm{G}} = \frac{4F}{w_1} = \frac{4\mathscr{K}_{\mathrm{z}}^{\mathrm{s}}}{1 + 2\alpha_{\mathrm{v}}(S) + \alpha_{\mathrm{v}}(S\sqrt{2})} \tag{B.7}$$

From this impedance function, the pile group stiffness is found taking the real part of the function, while the damping is calculated taking the imaginary part.

$$\begin{aligned} \bar{K}_{\mathrm{z}}^{\mathrm{G}} &= \mathfrak{Re}(\mathscr{K}_{\mathrm{z}}^{\mathrm{G}}) \\ C_{\mathrm{z}}^{\mathrm{G}} &= \frac{\mathfrak{Im}(\mathscr{K}_{\mathrm{z}}^{\mathrm{G}})}{a_0} \end{aligned} \tag{B.8}$$

For the pile group of two by two shown in Figure B.1, with $\frac{E_p}{E_s} = 1000$ and a ratio of $\frac{L}{d} = 15$, $\nu_s = 0.4$, $\beta_s = 0.05$, using the equations for $\mathscr{K}_z^{\mathbf{S}}$ as described in Appendix A, the response of the pile groups for different values of $\frac{S}{d}$ is derived. In Figure B.2 the results from Dobry and Gazetast [16] and the obtained results are compared. The stiffness and damping are normalised by dividing them by the sum of the stiffnesses of the individual piles. The trend that can be seen in Figure B.2 is similar for both the calculated values and the ones provided in the literature. However, there is a difference in the height of the peaks, which has to do with the way the stiffness and damping of a single pile is calculated.

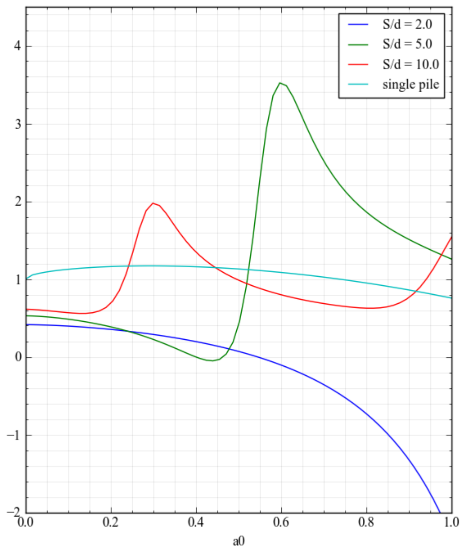

(a) Normalised stiffness 2x2 pile group, calculated

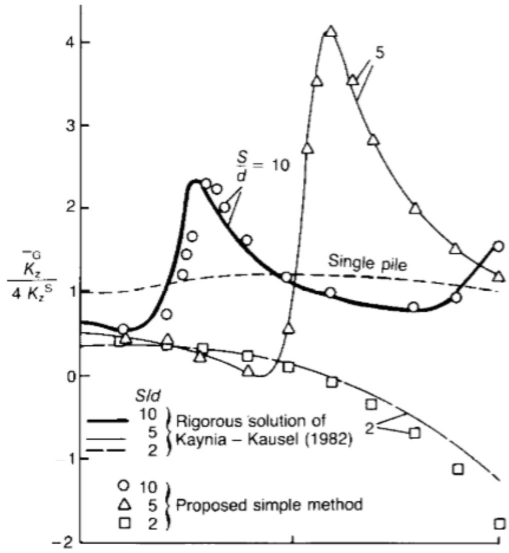

(b) Normalised stiffness 2x2 pile group, [16]

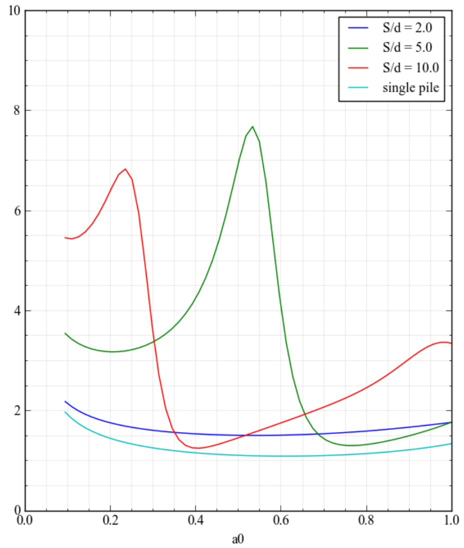

(c) Normalised damping factor 2x2 pile group, calculated

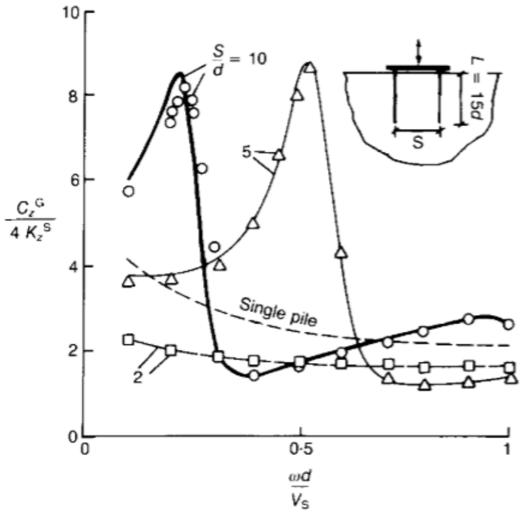

(d) Normalised damping factor 2x2 pile group, [16]

Figure B.2: Verification damping and stiffness of a two by two pile group

B.2. Verification three by three pile group

The same method can be followed for a three by three pile group, or a pile group of any other configuration. Due to symmetry, the edge piles and center piles can be grouped. Whereas for the two by two group the forces on each pile were the same, in the case of a three by three pile group, the forces on the piles are not equal to each other: the force that will be taken by the center pile will differ from the edge or corner piles.

When considering the effect of piles where there are also intermediate piles, these intermediate piles are considered "transparent"; they are assumed not to influence the interaction between the two piles considered. This principle is illustrated for the derivation of w_1 in Figure B.3.

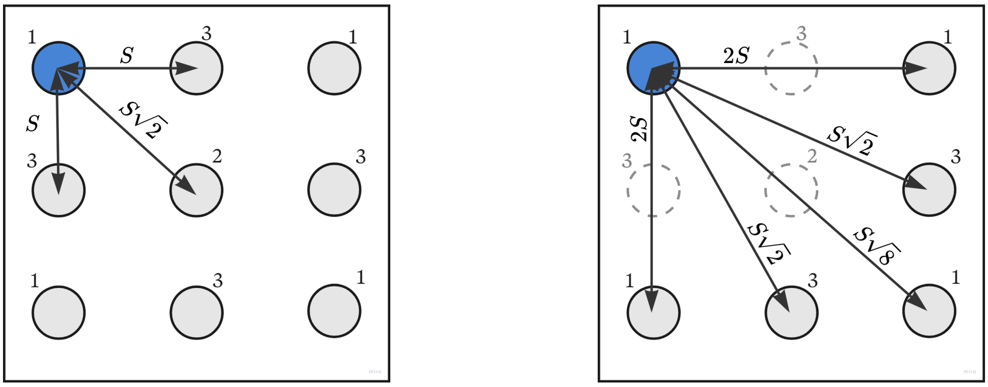

(a) Neighbouring piles w_1 **(b)** Transparent intermediate piles

Figure B.3: Interaction between piles, determination of w_1

Based on the geometry of the pile group with a pile distance of S, the following equations can be set up for the pile displacements:

$$
\begin{aligned}
w_1 &= w_{11} + w_{12} + w_{13} \\
w_2 &= w_{22} + 4w_{21} + 4w_{23} \\
w_3 &= w_{33} + w_{32} + w_{31} \\
w_{11} &= \frac{F_1(1 + 2a_v(S) + a_v(\sqrt{8}))}{\mathscr{K}_z^{\mathbf{S}}(\omega)} \\
w_{12} &= \frac{F_2 a_v(S\sqrt{2})}{\mathscr{K}_z^{\mathbf{S}}(\omega)} \\
w_{13} &= \frac{F_3(2a_v + 2a_v(S\sqrt{5}))}{\mathscr{K}_z^{\mathbf{S}}(\omega)} \\
w_{22} &= \frac{F_2}{\mathscr{K}_z^{\mathbf{S}}(\omega)} \\
w_{21} &= \frac{F_1 a_v(S\sqrt{2})}{\mathscr{K}_z^{\mathbf{S}}(\omega)} \\
w_{23} &= \frac{F_3 a_v}{\mathscr{K}_z^{\mathbf{S}}(\omega)} \\
w_{33} &= \frac{F_3(1 + 2a_v(\sqrt{\ }) + a_v(S))}{\mathscr{K}_z^{\mathbf{S}}(\omega)} \\
w_{32} &= \frac{F_2 a_v}{\mathscr{K}_z^{\mathbf{S}}(\omega)} \\
w_{31} &= \frac{F_1(2a_v + 2a_v(S\sqrt{5}))}{\mathscr{K}_z^{\mathbf{S}}(\omega)}
\end{aligned}
$$

The distribution of the pile forces $F^G G$ is the sum of all the individual forces:

$$F^G = 4F_1 + 4F_3 + F_2 \tag{B.9}$$

For each distance between two piles within the three by three pile group, the interaction factor α_v can again be calculated:

$$a_{op} = \frac{2\pi f d}{V_s}$$

$$a_v = \left(\frac{S}{\frac{d}{2}}\right)^{-\frac{1}{2}} \cdot \exp\left(-\beta_s(2\pi f)\frac{S}{V_s}\right) \cdot \exp\left(-i(2\pi f)\frac{S}{V_s}\right)$$

$$a_v(S) = \left(\frac{2S}{\frac{d}{2}}\right)^{-\frac{1}{2}} \cdot \exp\left(-\beta_s(2\pi f)\frac{2S}{V_s}\right) \cdot \exp\left(-i(2\pi f)\frac{2S}{V_s}\right)$$

$$a_v(S\sqrt{2}) = \left(\frac{S\sqrt{2}}{\frac{d}{2}}\right)^{-\frac{1}{2}} \cdot \exp\left(-\beta_s(2\pi f)\frac{S\sqrt{2}}{V_s}\right) \cdot \exp\left(-i(2\pi f)\frac{S\sqrt{2}}{V_s}\right)$$

$$a_v(S\sqrt{5}) = \left(\frac{S\sqrt{5}}{\frac{d}{2}}\right)^{-\frac{1}{2}} \cdot \exp\left(-\beta_s(2\pi f)\frac{S\sqrt{5}}{V_s}\right) \cdot \exp\left(-i(2\pi f)\frac{S\sqrt{5}}{V_s}\right)$$

$$a_v(\sqrt{8}) = \left(\frac{S\sqrt{8}}{\frac{d}{2}}\right)^{-\frac{1}{2}} \cdot \exp\left(-\beta_s(2\pi f)\frac{S\sqrt{8}}{V_s}\right) \cdot \exp\left(-i(2\pi f)\frac{S\sqrt{8}}{V_s}\right)$$

Using the equations for the displacements and the equation for F^G, the system can be solved (for example in Maple) and the pile group impedance $\mathscr{K}_\mathrm{z}^\mathrm{G}$ can again be found. With the pile group impedance, the stiffness of the group and the damping factor can be calculated:

$$\text{Then:} \quad \mathscr{K}_z^{\mathbf{S}}(\omega) = k_z^p \cdot (1 + 2i\beta_z^p)$$

$$\begin{aligned}\mathscr{K}_z^{\mathbf{G}}(\omega) = 4\Bigg(& 8a_v(S\sqrt{2})^2 + (-12a_v + a_v(S) - 4a_v(S\sqrt{5}) - \frac{a_v(\sqrt{8})}{2} - \frac{1}{2})a_v(S\sqrt{2}) \\ & + a_v^2 + (4a_v(S) - 2a_v(S\sqrt{5}) + 2a_v(\sqrt{8}) + 6)a_v - \frac{a_v(S)^2}{2} - \frac{a_v(\sqrt{8})}{4} - \frac{15}{4})a_v(S\sqrt{2}) \\ & + a_v(S\sqrt{5})^2 + 4a_v(S\sqrt{5}) - \frac{5a_v(\sqrt{8})}{4} - \frac{9}{4}\Bigg) \cdot \mathscr{K}_z^{\mathbf{S}}(\omega)\end{aligned}$$

$$\bar{K}_\mathrm{z}^\mathrm{G} = \mathfrak{Re}(\mathscr{K}_\mathrm{z}^\mathrm{G})$$

$$C_\mathrm{z}^\mathrm{G} = \frac{\mathfrak{Im}(\mathscr{K}_\mathrm{z}^\mathrm{G})}{a_{op}}$$

For the three by three pile group, with $\frac{E_p}{E_s} = 1000$ and a ratio of $\frac{L}{d} = 15$, $\nu_s = 0.4$, $\beta_s = 0.05$, using the equations for $\mathscr{K}_z^{\mathbf{S}}$ as described in Appendix A, the response of the pile groups for different values of $\frac{S}{d}$ is derived. In Figure B.4 the results from Dobry and Gazetast [16] and the obtained results are compared. The stiffness and damping are normalised by dividing them by the sum of the stiffnesses of the individual piles. Again, there is a difference in the height of the peaks, which has to do with the way the stiffness and damping of a single pile is calculated.

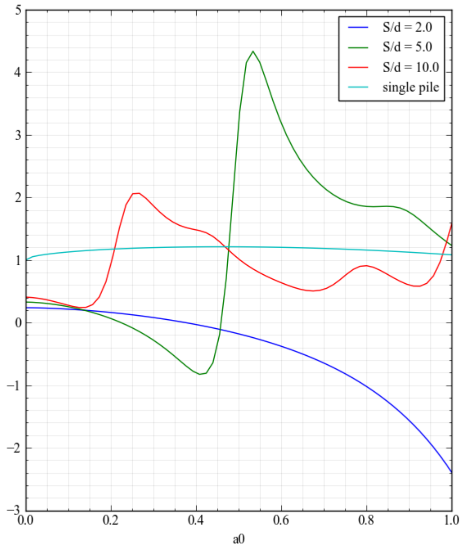

(a) Normalised stiffness 3x3 pile group, calculated

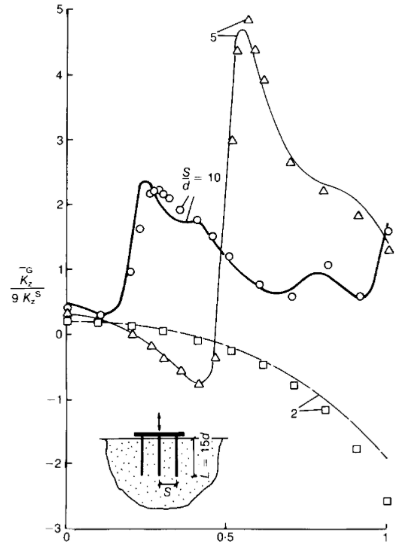

(b) Normalised stiffness 3x3 pile group, [16]

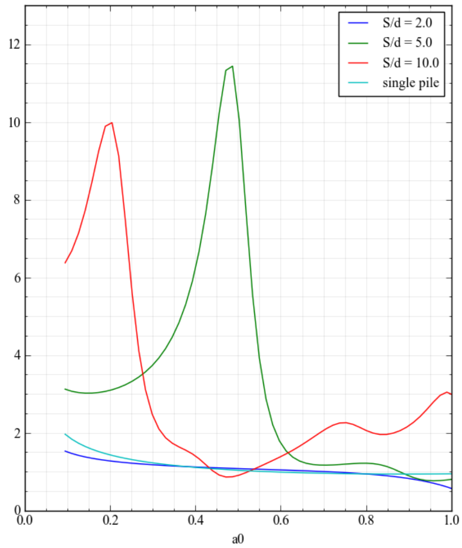

(c) Normalised damping factor 3x3 pile group, calculated

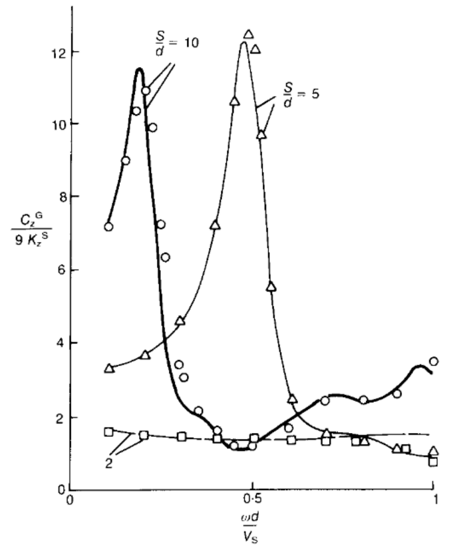

(d) Normalised damping factor 3x3 pile group, [16]

Figure B.4: Verification damping and stiffness of a two by two pile group

C
Derivation of transfer functions floor

For a flexible plate, the equation for the transfer function between the support force of the floor $P_{F,W}$ and the displacement at this location $U_{F,W}$ is as follows [6]:

$$\frac{P_{F,W}}{U_{F,W}} = (2\pi f)^2 (m_F + \mu \frac{f^2}{(1 + 2ci) f_{0,F}^2 - f^2}) \tag{C.1}$$

In this appendix, the derivation of this formula will be shown.

A floor system subjected to a harmonic base excitation at its support (the connecting wall or column) $U_{F,W}$ can be described by the following differential equation [6]:

$$K(U_R) - m\omega^2 U_R = m\omega^2 U_{F,W} \tag{C.2}$$

With $U_R = U - U_0$, the mass density of the floor m, the forcing frequency ω and the dynamic stiffness operator $K = k + i\omega c$. To solve the equation, the eigenfunctions ϕ_n and their corresponding eigenfrequencies ω_n have to be found that satisfy the homogeneous equation:

$$K(\phi_n) - m\omega_n^2 \phi_n = 0 \tag{C.3}$$

Assuming U_R can be written as an expansion of the eigenfunctions, results in:

$$U_R = \sum_{n=1}^{\infty} c_n \phi_n \tag{C.4}$$

By inserting this in the original differential equation Equation C.2 and making use of the orthogonality of the eigenfunctions, the expansion coëfficients can be found. To do so, the equation is multiplied with the eigenfunction ϕ_n and then integrated, after substituting Equation C.4:

$$\int (K(c_n \phi_n) - m\omega^2 c_n \phi_n) \phi_n \, dm = \int m\omega^2 U_{F,W} \phi_n \, dm \tag{C.5}$$

By dividing by m and making use of $\omega_n = \frac{K}{m}$ this equation can be rewritten:

$$c_n \int (\omega_n^2 - \omega^2) \phi_n^2 \, dm = \int m\omega^2 U_{F,W} \phi_n \, dm \tag{C.6}$$

And then by dividing the terms, the following equation can be found:

$$\frac{c_n}{U_{F,W}} = \frac{\int \omega^2 \phi_n \, dm}{\int (\omega_n^2 - \omega^2) \phi_n^2 \, dm} \tag{C.7}$$

Remembering that $U_R = U - U_{F,W}$, the transfer function between the displacement at x and the displacement of the support can be found as follows:

$$\frac{U(x)}{U_{F,W}} = \frac{U_{F,W} + U_R}{U_{F,W}} = 1 + \sum_{n=1}^{\infty} \frac{c_n}{U_{F,W}} \phi_n$$
$$= 1 + \phi_n \frac{\int \phi_n \, dm}{\int \phi_n^2 \, dm} \frac{\omega^2}{(\omega_n^2 - \omega^2)} \tag{C.8}$$

In this equation, α is the highlighted blue part of the formula.

Then, to find $\frac{P_{F,W}}{U_{F,W}}$, the transfer function between the support force $P_{F,W}$ and the support displacement, the integral of the inertial forces is taken:

$$\frac{P_{F,W}}{U_{F,W}} = \int -\omega^2 \frac{U_{F,W} + U_R}{U_{F,W}} \, dm$$
$$= \int -\omega^2 \, dm - \int \omega^2 \sum_{n=1}^{\infty} \frac{c_n}{U_{F,W}} \phi_n \, dm$$
$$= -m_F \omega^2 - \omega^2 \frac{(\int \phi_n \, dm)^2}{\int \phi_n^2 \, dm} \frac{\omega^2}{(\omega_n^2 - \omega^2)} \tag{C.9}$$
$$= -(\omega^2)(m_F - \mu \frac{\omega^2}{\omega_n^2 - \omega^2})$$

In this equation, μ is the highlighted blue part of the formula.

D

Verification transfer matrix model

The transfer matrix model has been used and verified with experimental results in different research papers. To verify the Python model that was written for this thesis, two different cases discussed by Auersch [7] are used to check if the results from the Python model are in agreeance with the results from the paper.

D.1. Wall model

First, a four-storey building is considered. The building has masonry walls and concrete floors of 5 m x 5 m and is made up of four apartments next to each other, creating a total floor area of 20 m^2. The floors are one-way slabs and are assumed to be clamped at the connection with the walls. The corresponding material properties are shown in Table D.1.

Table D.1: Material parameters four-storey building

		Wall - masonry	**Floor - concrete**	**Unity**
Modulus of Elasticity	E	$5 \cdot 10^9$	$30 \cdot 10^9$	N/m^2
Mass density	ρ	2500	2500	kg/m^3
Thickness	t	0.25	0.2	m
Area	A	$0.25 \cdot 20 = 5$	$5 \cdot 20 = 100$	m^2
Height	h_W	3	-	m
Poisson's ratio	ν	-	0.2	-
Damping ratio	D	-	0.05	-

The material properties of the soil can be found in Table D.2.

Table D.2: Soil parameters four-storey building

		Soil	**Unity**
Shear wave velocity	ν_s	100	m/s
Foundation area	A_s	$1 \cdot 20 = 20$	m^2
Shear modulus	G_s	$8.5 \cdot 10^7$	N/m

Using the transfer matrix method explained in chapter 4 results in the transfer matrices shown in Figure D.1c and Figure D.1a. These are in agreeance with the transfer matrices found by Auersch [7] shown in in Figure D.1d and Figure D.1b, although it can be seen that at the natural frequency of the floor the peaks seam to differ in amplitude. The shape of the functions is however equal. Most likely there is a small difference in input data, but this value can not specifically be found.

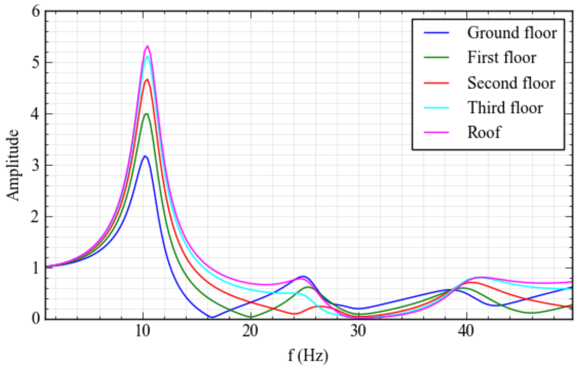

(a) Transfer functions wall, Python model

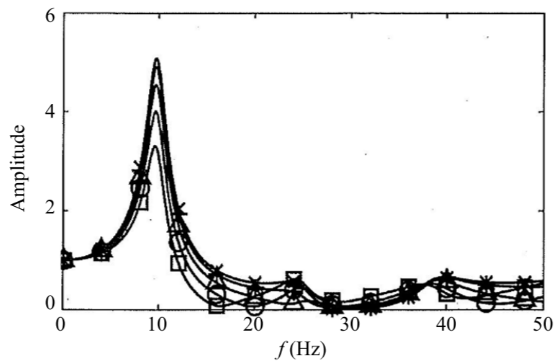

(b) Transfer functions wall from Auersch [7]

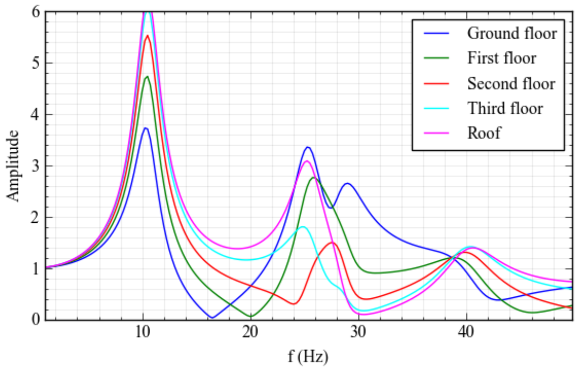

(c) Transfer functions floor, Python model

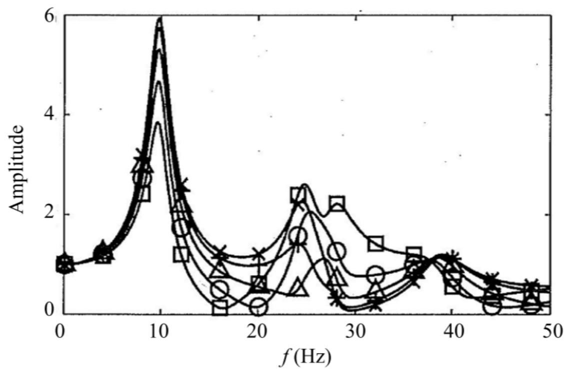

(d) Transfer functions floor from Auersch [7]

Figure D.1: Transfer functions four-storey building

D.2. Column model

To accommodate for the columns, the Python model is slightly adjusted by calculating the equivalent column area. To validate the column component, a twenty-storey building is considered. Every span has four columns and there are three spans in a row. The floors are considered to be point supported. Both the columns and the floors are constructed from concrete. The corresponding material properties are shown in Table D.3.

Table D.3: Material parameters twenty-storey building

		Columns - concrete	**Floor - concrete**	**Unity**
Modulus of Elasticity	E	$30 \cdot 10^9$	$30 \cdot 10^9$	N/m^2
Mass density	ρ	2500	2500	kg/m^3
Thickness	t	0.6	0.2	m
Area	A	$0.6 \cdot 0.6 \cdot 4 = 1.44$	$6 \cdot 18 = 108$	m^2
Height	h_W	3	-	m
Poisson's ratio	ν	-	0.2	-
Damping ratio	D	-	0.05	-

The material properties of the soil are shown in Table D.4.

Table D.4: Soil parameters twenty-storey building

		Soil	Unity
Shear wave velocity	ν_s	200	m/s
Foundation area	A_s	$1 \cdot 18 = 18$	m^2
Stiffness soil	k_s	$540 \cdot 10^6$	N/m

From Figure D.2a and Figure D.2b it can again be seen that these results are in agreeance with each other for the most important values: the eigenfrequency of the total building around 4 Hz, where the first and largest peak occurs; the second peak around 10 Hz, caused by the floor resonance; the small peaks between 20 and 30 Hz. The exact parameters used by Auersch [7] are not given in the paper and had to be partially assumed, which is assumed to be the explanation for small deviations between the results of Figure D.2a and Figure D.2b.

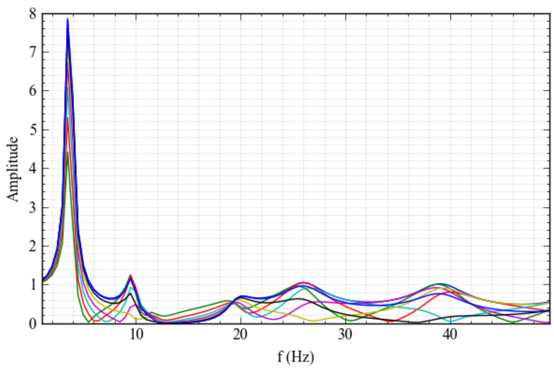

(a) Transfer functions columns, Python model

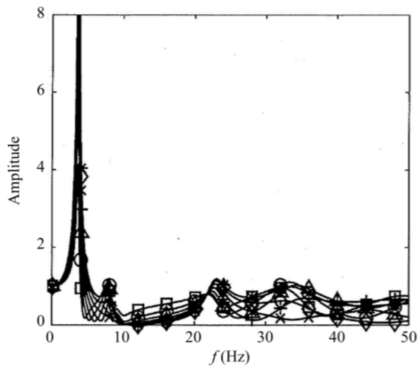

(b) Transfer functions columns from Auersch [7]

Figure D.2: Transfer functions twenty-storey building

E

Structural verifications

E.1. Floor system

Considering one of the floors of the building as shown in Figure E.1, the floor is checked on bending, shear force, walking-induced vibration criteria and deflections.

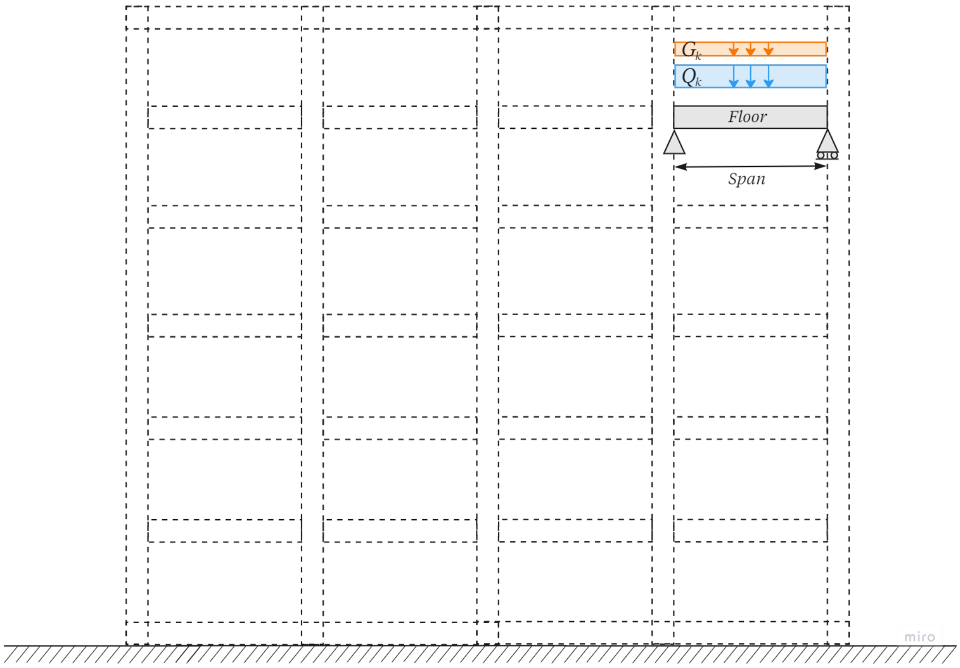

Figure E.1: Representative floor structural calculations

Two forces are considered to act on the floor: its self-weight g_k, including that of any floor finishes and the live load q_k for residential buildings of category A, equal to $1.75kN/m^2$ as prescribed in the EN 1991-1-1. Besides that, the self-weight of partitions has to be taken into account. In agreeance with the NEN-EN 1991-1-1+C1+C11:2019, this value is taken as $q_k = 0.8kN/m^2$, resulting in a total variable load on the floors of $q_{f,k} = 1.75 + 0.8 = 2.55kN/m^2$.

The design strength of a CLT or hollow box floor can be calculated with Equation E.1 conform 4.5.1 of the EN 1995-1-1:2011. For a CLT floor, $\gamma_M = 1.25$ and $k_{mod} = 0.8$ for the imposed floor load, with the medium-term load duration class in the ULS. For a LVL hollow box floor, $\gamma_M = 1.2$ and $k_{mod} = 0.8$.

$$f_d = \frac{k_{mod} \cdot f_k}{\gamma_M} \tag{E.1}$$

The design load combination for the floor in ULS is in agreeance with the NEN-EN 1990:2021 equal to Equation E.2, with $\gamma_G = 1.35 \cdot 0.89$ and $\gamma_G = 1.5$

$$q_d = \gamma_G \cdot g_k + \gamma_Q \cdot q_k \tag{E.2}$$

E.1.1. Bending

CLT floor

The floor is considered to be a simply supported single span, with a width $b_x = 1.0\ m$. The design bending moment for a single span simply supported beam of length L is given in Equation E.3.

$$M_d = \frac{1}{8} q_d L^2 \tag{E.3}$$

The design moment can be used to calculate the design bending stresses:

$$\sigma_d = \frac{M_d}{W_{x,net}} \tag{E.4}$$

In which $W_{x,net}$ represents the net moment of resistance of the cross-section. This moment is calculated differently for a CLT floor and a LVL hollow box floor.
The moment of resistance can be calculated after the net moment of inertia $I_{x,net}$ is found. The net moment resistance of a CLT floor is determined by considering the layers in which the fibres are oriented parallel to the span, as shown in Figure E.2.

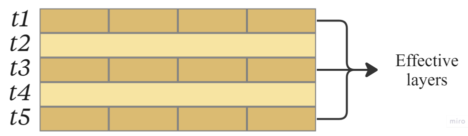

Figure E.2: Effective layers parallel to span for a CLT floor

Any floor finishes such as a screed are not taken into account in the flexural rigidity for the cross-sectional checks. For a symmetrical CLT panel of either 3 or 5 layers in which the layers are of equal thickness per direction, I_{net} is equal to:

$$\begin{aligned} I_{x,net} &= b_x \left(n \frac{t_1^3}{12} + 2 t_1 a_1^2 \right) \\ W_{x,net} &= \frac{2 I_{x,net}}{h_{CLT}} \end{aligned} \tag{E.5}$$

In which h_{CLT} is equal to the total thickness of the CLT, a_1 is the distance between the centre of gravity z_0 and the layers in the direction of the span, n is the number of layers in the direction of the span and t_1 is the thickness of the layers in the direction of the span.
For pure bending, the following needs to be satisfied:

$$k_{red} \cdot \frac{\sigma_d}{f_{m,d}} \leq 1.0 \tag{E.6}$$

For CLT floors, $k_{red} = 1.0$.

LVL hollow box floor

For hollow box sections, the design bending moment can be calculated with Equation E.7.

$$M_d = \frac{1}{8} q_d \cdot b_{ef,1} L^2 \tag{E.7}$$

Furthermore, the cross-section can be divided into middle sections and edge sections, as shown in Figure E.3.
For both sections, the effective width of the upper and lower flanges can be calculated. In Figure E.4, the dimensions of the cross sections are shown that are used in the calculations.

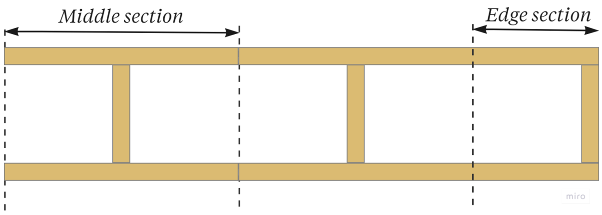

Figure E.3: Middle and edge sections LVL hollow box floor

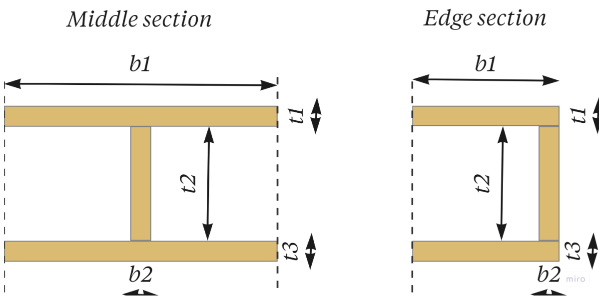

Figure E.4: Dimensions LVL cross section

To calculate the effective width for the flexural rigidity for bending, the limits for the effective width for the compression side $b_{c,ef}$ and the tension side $b_{t,ef}$ are calculated first:

$$\begin{aligned} b_{c,ef} &= \min(0.1L; 20t_1) \\ b_{t,ef} &= \min(0.1L; 20t_3) \end{aligned} \tag{E.8}$$

For the middle sections, the following limits apply:

$$\begin{aligned} b_{ef,1} &= \min(b_{c,ef} + b_2; b_1) \\ b_{ef,3} &= \min(b_{t,ef} + b_2; b_3) \end{aligned} \tag{E.9}$$

For the edge sections, the following limits apply:

$$\begin{aligned} b_{ef,1} &= \min(0.5b_{c,ef} + b_2; b_1) \\ b_{ef,3} &= \min(0.5b_{t,ef} + b_2; b_3) \end{aligned} \tag{E.10}$$

Since it is a hollow core slab with the same width b for both flanges, $b_{ef,1} = b_{ef,3}$. By taking into account the effective width of the upper and lower slab, the effective areas can be calculated, after which the centre of gravity z_0 can be determined. Similar to the CLT floor, any floor finishes such as a screed are not taken into account in the flexural rigidity for the cross-sectional checks. Now, the bending strength can be checked with the following equation:

$$k_h \cdot \frac{\sigma_d}{f_{m,d}} \leq 1.0 \tag{E.11}$$

In which k_h is a factor that takes into account the deviation of the height of the rib h if this is not equal to 300 mm:

$$k_h = \min(\left(\frac{300}{h}\right)^s; 1.2) \tag{E.12}$$

In which the factor s is a factor that takes into account the volume effect, and is determined for LVL with the help of the EN 14374:

$$s = 2 \cdot v - 0.05 \tag{E.13}$$

For this research, the factor v which takes into account the variation of the test results of the LVL element that is used in the design, is taken as 0.10, resulting in a value of $s = 0.15$.

The bending stress is calculated in four different points, as shown in Figure E.5.

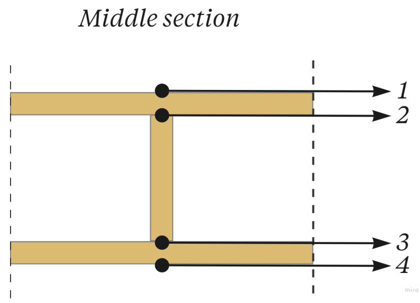

Figure E.5: Locations bending checks in LVL hollow box panel

E.1.2. Shear force

The design shear force for a simply supported single-span floor is equal to:

$$V_d = \frac{1}{2} q_d L \tag{E.14}$$

CLT floor

The design shear stress τ_d can be calculated for a CLT floor with Equation E.15.

$$\tau_d = \frac{V_d \cdot S_{x,net}}{I_{x,net} \cdot b_x} \tag{E.15}$$

The net static moment of longitudinal shear $S_{x,net}$ can be calculated as follows:

$$S_{x,net} = b_x t_1 a_1 + b_x \frac{t_c^2}{8} \tag{E.16}$$

In which t_c is the thickness of the middle panel. For the cross-section to be able to resist the shear force, the following has to be satisfied:

$$\tau_d \leq k_{cr} \cdot f_{v,d} \tag{E.17}$$

For CLT floors, $k_{cr} = 1.0$.

Furthermore, in the case of CLT slabs, the rolling shear stress has to be checked. This has to be verified because of the potential for shear forces to cause the layers of a CLT slab to slide over each other. The rolling design shear stress $\tau_{Rv,d}$ can be calculated in a similar manner as the shear stress, with Equation E.18.

$$\tau_{Rv,d} = \frac{V_d \cdot S_{Rx,net}}{I_{x,net} \cdot b_x} \tag{E.18}$$

The net static moment of rolling shear $S_{R,x,net}$ is found with Equation E.19.

$$S_{R,x,net} = b_x \cdot t_1 \cdot a_1 \tag{E.19}$$

For the panel to be able to resist the rolling shear force, the following equation has to be satisfied:

$$\tau_{Rv,d} \leq k_{r,pu} \cdot f_{Rv,d} \tag{E.20}$$

In which $k_{r,pu} = 1.60$ for CLT fully made of timber layers.

LVL hollow box floor

According to the NEN-EN 1995-1-1+C1+A1:2011, the shear force for a LVL hollow box cross-section should be comply to the following limits:

$$V_d \leq \begin{cases} b_2 h_2 \left(1 + \frac{0.5(t_1+t_3)}{h_2}\right) f_{v,0,d}, & \text{if } h_2 \leq 35 b_2 \\ 35 b_2^2 \left(1 + \frac{0.5(t_1+t_3)}{h_2}\right) f_{v,0,d}, & \text{if } 35 b_2 \leq h_2 \leq 70 b_2 \end{cases} \tag{E.21}$$

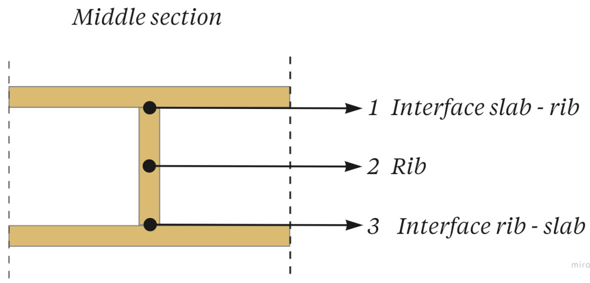

Figure E.6: Locations shear checks LVL hollow box panel

For a hollow box section, the design shear force is equal to:

$$V_d = \frac{1}{2} q_d \cdot b_{ef,1} \cdot L \tag{E.22}$$

Besides that, it needs to be checked that the shear stress τ_d does not exceed the shear resistance at the interface of the LVL rib with the flanges and at the center of gravity of the cross-section as shown in Figure E.6. The checks are carried out for both the middle section and the edge section. Similar to the CLT panel, $k_{cr} = 1.0$:

$$\tau_d \leq k_{cr} \cdot f_{v,d} \tag{E.23}$$

At each position shown in Figure E.6, the occuring shear force can be calculated with Equation E.24.

$$\tau_d(z) = E_i \frac{V_d \cdot S_y(z)}{EI_{y,ef} \cdot b_i} \tag{E.24}$$

In this equation, i denotes which element is checked (the upper flange, rib or lower flange) and $S_y(z)$ is the net static moment at that location of the cross section.

E.1.3. Deformations

To calculate the deformations of the floor, the initial deflection and the effect of creep have to be taken into account. The initial deflection due to the variable and permanent forces for a single-span simply supported system can be calculated with Equation E.25.

$$w_{inst} = \frac{5 \cdot q \cdot L^4}{384 \cdot E_{x,mean} \cdot I_{x,ef}} \tag{E.25}$$

To take into account the effect of creep, the initial deflection due to the permanent load is multiplied with a factor k_{def}. For floors, service class 1 is used, resulting in a value of $k_{def} = 0.85$.

$$w_{creep,G} = k_{def} \cdot w_{inst,G} \tag{E.26}$$

Since the creep is dependent on the time that the load is present, the factor k_{def} is multiplied with ψ_2 for the variable load.

$$w_{creep,Q} = k_{def} \cdot \psi_2 \cdot w_{inst,Q} \tag{E.27}$$

The total deformation w_{tot} of the creep and the initial deflections can then be calculated as follows:

$$w_{tot} = w_{inst,G} \cdot (1 + k_{def}) + w_{inst,Q} \cdot (1 + \psi_2 k_{def}) \tag{E.28}$$

The design criteria for the floor structure according to the EN 1995-1-1:2011 is a maximum deflection w_{tot} of $L/300$.

E.1.4. Vibration criteria

Timber floors that fall into the category of residential floors, have to be checked against human-induced vibrations caused by footfall. If the natural frequency of the floor is above $f_{1,lim} = 8Hz$, no resonant response will take place according to the prEN 1995-1-1:2023. The following criteria still need to be checked:

- stiffness criteria
- velocity criteria

If the natural frequency is however below $f_{1,lim} = 8Hz$, then the acceleration criterium also has to be taken into account. Besides that, the natural frequency has to be higher than $4.5Hz$. If a screed is present, the bending stiffness of this screed can be considered to contribute to the total floor stiffness due to the prEN 1995-1-1:2023. In the cross-sectional calculations, the screed is disregarded.

Stiffness criteria

The maximum deflection $w_{1,kN}$ due to a point load of 1 kN, for a simply supported single-span floor placed in the middle, should be lower than $w_{lim,max}$. For floors in residential buildings, $w_{lim,max} = 0.25mm$.

$$w_{1,kN} = \frac{FL^3}{48 \cdot EI_L \cdot b_{ef}} \leq w_{lim,max} \tag{E.29}$$

In this equation, the effective width b_{ef} can be determined as follows:

$$b_{ef} = \min(0.95 \cdot L \cdot \left(\frac{EI_T}{EI_L}\right)^{0.25}; b) \tag{E.30}$$

In which L is the span of the floor, EI_L and EI_T are for CLT the net bending stiffness in respectively the longitudinal and transverse direction and b represents the width of the floor.

Velocity criteria

To check the velocity criteria, first the modal impulse $I_{mod,mean}$ needs to be calculated:

$$I_{mod,mean} = \frac{42 \cdot f_w^{1.43}}{f_1^{1.3}} \tag{E.31}$$

With a walking frequency of $f_w = 1.5Hz$ for residential buildings and f_1 the natural frequency of the considered floor. The peak velocity $v_{1,peak}$ equals:

$$v_{1,peak} = k_{red} \frac{I_{mod,mean}}{M^* + 70} \tag{E.32}$$

In which $k_{red} = 0.7$ and M^* represents the modal mass in kg, The modal mass for a single span floor according to the prEN 1995-1-1:2023 is:

$$M^* = \frac{m \cdot L \cdot b}{4} \tag{E.33}$$

In which b is the width of the floor and m is the mass per unit area. This value should include any permanent loads, the self-weight of the floor and any partition walls. Besides that, it should include an additional mass, which should be taken as 10% of the imposed loads.

Then, to take into account other vibration modes apart from the natural frequency of the floor, k_{imp} can be calculated, after which it is multiplied with $v_{1,peak}$ to find the total peak response $v_{tot,peak}$:

$$\begin{gathered} k_{imp} = \max(0.48 \cdot \frac{b}{L} \left(\frac{EI_L}{EI_T}\right)^{0.25}; 1.0) \\ v_{tot,peak} = k_{imp} \cdot v_{1,peak} \end{gathered} \tag{E.34}$$

Finally, the root mean square velocity v_{rms} can be calculated:

$$v_{rms} = v_{tot,peak} \cdot (0.65 - 0.01 f_1) \cdot (1.22 - 11.0\xi) \cdot \eta \tag{E.35}$$

In Equation E.35 ξ is the damping ratio, which is 0.04 for a CLT floor with floating floor layer. η for a CLT floor is calculated with Equation E.36, as long as $1.0 \leq k_imp \leq 1.7$, otherwise $\eta = 0.67$.

$$\eta = 1.35 - 0.4 \cdot k_{imp} \tag{E.36}$$

Lastly, v_{rms} can be tested for the criteria that need to be satisfied:

$$v_{rms} < 0.0001\, R\, m/s \tag{E.37}$$

Acceleration criteria

For floors for which the natural frequency is lower than $f_{1,lim} = 8Hz$, the acceleration criteria also need to be checked. Besides that, the criteria $f_1 \geq 4.5Hz$ also need to be met.

The root mean square value of acceleration a_{rms} can be calculated as follows:

$$a_{rms} = \frac{k_{res} \mu_{res} F_{dyn}}{\sqrt{2} \cdot 2\xi M^*} \tag{E.38}$$

In which F_{dyn} is taken as 50 N in agreeance with the prEN 1995-1-1:2023, representing the assumed weight of a walking person. μ_{res} is a resonant build-up factor and taken as 0.4. ξ and M^* are again respectively the damping ratio and the modal mass. Lastly, k_{res} is calculated with Equation E.39.

$$k_{res} = \max(0.19 \cdot \frac{b}{L} \left(\frac{EI_L}{EI_T} \right)^{0.25}; 1.0) \tag{E.39}$$

The criteria that need to be satisfied:

$$a_{rms} < 0.005\, R\, m/s^2 \tag{E.40}$$

E.1.5. Fire safety

Although the importance of fire safety calculations should be stressed, in this research it is assumed that the fire safety requirements can be obtained by covering the upper part of the floor with a screed and the ceiling with gypsum plates.

E.2. CLT wall system

When assuming all cross-sections of all walls are the same when checking the walls on compressive forces, an inner wall as shown in Figure E.7 will be governing for the compressive stresses.

The forces that are taken into account are the variable loads on the floors above the column $Q_{f,k}$, the self-weight of these floors including their finishes $G_{f,k}$, the self-weight of the roof $G_{r,k}$ and the self-weight of all the columns above the considered column $G_{c,k}$. Like in section E.1 live load Q_k for residential buildings of category A is equal to $1.75kN/m^2$ as prescribed in the EN 1991-1-1.

Furthermore, the self-weight of partitions has to be taken into account. In agreeance with the NEN-EN 1991-1-1+C1+C11:2019, this value is taken as $q_k = 0.8kN/m^2$. The NEN-EN 1991-1-1:2002+C11:2019+NB:2019 prescribes that when a force is considered on two or more floors, for two floors the extreme value of the variable load has to be considered. In this case, that means that on the two upper floors, the applied load will be equal to $q_{f,k} = 1.75 + 0.8 = 2.55kN/m^2$. On the other floors including the roof, the reduction factor ψ_0 can be taken into account.

Furthermore, floors are again considered to be simply supported, resulting in a load transfer per floor to the governing wall of $\frac{1}{2}qL$. The total characteristic variable and permanent loads in kN/m will then be:

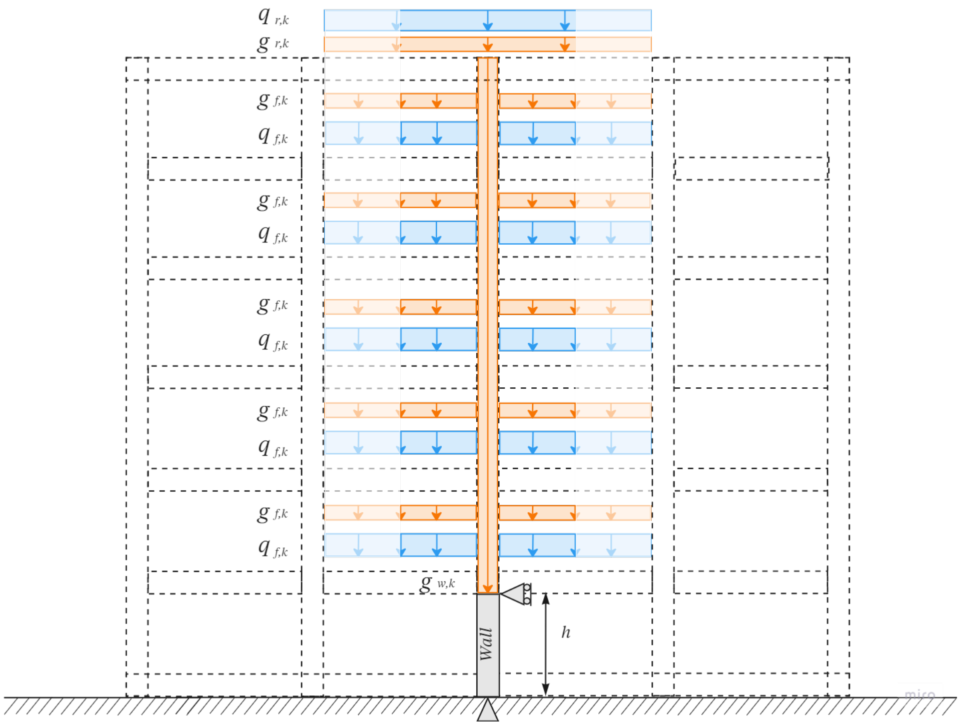

Figure E.7: Representative wall structural calculations

$$
\begin{aligned}
Q_k &= [(n-2)\cdot q_{f,k}\cdot L + q_{r,k}\cdot L]\psi_0 + 2\cdot q_{f,k}\cdot L \\
G_k &= n\cdot g_{f,k}\cdot L + g_{r,k}\cdot L + n\cdot G_{w,k}
\end{aligned} \tag{E.41}
$$

In which n is the number of storeys above the considered wall, L the span of the floors, h the height of each wall, and ρ_{wall} the mass density of each wall. The design load combination for the wall in kN/m in ULS is in agreement with the NEN-EN 1990:2021 equal to Equation E.42, with $\gamma_G = 1.35\cdot 0.89$ and $\gamma_G = 1.5$.

$$
F_d = \gamma_G\cdot G_k + \gamma_Q\cdot Q_k \tag{E.42}
$$

The design strength of a CLT floor can be calculated with Equation E.43 conform 4.5.1 of the prEN 1995-1-1:2023. For a CLT wall, $\gamma_M = 1.25$ and $k_{mod} = 0.8$ for the imposed floor load, with the medium-term load duration class in the ULS.

$$
f_d = \frac{k_{mod}\cdot f_k}{\gamma_M} \tag{E.43}
$$

E.2.1. Axial stress

The walls are subjected to compression, for which the design check for the axial strength of the wall has to be satisfied:

$$
\sigma_{c,0,d} \leq f_{c,0,d} \tag{E.44}
$$

In which:

$$
\sigma_{c,0,d} = \frac{N_d}{A_{x,net}} \tag{E.45}
$$

E.2.2. Buckling, pure compression

First, the cross-sectional properties of the wall, such as the net cross-section area $A_{x,net}$, the net and effective moment of inertia $I_{x,net}$ and $I_{x,ef}$, the net moment of resistance $W_{x,net}$ and the gamma values

γ should be calculated. With those values, the effective radius of gyration $i_{x,ef}$ and the slenderness factor λ_y can be determined:

$$\begin{aligned} A_{x,net} &= n \cdot b_x \cdot t_1 \\ I_{x,net} &= b_x \left(n\frac{t_1^3}{12} + 2t_1 a_1^2 \right) \\ W_{x,net} &= \frac{2I_{x,net}}{t_{CLT}} \\ i_{x,ef} &= \frac{I_{x,ef}}{A_{x,net}} \\ \lambda_y &= \frac{h}{i_{x,ef}} \end{aligned} \tag{E.46}$$

In which t_{CLT} is equal to the total thickness of the CLT wall, a_1 is the distance between the centre of gravity z_0 and the layers in the direction of the span, n is the number of layers in the direction of the span and t_1 is the thickness of the layers in the direction of the span.

The factor k_y that takes into account the second-order effect for flexural buckling on the compressive stresses can be calculated as follows, in agreeance with the NEN-EN 1995-1-1:2011:

$$\begin{aligned} \lambda_{y,rel} &= \frac{\lambda_y}{\pi}\sqrt{\frac{f_{c,0,k}}{E_{0.05}}} \\ k_y &= 0.5 \cdot (1 + \beta_c(\lambda_{y,rel} - 0.3) + \lambda_{y,rel}^2) \\ k_{c,y} &= \frac{1}{k_y + \sqrt{k_y^2 - \lambda_{y,rel}^2}} \end{aligned} \tag{E.47}$$

In which β_c is equal to 0.1 for CLT. The vertical load N_d is calculated over the width of a strip $b_x = 1m$, after which the compressive stresses $\sigma_{c,0,d}$ can be determined:

$$\begin{aligned} N_d &= b_x \cdot F_d \\ \sigma_{c,0,d} &= \frac{N_d}{A_{x,net}} \end{aligned} \tag{E.48}$$

Eventually, the following unity check needs to be satisfied:

$$\frac{\sigma_{c,0,d}}{k_{c,y}} \leq 1.0 \tag{E.49}$$

E.2.3. Wind load

When considering an outer wall such as shown in Figure E.8, the effect of the wind load also has to be taken into account, creating a combined effect between the bending moment caused by the wind load and the compressive force caused by the self-weight and variable loads of the elements above.

To calculate the wind load, it is assumed that the building will be build in a scarcely populated area, placing it in terrain category II according to the NEN-EN 1991-1-4+A1+C2/NB+C2. Furthermore, it is assumed the building is built in wind district II.

In the NEN-EN 1991-1-4+A1+C2:2011, it is taken into account that the wind exerts a different load on every part of the building. The facade can be divided into parts and each different load for each part can be calculated. The combined effect of these loads can then be calculated in a computational model. Because no computational model is being used in this research, only the dominant loads on the structure are calculated for the sake of simplifcation.

The wind pressure has to be calculated on both the outside and the inside walls. The wind pressure on the outside walls w_e is calculated with the external pressure coefficient $c_{pe,10}$ and the extreme pressure

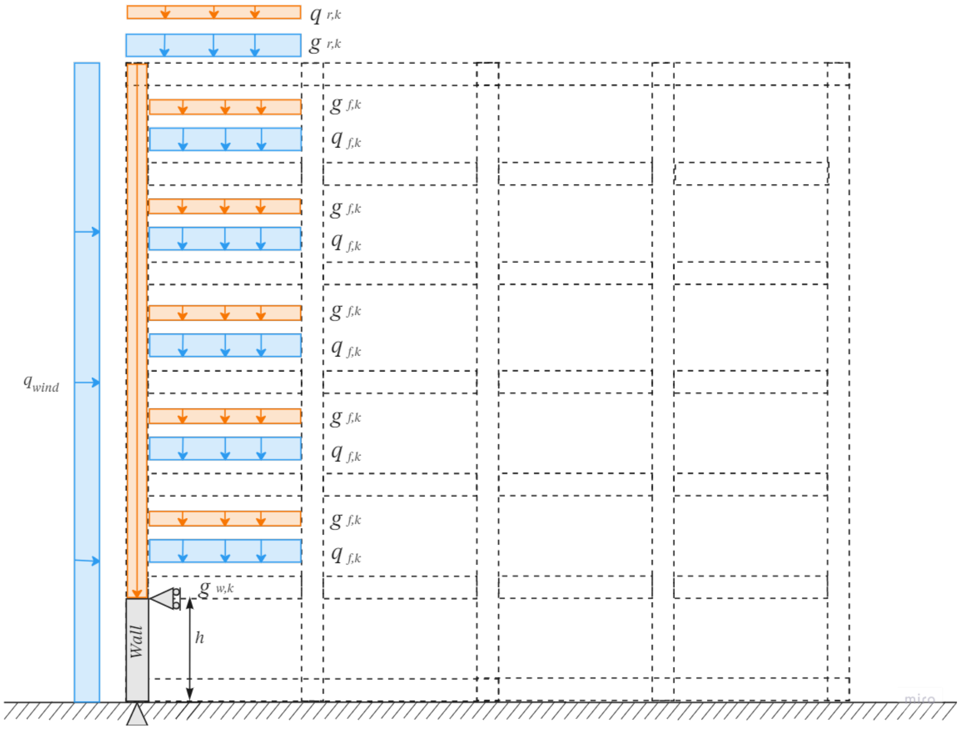

Figure E.8: Representative outer wall structural calculations

$q_p(z)$. The wind pressure on the inside walls w_i is calculated by taking into account the internal pressure coefficient c_{pi} and the extreme pressure $q_p(z)$:

$$\begin{aligned} w_e &= q_p(z_e) \cdot c_{pe,10} \\ w_i &= q_p(z_i) \cdot c_{pi} \end{aligned} \tag{E.50}$$

For a rectangular building, the values for $c_{pe,10}$ are shown in Table E.1, in agreement with the NEN-EN 1991-1-4+A1+C2/NB+C2. The zones represent the areas of the facade on which the specific external pressure coefficient has to be taken into account. In Figure E.9 it is shown when the values are interpreted as positive or negative for both the internal and external coefficients. The value for c_{pi} is taken as the most unfavourable value of $+0.2$ or -0.3

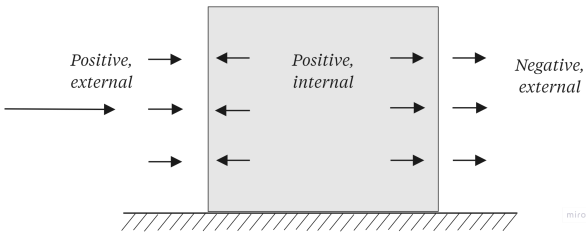

Figure E.9: Internal and external pressure on facades

Table E.1: Values of $c_{pe,10}$ for rectangular facades of buildings with rectangular floor plans

Zone	A	B	C	D	E
h/d $\leq$ 1.0	-1.2	-0.8	-0.5	0.8	-0.5

In Figure E.10 the building is divided in zones as described in the NEN-EN 1991-1-4+A1+C2:2011 and the external pressure coefficients are applied corresponding to Table E.1. For the internal pressure coefficients the most unfavourable combination in chosen. As mentioned, only the dominant wind load is taken into account, meaning the side of the building with the highest resulting force, marked in blue in Figure E.10. That means that on zone D, the internal pressure coefficient $c_{pi} = -0.3$ and on zone E $c_{pi} = +0.2$.

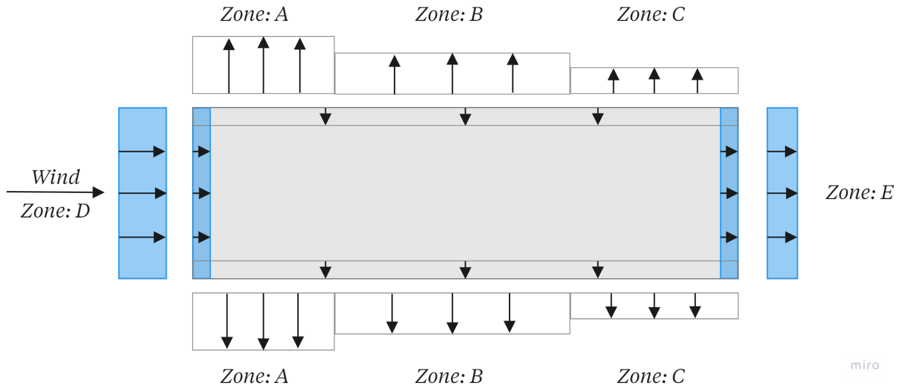

Figure E.10: Internal and external pressure on facades

The value for the extreme pressure $q_p(z)$ can be found with the help of Table E.2, as given in NEN-EN 1991-1-4+A1+C2/NB+C2. Depending on the height of the building, to find the corresponding $q_p(z)$ value, linear interpolation may be applied.

Table E.2: Values of $q_p(z)$ for terrain category II and wind district II

h (m)	**1**	**2**	**3**	**4**	**5**	**6**	**7**	**8**	**9**
$q_p(z)$	0.6	0.6	0.6	0.6	0.66	0.71	0.75	0.79	0.82
h (m)	**10**	**15**	**20**	**25**	**30**	**35**	**40**	**45**	
$q_p(z)$	0.85	0.98	1.07	1.14	1.2	1.25	1.3	1.34	

Finally, the governing resulting force q_{wind} per kN/m^2 can be calculated by combining the pressure on wind zone D with the pressure on wind zone E:

$$q_{wind} = (0.8 + 0.3) \cdot q_p(z) + (0.5 + 0.2) \cdot q_p(z) \tag{E.51}$$

E.2.4. Buckling, combined effect

To calculate the combined effect of bending and compression on the outer wall, a representative part of the wall is taken with a width of $b_x = 1.0m$ and the loads in ULS are applied as shown in Figure E.11. The wind load q_{wind} is applied as a variable load as shown in Figure E.11. The load F_d is now half of the load used in Equation E.42 as can be seen from Figure E.8. Equation E.48 can be used again to calculate the compressive stresses occurring in the wall.
Additionally, for the outer wall, the moment caused by the wind $M_{y,d}$ from Figure E.11 and the bending stresses $\sigma_{m,d}$ are calculated for the same 1m strip

$$\begin{gathered} M_{y,d} = \frac{1}{8} \cdot q_{wind} \cdot L^2 \\ \sigma_{m,d} = \frac{M_{y,d}}{W_{x,net}} \end{gathered} \tag{E.52}$$

For the verification of the compressive and bending stresses in the cross-section, the following should be satisfied:

$$\frac{\sigma_{c,0,d}}{k_{c,y} \cdot f_{c,0,d}} + \frac{\sigma_{m,d}}{f_{m,d}} \leq 1.0 \tag{E.53}$$

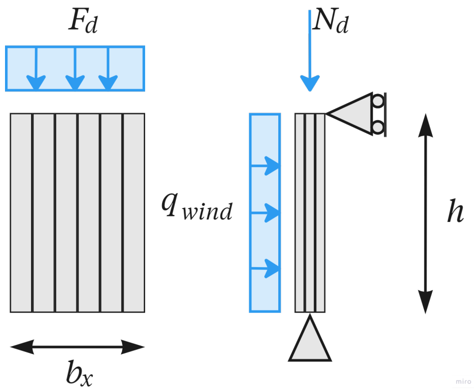

Figure E.11: Wall panel, buckling calculations

E.2.5. Fire safety

Similar to the floor system, in this research it is assumed that the fire safety requirements can be met by covering the CLT walls with gypsum plates.

F

Standard dimensions LVL hollow box floor

Table F.1: Standard dimensions LVL-S ribs, taken from [56]

Thickness [mm]	Height/Width							
45	200	240	300	350	400	450	500	600
51	200	240	300	350	400	450	500	600
57	-	240	300	350	400	-	-	-
63	-	240	300	350	400	450	500	600
69	-	240	300	350	400	-	-	-
75	200	240	300	350	400	450	500	600

Table F.2: Standard dimensions LVL-X top- and bottom panels, taken from [56]

Thickness [mm]	Height/Width							
27	200	240	300	350	400	450	500	600
30	200	240	300	350	400	450	500	600
33	200	240	300	350	400	450	500	600
39	200	240	300	350	400	450	500	600
45	200	240	300	350	400	450	500	600
51	200	240	300	350	400	450	500	600
57	-	240	300	350	400	-	-	-
63	-	240	300	350	400	450	500	600
69	-	240	300	350	400	-	-	-
75	200	240	300	350	400	450	500	600

G

Results structural verifications

This appendix contains the results of the structural verifications of the timber floors of the initial design for the parameter study.

G.1. CLT floor, dry screed

G.1.1. Parameters

CLT floor
Span: 3.6 [m]
Width floor: 5 [m]
Layup: [40, 20, 20, 20, 40] [mm]
Mass density: 490 [kg/m3]
Modulus of elasticity, mean, 0: 11000000000 [N/m2]

Screed and finishes
Thickness screed: 0.0 [mm]
Modulus of Elasticity screed: 26000 [N/m2]
Mass density screed: 2500 [kg/m3]
Other additional weight finishes: 117 [kg/m2]

G.1.2. Loads

$$q_k = 2.55[kN/m2]$$

$$g_k = 1.86[kN/m2]$$

$$q_d = \gamma_G \cdot g_k + \gamma_Q \cdot q_k = 6.05[kN/m2]$$

G.1.3. Bending

$$M_d = \frac{1}{8} q_d L^2 = 9.81[kNm]$$

$$I_{x,net} = b_x \left(n \frac{t_1^3}{12} + 2t_1 a_1^2 \right) = 216666666.67[mm4]$$

$$W_{x,net} = \frac{2I_{x,net}}{h_{CLT}} = 3095238.1[mm3]$$

$$\sigma_d = \frac{M_d}{W_{x,net}} = 3.17[Mpa]$$

ULS: 0.206 [-]

G.1.4. Shear force

$$V_d = \frac{1}{2} q_d L = 10.9[kN]$$

$$S_{x,net} = b_x t_1 a_1 + b_x \frac{t_c^2}{8} = 2050000.0[mm3]$$

$$\tau_d = \frac{V_d \cdot S_{x,net}}{I_{x,net} \cdot b_x} = 0.1[Mpa]$$

ULS: 0.04 [-]

G.1.5. Rolling shear force

$$V_d = \frac{1}{2} q_d L = 10.9[kN]$$

$$S_{R,x,net} = b_x \cdot t_1 \cdot a_1 = 2000000.0[mm3]$$

$$\tau_{Rv,d} = \frac{V_d \cdot S_{Rx,net}}{I_{x,net} \cdot b_x} = 0.1[Mpa]$$

ULS: 0.225 [-]

G.1.6. Deformations

$$w_{inst} = \frac{5 \cdot q \cdot L^4}{384 \cdot E_{x,mean} \cdot I_{x,ef}} = 4.67[mm]$$

$$w_{tot} = w_{inst,G} \cdot (1 + k_{def}) + w_{inst,Q} \cdot (1 + \psi_2 k_{def}) = 8.63[mm]$$

SLS: 0.586 [-]

G.1.7. Human-induced vibration criteria

Stiffness criteria

$$f_1 = 12.94[Hz]$$

$$EI_L = 2115981103234.94[Nmm2]$$

$$EI_T = 190666666666.67[Nmm2]$$

$$b_{ef} = \min(0.95 \cdot L \cdot \left(\frac{EI_T}{EI_L}\right)^{0.25}; b) = 1.87[m]$$

$$w_{1,kN} = \frac{FL^3}{48 \cdot EI_L \cdot b_{ef}} = 0.2452[mm]$$

SLS: 0.981 [-]

Velocity criteria

$$I_{mod,mean} = \frac{42 \cdot f_w^{1.43}}{f_1^{1.3}} = 2.69[-]$$

$$v_{1,peak} = k_{red}\frac{I_{mod,mean}}{M^* + 70} = 0.00208[mm/s]$$

$$k_{imp} = \max(0.48 \cdot \frac{b}{L}\left(\frac{EI_L}{EI_T}\right)^{0.25}; 1.0) = 1.22[-]$$

$$v_{tot,peak} = k_{imp} \cdot v_{1,peak} = 0.00253[mm/s]$$

$$v_{rms} = v_{tot,peak} \cdot (0.65 - 0.01f_1) \cdot (1.22 - 11.0\xi) \cdot \eta = 0.00089[mm/s]$$

SLS: 0.739 [-]

Acceleration criteria, only if f1 < 4.5 Hz

$$k_{res} = \max(0.19 \cdot \frac{b}{L}\left(\frac{EI_L}{EI_T}\right)^{0.25}; 1.0) = 1[-]$$

$$a_{rms} = \frac{k_{res}\mu_{res}F_{dyn}}{\sqrt{2} \cdot 2\xi M^*} = 0.21166[mm/s2]$$

SLS: 3.528 [-]

G.2. CLT floor, wet screed

G.2.1. Parameters

CLT floor
Span: 3.6 [m]
Width floor: 5 [m]
Layup: [40, 20, 20, 20, 40] [mm]
Mass density: 490 [kg/m3]
Modulus of elasticity, mean, 0: 11000000000 [N/m2]

Screed and finishes
Thickness screed: 70 [mm]
Modulus of Elasticity screed: 26000 [N/m2]
Mass density screed: 2500 [kg/m3]
Other additional weight finishes: 162 [kg/m2]

G.2.2. Loads

$$q_k = 2.55[kN/m2]$$

$$g_k = 4.06[kN/m2]$$

$$q_d = \gamma_G \cdot g_k + \gamma_Q \cdot q_k = 8.7[kN/m2]$$

G.2.3. Bending

$$M_d = \frac{1}{8} q_d L^2 = 14.09[kNm]$$

$$I_{x,net} = b_x \left(n \frac{t_1^3}{12} + 2 t_1 a_1^2 \right) = 216666666.67[mm4]$$

$$W_{x,net} = \frac{2 I_{x,net}}{h_{CLT}} = 3095238.1[mm3]$$

$$\sigma_d = \frac{M_d}{W_{x,net}} = 4.55[Mpa]$$

ULS: 0.296 [-]

G.2.4. Shear force

$$V_d = \frac{1}{2} q_d L = 15.66[kN]$$

$$S_{x,net} = b_x t_1 a_1 + b_x \frac{t_c^2}{8} = 2050000.0[mm3]$$

$$\tau_d = \frac{V_d \cdot S_{x,net}}{I_{x,net} \cdot b_x} = 0.15[Mpa]$$

ULS: 0.058 [-]

G.2.5. Rolling shear force

$$V_d = \frac{1}{2} q_d L = 15.66[kN]$$

$$S_{R,x,net} = b_x \cdot t_1 \cdot a_1 = 2000000.0[mm3]$$

$$\tau_{Rv,d} = \frac{V_d \cdot S_{Rx,net}}{I_{x,net} \cdot b_x} = 0.14[Mpa]$$

ULS: 0.323 [-]

G.2.6. Deformations

$$w_{inst} = \frac{5 \cdot q \cdot L^4}{384 \cdot E_{x,mean} \cdot I_{x,ef}} = 7.0[mm]$$

$$w_{tot} = w_{inst,G} \cdot (1 + k_{def}) + w_{inst,Q} \cdot (1 + \psi_2 k_{def}) = 12.95[mm]$$

SLS: 0.945 [-]

G.2.7. Human-induced vibration criteria

Stiffness criteria

$$f_1 = 10.18[Hz]$$

$$EI_L = 2859147769901.61[Nmm2]$$

$$EI_T = 933833333333.33[Nmm2]$$

$$b_{ef} = \min(0.95 \cdot L \cdot \left(\frac{EI_T}{EI_L}\right)^{0.25}; b) = 2.59[m]$$

$$w_{1,kN} = \frac{FL^3}{48 \cdot EI_L \cdot b_{ef}} = 0.1315[mm]$$

SLS: 0.526 [-]

Velocity criteria

$$I_{mod,mean} = \frac{42 \cdot f_w^{1.43}}{f_1^{1.3}} = 3.67[-]$$

$$v_{1,peak} = k_{red}\frac{I_{mod,mean}}{M^* + 70} = 0.00136[mm/s]$$

$$k_{imp} = \max(0.48 \cdot \frac{b}{L}\left(\frac{EI_L}{EI_T}\right)^{0.25}; 1.0) = 1[-]$$

$$v_{tot,peak} = k_{imp} \cdot v_{1,peak} = 0.00136[mm/s]$$

$$v_{rms} = v_{tot,peak} \cdot (0.65 - 0.01f_1) \cdot (1.22 - 11.0\xi) \cdot \eta = 0.00055[mm/s]$$

SLS: 0.459 [-]

Acceleration criteria, only if f1 < 4.5 Hz

$$k_{res} = \max(0.19 \cdot \frac{b}{L}\left(\frac{EI_L}{EI_T}\right)^{0.25}; 1.0) = 1[-]$$

$$a_{rms} = \frac{k_{res}\mu_{res}F_{dyn}}{\sqrt{2} \cdot 2\xi M^*} = 0.09685[mm/s2]$$

SLS: 1.614 [-]

G.3. Hollow box floor, dry screed

G.3.1. Parameters

Hollow box floor
Span: 3.6 [m]
Width floor: 5 [m]
b1: 600.0 [mm]
t1: 27.0 [mm]
b2: 45.0 [mm]
h2: 200.0 [mm]
b3: 600.0 [mm]
t3: 27.0 [mm]
Mass density: 510 [kg/m3]
Modulus of elasticity, E1: 10500000000.0 [N/m2]
Modulus of elasticity, E2: 13800000000.0 [N/m2]
Modulus of elasticity, E3: 10500000000.0 [N/m2]

Screed and finishes
Thickness screed: 0 [mm]
Modulus of Elasticity screed: 26000000000 [N/m2]
Mass density screed: 2500 [kg/m3]
Other additional weight finishes: 194 [kg/m2]

G.3.2. Loads

$$q_{d,middle} = \gamma_G \cdot g_k + \gamma_Q \cdot q_k = 3.95[kN/m2]$$

$$q_{d,edge} = \gamma_G \cdot g_k + \gamma_Q \cdot q_k = 1.97[kN/m2]$$

G.3.3. Shear force, middle

$$\tau_1 = 0.63[Mpa]$$
$$\tau_2 = 0.73[Mpa]$$
$$\tau_3 = 0.63[Mpa]$$

ULS: 0.73 [-]

G.3.4. Shear force, edge

$$\tau_1 = 0.58[Mpa]$$
$$\tau_2 = 0.77[Mpa]$$
$$\tau_3 = 0.58[Mpa]$$

ULS: 0.67 [-]

G.3.5. Normal stress, middle

$$M_d = 6.39451375[kNm]$$
$$\sigma_{1,1} = -1.77[Mpa]$$
$$\sigma_{1,2} = -1.39[Mpa]$$
$$\sigma_{2,2} = -1.83[Mpa]$$
$$\sigma_{2,3} = 1.83[Mpa]$$
$$\sigma_{3,3} = 1.39[Mpa]$$
$$\sigma_{3,4} = 1.77[Mpa]$$

ULS: 0.074 [-]

G.3.6. Normal stress, edge

$$M_d = 3.19725688[kNm]$$
$$\sigma_{1,1} = -1.62[Mpa]$$
$$\sigma_{1,2} = -1.28[Mpa]$$
$$\sigma_{2,2} = -1.68[Mpa]$$
$$\sigma_{2,3} = 1.68[Mpa]$$
$$\sigma_{3,3} = 1.28[Mpa]$$
$$\sigma_{3,4} = 1.62[Mpa]$$

ULS: 0.068 [-]

G.3.7. Deformations

$$w_{inst} = \frac{5 \cdot q \cdot L^4}{384 \cdot E_{x,mean} \cdot I_{x,ef}} = 2.36[mm]$$

$$w_{tot} = w_{inst,G} \cdot (1 + k_{def}) + w_{inst,Q} \cdot (1 + \psi_2 k_{def}) = 3.26[mm]$$

SLS: 0.226 [-]

G.3.8. Human-induced vibration criteria

Stiffness criteria

$$f_1 = 22.69[Hz]$$

$$EI_L = 8028681000000.0[Nmm2]$$

$$EI_T = 6561000000.0[Nmm2]$$

$$b_{ef} = \min(0.95 \cdot L \cdot \left(\frac{EI_T}{EI_L}\right)^{0.25}; b) = 0.58[m]$$

$$w_{1,kN} = \frac{FL^3}{48 \cdot EI_L \cdot b_{ef}} = 0.2094[mm]$$

SLS: 0.837 [-]

Velocity criteria

$$I_{mod,mean} = \frac{42 \cdot f_w^{1.43}}{f_1^{1.3}} = 1.3[-]$$

$$v_{1,peak} = k_{red} \frac{I_{mod,mean}}{M^* + 70} = 0.00082[mm/s]$$

$$k_{imp} = \max(0.48 \cdot \frac{b}{L} \left(\frac{EI_L}{EI_T}\right)^{0.25}; 1.0) = 3.94[-]$$

$$v_{tot,peak} = k_{imp} \cdot v_{1,peak} = 0.00325[mm/s]$$

$$v_{rms} = v_{tot,peak} \cdot (0.65 - 0.01 f_1) \cdot (1.22 - 11.0\xi) \cdot \eta = 0.00072[mm/s]$$

SLS: 0.599 [-]

Acceleration criteria, only if f1 < 4.5 Hz

$$k_{res} = \max(0.19 \cdot \frac{b}{L} \left(\frac{EI_L}{EI_T}\right)^{0.25}; 1.0) = 1.56[-]$$

$$a_{rms} = \frac{k_{res}\mu_{res}F_{dyn}}{\sqrt{2} \cdot 2\xi M^*} = 0.26752[mm/s2]$$

SLS: 4.459 [-]

G.4. Hollow box floor, wet screed

G.4.1. Parameters

Hollow box floor
Span: 3.6 [m]
Width floor: 5 [m]
b1: 600.0 [mm]
t1: 27.0 [mm]
b2: 45.0 [mm]
h2: 200.0 [mm]
b3: 600.0 [mm]
t3: 27.0 [mm]
Mass density: 510 [kg/m3]
Modulus of elasticity, E1: 10500000000.0 [N/m2]
Modulus of elasticity, E2: 13800000000.0 [N/m2]
Modulus of elasticity, E3: 10500000000.0 [N/m2]

Screed and finishes
Thickness screed: 70 [mm]
Modulus of Elasticity screed: 26000000000 [N/m2]
Mass density screed: 2500 [kg/m3]
Other additional weight finishes: 99 [kg/m2]

G.4.2. Loads

$$q_{d,middle} = \gamma_G \cdot g_k + \gamma_Q \cdot q_k = 4.52[kN/m2]$$

$$q_{d,edge} = \gamma_G \cdot g_k + \gamma_Q \cdot q_k = 2.26[kN/m2]$$

G.4.3. Shear force, middle

$$\tau_1 = 0.73[Mpa]$$
$$\tau_2 = 0.84[Mpa]$$
$$\tau_3 = 0.73[Mpa]$$

ULS: 0.837 [-]

G.4.4. Shear force, edge

$$\tau_1 = 0.67[Mpa]$$
$$\tau_2 = 0.88[Mpa]$$
$$\tau_3 = 0.67[Mpa]$$

ULS: 0.768 [-]

G.4.5. Normal stress, middle

$$M_d = 7.32880015[kNm]$$
$$\sigma_{1,1} = -2.03[Mpa]$$
$$\sigma_{1,2} = -1.6[Mpa]$$
$$\sigma_{2,2} = -2.1[Mpa]$$
$$\sigma_{2,3} = 2.1[Mpa]$$
$$\sigma_{3,3} = 1.6[Mpa]$$
$$\sigma_{3,4} = 2.03[Mpa]$$

ULS: 0.085 [-]

G.4.6. Normal stress, edge

$$M_d = 3.66440008[kNm]$$
$$\sigma_{1,1} = -1.86[Mpa]$$
$$\sigma_{1,2} = -1.47[Mpa]$$
$$\sigma_{2,2} = -1.93[Mpa]$$
$$\sigma_{2,3} = 1.93[Mpa]$$
$$\sigma_{3,3} = 1.47[Mpa]$$
$$\sigma_{3,4} = 1.86[Mpa]$$

ULS: 0.078 [-]

G.4.7. Deformations

$$w_{inst} = \frac{5 \cdot q \cdot L^4}{384 \cdot E_{x,mean} \cdot I_{x,ef}} = 2.76[mm]$$

$$w_{tot} = w_{inst,G} \cdot (1 + k_{def}) + w_{inst,Q} \cdot (1 + \psi_2 k_{def}) = 3.89[mm]$$

SLS: 0.27 [-]

G.4.8. Human-induced vibration criteria

Stiffness criteria

$$f_1 = 20.41[Hz]$$

$$EI_L = 8771847666666.67[Nmm2]$$

$$EI_T = 749727666666.67[Nmm2]$$

$$b_{ef} = \min(0.95 \cdot L \cdot \left(\frac{EI_T}{EI_L}\right)^{0.25}; b) = 1.85[m]$$

$$w_{1,kN} = \frac{FL^3}{48 \cdot EI_L \cdot b_{ef}} = 0.0599[mm]$$

SLS: 0.24 [-]

Velocity criteria

$$I_{mod,mean} = \frac{42 \cdot f_w^{1.43}}{f_1^{1.3}} = 1.49[-]$$

$$v_{1,peak} = k_{red} \frac{I_{mod,mean}}{M^* + 70} = 0.00071[mm/s]$$

$$k_{imp} = \max(0.48 \cdot \frac{b}{L} \left(\frac{EI_L}{EI_T}\right)^{0.25}; 1.0) = 1.23[-]$$

$$v_{tot,peak} = k_{imp} \cdot v_{1,peak} = 0.00088[mm/s]$$

$$v_{rms} = v_{tot,peak} \cdot (0.65 - 0.01 f_1) \cdot (1.22 - 11.0\xi) \cdot \eta = 0.00026[mm/s]$$

SLS: 0.218 [-]

Acceleration criteria, only if f1 < 4.5 Hz

$$k_{res} = \max(0.19 \cdot \frac{b}{L} \left(\frac{EI_L}{EI_T}\right)^{0.25}; 1.0) = 1[-]$$

$$a_{rms} = \frac{k_{res} \mu_{res} F_{dyn}}{\sqrt{2} \cdot 2\xi M^*} = 0.12705[mm/s2]$$

SLS: 2.118 [-]